Origin, migration and alteration of hydrocarbons in the Austrian sector of Alpine Foreland Basin

PhD Thesis

Łukasz Pytlak, MSc

Supervisor:

Univ.-Prof. Mag.rer.nat Dr. mont. Reinhard F. Sachsenhofer,

Department Applied Geosciences and Geophysics

Chair of Petroleum Geology

Montanuniversität Leoben

Leoben, 2017

Affidavit

I declare in lieu of oath, that I wrote this thesis and performed the associated research myself, using only literature cited in this volume.

MSc Łukasz Pytlak

Acknowledgements

First and foremost, I would like to thank my supervisors, Reinhard Sachsenhofer and Doris Gross, for their invaluable guidance throughout the process of writing this thesis.

Secondly, I would like to extend my gratitude to Rohoel-Aufsuchungs AG for providing me the access to the samples and data which made this thesis possible. I also owe my thanks to Rohoel-Aufsuchungs AG employees Hans-Gert Linzer, Alan Reingruber, Wilma Troiss, Werner Tschelaut and Christoph Janka for their motivation and dedicating their time to assist me in all aspects of this thesis.

Co-operation between Montanuniversität Leoben and Rohoel-Aufsuchungs AG in the frame of the FFG-Bridge Project (836527) resulted as numerous articles and conference papers. The most meaningful full research articles are:

- Pytlak et al., 2016. Generation, mixing and alteration of thermogenic and microbial gas in oil deposits: The case of the Alpine Foreland Basin (Austria). Marine and Petroleum Geology 78, 575-592
- Pytlak et al., 2016. Gas accumulations in Oligocene-Miocene reservoirs in the Alpine Foreland Basin (Austria): evidence for gas mixing and gas degradation. International Journal of Earth Sciences
- Pytlak et al., 2017. Composition of diamondoids in oil samples from the Alpine Foreland Basin, Austria: potential as indices of source rock facies, maturity and biodegradation. Journal of Petroleum Geology 40, 153-171
- Pytlak et al., (under review). Light hydrocarbon geochemistry of oils in the Alpine Foreland Basin: Impact of geothermal fluids on the petroleum system. Geofluids
- Pytlak et al., (under review). Origin of condensates co-produced with microbial gas in the Alpine Foreland Basin (Austria): lessons learned from ancillary geochemical methods. Organic Geochemistry

Here I want to thank the editors Christopher Tiratsoo (Journal of Petroleum Geology), Robert Ondrak (GFZ German Research Centre for Geoscience, Marine and Petroleum Geology) and Wolf-Christian Dullo (International Journal of Earth Sciences), the reviewers Andrea Vieth-Hillebrand (GFZ), Gabor C. Tari (OMV), C. Ungureanu (OMV), G.N. Gordadze (Gubkin University) and two anonymous reviewers for their suggestions, which helped to improve the articles (and the present thesis) considerably.

I am immensely grateful to Adam Kowalski (AGH University of Science and Technology) for help with GC-MS/MS, enabling a part of my thesis which resulted from an Elsevier Research Scholarship 2015 (see section 8).

Special thanks go to Achim Bechtel and Reinhard Gratzer (both from Montanuniversität Leoben) for sharing with me their knowledge on geochemistry and guiding me through the laboratory work. A big “thank you” goes to Walter Prochaska (Montanuniversität Leoben), Albrecht Leis (JR-AquaConSol GmbH) and Suryendu Dutta (Indian Institute of Technology Bombay) for providing me the results, which became an integral part of this thesis and help with establishing the analytical method.

A sincere thank-you to my colleagues at the Chair of Petroleum Geology for all the support and help during hard times.

Last but not least, “thank-you” to my wife Joanna, my family and friends for being the people I can always count on.

Abstract

Two petroleum systems are present in the eastern (Austrian) sector of the Alpine Foreland Basin. Whereas oil and thermogenic gas in Mesozoic and Eocene reservoir rocks have been generated beneath the Alps in Lower Oligocene source rocks, relative dry gas in Oligocene–Miocene clastic rocks deposited in the deep marine basin-axial channel system (Puchkirchen Channel) is interpreted as microbial in origin.

Detailed investigations of the molecular and isotope composition of hydrocarbon samples from Cretaceous, Eocene and Oligocene/Miocene reservoirs (representing all producing fields) give new insight into the filling history of traps.

Maturity parameters based on the light hydrocarbons fraction, as well as diamondoid isomerization indices and $\delta^{13}C$ of ethane and propane show that light hydrocarbons in oils from Cenomanian/Eocene reservoirs have been generated from a source rock with late oil window maturity (1.1-1.2% Rr). This is a higher maturity level than indicated by biomarker isomerization ratios and MPI-1 (0.6-0.9 %Rr) and points to mixing of two end-member oil phases, both generated from the same source rock, but at different maturity levels. API gravity of (non-altered) oils and the development of gas caps in the eastern part of the study area are controlled by the relative percentage of the hydrocarbons with higher maturity. Mixing of fluids with different maturities is also supported by evidences for evaporative fractionation. In contrast, most Cenomanian/Eocene fields trap methane derived from a source which is not thermogenic. Shallow northeastern reservoirs trap methane interpreted as secondary microbial in origin. The same process is proposed here as source of methane in north-western deposits. However, those gases are enriched in ^{2}H isotope suggesting different methanogenesis pathways. Fields along the southern margin of the Alpine Foreland Basin, where reservoir temperature exceeds 80°C, host methane generated during primary organic matter degradation. Thus, Eocene layers should be considered as additional potential source rocks.

Presence of pure microbial gas in Oligocene/Miocene reservoirs is rare and limited mainly to the northern basin flank (e.g., KK field). All other fields contain varying amounts of thermogenic gas/condensate, which have been generated from a source rock with oil-window maturity. Moreover, concentration of diamondoids (and their isomerization indices) in the condensates are positively correlated with percentages of thermogenic methane in co-produced (microbial) gas. Consequently, the condensates are explained as products of evaporative fractionation of oils in Cenomanian/Eocene

reservoirs. Upward migration occurred along discrete fault zones (e.g., H field) or through low-permeability caprocks. Local erosion of Lower Oligocene sediments, the principal seal for the thermogenic petroleum system, as well as a high percentage of permeable rocks within the Puchkirchen Channel favored upward migration and mixing of thermogenic and microbial gas. The same (Lower Oligocene) source rock for condensates in Oligocene/Miocene reservoirs and oils in Cenomanian/Eocene reservoirs is proven by geochemical features. All gas and condensate samples in Oligocene/Miocene reservoirs are biodegraded. Biodegradation and the formation of secondary microbial gas resulted in gas drying. Therefore, the gas samples analyzed in this study are relative dry, despite significant contributions of thermogenic hydrocarbons. Biodegradation probably continues at present time. The degree of biodegradation, however, decreases with depth.

Diamondoid hydrocarbons were detected in the saturated fraction of all analysed oils. A biodegraded oil sample from a shallow reservoir in the northeastern part of the study area showed an enrichment in diamondoids due to the molecule's high resistance to microbial degradation. In the Alpine Foreland Basin, biomarker-derived maturity parameters do not show a convincing correlation with diamondoid maturity parameters. Moreover, no cracking trend based on biomarkers and diamondoid concentrations was observed. The results indicate that the composition of diamondoids in oils from the Austrian part of the Alpine Foreland Basin is mainly controlled by heterogeneities in the Lower Oligocene source rocks, including the occurrence of a redeposited source rock succession in the western part of the study area. By contrast, EAI-1 (the ethyladamantane index) shows a good correlation with various maturity parameters and seems to be independent of source rock facies.

Apart from petroleum, the basin hosts a significant geothermal potential, which is based on the regional flow of meteoric water through Malmian carbonate rocks. 57 oil samples and 19 water samples (representing 28 fields) were measured for chemical snd isotopic compositions. Oils are predominantly composed of *n*-alkanes, while some samples are progressively depleted in light aromatic components. The depletion in aromatic components relative to abundant *n*-alkanes is an effect of water washing. Besides a progressive depletion in aromatics, water washing causes a reduction in API gravity and removal of sulphur bearing compounds. Waters co-produced with oils that are affected by water washing show a progressive reduction in salinity and depletion in

^{2}H and ^{18}O isotopes, indicating that the degree of water washing is mainly controlled by the inflow of meteoric water from Malmian carbonates. Most strongly affected oils are located in the shallow northern and northeastern part of the study area. In some fields with Cenomanian reservoirs, a hydraulic connectivity with the thermal aquifer is evident. However, water washing is also recognized in Eocene reservoirs in areas where the Malmian aquifer is missing. This shows that existing flow models for the regional geothermal aquifer have to be modified. Therefore, the results emphasize the importance of combining data from the petroleum and geothermal industry, which are often handled separately.

Zusammenfassung

Zwei Kohlenwasserstoffsysteme existieren im östlichen (österreichischen) Teil des Alpinen Vorlandbeckens. Während die in den mesozoischen und eozänen Reservoireinheiten akkumulierten Kohlenwasserstoffe (Öl und thermisches Gas) von vom Nordrand der Alpen überschobenen unteroligozänen Muttergesteinen generiert wurden, kann für relativ trockenes Gas in oligozänen und miozänen Speichergesteinen entlang des tiefmarinen Puchkirchen Channels ein biogener Ursprung postuliert werden.

Neue Untersuchungen hinsichtlich der molekularen und isotopischen Zusammensetzung von Kohlenwasserstoffproben aus kretazischen, eozänen und oligo-/miozänen Speichergesteinen (aus allen aktuell produzierenden Feldern) ermöglichen eine detaillierte Interpretation der Füllungsgeschichte der vorhandenen, produktionsrelevanten Fallenstrukturen.

Reifeparameter auf Basis der leichten Kohlenwasserstofffraktionen, sowie Isomerisierungsverhältnisse der Diamantoide und δ^{13}C-Werte von Methan und Ethan zeigen, dass die leichten Kohlenwasserstofffraktionen in cenomanen und eozänen Reservoirs von einem Muttergestein mit einer Reife im Bereich des späten Ölfensters (1.1-1.2 %Rr) generiert wurden. Diese relativ hohe thermische Reife wird jedoch von konventionellen geochemischen Reifeparametern (Hopan/Steran-Isomerisierung, MPI-1) nicht bestätigt, welche auf eine deutlich geringer Reife (0.6-0.9 %Rr) hindeuten. Dieses Phänomen kann vermutlich auf Mischungsprozesse zwischen zwei Ölphasen zurückgeführt werden, welche von demselben Muttergestein, allerdings in unterschiedlichen Phasen der Versenkungsgeschichte, gebildet wurden. Die Dichte (in °API) der nicht biodegradierten Öle sowie die Bildung von Gaskappen im östlichen Teil des Untersuchungsgebiets werden von dem relativen Anteil an Kohlenwasserstoffen höherer thermischer Reife kontrolliert. Die Theorie der Mischung zweier Phasen unterschiedlicher thermischer Reife wird weiters durch die Tatsache untermauert, dass Indizien für evaporitische Fraktionierung vorliegen. Im Gegenzug beinhaltet die Mehrzahl an cenomanen und eozänen Reservoirs Methan, welches nicht thermisch gebildet wurde. Seichte Lagerstätten im Nordosten beinhalten Methan sekundären, biogenen Ursprungs. Die Ergebnisse dieser Studie deuten auf einen ähnlichen Bildungsmechanismus für Methan in nordwestlich gelegenen Lagerstätten. Allerdings variieren nordöstliche und nordwestliche Lagerstätten hinsichtlich der isotopischen Zusammensetzung des Wasserstoffs, was auf unterschiedliche Pfade der Methanogenese hindeutet. Felder entlang des Molasse-Südrands erreichen

Lagerstättentemperaturen >80 °C und weisen primär mikrobiell gebildetes Methan auf, demzufolge können eozäne Gesteine als zusätzliche potentielle Muttergesteine betrachtet werden.

Das Vorhandensein von rein mikrobiell gebildetem Gas in oligo-/miozänen Speicherstrukturen ist generell auf den nördlichen Beckenrand beschränkt (z.B. KK Feld). Alle anderen Felder beinhalten variierende Mengen einer thermischen Gas/Kondensat-Phase, welche auf ein Muttergestein im Ölfenster zurückzuführen ist. Weiters korreliert die Konzentration an Diamantoiden (und deren Isomerisierungsverhältnisse) in der Kondensatphase positiv mit dem Anteil an thermischem Methan innerhalb des gleichzeitig produzierten mikrobiellen Gases. Demzufolge wird der Anteil an Kondensat in den untersuchten oligo-/miozänen Lagerstätten als ein Resultat von evaporitischer Fraktionierung cenomaner und eozäner Öle interpretiert. Die Migration in jüngere Speicherhorizonte erfolgte entweder entlang diskreter Störungszonen (z.B. H Feld), oder durch geringpermeable Deckschichten. Lokale Erosion von unteroligozänen Sedimenten, welche die hauptsächliche Deckschicht des thermischen Kohlenwasserstoffsystems darstellen, sowie ein hoher Anteil permeabler Schichten innerhalb des Puchkirchen Channels, ermöglichen vertikale Migration und die Mischung von thermischem und mikrobiellem Gas in seichten Lagerstätten. Sowohl für Kondensate in oligo-/miozänen Lagerstätten, als auch für Öle in cenomanen und eozänen Lagerstätten, wurde anhand der geochemischen Signatur dasselbe (unteroligozäne) Muttergestein festgestellt. Alle untersuchten Gas- und Kondensatproben weisen Anzeichen von Biodegradation auf. Diese Degradationsprozesse gingen mit der Bildung von sekundärem, mikrobiellem Gas einher, welches zu einer Erhöhung der „Dryness“ führte. Demzufolge sind alle untersuchten Gase trotz signifikantem Anteil an thermischen Kohlenwasserstoffen als eher trocken zu klassifizieren. In-situ Biodegradation spielt vermutlich auch in rezenten Lagerstätten eine wichtige Rolle, wobei der Grad an Degradation mit der Tiefe abnimmt.

Diamantoide wurden in der aliphatischen Fraktion aller analysierten Öle nachgewiesen. Ein biodegradiertes Öl aus einer seichten Lagerstätte im nordöstlichen Teil des Untersuchungsgebiets zeigte deutlich eine Anreicherung von Diamantoiden aufgrund der hohen Resistenz dieser Molekülgruppe gegen Degradationsprozesse. Konventionelle Reifeparameter auf Basis von Biomarkermolekülen zeigen im Alpinen Vorlandbecken eine nur unzureichende Korrelation mit Reifeparametern auf Basis von

Diamantoidkonzentrationen. Dies ist vermutlich darauf zurückzuführen, dass die Zusammensetzung von Diamantoiden in den untersuchten Ölen in erster Linie von Heterogenitäten innerhalb des unteroligozänen Muttergesteins zurückzuführen ist. Die Umlagerung von organisch-reichen, unteroligozänen Sedimenten im westlichen Teil des Untersuchungsgebiets spielt in dieser Hinsicht vermutlich ebenfalls eine wichtige Rolle. Im Gegensatz dazu korreliert der EAI-1 Index (Ethyladamantan-Index) gut mit verschiedenen etablierten Reifeparametern, was eine weitgehende Faziesunempfindlichkeit dieses Indexes nahelegt.

Neben dem Kohlenwasserstoffpotential kann für das Alpine Vorlandbecken auch ein beträchtliches Nutzungspotential hinsichtlich geothermischer Energiegewinnung zugrunde gelegt werden. Dieses Potential ist auf regionale Tiefenströmungen von meteorischen Wässern innerhalb von Malmaquiferen karbonatischer Lithologie zurückzuführen. 57 Ölproben und 19 Wasserproben (aus 28 Feldern) wurden hinsichtlich der chemischen und isotopischen Zusammensetzung untersucht. Die untersuchten Öle weisen Anzeichen von „water-washing“ auf (z.B. Abreicherung leichter aromatischer Verbindungen), welches unter anderem zu einer Reduktion der Öldichte (°API) und geringen relativen Anteilen an schwefelhaltigen Verbindungen führte. Lagerstättenwässer, welche gemeinsam mit den produzierten Ölen gefördert wurden, weisen eine progressive Reduktion der Salinität sowie eine Abreicherung von schweren Wasserstoff- und Sauerstoffisotopen (^{2}H, ^{18}O) auf. Dies deutet darauf hin, dass der Grad an „water-washing“ in erster Linie durch den Zufluss meteorischer Wässer aus den Malm-Karbonaten kontrolliert wird. Die größte Beeinflussung wurde dabei für seichte Lagerstätten im nördlichen und nordöstlichen Bereich des Untersuchungsgebiets festgestellt. Für einige Felder mit cenomanen Speichergesteinen wird ein hydraulischer Kontakt mit dem Malmaquifer postuliert, wobei Anzeichen für „water-washing“ auch für eozäne Lagerstätten bestehen, für welche ein Konnex zum oben erwähnten Malmaquifer ausgeschlossen werden kann. Dies beweist, dass die existierenden hydrogeologischen Strömungsmodelle für den regionalen geothermischen Aquifer lückenhaft und verbesserungsbedürftig sind. Die Zusammenarbeit von Kohlenwasserstoffproduzenten und Geothermiebetreibern verspricht essentielle Synergieeffekte welche in zukünftigen Studien genutzt werden sollten.

Table of Contents

1. Oil and gas generation: theoretical background

Significant progress has been achieved in the last decades in understanding the formation of natural gas accumulations as well as gas-oil and gas-source rock correlations. The generation and accumulation of hydrocarbons are related to three main stages of thermal maturity of organic matter in sedimentary rocks: (I) diagenesis, (II) catagenesis and (III) metagenesis.

(I) Diagenesis is the process involving biological, physical and chemical alteration of the organic matter in sediments without a pronounced effect of rising temperature. This process leads from biopolymers synthesized by plants and animals to geopolymers called kerogen – the main organic material in ancient sediments. Moving downward in a column of accumulating sediment, following consumption of free oxygen, a series of zones where nitrate, Mn^{IV}, Fe^{III}, sulfate and methane reduction occur (Whiticar, 1999). The proteins, carbohydrates and lipids are broken down into amino acids, simple sugars and long-chain fatty acids. These smaller molecules are attacked by fermenting bacteria that produce acetic acids, other short-chain carboxylic acids, alcohols, hydrogen and carbon dioxide. In the final step, these are converted to methane (called in this thesis primary microbial methane; Milkov, 2011) by methanogenic bacteria. Methane production and accumulation is restricted to oxygen-free environments as methane-producing microorganisms are strict anaerobes (Whiticar, 1999). Moreover, methane does not accumulate in significant amounts in the presence of high concentration of dissolved sulfate. Above restrictions confine the production of methane to certain environments like: dung heaps, poorly drained swamps, bays, paddy fields, anoxic freshwater lake bottoms, landfills, glacial drift and marine sediment below the sulfate reduction zone (Rice & Claypool, 1981 and references therein). Beside of methane, only traces of higher hydrocarbons can be generated in laboratory-conducted studies (Davis & Squires, 1954; Kim & Douglas, 1972; Oremland et al., 1988) and are founded in recent sediments (Weber & Maximov, 1976, Hinrichs et al., 2006).

(II) With increasing temperature and advancing geologic time, a wide range of hydorcarbons is produced from kerogen by thermal alteration and cracking reactions (thermogenic processes). Thermal maturity ranges between 0.6 and 2.0% vitrinite reflectance. Oil generation occurs during this stage and is accompanied by the production of significant amounts on natural gas depending on the type of organic matter. While generation proceeds through the oil window (mature stage) and into the

advanced stage of catagenesis, the gas becomes progressively drier and isotopically more positive (Schoell, 1983). The change in molecular composition mostly results because the C_2-C_5 components are less stable than methane at higher temperature.

(III) At the end of the catagenesis and beginning of metagenesis, the kerogen becomes highly polymerized, condensed in structure and chemically stable. The main hydrocarbon generated is methane, which mainly results from cracking of generated hydrocarbons. The level of maturity is equivalent to the range 2.0 to 3.3% vitrinite reflectance.

The carbon and hydrogen isotopic composition of hydrocarbons and CO_2 are useful for recognition of the gas origin. It has been shown that isotopic ratios are mainly controlled by the formation mechanisms (e.g. CO_2 reduction vs. fermentation, thermogenic vs. microbial), the isotopic signature of the source rock and its thermal maturity (e.g. Berner & Faber, 1987; Chung et al., 1988; Clayton, 1991; Fuex, 1977; Galimov, 2006; James, 1983; 1990; Krooss et al., 1995; Littke et al., 1995; Rice & Claypool, 1981; Rooney et al., 1995; Schoell, 1980; 1983; Stahl, 1977; Whiticar et al., 1994; Milkov, 2011). Low temperature bacterial reduction of CO_2 to CH_4 leads to $\delta^{13}C$ values of CH_4 as negative as -110‰ V-PDB (Vienna-Pee Dee Belemnite). Fermentation of methylated substrates results in values of -50‰ to -60‰ V-PDB. Hydrogen isotope fractionation effects during fermentation can lead to δ^2H values of CH_4 as low as -530‰ V-SMOW (Vienna-Standard Mean Ocean Water), while CO_2 reduction gives more positive values (-170‰ to -250‰ V-SMOW) (Whiticar, 1999). In early catagenesis gas is formed concurrently with oil from kerogen in source rocks. This thermogenic gas contains higher amounts of the C_2-C_5 hydrocarbons than microbial gas. The methane generated during thermogenic processes is generally enriched in ^{13}C and ^2H compared to microbial methane and can reach values of -25‰ to -55‰ V-PDB and -100‰ to -300‰ V-SMOW, for carbon and hydrogen, respectively. However, the isotopic signature strongly depends on organic matter type and source rock maturity.

In addition, the hydrogen isotope compositions are controlled by hydrogen exchange between water and thermally maturing organic matter (Lewan, 1993; 1997; Schimmelmann et al., 2001; 2004; Yoneyama et al., 2002), whereas isotope exchange between already formed *n*-alkanes and water is limited (Hoering, 1984; Seewald et al., 1998; Sessions et al., 2004). An enrichment in ^2H with increasing thermal stress is observed in natural samples (Dai, 1990; Radke et al., 2005; Schoell, 1980) as well as in theoretical and laboratory studies (e.g. Ni et al., 2011; Tang et al., 2005).

Once the hydrocarbons are expelled from the source rock, different alteration processes can influence their composition. The most important processes are biodegradation, water washing, in-reservoir cracking, thermochemical sulphur reduction, deasphaltening, evaporative fractionation.

Microbial petroleum biodegradation has been identified as a significant factor influencing molecular and isotopic gas compositions and thus pressure-volume-temperature (PVT) properties (James & Burns, 1984; Larter & di Primo, 2005; Palasser, 2000). Significant amounts of (secondary microbial) methane can be generated via hydrocarbon biodegradation (e.g. Head et al., 2003; Huang & Larter, 2014; Jones et al., 2008; Milkov, 2010; Zengler et al, 1999). Secondary microbial methane is characterized by varying carbon isotope ratio depending on methanogenic community and reaction pathways, isotopic signature of the substrate, progress of alteration, reservoir temperature etc. (Jones et al., 2008; Brown, 2011). Diagnostic features of secondary microbial gas include CO_2 enriched in ^{13}C (Milkov, 2011 and references therein). The enrichment results from CO_2-CH_4 isotopic fractionation during methanogenesis (Botz et al, 1996; Feisthauer et al, 2010). When CO_2 reduction commences, isotopically light methane (-65 ‰ or lower) and CO_2 with moderately high $\delta^{13}C$ values are produced (Jones et al., 2008).

Often biodegradation is accompanied by water washing as bacteria and necessary nutrients can be introduced from the water. The interaction of water with hydrocarbons may result in the removal of relative water-soluble compounds (e.g. light aromatics: benzene, toluene, xylenes etc.) from oil. Water washing may occur either during oil migration or within the reservoir (e.g. Lafargue & Barker, 1988).

The most common understanding of the origin of gas condensates is that they are thermally generated by cracking of kerogen and liquid oil at vitrinite reflectance of 1.2% and higher (e.g. Tissot & Welte, 1984) or that they are formed from coaly (type III) kerogen. However, evaporative fractionation (Thomson, 1987), a process akin to natural distillation, in which lighter hydrocarbons and gases escape from deeper reservoirs and migrate upwards into shallower reservoirs, is an additional important process, which may lead to condensate deposits.

Condensates are rarely included in oil-oil correlation, as biological markers are often below detection limit and light hydrocarbons do not preserve evidence of a unique, biological origin due to too small carbon skeletons. Actually most of the light hydrocarbons are formed by catagenetic cracking of larger precursors, whereas only

some isomers may have direct biological origin. Nevertheless, light hydrocarbons can yield information about source, thermal maturity and post-expulsion history.

2. Geology of the Austrian part of the Alpine Foreland Basin

The Alpine Foreland Basin (often also called Molasse Basin) extends along the northern margin of the Alps from Geneva (Switzerland) in the west to Vienna (Austria) in the east. The present study focusses on its Austrian part (Fig. 1b). A brief overview on its geological evolution is provided below.

2.1. The geological evolution of the pre-Molasse sediments

The pre-Cenozoic basement of the Alpine Foreland Basin is formed by crystalline rocks of the Bohemian Massif, which are overlain by Jurassic to Cretaceous siliciclastics and carbonate rocks (Fig. 2). Permo-Carboniferous sediments are only locally preserved in narrow graben structures (Wagner, 1996; 1998).

The oldest Mesozoic rocks in the study area are Middle Jurassic shallow-marine to fluvial sandstones with intercalated layers of coal. An extensive carbonate platform formed in Late Jurassic time on the tropical shelf of the Bohemian Massif. Its facies distribution indicates progressive deepening of the sea from north towards south(west).

During the Early Cretaceous, the area became uplifted, eroded and karstified. Tectonic activity occurred along NW-SE striking fault systems southwest of the Central Swell Zone (for location see Fig. 3) and the Bohemian Massif.

The Late Cretaceous started with the deposition of transgressive Cenomanian marls and storm-dominated glauconitic sandstones underlain by fluvial sandstones. The latter, so called “Schutzfels Beds”, infill the Jurassic karst (Nachtmann & Wagner 1987). The Cenomanian clastics are overlain by Turonian clays containing storm deposits. Campanian sediments consist of shallow marine sandstones derived form the Bohemian Massif and shallow marine mudstones. Due to major tectonic deformations in latest Cretaceous to earliest Paleogene time, the top of the Cretaceous corresponds to a regional unconformity. During this time the basin was uplifted and transected by NW-SE and NNW-SSE trending fault systems. The tilting of individual fault blocks to the east preserved Upper Cretaceous sediments in their eastern parts. Faults along the Central Swell Zone became reactivated, resulting in uplift and erosion of Cretaceous and locally Jurassic layers above this structural high.

2.2. Basin fill

During Late Eocene time, the (Peri-Tethyan) sea transgressed progressively on the evolved peneplain. Therefore, an Upper Eocene transgressive succession including fluvial and shallow marine sandstones, as well as shallow marine carbonates ("Lithothamnium Limestone") overlies Mesozoic or crystalline basement rocks. Due to subsequent overthrusting and tectonic shortening the present-day basin is much narrower than the original one (Wagner, 1996). Flexural downward bending of the European lithosphere due to the advancing Alpine nappe system led to the development of mainly south-dipping E-W trending faults, but also to reactivation of NNW-SSE trending normal fault systems, rapid subsidence of the area to deep water conditions, and southward increasing basement depth.

Extensive tectonic activity at the Eocene-Oligocene boundary changed the configuration of Eurasia and separated the (Peri-)Tethys into the Paratethys and the Mediterranean Sea (Roegl, 1999). Deep basins with reduced circulation and oxygen-depleted bottom conditions led to the deposition of organic matter-rich pelitic rocks with thin carbonate layers during Early Oligocene time (Schöneck, Dynow, Eggerding formations; Schulz et al., 2005; Sachsenhofer et al., 2010). Locally these rocks, about 60 m thick, have been removed by submarine erosion before deposition of the overlying Zupfing Formation (Sachsenhofer & Schulz, 2006).

Ssubsequently the re-opening of seaways from the Paratethys to the Mediterranean Sea and the Indian Ocean allowed oxygenated bottom water entering the Paratethys Sea. This caused a breakdown of water column stratification and terminated deposition of organic matter-rich rocks (Schulz et al., 2002).

During Late Oligocene and Early Miocene times, gravity flow deposits accumulated in a deep marine basin-axial channel system (Puchkirchen Channel) originating in the west (near Munich) from a prograding-retrograding delta system (Covault et al., 2009; Hubbard et al., 2005, 2009). The coarse-grained clastic rocks form part of the Lower Puchkirchen Formation (uppermost Chattian to lowermost Aquitanian), the Upper Puchkirchen Formation (Aquitanian to lower Burdigalian) and the Hall Formation, which follows above a major erosional event (Grunert et al., 2013, 2015; Fig. 2). Pelitic rocks, typically with low organic matter contents, were deposited outside of the channel system. However, organic matter-rich intervals, including a "fish shale" near the top of the Upper Puchkirchen Formation, occur as well (Wagner, 1996, 1998). Decreased

subsidence and increased sedimentation rates resulted in filling of the basin between late Eggenburgian and Ottnangian times. Coal-bearing freshwater sediments with a Middle to Late Miocene age dominate the uppermost part of the Cenozoic succession.

2.3. Tectonic evolution

Several fault systems occur in the Austrian part of the foreland basin (Fig. 1c). NW–SE- and NE–SW-trending faults existed already during Palaeozoic times and were reactivated in Mesozoic and Palaeogene times. Roughly W–E-trending extensional faults result from the down-bending of the foreland crust due to the subduction of the European Plate under the Periadriatic Plate and the weight of the advancing Alpine nappe system (Wagner, 1998). Almost all Early Oligocene faults were reactivated during Miocene times (Fig. 4).

The southern part of the basin was overthrusted by the Alpine nappes. During overthrusting, Cenozoic molasse sediments were incorporated into the Alpine thrusts (Imbricated or Allochthonous Molasse) and moved tectonically into, and across, the southern autochthonous sediments (Autochthonous Molasse) (Fig. 1d).

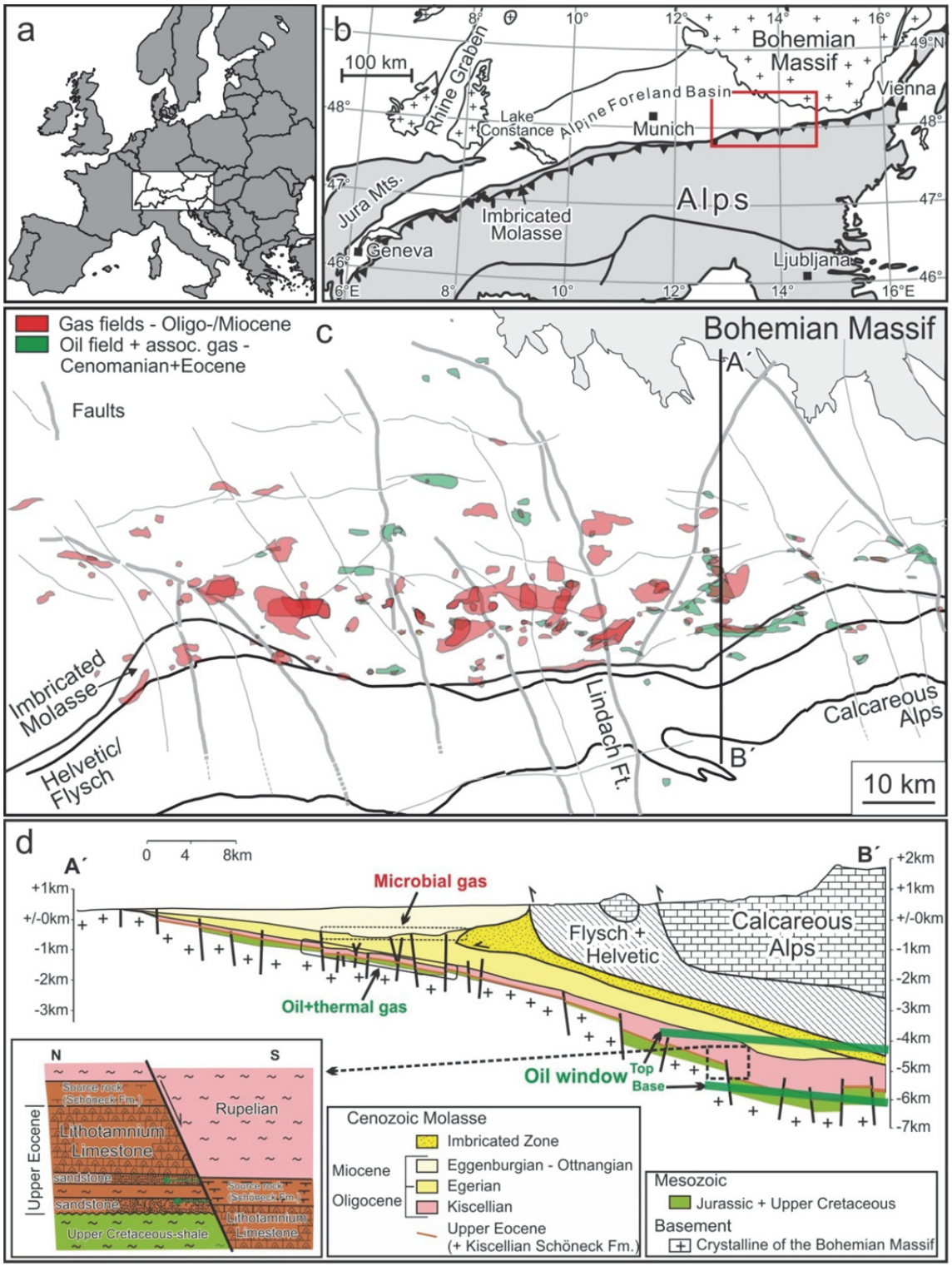

Fig. 1. (a, b) Location maps of study area, (c) location of oil and gas fields in study area. Cross section A'-B' is presented in Fig. 1d. (d) cross section through the Alpine Foreland Basin (modified after Wagner 1996). Inset in figure "d" explains migration from source rocks into stratigraphically deeper carrier beds across normal faults (Malzer et al., 1993).

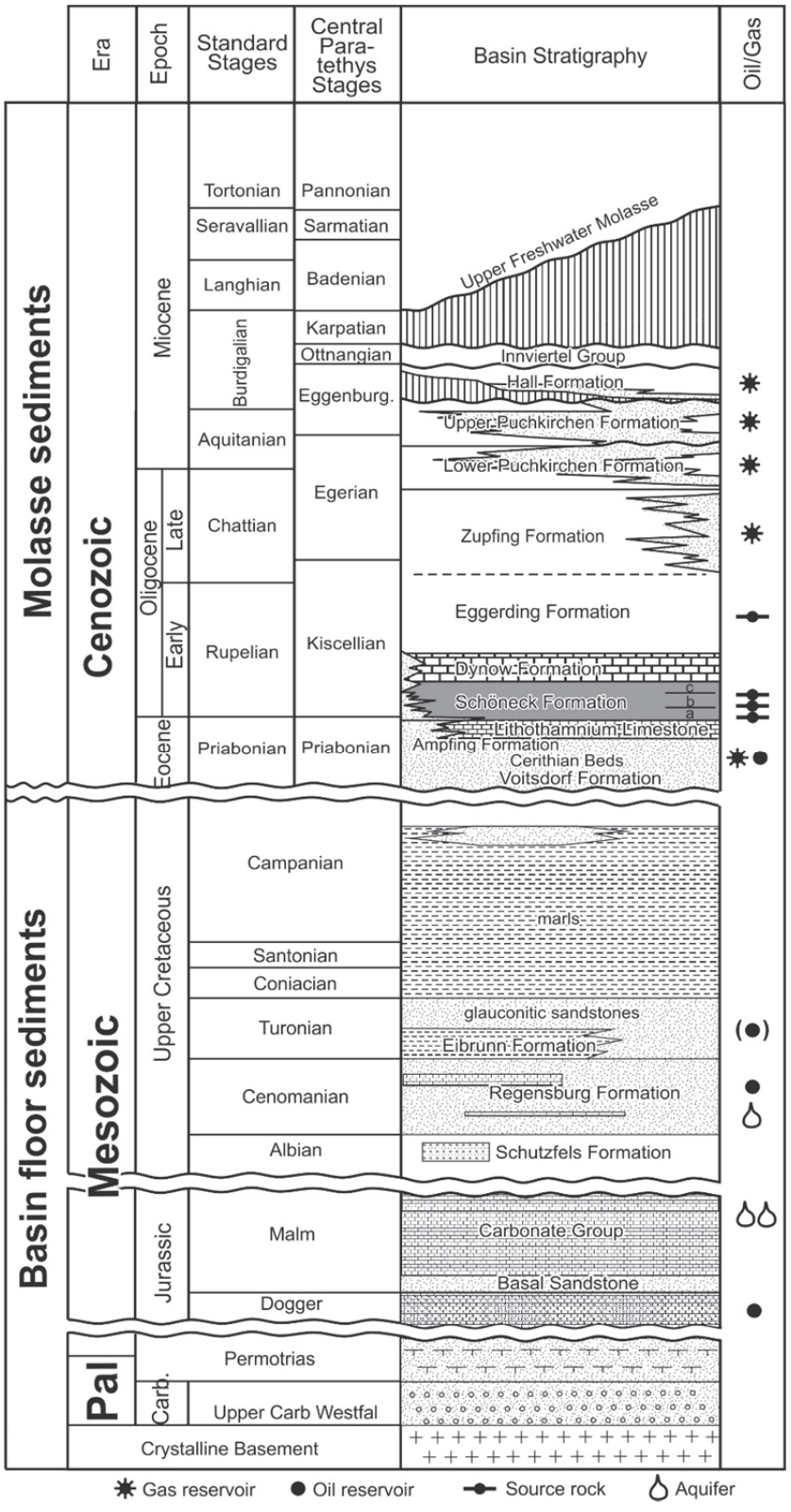

Fig. 2. Stratigraphy of Cenozoic and Mesozoic rocks in the Austrian part of the Alpine Foreland Basin (after Wagner 1996).

2.4. Petroleum systems

Traditionally two petroleum systems are distinguished in the Austrian part of the Alpine Foreland Basin: A thermogenic petroleum system and isotopically light methane interpreted as microbial in origin.

2.4.1. Thermogenic petroleum system

The thermogenic system is based on Lower Oligocene source rocks, which became mature beneath the Alpine nappes in the Miocene time (Gusterhuber et al., 2013, Gusterhuber et al., 2014). In the western part of the study area the Lower Oligocene source rocks are incorporated into molasses imbricates (Sachsenhofer et al., 2010). Main reservoir rocks are Cenomanian and Eocene shallow marine sandstones in front of the Alps indicating long-distance, lateral oil migration (Bechtel et al., 2013).

Source rocks

- **Schöneck Formation**

The Schöneck Formation is about 10 m thick and includes two marly units ("a", "b") and a largely carbonate free black shale unit ("c"; Schulz et al., 2002, Sachsenhofer & Schulz, 2006). Oxygen depleted conditions resulted in high organic matter contents and high hydrogen index (HI; 400-600 mgHC/g TOC) values. TOC contents in the units "a/b" range from 2 to 3 wt.% and exceed 5 wt.% in unit "c". Photic zone anoxia occurred during deposition of unit "c". Brackish surface water conditions were established during deposition of the upper part of unit "c" and continued during deposition of the overlying Dynow Formation, which is characterized by light-colored coccolith limestones and marls (Schulz et al., 2004). Dilution by carbonate resulted in reduced TOC contents between 0.5 and 3.0 wt.%, but HI values remained high (500-600 mgHC/g TOC).

- **Eggerding Formation**

Marine ingressions into the Paratethys resulted in increased salinity and deposition of marly shales of the Eggerding Formation (Schulz et al., 2004, Sachsenhofer et al., 2010), about 45 m thick. The lower part of the formation is rich in organic matter (TOC 1.9-6.0 wt.%; HI up to 600 mg HC/g TOC), whereas the average TOC in its upper part is only 1.5 wt.%.

Slope instabilities during deposition of the Eggerding Formation resulted in submarine mass movements. Locally, Lower Oligocene rocks, up to 70 m thick, were removed from the northern slope and re-deposited along the lower basin slope (Sachsenhofer et al., 2010). The re-deposited rocks, present beneath the Alpine nappes, predominate west of the Lindach Fault ("Oberhofen facies", Schulz et al., 2002; see Fig. 1c for position of the Lindach Fault).

Reservoir rocks

The most important reservoir rocks for oil and associated gas are Upper Eocene basal sandstones and carbonates. The sequence, up to 30 m thick, comprises shallow marine sandstones onlapping northwards onto coastal to fluvial deposits. Within the Eocene succession the coastal sandstones show the best reservoir quality with average porosities of 15 to 25 % and permeabilities ranging from several to 2000 mD (Wagner, 1980). The lower part of the overlying "Lithothamnium Limestone" contains less oil bearing sandstones. Secondary reservoirs occur in Cenomanian sandstones, up to 60 m thick, near the base of the Upper Cretaceous succession. Their porosity values can reach 17 % while permeabilities range from 10 to 400 mD (Malzer, 1993).

Oil families

Gratzer et al. (2011) recognized two oil families (Fig. 5). The western family includes (type "A") oil, which contains slightly more sulphur than type "B" oil from the eastern family. Moreover, dibenzothiophene/phenanthrene (DBT/Ph) ratios of type "B" oils are reduced indicating limited availability of reduced sulphur for incorporation into organic matter (Hughes et al., 1995) and Ts/Tm (18α-22,29,30-trisnorneohopane/17α-22,29,30-trisnorneohopane) ratios are increased. The saturated fraction of the western oil family is isotopically enriched in ^{13}C compared to the eastern family. These differences reflect differences in the source rock facies beneath the Alpine nappes. Areas with different oils facies are separated by a roughly N-S trending zone along the Lindach Fault. It is evident that type "B" oils have been generated from the "normal" Lower Oligocene source rock facies. The negative $\delta^{13}C$ values and the low DBT/Ph ratios suggest that a large proportion of the oils has been generated from unit "c". In contrast, type "A" oils have been generated from redeposited Oligocene rocks ("Oberhofen facies"), which prevail west of the Lindach Fault and which have a reduced hydrocarbon potential (Sachsenhofer & Schulz, 2006). Alternatively, type "A" oils may have received a charge of hydrocarbons generated from units "a/b" of the Schöneck Formation, which

generated oil with a relative high amount of sulphur-bearing compounds (Gratzer et al., 2011). DBT/Ph ratios and $\delta^{13}C$ values of *n*-alkanes are, therefore, clear facies-related parameters. Gratzer et al. (2011) emphasized that Ts/Tm ratios in the Alpine Foreland Basin are also mainly influenced by changes in depositional environment of source rocks. This is further supported by the fact that Ts/Tm ratios in the "Oberhofen Facies" shows a clear upward increasing trend from 1 to 4 within a depth interval, less than 40 m thick.

Oil in the AE* field and oil stains within molasses imbricates (Obhf-1) belong to the type "B" group and are the only exceptions from the geographical west-east separation (Fig. 5). These hydrocarbons probably have been generated from non-redeposited ("normal") source rock facies within the molasses imbricates (Gusterhuber et al., 2013).

Heavily biodegraded oils with low API gravity values occur along the northern margin of the basin in shallow marine Oligocene sands (Fig. 1c; Gratzer et al., 2011). Reischenbacher & Sachsenhofer (2011) compiled gas data from a high number of samples. They showed that gas samples are typically wet (CH4/(C2H5+C3H6) <50). Higher values are restricted to samples in the northeastern part of the study area. Many of these samples are also characterized by i-C4/n-C4 ratios >1 indicating biodegradation.

Biomarker ratios related to maturity (e.g., MPI-1; Radke & Welte, 1983) suggest that the oils have been generated in the vitrinite reflectance interval between 0.69 and 0.93%Rr (Gratzer et al., 2011). Iso-maturity lines display a general W-E trend (Figs. 10, 12 in Gratzer et al., 2011).

2.4.2. Microbial petroleum system

Isotopically light gas, traditionally interpreted as microbial in origin (e.g. Schoell 1984; Schulz & van Berk 2009), prevails in clastic deep water sediments with a Late Oligocene to Early Miocene age (Puchkirchen Group, Hall Fm.; Covault et al. 2009; Hubbard et al. 2005, 2009; Fig. 2). Source and reservoir rocks are closely related. The bacterial gas was generated form thermally immature source rocks which contain more than 0.5 % TOC (Schulz & van Berk, 2009). Different facies of the Puchkirchen and Hall channel and delta systems are the gas reservoirs (De Ruig & Hubbard 2006;

Hubbard et al. 2009), including main channel fill, tributary channels and minor overbank lobes. Ponded slope fans occur directly in front of the Alpine nappes or in piggyback basins on the thrust sheet. The top seal for many gas fields in the Puchkirchen channel system is represented by overbank wedges.

2.5. Thermal aquifer

The Alpine Foreland Basin is not only an important hydrocarbon province, but hosts also a major geothermal potential (e.g. Goldbrunner 2015), which is related to an active aquifer in Upper Jurassic carbonates ("Malmian aquifer" sensu Goldbrunner, 2012). The general characteristics of the aquifer system, like charge and discharge area, residence time etc. are reasonably well understood (e.g. Andrews et al., 1987; Figs. 3, 4).

The Upper Jurassic Carbonate Group (Fig. 2), comprising limestones and dolostones, is up to 500 m thick (Fig. 3). These fractured and karstified carbonates are the most important deep aquifer for thermal water (Goldbrunner 2015). The Malmian water differs hydrochemically from waters in overlying Cretaceous and Tertiary horizons. In the northwestern part of study area, the Malmian connate brines have been replaced by meteoric water with very low total mineralization (average 2.2 g/l; Goldbrunner, 2000). In contrast, high salinity water is found in the southern part of basin indicating stagnant conditions in this area (Andrews et al., 1987, Fig. 3). The Malmian aquifer is charged in areas where carbonates are denuded prior to Tertiary deposition and where water can flow through permeable Cenozoic sediments or basement rocks (Fig. 4). Upper Jurassic sediments are absent in the northern and eastern part of the study area (discharge area) due to erosion. Therefore, in this area shallow marine Oligocene sandstones and locally fractured crystalline basement rocks provide an active aquifer for low salinity waters (Goldbrunner, 1984; Bayrisches Landesamt für Wasserwirtschaft, 1999).

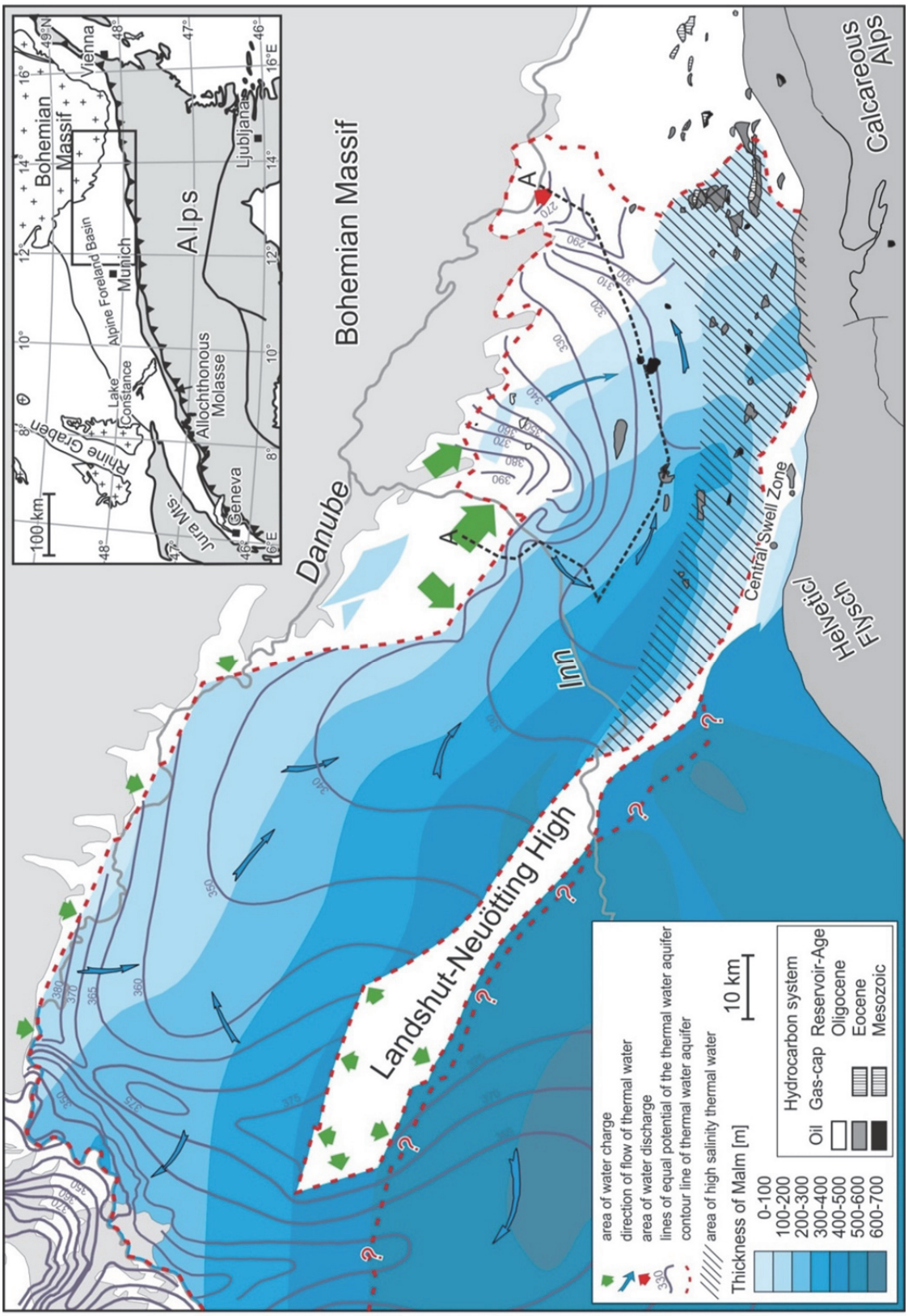

Fig. 3. Thickness map of Malmian horizon. Simplified thermal water system, regional water flow (modified after Bayrisches Landesamt für Wasserwirtschaft, 1999) and location of oil fields are indicated. Inset presents location of map. Faults have been ommited to simplify the map. The A-A` cross section is presented in Fig. 4.

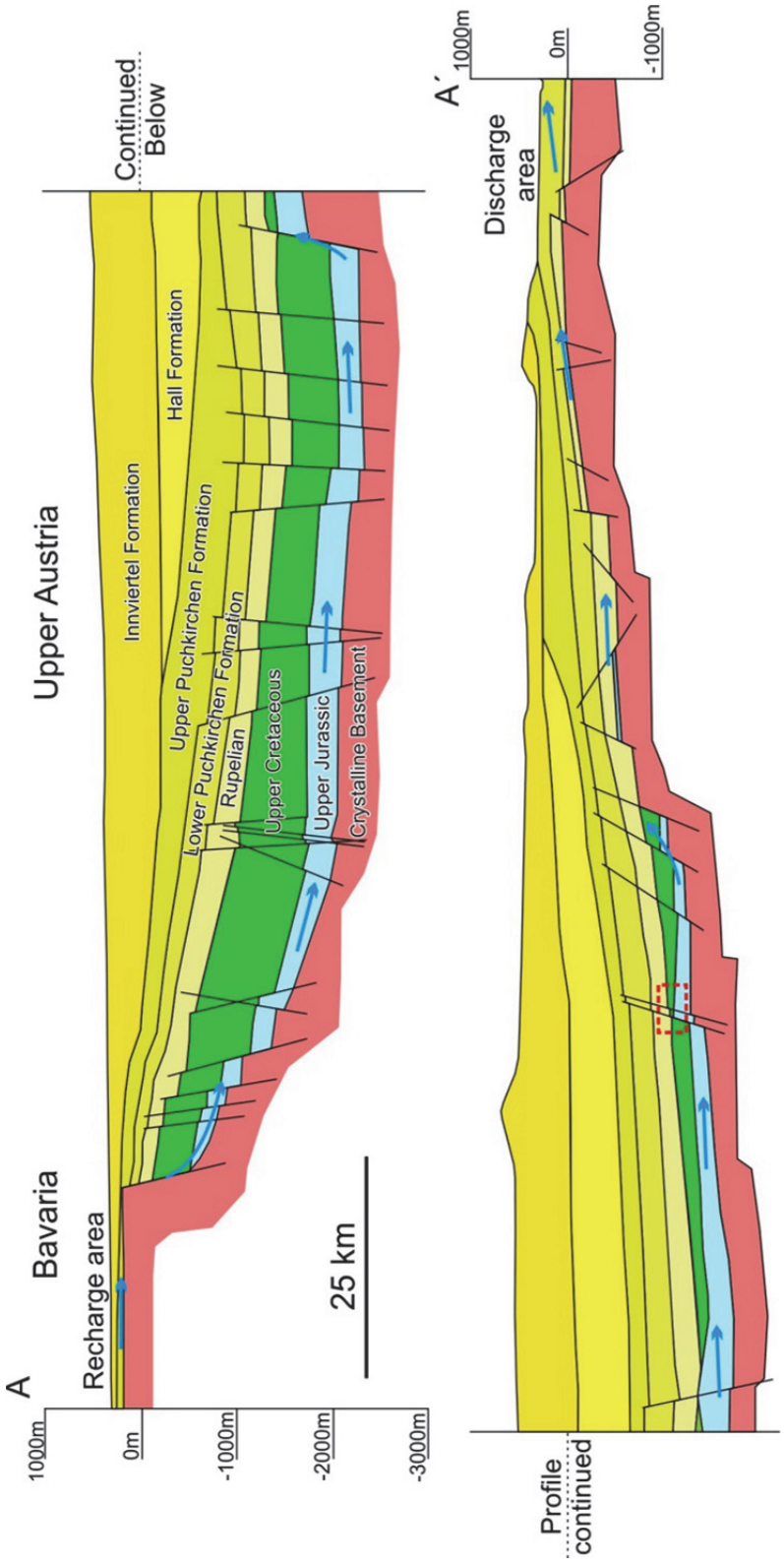

Fig. 4. Reginal cross-section from the recharge area in Lower Bavaria to the discharge area west of Linz (Upper Austria). Position of cross-section is indicated in Fig. 3 by a dashed line. Area marked by red rectange is presented in Fig. 62.

3. Aims of this thesis

Since the pioneering work of Schoell (1977, 1984) on carbon and hydrogen isotope ratios it is known that both, oil-associated thermogenic gas and microbial methane exist in the Alpine Foreland Basin (Fig. 1a,b). According to traditional concepts, thermogenic hydrocarbons are found in Mesozoic and Eocene reservoirs, whereas microbial gas prevails in Oligocene-Miocene reservoirs separated effectively from the underlying thermogenic petroleum system by several hundred meters of shales (e.g. Brix & Schultz 1993, Fig. 2). However, recently Reischenbacher & Sachsenhofer (2011) emphasized that molecular and isotopic gas data from the Austrian part of the Alpine Foreland Basin are in conflict with this simple model. Therefore, the main aim of the present thesis is to determine the origin of gaseous hydrocarbons in Mesozoic, Eocene and Oligocene-Miocene reservoirs including possible mixing and alteration processes.

The second aim of the study is to reveal the origin of condensates co-produced with methane from Oligocene/Miocene reservoirs. This includes the determination of the source rock of the condensates, its thermal maturity and possible migration mechanisms.

Apart from hydrocarbons, the Alpine Foreland Basin hosts also a major geothermal potential, related to the active "Malmian aquifer" (Goldbrunner, 2012). In hydrogeological models the Malmian aquifer is typically considered as separated from aquifers in overlying stratigraphic units (Bayrisches Landesamt für Wasserwirtschaft, 1999). However, Andrews et al. (1987), Goldbrunner (2000) and Gross et al. (2015) suggested hydraulic connections between the Malmian aquifer and oil-bearing rocks. Recently, Gruner et al. (2017) detected metabolites in reservoir water, which are products of ongoing oil biodegradation. Hence, a third aim of this study is to reveal the possible effect of waters from the active Malmian aquifer on the composition of oil in Cretaceous and Eocene reservoirs.

4. Methods

4.1. Sampling procedure

4.1.1. Gases

Two different types of gas samples have been taken within the frame of the study: (I) gas dissolved in oil and (II) free gas.

(I) Gases dissolved in oil were sampled (n=48) from actively producing Cenomanian and Eocene reservoirs (Fig. 5). Samples were taken directly from the wellhead or production pipe. For this, the wells were connected with a glass bottle, initially filled with NaCl-saturated water. During sampling, the brine was displaced by the same volume of reservoir fluids.

(II) Gas samples from (n=87) fields producing free gas form Oligocene/Miocene reservoirs (Fig. 6) have been taken using the IsoTube® gas sampling system. The aluminum-made sampling cylinders were attached directly to the wellheads via the pressure reduction unit and purged with produced gas several times to avoid air contamination. Finally the IsoTubes were filled to the maximum allowed pressure of 8 bar.

4.1.2. Fluids

38 oil and 15 water samples were collected from producing wells. Special precautions were taken during sampling and laboratory handling to avoid any possible losses of volatile hydrocarbons. Glass bottles were filled with reservoir fluids (oil and water), immediately crimped and stored at 4°C. In the lab water and oil were separated and stored in crimped bottles at 4°C for further investigations. In addition, oil and water samples stored at the Chair of Petroleum Geology, Montanuniversitaet Leoben, were also investigated.

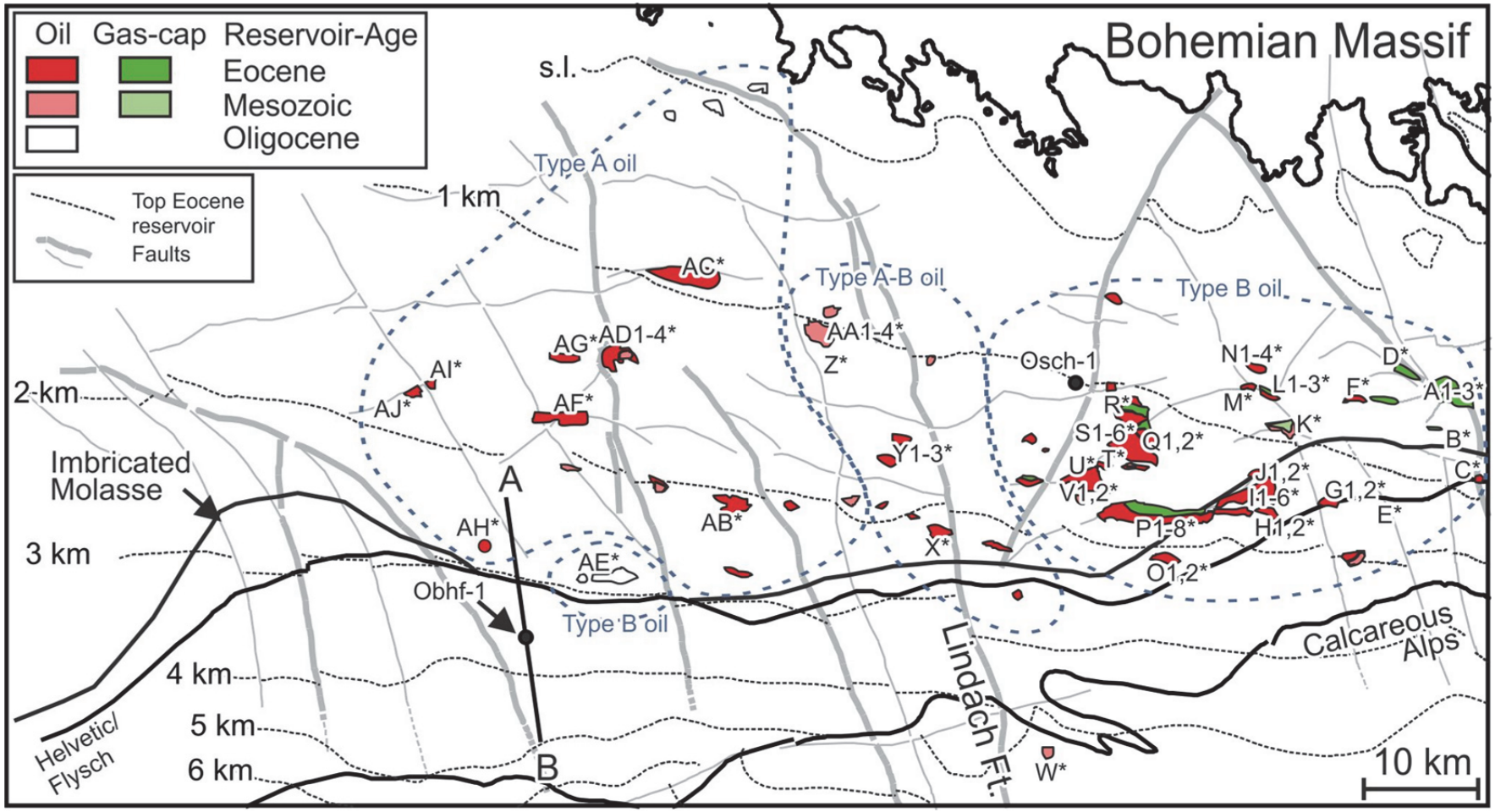

Fig. 5. Location of oil and associated gas fields in Mesozoic, Eocene and Oligocene reservoirs. Numbers indicate the location of wells sampled in the frame of this thesis. Wells are listed in Tab.1. The cross section A-B is presented in Fig. 60.

Tab. 1. List of wells producing from Eocene/Cenomanian reservoirs. For well location see Fig. 5

Well	Type of sample	Measurements
A1*	OA	Gas data archive
A2*	OA	Gas data archive
A3*	OA	
B*		Gas data archive
C*		Gas data archive
D*	OA	GC-MS/MS
E*	O	GC-MS/MS, GC-FID
F*	OA	GC-MS/MS, GC-FID
G1*	OA	GC-FID
G2*	O, G	GC-gas, IRMS, GC-MS/MS, GC-FID
H1*	O, G	GC-gas, IRMS, GC-FID
H2*	O, G	GC-gas, IRMS, GC-MS/MS, GC-FID
I1*	OA, G	GC-gas, IRMS, GC-FID
I2*	G	GC-gas, IRMS
I3*	G	GC-gas, IRMS
I4*	G	GC-gas, IRMS
I5*	G	GC-gas, IRMS
I6*	OA, G	GC-gas, IRMS, GC-MS/MS, GC-FID
J1*	G	GC-gas, IRMS
J2*	OA, G	GC-gas, IRMS, GC-FID
K*		Gas data archive
L1*	OA	GC-FID
L2*	OA	GC-FID
L3*	OA	GC-FID
M*	O, W, G	GC-gas, IRMS, GC-FID
N1*	OA	GC-FID
N2*	O, W, G	GC-gas, IRMS, GC-MS/MS, GC-FID
N3*	OA	GC-FID
N4*	O, W, G	GC-gas, IRMS, GC-FID
O1*	O, W, G	GC-gas, IRMS, GC-FID
O2*	O, G	GC-gas, IRMS, GC-MS/MS, GC-FID
P1*	O, G	GC-gas, IRMS, GC-FID
P2*	O, G	GC-gas, IRMS, GC-FID
P3*	WA	
P4*	WA	
P5*	O, G	GC-gas, IRMS, GC-FID
P6*	O, G	GC-gas, IRMS, GC-MS/MS, GC-FID
P7*	WA	
P8*	G	GC-gas, IRMS
Q1*	G	GC-gas, IRMS
Q2*	O, G	GC-gas, IRMS, GC-MS/MS, GC-FID
R*	O, G	GC-gas, IRMS, GC-MS/MS, GC-FID
S1*	O, G	GC-gas, IRMS, GC-FID
S2*	O, G	GC-gas, IRMS, GC-MS/MS, GC-FID
S3*	O, G	GC-gas, IRMS, GC-FID
S4*	O, W, G	GC-gas, IRMS, GC-FID
S5*	O, G	GC-gas, IRMS,GC-FID
S6*	O, W, G	GC-gas, IRMS, GC-FID
T*	OA	GC-FID
U*	O, G	GC-gas, IRMS, GC-MS/MS, GC-FID
V1*	OA	GC-FID

V2*	O, W, G	GC-gas, IRMS, GC-MS/MS, GC-FID
V3*	O, W, G	GC-gas, IRMS, GC-FID
W*	OA	GC-MS/MS, GC-FID
X*	OA	GC-MS/MS, GC-FID
Y1*	OA	GC-FID
Y2*	O, G	GC-gas, IRMS, GC-FID
Y3*	O, G	GC-gas, IRMS, GC-MS/MS, GC-FID
Z*	OA	GC-MS/MS, GC-FID
AA1*	OA	GC-FID
AA2*	O, W, G	GC-gas, IRMS, GC-FID
AA3*	O, G	GC-gas, IRMS, GC-FID
AA4*	O, W, G	GC-gas, IRMS, GC-MS/MS, GC-FID
AB*	O, G	GC-gas, IRMS, GC-MS/MS, GC-FID
AC*	O, W, G	GC-gas, IRMS, GC-MS/MS, GC-FID
AD1*	O, W, G	GC-gas, IRMS, GC-FID
AD2*	O, W, G	GC-gas, IRMS, GC-MS/MS, GC-FID
AD3*	O, W, G	GC-gas, IRMS, GC-FID
AD4*	OA, G	GC-gas, IRMS, GC-FID
AE*		Gas data archive
AF*	O, W, G	GC-gas, IRMS, GC-MS/MS, GC-FID
AG*	OA	GC-MS/MS, GC-FID
AH*	O, G	GC-gas, IRMS, GC-MS/MS, GC-FID
AI*	O, G	GC-gas, IRMS, GC-MS/MS, GC-FID
AJ*	O, G	GC-gas, IRMS, GC-MS/MS, GC-FID

Sample type: OA - archival oil measured in the frame of this thesis, O - oil sampled and measured in the frame of this thesis, G - gas sampled and measured in the frame of this thesis, W - water sampled and measured in the frame of this thesis, WA – archival water measured in the frame of this thesis,

Measurements: Gas data archive – published and industrial data used for interpretation, GC-gas - molecular composition of gas sample, IRMS – stable carbon and hydrogen isotopic composition of gaseous hydrocarbons and carbon dioxide, GC-FID - molecular composition of oil fraction, GC-MS/MS - composition of diamondoids in oil fraction

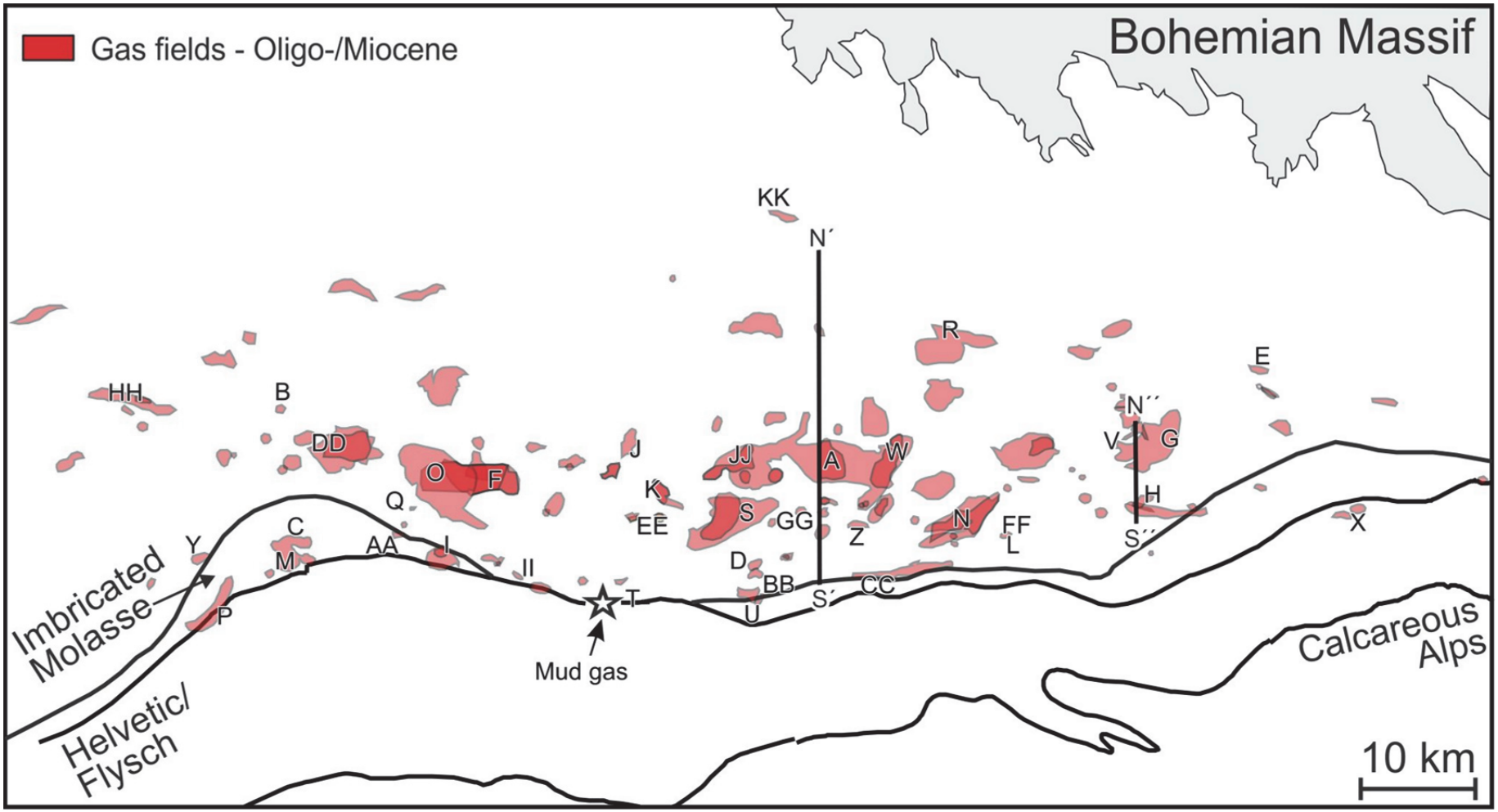

Fig. 6. Location of gas fields producing from Oligocene-Miocene reservoirs. Labels denote currently producing gas fields sampled in the frame of this thesis. Fields and wells are listed in Tab. 2. The cross sections N'-S' and N''-S'' are presented in Fig. 59a, b.

Tab. 2. List of wells producing from Oligocene/Miocene reservoirs. For well location see Fig. 6

Well	Age	Type of sample	Measurements
A1	UPF	G, C	GC-gas, GC-FID, GC-MS, IRMS-gas, IRMS-cond.
A2	HF	G	GC-gas, IRMS-gas
A3	UPF	G	GC-gas, IRMS-gas
A4	UPF	G, C	GC-gas, GC-FID, IRMS-gas
A5	UPF	G	GC-gas, IRMS-gas
A6	UPF	G, C	GC-gas, GC-FID, IRMS-gas, IRMS-cond.
A7	UPF	G, C	GC-gas, GC-FID, GC-MS, GC-MS/MS, IRMS-gas, IRMS-cond.
B1	HF	G, C	GC-gas, GC-FID, GC-MS, GC-MS/MS, IRMS-gas, IRMS-cond.
C1	UPF	G	GC-gas, IRMS-gas
D1	UPF	G, C	GC-gas, GC-FID, GC-MS, GC-MS/MS, IRMS-gas, IRMS-cond.
E1	HF	G	GC-gas, IRMS-gas
F1	UPF	G	GC-gas, IRMS-gas
F2	HF	G	GC-gas, IRMS-gas
F3	UPF	G	GC-gas, IRMS-gas
F4	UPF	G,C	GC-gas, GC-MS, IRMS-gas
F5	HF	G,C	GC-gas, GC-FID, IRMS-gas
F6	HF	G	GC-gas, IRMS-gas
G1	HF	G	GC-gas, IRMS-gas
H1	HF	G	GC-gas, IRMS-gas
I1	HF	G	GC-gas, IRMS-gas
I2	UPF	G	GC-gas, IRMS-gas
I3	UPF	G	GC-gas, IRMS-gas
J1	UPF	G, C	GC-gas, GC-FID, GC-MS/MS, IRMS-gas, IRMS-cond.
K1	UPF	G	GC-gas, IRMS-gas
L1	HF	G	GC-gas, IRMS-gas
M1	UPF	G	GC-gas, IRMS-gas
M2	UPF	G	GC-gas, IRMS-gas
M3	UPF	G, C	GC-gas, IRMS-gas, IRMS-cond.
M4	UPF	G, C	GC-gas, GC-FID, IRMS-gas
M5	UPF	G, C	GC-gas, GC-FID, IRMS-gas, IRMS-cond.
M-6	UPF	G	GC-gas, IRMS-gas
N1	HF	G	GC-gas, IRMS-gas
N2	HF	G	GC-gas, IRMS-gas
N3	HF	G	GC-gas, IRMS-gas
O1	HF	G	GC-gas, IRMS-gas
O2	HF	G	GC-gas, IRMS-gas
O3	HF	G	GC-gas, IRMS-gas
O4	HF	G, C	GC-gas, IRMS-gas, IRMS-cond.
O5	HF	G,C	GC-gas, GC-FID, IRMS-gas
O6	HF	G,C	GC-gas, GC-FID, IRMS-gas
O7	HF	G	GC-gas, IRMS-gas
P1	UPF	G	GC-gas, IRMS-gas
P2	UPF	G,C	GC-gas, GC-FID, IRMS-gas
Q1	UPF	G	GC-gas, IRMS-gas
R1	HF	G	GC-gas, IRMS-gas
R2	HF	G	GC-gas, IRMS-gas
R3	HF	G	GC-gas, IRMS-gas
R4	HF	G	GC-gas, IRMS-gas
R5	HF	G	GC-gas, IRMS-gas

S1	HF	G	GC-gas, IRMS-gas
S2	UPF	G,C	GC-gas, GC-FID, IRMS-gas
S3	UPF	G	GC-gas, IRMS-gas
S4	HF	G	GC-gas, IRMS-gas
T1	UPF	G, C	GC-gas, GC-FID, GC-MS, GC-MS/MS, IRMS-gas, IRMS-cond.
U1	UPF	G	GC-gas, IRMS-gas
U2	UPF	G	GC-gas, IRMS-gas
U3	UPF	G, C	GC-gas, IRMS-gas, IRMS-cond.
V1	HF	G	GC-gas, IRMS-gas
V2	HF	G	GC-gas, IRMS-gas
W1	HF	G, C	GC-gas, GC-FID, GC-MS, IRMS-gas
W2	HF	G	GC-gas, IRMS-gas
W3	UPF	G, C	GC-gas, GC-FID, GC-MS, IRMS-gas, IRMS-cond.
W4	UPF	G	GC-gas, IRMS-gas
X1	Imbr	G	GC-gas, IRMS-gas
X2	Imbr	G, C	GC-gas, GC-FID, GC-MS/MS, IRMS-gas, IRMS-cond.
X3	Imbr	G	GC-gas, IRMS-gas
X4	Imbr	G	GC-gas, IRMS-gas
Y1	LPF	G, C	GC-gas, GC-FID, GC-MS, GC-MS/MS, IRMS-gas, IRMS-cond.
Z1	HF	G	GC-gas, IRMS-gas
AA1	HF	G	GC-gas, IRMS-gas
BB1	HF	G	GC-gas, IRMS-gas
CC1	HF	G	GC-gas, IRMS-gas
DD1	LPF	G, C	GC-gas, GC-FID, GC-MS, IRMS-gas, IRMS-cond.
DD2	UPF	G	GC-gas, IRMS-gas
EE1	HF	G	GC-gas, IRMS-gas
FF1	UPF	G, C	GC-gas, GC-FID, GC-MS/MS, IRMS-gas, IRMS-cond.
GG1	HF	G	GC-gas, IRMS-gas
GG2	HF	G	GC-gas, IRMS-gas
HH1	UPF	G	GC-gas, IRMS-gas
II1	HF	G	GC-gas, IRMS-gas
II2	HF	G, C	GC-gas, GC-MS, IRMS-gas
JJ1	UPF	G, C	GC-gas, GC-FID, IRMS-gas
JJ2	UPF	G, C	GC-gas, GC-FID, GC-MS, GC-MS/MS, IRMS-gas, IRMS-cond.
JJ3	UPF	G, C	GC-gas, GC-FID, GC-MS, IRMS-gas
JJ4	UPF	G	GC-gas, IRMS-gas
KK1	UPF	G	GC-gas, IRMS-gas
KK-2	UPF	G	GC-gas, IRMS-gas
A2,3*[a]	Eo	CA	GC-FID, GC-MS, GC-MS/MS, IRMS-cond.
A1*[a]	Eo	CA	GC-FID, GC-MS, GC-MS/MS, IRMS-cond.

[a] well producing condensate from Eocene reservoirs, used for comparison,
Sample type: G - gas sampled and measured in the frame of this thesis, C – condensate sampled and measured in the frame of this, CA – archival condensate sample measured in the frame of this thesis
Age: HF - Hall Formation, UPF - Upper Puchkirchen Formation, LPF - Lower Puchkirchen Formation
Measurements: GC-gas - molecular composition of gas sample, GC-FID - molecular composition of condensate fraction, GC-MS – biomarkers and specific compounds in condensate fraction, GC-MS/MS - composition of diamondoids in condensate fraction, IRMS-gas - stable carbon and hydrogen isotopic composition of gaseous hydrocarbons and carbon dioxide, IRMS-cond. - stable carbon isotopic composition of condensate.

4.2. Analysis of chemical composition

4.2.1. Gas molecular composition

Molecular compositions were determined with a gas chromatograph equipped with three different columns and detectors. Hydrocarbons were resolved on a 30 m Rtx-Alumina capillary column (i.d. 0.53 mm; filling Na_2SO_4, 10 μm film thickness) and detected by FID. Permanent gases were resolved on two packed columns: HayeSep Q (2 m x 1/8" OD) and MolSieve 5A (2 m x 1/8" OD) and detected by TCD. Sulfur compounds were determined using Rtx-Sulfur packed column (2 m x 1/8" OD) and FPD detector. All columns were mounted in one oven programmed to hold at 50°C for 4.3 minutes and then increase to 165°C at 10°C/min, at which point it was held for 0.5 minutes. Helium was used as carrier gas for all three channels. Peak identification has been performed based on comparison of retention times of calibration gas mixture and analyzed sample. Concentration of compounds has been determined by comparison of their peak areas with peak areas of the same components with known concentration. Calibration gases contained mixtures of all compounds observed in the investigated samples.

4.2.2. Oil/condensate molecular composition

4.2.2.1. GC-FID (gas chromatography-flame ionization detector)

In laboratory the oils were separated from water. Thereafter 50 mg of oil were diluted in *n*-pentane and the insoluble fraction (asphaltenes) was separated by centrifuging. The condensate samples were not treated to remove asphaltenes prior to analysis. The pentane-soluble fractions of oils were analyzed on a gas chromatograph equipped with a J&W DB-1 PONA (50 m length, ID 0.2 mm, 0.5 μm film thickness) fused silica capillary column. The sample was injected with split mode at a temperature of 270°C. The GC oven temperature was programmed as followed: 32°C hold for 5 min, then heated 2.5°C/min to 310°C hold for 30 min. Helium was used as carrier gas with constant flow 1.3 ml/min. The flame ionization detector was operated at a temperature of 320°C with 350ml/min and 35 ml/min flows for air and hydrogen, respectively.

4.2.2.2. GC-MS (gas chromatography-mass spectrometry)

Two types of mass spectrometry detectors were use in present study: (I) single quadrupole and (II) triple quadrupole.

(I) Bulk composition analyses of condensates were performed without prior sample preparation. Selected oils were treated to remove asphaltenes: 50 mg of oil were diluted in *n*-pentane and the insoluble fraction was separated by centrifuging. The pentane-soluble fractions and crude condensates were analyzed on a gas chromatograph equipped with a J&W DB-5MS (30 m length, ID 0.25 mm, 0.25 μm film thickness) fused silica capillary column coupled with single-quadrupole mass spectrometer. The sample was injected with split mode at temperature 270°C. The GC oven temperature was programmed as followed: 32°C hold for 5 min, then heated 2°C/min to 100°C hold for 1 min and heated to 300°C hold for 15 min. Helium was used as carrier gas with constant flow of 1.2 ml/min. Mass spectrometer was operated in electron impact (EI) mode. Mass transfer line and ion source were hold at temperatures of 270 and 250°C, respectively. Compounds were detected by monitoring mass range from 50 to 650 (amu) and recorded at a scan time 0.5 sec.

Cyclic/branched hydrocarbons fractions were analyzed for steranes/hopanes composition. To do so, a gas chromatograph equipped with a J&W DB-5MS (30 m length, ID 0.25 mm, 0.25 mm film thickness) fused silica capillary column coupled with single quadrupole mass spectrometer operating in Single Ion Mode (SIM). Steranes were detected by selected ions (m/z): 149, 177, 191, 205, 370, 398, 412, 426, 440, whereas hopanes (m/z): 217, 218, 231, 259, 372, 386, 400, 414.

(II) Gas chromatography-triple quadrupole mass spectrometry has been applied to determine the composition of diamondoid hydrocarbons. The saturated oil fraction was analyzed using an Agilent 7000 series GC-MS System. The gas chromatograph was equipped with a J&W DB-5MS (60 m length, ID 0.25 mm, 0.25 μm film thickness) fused silica capillary column. Helium was used as carrier gas with a constant flow of 2.2 ml/min. 1 μl of sample was injected on a split-splitless inlet hold at a temperature of 300°C. The GC oven temperature was programmed as followed: initial 40°C heated 4°C/min to 290°C hold for 30 min. The triple quadrupole was operated in EI mode at 70 eV. MSD transfer line

and source were heated to 300°C and 230°C, respectively. Nitrogen was used as collision gas at 1.5 ml/min flow. To reduce any possible effects of instrument variability, all samples were run in a single batch. GC and MS-MS conditions (e.g., collision energy, scan time) were optimized experimentally by multiple repeating of a commercial diamondoid standard. Samples were analyzed in MRM mode (multiple reaction monitoring; parent-daughter mode). The analytical work was performed in the Laboratory of Petroleum Geochemistry, AGH University of Science and Technology, Krakow in co-operation Dr Adam Kowalski.

4.2.3. Chemical composition of water

Fresh and archive samples (19 in total) were measured by ion chromatography. The samples were filtered through a 0.2 μm nylon filter prior to analysis. The final filtrate was diluted and analyzed for cations and anions using two different sets of ion chromatography equipment. Anions were determined on a Dionex DX-3000 system with an external suppression. For standard runs, a 25 μl sample loop was used. All analyzed values were well above the detection limits. Cations were analyzed using a Dionex DX-120 system with electrochemical micro-membrane suppression and a 25 μl sample loop. The analytical work was performed at Chair of Geology and Economic Geology, Montanuniversitaet Leoben by Prof. Walter Prochaska.

4.3. Isotopic composition

4.3.1. Stable carbon and hydrogen isotopic composition of gaseous hydrocarbons and carbon dioxide

Stable C and H isotope measurements were carried out using a Trace GC-ultra gas chromatograph attached to the ThermoFisher Delta-V isotope ratio mass spectrometer (IRMS) via a combustion and high temperature reduction interface, respectively (GC Isolink, ThermoFisher). The GC coupled to the IRMS was equipped with a 25 m PoraPlot capillary column (i.d. 0.32 mm; 0.10 μm film thickness). The oven temperature was programmed from 30–180°C at a rate of 5°C/min followed by an isothermal period of 5 min. Helium was used as carrier gas. For calibration, a CO_2 or H_2

in-house standard gas was injected at the beginning and at the end of each analysis. Analytical reproducibility was controlled by repeated measurements of in-house calibration gas composed of C_1-C_6 hydrocarbons and CO_2 with known isotopic composition. $^{2}H/^{1}H$ and $^{13}C/^{12}C$ relative ratios are expressed relative to V-SMOW and V-PDB, respectively.

4.3.2. Stable carbon and hydrogen isotopic composition of oil/condensate samples

Selected samples were separated for saturated hydrocarbons, polar compounds and aromatic hydrocarbons by MPLC (Radke et al., 1980). Then, *n*-alkanes were separated from cyclic/branched hydrocarbons by an improved 5Å molecular sieve method (Grice et al., 2008). The separated fraction was analyzed for stable carbon isotopic composition of individual *n*-alkanes and acyclic isoprenoids (GC-IRMS). Stable C isotope measurements were performed using a Trace GC-Ultra gas chromatograph equipped with a J&W DB-5MS (30 m length, ID 0.25 mm, 0.25 mm film thickness) fused silica capillary column coupled with a ThermoFisher Delta-V isotope ratio mass spectrometer via combustion and reduction interface (GC Isolink, ThermoFisher). The oven temperature was programmed as follows: 70-300°C at a rate of 4°C/min followed by an isothermal period of 15 min. Helium was used as carrier gas. For calibration, a CO_2 standard gas was injected at the beginning and at the end of each analysis. Isotopic compositions are reported in the δ notation relative to the V-PDB standard.

4.3.3. Stable oxygen and hydrogen isotopic composition of waters

The oxygen isotopic composition ($\delta^{18}O$) of the water samples was measured by the classic CO_2–H_2O equilibrium technique (Epstein & Mayeda, 1953) with a fully automated device adapted from Horita et al. (1989) coupled to a Finnigan DELTAplus mass spectrometer. Measurement reproducibility of duplicates was better than ±0.05‰ for $\delta^{18}O$. Deuterium ($\delta^{2}H$) was measured with a Finnigan DELTAplus XP continuous flow stable isotope ratio mass spectrometer by chromium reduction using a ceramic reactor slightly modified from Morrison et al. (2001). The analytical precision of the $\delta^{2}H$ measurements was better than 1.5‰. Stable hydrogen and oxygen isotopes of water

are expresses against V-SMOW. The analytical work was performed in the laboratory of JR-AquaConSol GmbH (Graz) by Dr Albrecht Leis.

5. Generation, mixing and alteration of thermogenic and microbial gas in oil deposits

Analytical data from 48 samples studied within the frame of the present thesis are presented in this section together with data from six wells representing fields, which were abandoned before 2012 (Tabs. 1, 3). The latter data are from Schoell (1984) and industry sources. Molecular composition of gas from 75 wells compiled by Reischenbacher & Sachsenhofer (2011; their Fig. 3) are used in Fig. 7a.

5.1. Molecular composition

The studied gas samples are dominated by methane with varying concentrations of C_{2+} hydrocarbons, nitrogen and carbon dioxide. In some samples traces of hydrogen sulfide (wells: V2*, AA2*, AD1*, AD3*) and carbon monoxide (wells: AH* and AA4*) have been detected. The C_{6+} fraction (Tab. 4) consists of *n*-hexane and undefined or unresolved hydrocarbons. Methane content ranges from 32.1-97.6%.

Gas dryness, defined by the $C_1/(C_2+C_3)$ ratio (Bernard et al., 1978), of samples taken within the frame of this study varies between 1 and 35 (Tab. 4) and, thus, all samples can be considered wet. However, drier gases with $C_1/(C_2+C_3)$ ratios between 50 and 425 occur in gas accumulations in the northeastern part of the study area (Reischenbacher & Sachsenhofer, 2011; Fig. 7a).

Concentration ratios of branched versus straight butanes (i-C_4/n-C_4) range between 0.34 and 0.72. Significantly higher ratios (1 – 30) occur in gas fields containing relative dry gas (Fig. 7a). i-C_5/n-C_5 ratios of studied samples range between 0.58 and 1.38 for pentanes (Tab. 4).

Nonhydrocarbon gases are dominated by nitrogen and carbon dioxide (CO_2). Nitrogen concentrations range from 0.2 to 19.3% (Tab.4). The concentration of CO_2 varies from 0.1 to 44.7 % with an average concentration of 2.3 %. Elevated CO_2 concentration in well AC* is caused by CO_2-enhanced oil recovery (EOR), while the reason for high CO_2 concentration in well AD1* remains unclear. Reservoir stimulation techniques have been also applied in the wells AI* and AJ*. Therefore, at least some CO_2 may result from the reaction of carbonate minerals with injected acids. Therefore, CO_2 isotope compositions in samples from these wells, which have to be considered with great caution, are indicated by asterisks in Table 4.

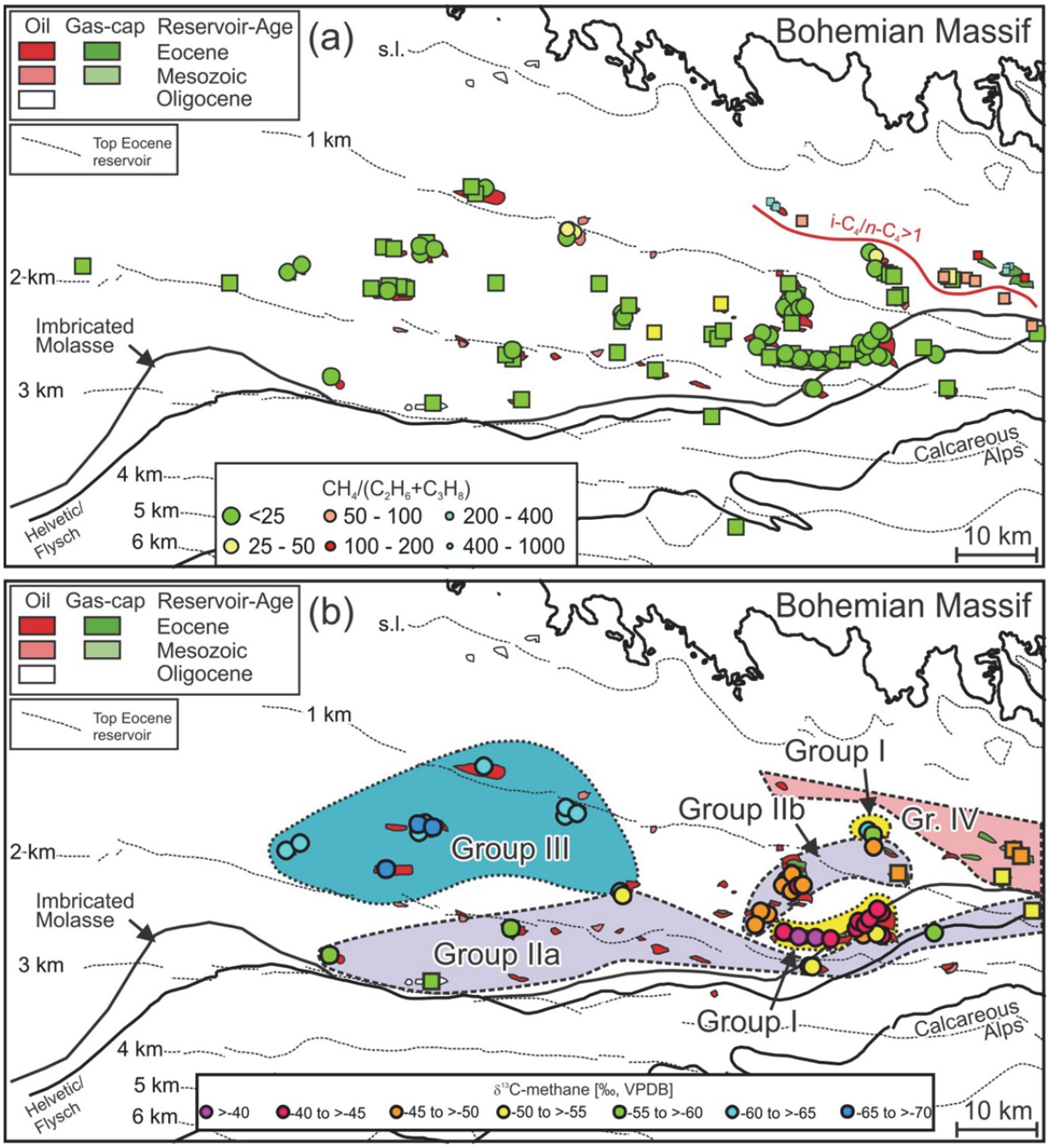

Fig. 7. Spatial distribution of parameters characterizing associated gas in oil deposits in the Austrian part of Alpine Foreland Basin. (a) Dryness: data are from this study (circles) and from Reischenbacher & Sachsenhofer (2011; squares). The boundary delineating gases with *i*-C4/*n*-C4 ratios >1 follows Reischenbacher & Sachsenhofer (2011). (b) Stable carbon isotope ratios of methane: data are summarized in Table 5. Data from this study are marked by circles. Squares mark industrial data and data from Schoell (1984).

5.2. Isotopic composition

The stable carbon and hydrogen isotopic compositions of hydrocarbons scatter widely. Stable carbon isotopic compositions in methane range from -66.0‰ to -38.4‰ (Tab. 5, Fig. 7b). The isotopically heaviest methane is trapped in wells P1* to P8* and I1,2*. According to many authors (see references in introduction section), methane characterized by $\delta^{13}C$ values measured in above wells (about -40‰) can be interpreted as product of thermogenic maturation of organic matter. In contrast, others wells produce methane depleted in ^{13}C. C_2 to C_5 hydrocarbons show a decreasing variability in isotopic values, with the exception of *n*-pentane. Therefore, we do not see clear regional trends. $\delta^{13}C$ values range from -40.1‰ to -28‰, -32.8‰ to -27.7‰, -32.2‰ to -27.4‰, -30.1‰ to -26.2‰, -28.6‰ to -25.4‰, -29.3‰ to -24.9‰, for ethane, propane, *i*-butane, *n*-butane, *i*-pentane, *n*-pentane, respectively (Tab. 5).

Due to relative high concentrations of C_{2+} hydrocarbons, it was possible to report stable hydrogen isotopes up to butanes. $\delta^{2}H$ ratios vary between -161 to -233 for methane, -255 to -151 and -220 to -131 for ethane and propane, respectively.

Carbon isotopes of CO_2 vary significantly between -17.5 ‰ and -1.4 ‰.

Tab. 3. Reservoir data of wells producing oil and associated gas. For location see Fig. 5.

Well	Age	Depth[a]	Res.Temp.[b]	°API[c]	GOR[d]
A1*	Eo	590			
A2*	Eo	670			
A3*	Eo				
B*	Eo				
C*	Eo	1158			
D*				21	
E*	Eo				
F*	Eo			31.8	
G1*	Eo				
G2*	Eo	1378	65	33.1	33
H1*	Eo+Ce	1593		34.8	15
H2*	Ce	1676		33.1	7.5
I1*	Ce	1420	70	36.6	60
I2*	Eo	1623	63	35.4	60
I3*	Eo	1501	74	37.5	110
I4*	Eo	1499		37.5	110
I5*	Eo	1610	75	37.5	110
I6*	Eo	1570		37.5	110
J1*	Eo+Ce	1408	68	34.4	110
J2*	Eo	1399	69		1000
K*	Eo	1233			
L1*	Eo				
L2*	Eo				
L3*	Eo				
M*	Eo	778		36.1	60
N1*	Eo	723			
N2*	Eo	706	55	32.6	13
N3*	Eo				
N4*	Eo	701	48	32.6	13
O1*	Eo	1893	86	32.1	58.2
O2*	Eo	1902	86	32.1	58.2
P1*	Eo	1596	68	35.3	1000
P2*	Eo	1626	80	37.1	126
P3*	Eo				
P4*	Eo				
P5*	Eo	1634	79	35.3	126
P6*	Eo	1651	69	35.8	126
P7*	Eo				
P8*	Eo+Ce	1697	75	27	200
Q1*	Eo	1176	60		
Q2*	Eo	1224	60	37.8	86
R	Eo	1147	58	37.2	97
S1*	Eo	1292	62	36.4	109
S2*	Eo	1354	62	36.4	109
S3*	Eo	1343	62	36.4	109
S4*	Eo	1280	62	36.4	109
S5*	Eo	1290	62	36.4	109
S6*	Eo	1310	62	36.4	109
T*	Eo				
U*	Ce	1777	71	33.2	15
V1*	Eo				

V2*	Eo	1642	69	36.6	102.2
V3*	Eo	1619	69	36.6	102.2
W*	Ce			34.4	
X*	Eo			33.4	
Y1*	Eo				
Y2*	Ce	1916	90	31.7	30
Y3*	Eo	1625	85	31.9	35
Z*	Ce				
AA1*	Ce				
AA2*	Ce	1124	62	30.2	5.1
AA3*	Ce	1092	57	30.2	5.1
AA4*	Ce	1093	57	30.2	5.1
AB*	Eo	2049	87	34.7	22
AC*	Eo	910	63	35.5	24
AD1*	Eo	1304	70	35.5	29.4
AD2*	Eo	1280	73	35.6	29.4
AD3*	Eo	1323	71	35.3	29.4
AD4*	Eo	1330	75	35.5	29.4
AE*	Eo	3218			
AF*	Eo	1646	85	32.8	48
AG*	Eo			33	
AH*	Eo	2650	110	31.4	27.6
AI*	Eo	1543	85	34.5	10
AJ*	Eo	1621	86	33.5	5

[a] reservoir depth, True Vertical Depth Subsea (TVDSS) [m], [b] reservoir temperature [°C], [c] API gravity values (industrial data), [d] gas to oil ratio [Nm3/m3], Eo - Eocene, Ce – Cenomanian

Tab. 4. Molecular compositions [% vol.] of gas from wells producing oil and associated gas. All gas samples listed in this table were sampled and measured in the frame of this study with exception of six samples originating from industrial data or literature (see footnote). For location see Fig. 5.

Well	CH_4	C_2H_6	C_3H_8	*i*-C_4H_{10}	*n*-C_4H_{10}	*i*-C_5H_{12}	*n*-C_5H_{12}	C_6H_{14+}[a]	CO_2	N_2	H_2S	CO	*i*/*n*C4	*i*/*n*C5	C1/(C2+C3)
A1*[c]	97.60	0.17	0.06	0.18	0.00	0.43									424
A2*[c]	97.00	0.19	0.06	0.20	0.00										388
B*[b]	90.30	0.50	0.80	0.30	0.40	0.20	0.10						0.75	2.00	69
C*[b]	90.69	2.20	2.60	0.61	1.23	0.44	0.35	0.40	0.12	1.36			0.50	1.26	19
G2*	49.13	9.73	20.22	5.03	9.10	2.53	1.79	1.15	0.48	0.84			0.55	1.42	2
H1*	67.12	7.73	10.77	2.84	5.80	1.85	1.56	1.09	0.36	0.89			0.49	1.19	4
H2*	60.54	8.58	13.43	3.09	7.21	2.12	1.71	1.21	0.12	1.98			0.43	1.24	3
I1*	67.70	7.38	10.01	2.53	5.98	2.02	1.78	0.45	0.07	2.07			0.42	1.13	4
I2*	75.59	7.42	7.97	1.56	3.54	1.03	0.95	0.27	0.48	1.18			0.44	1.08	5
I3*	78.73	8.67	6.77	1.07	2.35	0.57	0.51	0.13	0.39	0.80			0.45	1.11	5
I4*	80.45	6.11	5.59	1.10	2.70	0.89	0.85	0.25	0.31	1.74			0.41	1.04	7
I5*	81.12	6.51	5.40	1.00	2.35	0.61	0.54	0.10	0.36	2.00			0.43	1.12	7
I6*	71.47	8.28	8.90	1.93	4.78	1.41	1.29	0.28	0.49	1.16			0.40	1.10	4
J1*	85.44	5.17	3.79	0.67	1.54	0.40	0.37	0.10	0.28	2.24			0.44	1.08	10
J2*	89.87	3.59	1.84	0.30	0.69	0.20	0.18	0.04	0.20	3.07			0.44	1.09	17
K*[c]	86.40	4.14	2.36	0.43	1.03								0.42		13
M*	77.02	4.71	5.43	1.91	4.24	1.49	1.26	0.95	0.57	2.41			0.45	1.18	8
N2*	83.44	2.10	0.87	0.59	1.15	1.15	0.99	0.97	0.45	8.29			0.52	1.17	28
N4*	87.87	3.94	1.18	0.58	1.01	0.93	0.78	0.87	1.24	1.60			0.58	1.18	17
O1*	47.42	9.30	20.46	3.76	10.82	2.56	2.14	1.25	1.11	1.17			0.35	1.20	2
O2*	49.28	9.94	20.77	3.59	9.73	2.23	1.87	1.12	0.43	1.04			0.37	1.19	2
P1*	61.07	10.69	11.24	2.17	5.12	1.40	1.26	1.08	0.89	5.06			0.42	1.11	3
P2*	83.57	5.15	4.01	0.72	1.76	0.52	0.50	0.33	0.31	3.14			0.41	1.05	9
P5*	81.04	6.23	5.37	0.66	1.59	0.55	0.52	0.50	0.45	3.10			0.42	1.06	7
P6*	45.09	13.86	21.60	3.84	8.88	2.22	1.92	1.27	0.71	0.60			0.43	1.16	1
P8*	81.66	5.62	5.22	1.06	2.39	0.78	0.75	0.29	0.41	1.81			0.44	1.04	8
Q1*	83.36	5.23	4.74	1.22	2.09	0.68	0.56	0.16	0.39	1.58			0.58	1.22	8
Q2*	47.88	11.67	18.01	5.25	9.35	2.83	2.25	1.57	0.29	0.90			0.56	1.26	2
R*	83.78	4.52	3.90	1.09	1.98	0.75	0.66	0.70	0.30	2.33			0.55	1.14	10
S1*	77.88	9.34	6.68	1.28	2.17	0.58	0.49	0.46	0.78	0.34			0.59	1.19	5
S2*	52.59	9.33	16.26	4.74	9.01	2.59	2.09	1.43	0.72	1.24			0.53	1.24	2
S3*	55.55	9.36	14.86	4.34	7.95	2.28	1.81	1.23	0.36	2.25			0.55	1.26	2

S4*	40.90	13.34	21.09	5.63	10.49	2.81	2.25	1.47	1.48	0.54		0.54	1.25	1
S5*	53.59	10.81	14.51	3.85	7.20	2.08	1.71	1.14	0.74	4.36		0.54	1.22	2
S6*	40.75	11.81	21.00	6.10	11.28	3.05	2.40	1.52	0.56	1.53		0.54	1.27	1
U*	61.78	11.48	11.73	3.38	5.84	1.89	1.53	1.03	0.94	0.38		0.58	1.23	3
V2*	35.65	18.17	28.23	4.16	7.50	1.92	1.56	0.83	1.76	0.19	tr	0.56	1.23	1
V3*	53.67	7.77	13.48	3.46	8.87	2.99	5.19	3.13	0.50	0.93		0.39	0.58	3
Y2*	70.74	8.27	8.17	2.26	3.95	1.15	1.15	0.76	1.33	2.22		0.57	1.01	4
Y3*	88.75	1.99	2.40	1.16	1.70	1.06	0.77	0.87	0.39	0.93		0.68	1.38	20
AA2*	69.87	1.36	0.84	0.30	0.45	0.41	0.39	0.48	6.62	19.29	tr	0.66	1.03	32
AA3*	87.43	1.50	1.00	0.44	0.71	0.65	0.62	0.71	1.89	5.04		0.62	1.05	35
AA4*	79.72	2.18	1.20	0.44	0.61	0.51	0.47	0.56	1.99	12.32	tr	0.72	1.09	24
AB*	71.09	7.21	9.37	1.52	3.11	0.84	0.82	0.67	2.61	2.77		0.49	1.02	4
AC*	64.01	1.26	3.43	1.35	2.76	1.12	1.10	1.16	23.00	0.82		0.49	1.02	14
AD1*	32.14	1.32	2.98	0.79	2.31	1.08	1.27	1.55	44.70	11.86	tr	0.34	0.85	7
AD2*	78.91	3.23	7.06	2.03	3.40	0.92	0.78	0.67	1.42	1.60		0.60	1.17	8
AD3*	72.28	1.62	4.91	2.18	5.43	3.23	3.47	3.82	1.75	1.30	tr	0.40	0.93	11
AD4*	84.42	2.18	4.36	1.26	2.30	0.58	0.47	0.22	1.61	2.58		0.55	1.23	13
AE*[b]	75.95	2.25	2.35	0.70	0.50	0.10	0.20	0.00	0.65	4.43		1.40	0.50	17
AF*	56.37	4.35	13.61	4.58	8.09	2.32	1.86	1.18	3.73	3.92		0.57	1.25	3
AH*	70.05	4.89	11.91	2.56	5.33	1.08	0.79	0.33	1.31	1.75	tr	0.48	1.36	4
AI*	58.47	6.77	16.40	4.27	7.37	1.83	1.43	0.83	2.02	0.61		0.58	1.28	3
AJ*	45.02	10.68	22.74	5.22	9.71	1.69	1.70	0.39	1.79	1.07		0.54	1.00	1

[a] fraction of *n*-hexane and undefined or unresolved isomers, [b] unpublished industrial data, [c] data from Schoell (1984), tr- traces, Ce- Cenomanian, Eo- Eocene

Tab. 5. Stable carbon and hydrogen isotopic composition of gas from wells producing oil and associated gas. All gas samples listed in this table were sampled and measured in the frame of this study with exception of five samples originating from industrial data or literature (see footnote).

Well	$\delta^{13}C$ [V-PDB]								$\delta^{2}H$ [V-SMOW]						
	CH_4	C_2H_6	C_3H_8	*i*-C_4H_{10}	*n*-C_4H_{10}	*i*-C_5H_{12}	*n*-C_5H_{12}	CO_2	CH_4	C_2H_6	C_3H_8	*i*-C_4H_{10}	*n*-C_4H_{10}	*i*-C_5H_{12}	*n*-C_5H_{12}
A1*[f]	-47.8								-218						
A2*[f]	-47.8								-213						
B*[e]	-50.2														
C*[e]	-53	-35.8							-248						
G2*	-59.0	-32.7	-31.2	-30.1	-29.4	-27.4	-28.1	-16.5	-219	-225	-185	-121	-156	-108	-122
H1*	-52.8	-32.0	-29.9	-29.6	-28.5	-27.4	-27.7	-15.5	-193	-186	-163	-110	-145	-104	-121
H2*	-44.8	-34.1	-31.1	-31.0	-29.5	-28.1	-28.5	-13.4	-176	-199	-178	-124	-157	-102	-128
I1*	-43.3	-32.3	-30.1	-30.0	-29.0	-28.0	-25.8	-1.4	-176	-179	-160	-117	-147	-99	-123
I2*	-45.6	-31.0	-29.4	-29.0	-28.2	-27.4	-27.7	-11.8	-175	-167	-138	-80	-127	-86	-107
I3*	-40.0	-31.4	-29.6	-28.9	-27.9	-27.1	-27.9	-10.2	-165	-160	-142	-78	-129	-71	-92
I4*	-41.8	-31.3	-29.7	-28.2	-28.5	-27.5	-28.2	-7.9	-162	-162	-140	-83	-126	-75	-110
I5*	-40.3	-31.3	-29.4	-29.2	-28.2	-27.1	-27.5	-10.7	-162	-156	-147	-69	-122	-54	-90
I6*	-42.3	-31.6	-29.6	-29.2	-28.3	-27.5	-27.2	-10.0	-163	-165	-143	-88	-133	-73	-118
J1*	-41.2	-31.0	-29.2	-28.9	-28.0	-26.9	-26.8	-7.8	-165	-163	-146	-96	-141		-79
J2*	-40.0	-30.5	-28.7	-28.9	-27.5	-26.5	-26.5	-7.6	-161	-151	-131	-94	-125	-95	-69
K*[f]	-46.3								-171						
M*	-46.7	-30.5	-28.8	-29.1	-27.3	-26.2	-25.4	-15.6	-183	-165	-154	-99	-136	-93	-92
N2*	-59.5	-39.2	-32.7	-29.9	-28.6	-27.8	-28.3	-12.5	-222	-208	-168	-96	-120	-102	
N4*	-60.5	-40.1	-32.8	-30.1	-28.8	-27.9	-27.8	-5.8	-233	-217	-182	-110	-124	-112	-111
O1*	-52.9	-35.5	-32.2	-32.2	-30.1	-28.6	-29.3	-17.5	-206	-231	-198	-127	-170	-110	-146
O2*	-53.1	-35.4	-32.2	-31.9	-29.9	-28.5	-29.1	-13.0	-203	-223	-190	-118	-162	-107	-140
P1*	-38.8	-30.8	-29.1	-29.1	-27.3	-26.5	-25.8	-14.9	-167	-175	-154	-100	-134	-82	-109
P2*	-38.4	-30.6	-29.0	-28.7	-27.2	-26.6	-26.4	-17.0	-163	-170	-153	-70	-122	-62	-124
P5*	-40.6	-31.6	-29.9	-29.5	-28.7	-27.6	-28.6	-13.5	-165	-174	-158	-80	-136	-88	-109
P6*	-41.1	-32.2	-30.3	-30.0	-29.0	-27.8	-28.4	-15.6	-165	-181	-160	-110	-143	-84	-112
P8*	-42.1	-30.5	-29.0	-28.7	-27.9	-26.8	-26.8	-7.6	-165	-157	-139	-63	-124	-76	
Q1*	-49.0	-29.2	-28.4	-28.0	-27.3	-26.3	-26.8	-6.8	-174	-155	-143	-89	-119		
Q2*	-48.8	-29.3	-28.3	-28.0	-26.7	-25.7	-25.3	-17.2	-180	-165	-149	-104	-135	-93	-116
R*	-46.2	-29.1	-28.1	-27.9	-26.9	-26.7	-26.3	-10.5	-172	-157	-142	-103	-122	-89	-94
S1*	-44.7	-28.0	-27.7	-27.5	-26.2	-26.2	-24.9	-9.7	-180	-153	-142	-102	-110	-81	-64
S2*	-48.4	-29.2	-28.5	-28.2	-27.0	-26.2	-25.8	-14.3	-178	-153	-139	-89	-116	-66	-101
S3*	-48.6	-29.1	-28.5	-28.2	-27.0	-25.8	-25.4	-11.8	-182	-158	-143	-103	-134	-90	-79
S4*	-46.7	-29.3	-28.2	-27.9	-26.6	-25.9	-24.9	-10.6	-175	-159	-146	-106	-129	-85	-115
S5*	-47.3	-29.1	-28.1	-27.9	-26.7	-25.6	-25.3	-17.3	-175	-163	-147	-98	-131	-92	-112
S6*	-47.8	-29.3	-28.3	-27.9	-26.6	-25.4	-25.0	-15.7	-178	-163	-149	-104	-127	-101	-110
U*	-45.1	-30.2	-28.4	-28.3	-27.7	-27.7	-27.0	-15.0	-179	-163	-145	-110	-135	-80	-111
V2*	-48.0	-30.4	-29.4	-28.8	-28.4	-27.2	-27.7	-13.9	-187	-175	-157	-112	-137	-107	-120
V3*	-47.2	-30.0	-29.3	-28.7	-28.3	-27.2	-27.9	-15.0	-178	-172	-157	-114	-143	-109	-124
Y2*	-50.6	-30.7	-27.9	-28.4	-27.0	-26.0	-27.0	-8.3	-189	-190	-157	-123	-140	-86	-112
Y3*	-62.9	-35.3	-32.5	-29.5	-28.7	-26.9	-28.0	-13.0	-201	-238	-220	-133	-179	-112	-155
AA2*	-62.5	-34.9	-31.2	-28.7	-28.5	-27.1	-28.0	-7.6	-215	-211	-175	-112			
AA3*	-63.8	-36.8	-32.6	-27.4	-28.4	-27.0	-27.9	-9.9	-207	-234	-184	-85	-143		
AA4*	-63.7	-36.1	-31.8	-28.5	-28.5	-26.9	-27.6	-9.0	-211	-222	-179	-91	-125		
AB*	-57.4	-32.5	-29.8	-29.3	-28.4	-27.7	-27.8	-15.3	-208	-223	-162	-104	-139	-97	-131
AC*	-64.6	-34.0	-30.4	-30.3	-28.5	-27.8	-27.9	*	-206	-215	-176	-128	-141	-83	-115
AD1*	-64.7	-32.1	-29.4	-29.4	-28.1	-27.6	-27.8	*-4.3	-202	-162	-144	-99	-130	-101	-111
AD2*	-66.0	-32.7	-29.4	-29.5	-27.7	-27.1	-26.8	-6.8	-202	-216	-166	-107	-129	-85	-108
AD3*	-65.0	-32.5	-29.5	-29.2	-28.0	-27.2	-27.6	-15.1	-195	-208	-162	-129	-141	-113	-126
AD4*	-64.0	-32.8	-29.7	-29.6	-27.9	-27.1	-27.2	-8.4	-206	-218	-163	-115	-130		
AE*[e]	-58.3	-35.1	-30.1					-10.0	-210						
AF*	-65.1	-32.8	-29.4	-29.0	-27.6	-26.9	-26.8	-9.0	-200	-221	-174	-124	-142	-112	-133

AH*	-56.8	-35.3	-31.8	-31.4	-29.1	-28.0	-28.6	-16.0	-215	-255	-209	-119	-178	-102	-128
AI*	-64.9	-32.2	-29.8	-29.6	-27.9	-27.1	-27.3	*-8.4	-207	-220	-166	-128	-144	-105	-120
AJ*	-63.8	-31.7	-29.7	-30.0	-28.0	-27.3	-27.5	*-8.4	-206	-210	-162	-127	-136	-105	-124

[a] unpublished industrial data, [b] data from Schoell (1984), * – uncertain due to EOR.

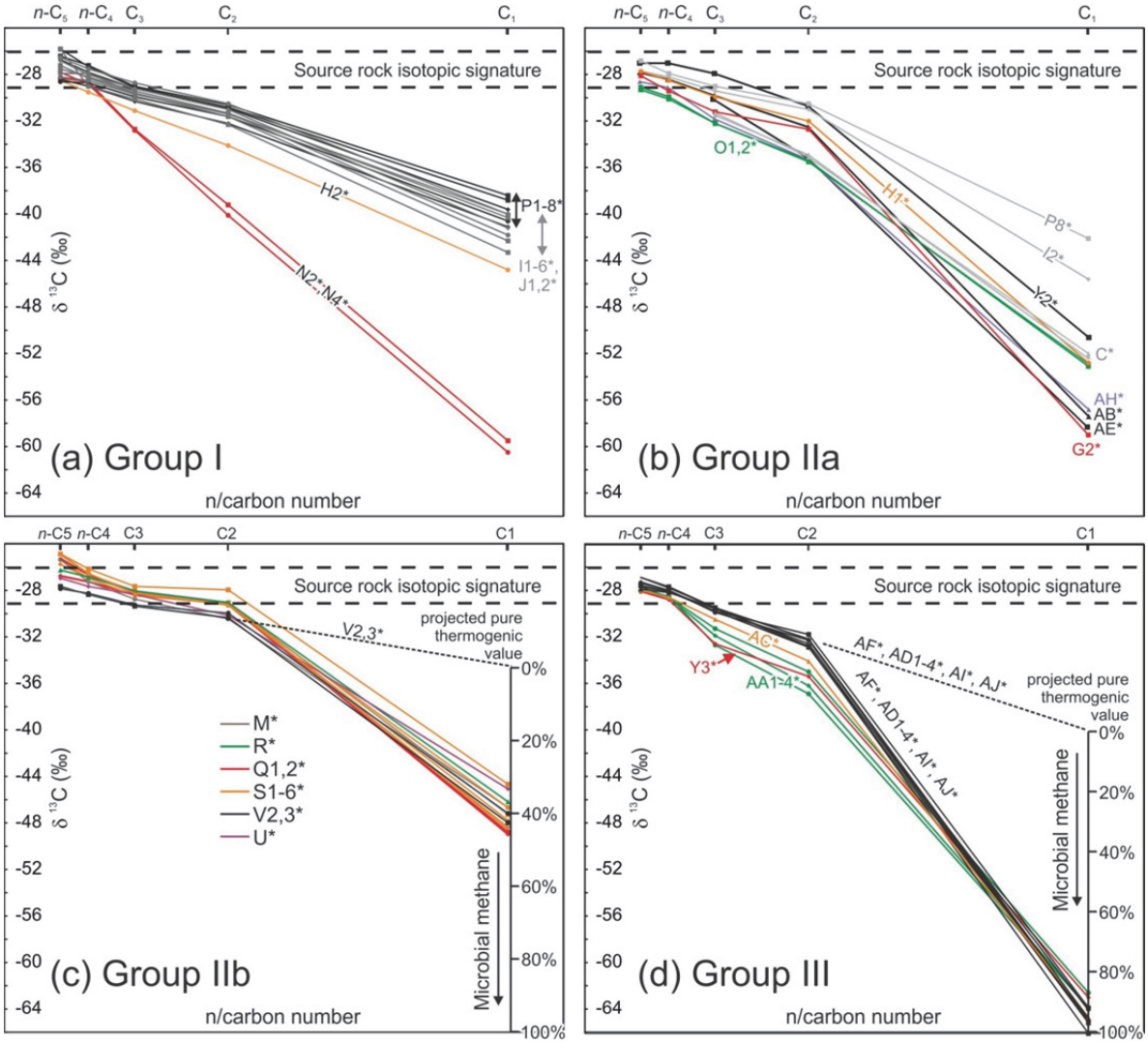

Fig. 8. The natural gas plot (Chung et al., 1988) showing the carbon isotopic compositions of individual hydrocarbons (C_1 to n-C_5) as a function of the carbon number. (a) Group I gases display straight lines characteristic for a thermogenic origin. The slope of the straight lines reflects differences in maturity. (b-d) Groups IIa, IIb, and III gases show addition of varying amounts of isotopically light (microbial) methane. The amount of microbial methane for Group IIb and III gases is estimated using the percentage scale in the right side of Figs. 8c, d (see text for details). The regional distribution of different gas groups is shown in Fig. 7b. Ranges of the carbon isotopic composition of kerogen from the source rock are shown after Schulz et al. (2002).

5.3. Genetic characterization

To define the origin of gas samples, the data have been plotted on different diagrams. In the "Natural Gas Plot" (Chung et al., 1988; Fig. 7), carbon isotopic compositions of individual hydrocarbons are plotted as a function of the carbon number. Samples generated by cracking of source kerogens should plot on a straight line when the carbon number is plotted as its inverse. Changes in isotopic composition of organic matter in the source kerogen and its variable contribution to gas components (Chung et al., 1988 and references therein) can cause deviations from straight lines between *n*-pentane - ethane endpoints. Furthermore, mixing with isotopically light or heavy methane (or C_{2+}) and biodegradation of light hydrocarbons may result in anomalous trend lines.

Stable carbon isotopic composition of methane versus dryness ("Bernard Diagram", Bernard et al., 1978) and stable hydrogen versus carbon isotope ratios of methane (Schoell, 1980; 1983; Whiticar et al., 1986) are plotted in Figs. 9 and 10, respectively.

Based on $\delta^{13}C$ values of C_1 to C_5 hydrocarbons, three different gas groups (I to III) are defined (Fig. 8). Group I gas shows a straight line behavior in the Natural Gas Plot, whereas gas from Groups II and III show a kinked line. Groups II and III are distinguished by $\delta^{13}C_{CH4}$ of >-60‰ and <-60‰, respectively. In addition, based on geographic distribution, Group II is split into subgroups IIa (samples near the Alpine front; Fig. 7b) and IIb (samples north of the wells P1-8*, I1-6* and J1, 2*). Based on dryness (Fig. 9), a fourth Group (IV) containing relative dry gas (>60; Table 4) has been defined.

Group I

Group I comprises most gas samples from the wells P1-8*, I1-6*, J1, 2* and H2*. These samples plot into the field characteristic for thermogenic gas (Fig. 9). In the natural Gas Plot (Chung et al., 1988) C_{1-5} hydrocarbons plot on straight lines (Fig. 8a) indicating genesis from an isotopically homogenous source and similar reaction mechanisms of methane, ethane, propane, *n*-butane, *n*-pentane. Differences in carbon isotope ratios between P1-8*, I1-6*, J1, 2* and H2* wells may be due to subtle differences in the isotopic composition of the parent kerogen or small maturity variations. It is known that subtle vertical $\delta^{13}C_{TOC}$ variations exist in source rocks (lower marly part of the Schöneck Fm.: -26‰; upper shaly part: -29‰; (Schulz et al., 2002). Nevertheless, slightly lower maturity of the well H2* sample compared to the P1-8*, and I1-6*, J1, 2* wells seems more likely (see discussion of example below). Methane trapped in wells P1-8* is isotopically the heaviest of all sampled hydrocarbon pools.

Considering that wells N2* and N4* plot also on straight lines in Fig. 8a, these samples are included in Group I. Methane carbon in the wells N2* and N4* is more negative (about -60‰) than commonly accepted for thermogenic methane (e.g. Bernard et al., 1978; Whiticar et al., 1994; Fig. 9). However, ethane and propane are isotopically light as well. Although ethane and propane can be generated by microbial activity, their contribution is believed to be very low (Hinrichs et al., 2006; Oremland et al., 1988; Rice & Claypool, 1981). Moreover, field observations (Colemann, 2001; Milkov & Dzou, 2007) and mathematical models (Ni et al., 2011; Tang et al., 2000) suggest that isotopically very light methane can be generated during early thermogenic transformations of kerogen. Thus, we prefer the interpretation that gas from wells N2* and N4* was formed at very low maturity. Within this context it is worth mentioning that oil from wells N2* and N4* has lower sterane isomerization ratios (0.4) than any other oil in the study area indicating relative low maturity of saturated hydrocarbons. However, the methylphenanthrene index (Radke and Welte, 1983) suggests that aromatic hydrocarbons were generated at similar maturity levels (~ 0.8%Rr) as other molasse oils (Gratzer et al., 2011).

Group II

The C_{1-5} compounds of Group II samples do not plot on straight lines in the natural gas plot (Fig. 8b, c) indicating that light isotope compositions of methane are due to mixing with different amounts of additional light methane, probably microbial in origin. In addition deviations from straight lines between *n*-pentane - ethane endpoints observed in several samples (e.g. wells G2*; Fig. 8b) indicate isotopic heterogeneities within precursor functional groups (Chung et al., 1988). Despite of the considerable portion of microbial methane, about half of the samples plot into the thermogenic field (Fig. 9). More details about microbial methane are presented in next sections.

$\delta^{13}C$ and $\delta^{2}H$ values of methane in Group II samples show a linear relation (Fig. 10). Interestingly, Group I samples (wells P1-8*, I1-6* and J1, 2*) follow the same trend. In the case of Group I samples the trend may originate from increasing maturity of parent kerogen (Schoell, 1980; 1983). However, in the case of Group II samples, we interpret a similar source for thermogenic and microbial methane.

Group II is split into subgroups IIa and IIb in view of geographical distribution. Group IIa comprises samples from wells located along the southern margin of the foreland basin (Fig. 7b). This group includes two wells (I2* and P8*), from the fields which are located in tectonically separated compartments. Group IIb includes oil wells M*, U*, V2, V3*, Q1*, Q2*, S1-6*, R* located north of the P1-8* and I1-6* and J1, 2* wells (Fig. 5).

Group III

Group III gas occurs in the western part of the study area. The gases are wet and contain a very high amount of microbial methane strongly depleted in ^{13}C (Figs. 8d, 9, 10). Differences exist in the δ^2H-$\delta^{13}C$ relation between methane from Groups III and I/II. This suggests that methane was generated from different sources or by different reaction pathways.

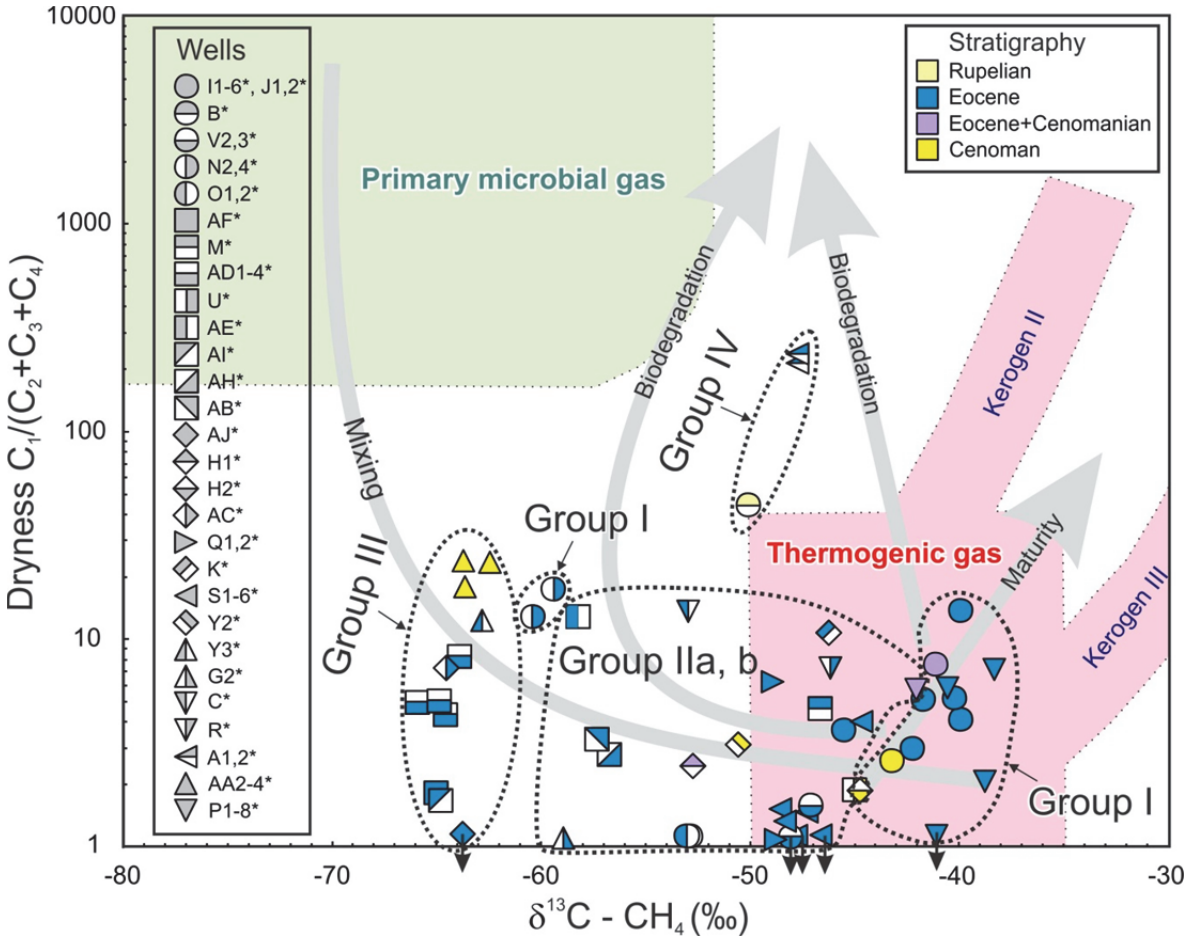

Fig. 9. Genetic characterization of oil associated gas from the Austrian part of the Alpine Foreland Basin using the discrimination plot of Bernard et al. (1978). The effects of different processes on gas composition are indicated by grey arrows and curve (after Milkov, 2011; Jones et al., 2008). Gas groups shown in Figs. 7b, are indicated.

Group IV

Gas from the wells B*, A1* and A2* is drier (>60) than gas from other wells (<35). Moreover, the ^{2}H and ^{13}C signature of samples from the wells A1* and A2* do not follow the trend defined by Group I and II samples (Fig. 10). Therefore, these samples are separated as Group IV. The gas from wells A1* and A2* has a high i-C_4/n-C_4 ratio (Tab. 4). Moreover, it is associated with heavily biodegraded heavy oil (Gratzer et al., 2011), suggesting that methane was formed by anaerobic biodegradation. The gas from wells A1* and A2* shares high i-C_4/n-C_4 ratios and the presence of a biodegraded oil rim with gas from the wells D* and F* (Harm and Wir fields after Gratzer et al., 2011; Reischenbacher & Sachsenhofer, 2011). Although isotopic data are not available, gases from these fields are included in Group IV (Fig. 7b).

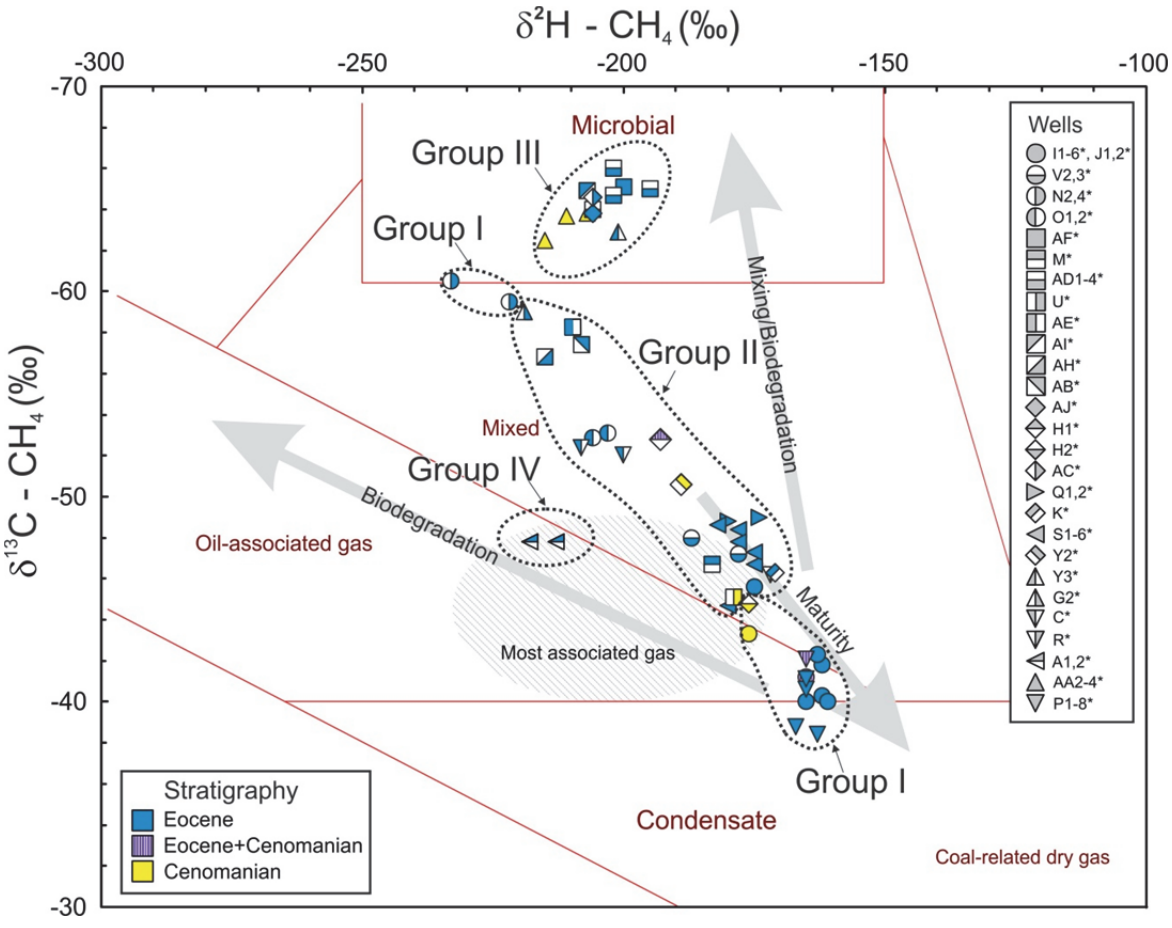

Fig. 10. Genetic characterization of oil associated gas from the Austrian part of the Alpine Foreland Basin using the discrimination plot of Schoell (1980), Whiticar (1986) and Milkov (2011). The effects of different processes on gas composition are indicated by grey arrows (after Milkov, 2011). Gas groups shown in Figs. 7b, 8, 9 are indicated.

5.4. Maturity

Models developed by Berner & Faber (1996) have been applied to estimate the maturity of source rocks during gas generation (Fig. 11). The maturity estimation was done for two isotopically distinct source rocks with $\delta^{13}C$ of -26‰ and -29‰ (Schulz et al., 2002).

It is obvious that the methane-ethane plot is influenced by the presence of microbial methane (Fig. 11a). As contributions of microbial ethane and propane are very low (e.g. Oremland et al., 1988), more reliable results may be expected from a plot of $\delta^{13}C$ of ethane versus propane (Fig. 11b). According to this plot gas was generated at oil window maturities (0.6 – 1.2 %Rr). In general, this interval fits with oil biomarker-derived oil maturities (0.70 – 0.95 %Rr, Gratzer et al., 2011), but the spread of maturity values is higher.

Because fractionation during organic matter cracking due to bond energy differences between CH_2D and CH_3 terminal groups results in an increase of the $\delta^{13}C$ values concentration of heavy isotopes with increasing thermal overprint (Sackett et al., 1970), maturity trends are also visible in plots of $\delta^{13}C$ versus $\delta^{2}H$ for ethane and propane (Fig. 12). These plots suggest that east of the Lindach Fault (Fig. 5) maturity increases northwards from the wells O1*, O2* and G2* to the I1-6*, J1-J2*, H2* and P1-8*. Gas from the wells U*, Q1*, Q2*, S1-6* and R* was generated at the highest maturity. A similar northward increase is observed in oil maturity (Gratzer et al., 2011).

As discussed in section 5.3, gas produced in the wells N2* and N4* was probably generated at very low maturity, which is in agreement with alkane-based biomarker ratios (sterane isomerization: 0.41), but not with aromatic hydrocarbons (MPI-1: 0.70 corresponding to a vitrinite reflectance of 0.82 %Rr; En field after Gratzer et al., 2011).

In the area west of the Lindach Fault (Fig. 5), the lowest maturity is established for the wells AH* and AA2-4*. Maturity of the well AC* is slightly higher and reaches maxima in the wells AF*, AD1-4*, AI*, AJ*.

The changes in isotopic composition are interpreted to reflect maturity trends (Fig. 12). The large difference in maturity of the wells I1-6*, J1, J2* and P1-8* on one hand and the wells N2* and N4* on the other hand is also reflected by largely different slopes in the natural gas plot (Fig. 8). This is due to kinetic isotope effects and depletion of gas-parent functional groups caused by its thermal maturation (Chung et al., 1988; and authors cited).

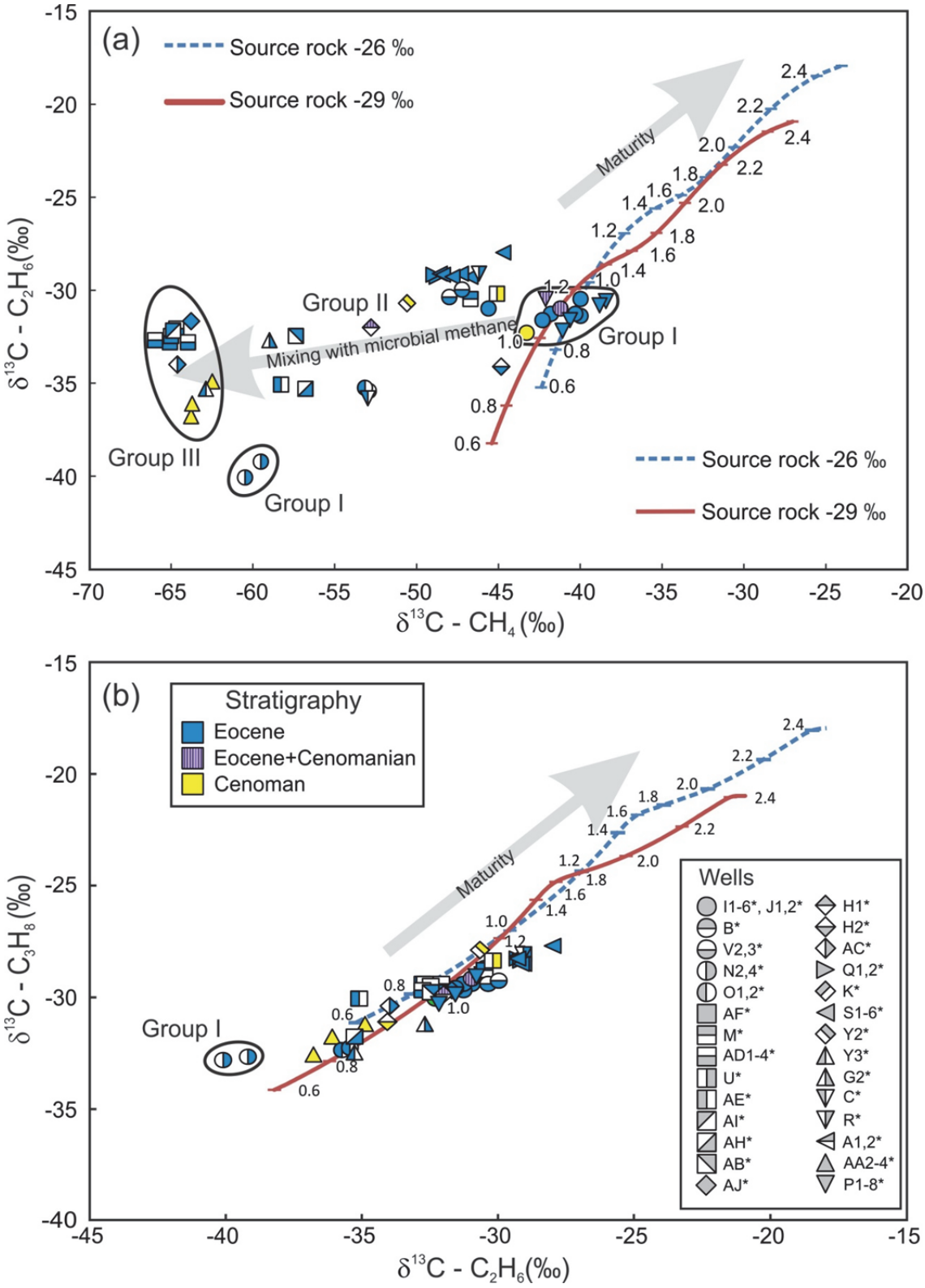

Fig. 11. Estimation of gas maturity based on plots of $\delta^{13}C$ of (a) methane vs. ethane and (b) ethane vs. propane according to models of Berner & Faber (1996). Arrows indicating maturity of source rocks during gas generation are expressed in vitrinite reflectance scale (%Rr). Two boundary isotopic compositions of source rocks (after Schulz et al., 2002) were used for calibration of maturity curves.

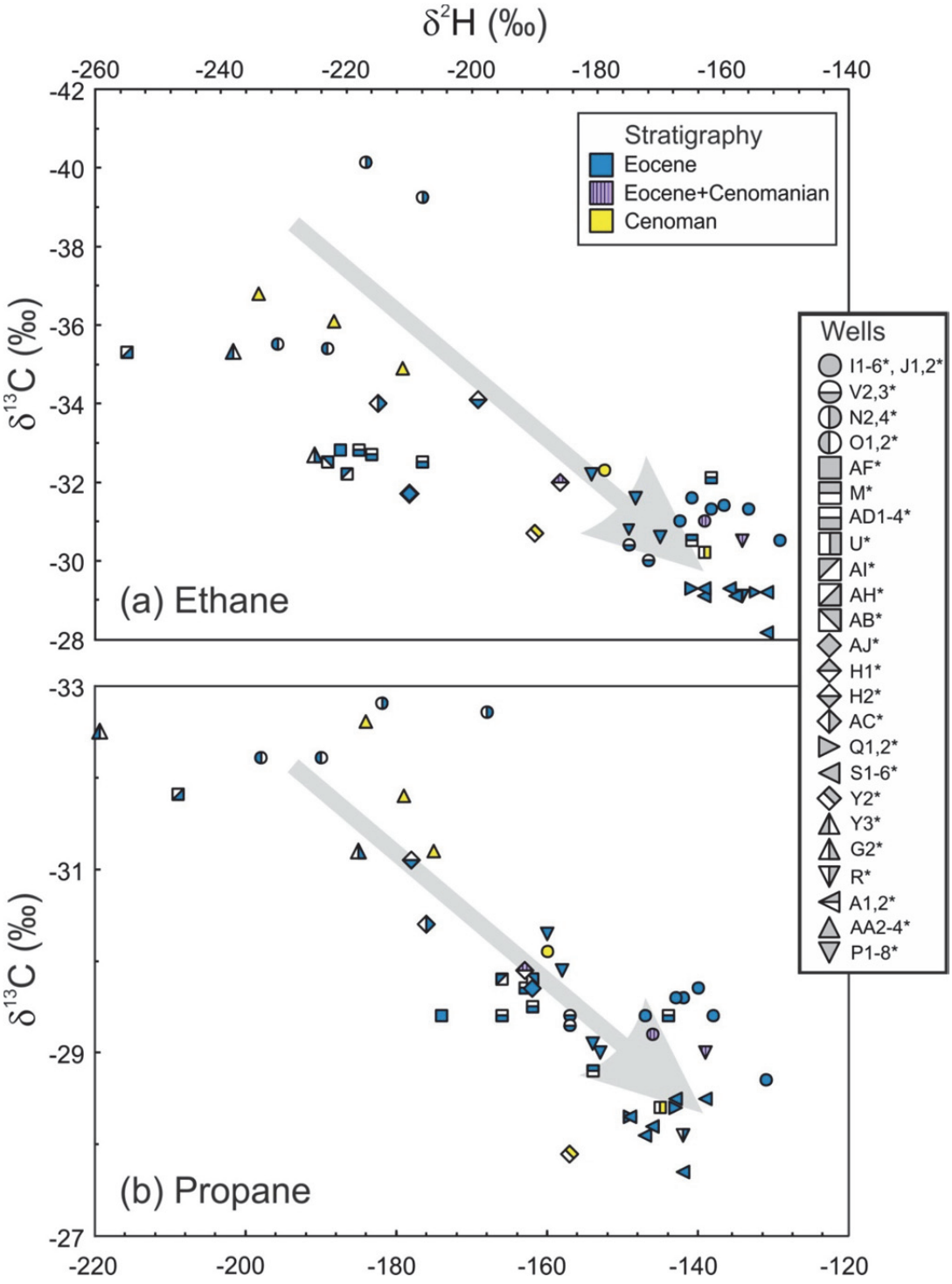

Fig. 12. Correlations of stable carbon and hydrogen isotopes in ethane (a) and propane (b). Increasing maturities are indicated by grey arrows according to Ni et al. (2011).

5.5. Amount of microbial methane

Carbon isotope ratios of thermogenic methane vary widely as a function of maturity and may even attain values considered diagnostic for microbial methane (e.g. wells N2* and N4*: -60‰; Fig. 10). Therefore, the application of methane isotope ratios alone is not sufficient to estimate the amount of microbial methane. In the present paper we use the natural gas plot to estimate proportions of microbial methane (Fig. 8). This approach is based on the observation that gas samples generated by cracking of kerogens plot on straight lines (Chung et al., 1988). Hence the extrapolation of the *n*-pentane – ethane trend lines helps to estimate the isotopic composition of pure thermogenic methane in mixtures of thermogenic gas with microbial methane (Figs. 8c, d). If the $\delta^{13}C$ value of pure microbial methane is known, the relative proportions of microbial and thermogenic methane can be estimated (see percentage scale on the right side of Figs. 8c, d). In this study it is assumed that the lightest recorded methane signature (-66‰) is diagnostic for pure microbial methane. This assumption is supported by the most negative $\delta^{13}C$ values of microbial methane in Oligo-Miocene reservoirs in the Austrian part of the Alpine Foreland Basin (-65.1‰; Pytlak et al., 2014). However, a value of -71.4‰ was measured by Schoell (1984) for methane produced from the same field as wells AA2-4* of present study. Adopting -71.4 as an end-member would result in slightly lower percentages of microbial methane.

Samples from Group I contain no or negligible amounts of microbial gas, whereas the rest of the samples contain significant amounts. The highest proportion of microbial methane is observed in samples from Group III (wells AF*, AD1-4*, AI* and AC*). A plot of estimated proportions of microbial methane versus gas-oil-ratios (GOR; Fig. 13) shows that samples rich in microbial methane are typically found in fields with low GOR (<50 m^3/m^3) implying a small overall methane volume.

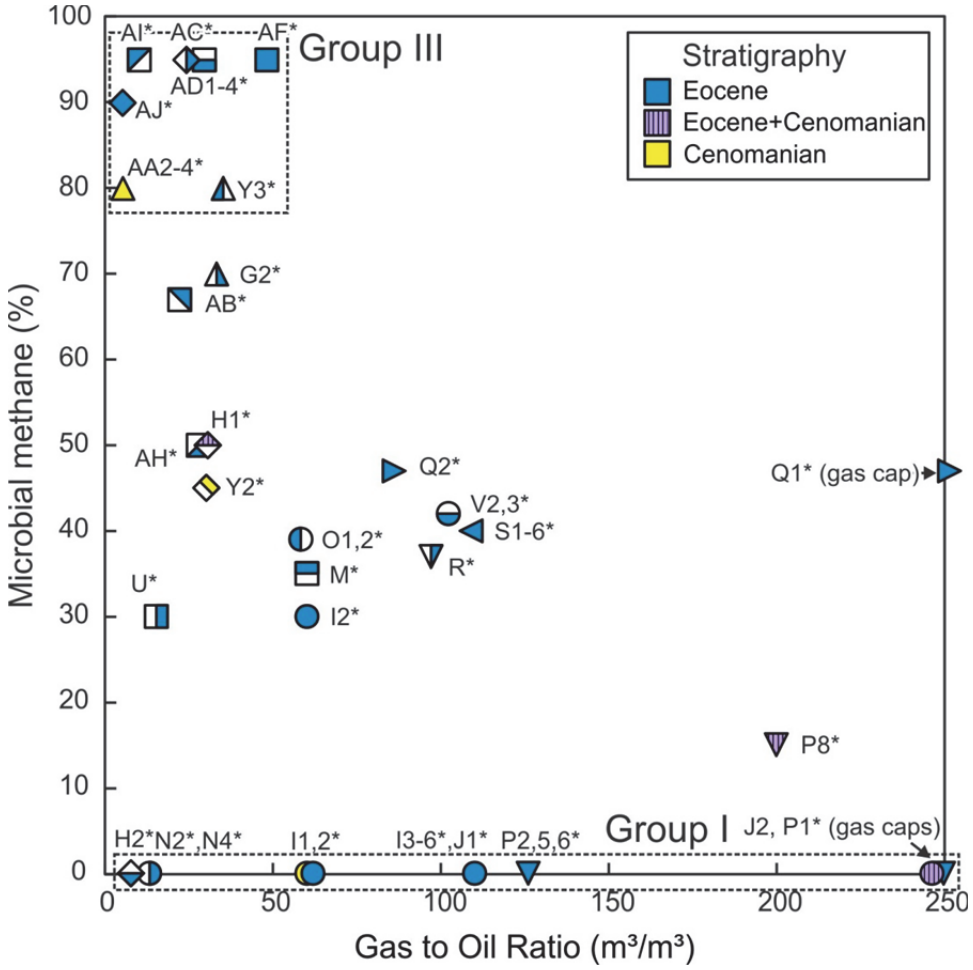

Fig. 13. Gas to Oil Ratio plotted against estimated proportion of microbial methane. High Gas to Oil Ratios are interpreted as gas cap above oil body.

5.6. Biodegradation

During microbial degradation of gas, straight chain alkanes are removed more effectively than branched ones (Palmer, 1993). Moreover propane is utilized much easier than ethane (Head et al., 2003). Hence gas degradation results in increased *i*-/*n*-C_4 and C_2H_6/C_3H_8 ratios as well as in gas drying. Moreover, biodegradation leads to an enrichment of heavier isotopes in the residual fraction. Simultaneously, the API gravity of residual oil decreases (Head et al., 2003 and reference therein).

Gases overlying biodegraded oil rims are limited to the northeastern part of the study area and have been classified as Group IV (Fig. 10). Because fields hosting Group IV gas have been abandoned or are used as storage facilities, original gas samples are no longer available. For this reason oil and gas data gathered by the industry during the last 50 years are used in Fig. 14 to demonstrate that oil and gas from shallow reservoir (<650 m below sea-level) are biodegraded. Biodegradation is reflected by decreasing oil gravity, increasing *i*-/*n*-C_4 ratios, increasing methane and decreasing propane contents (Fig. 14).

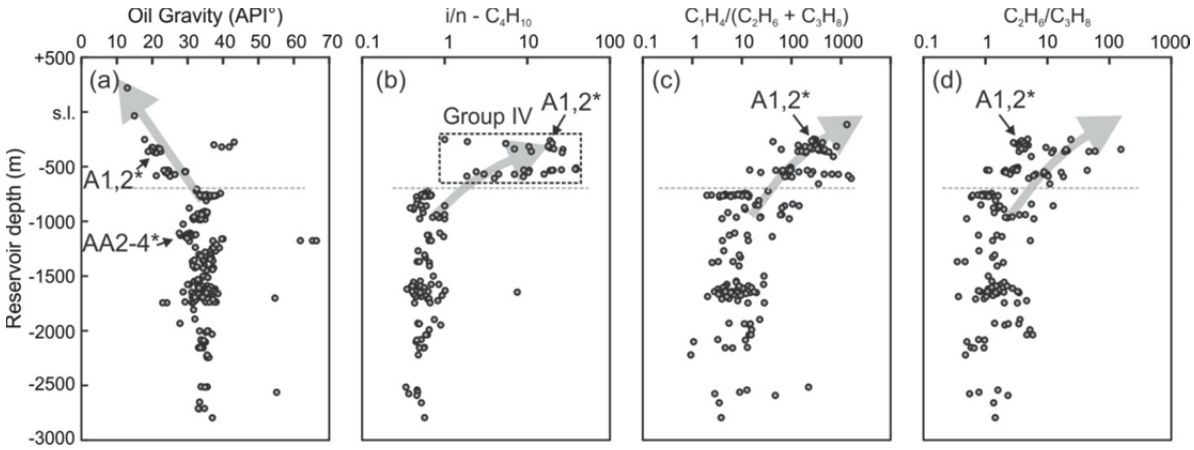

Fig. 14. Compilation of (a) oil gravity data and (b-d) different gas parameters from an unpublished industrial data base. s.l. – sea level. The depth plots show that significant biodegradation of oil and gas is limited to reservoirs depth shallower than -650 m below sea level (dashed line). Grey arrows indicate biodegradation trends.

Gas samples investigated in the present study are from oil fields at depths greater than 650 m below sea-level (Tab. 3). The C_{15+} fractions of oils from these deep fields are not biodegraded (Gratzer et al., 2011). Within the frame of the present study, we use the gaseous fraction, which is known to provide information already of slight biodegradation (e.g. Vieth & Wilkes, 2006).

A compilation of all data does not show clear trends (Fig. 15), probably because any biodegradation signals are overprinted by primary controls (e.g. source rocks variability, gas maturity; Alexander et al., 1981; Gratzer et al., 2011). However, samples from Group III, for which methane isotope data suggest a different source or reaction pathways, display indications for slight biodegradation (Fig. 16). For example, *i*-/*n*-C_4 and *i*-/*n*-C_5 ratios correlate well with $\delta^{13}C$ of *n*-C_4 and *n*-C_5 in the wells AD1-4* (Fig. 16a, b) and wells AA2-4* (Fig. 16b). In addition, the *i*/*n*-C_4 ratio correlates positively with C_2H_6/C_3H_8 ratio in the wells AA2-4* (Fig. 16c) (see section 5.1. for possible reason).

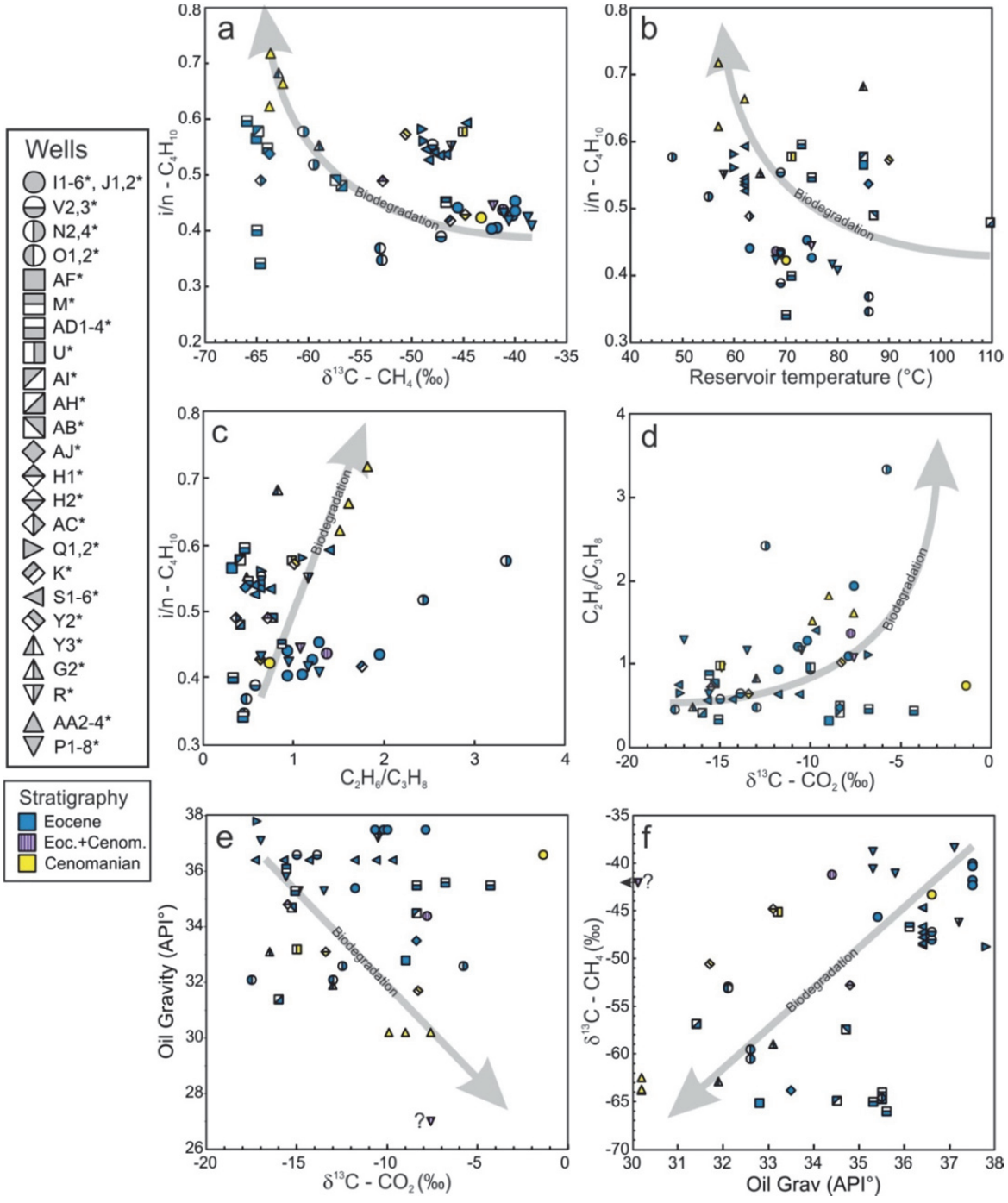

Fig. 15. Geochemical parameters used to assess biodegradation of gas samples. Oil gravity is plotted versus carbon isotopic ratios of carbon dioxide (e) and methane (f). Expected biodegradation trends are marked by grey arrows.

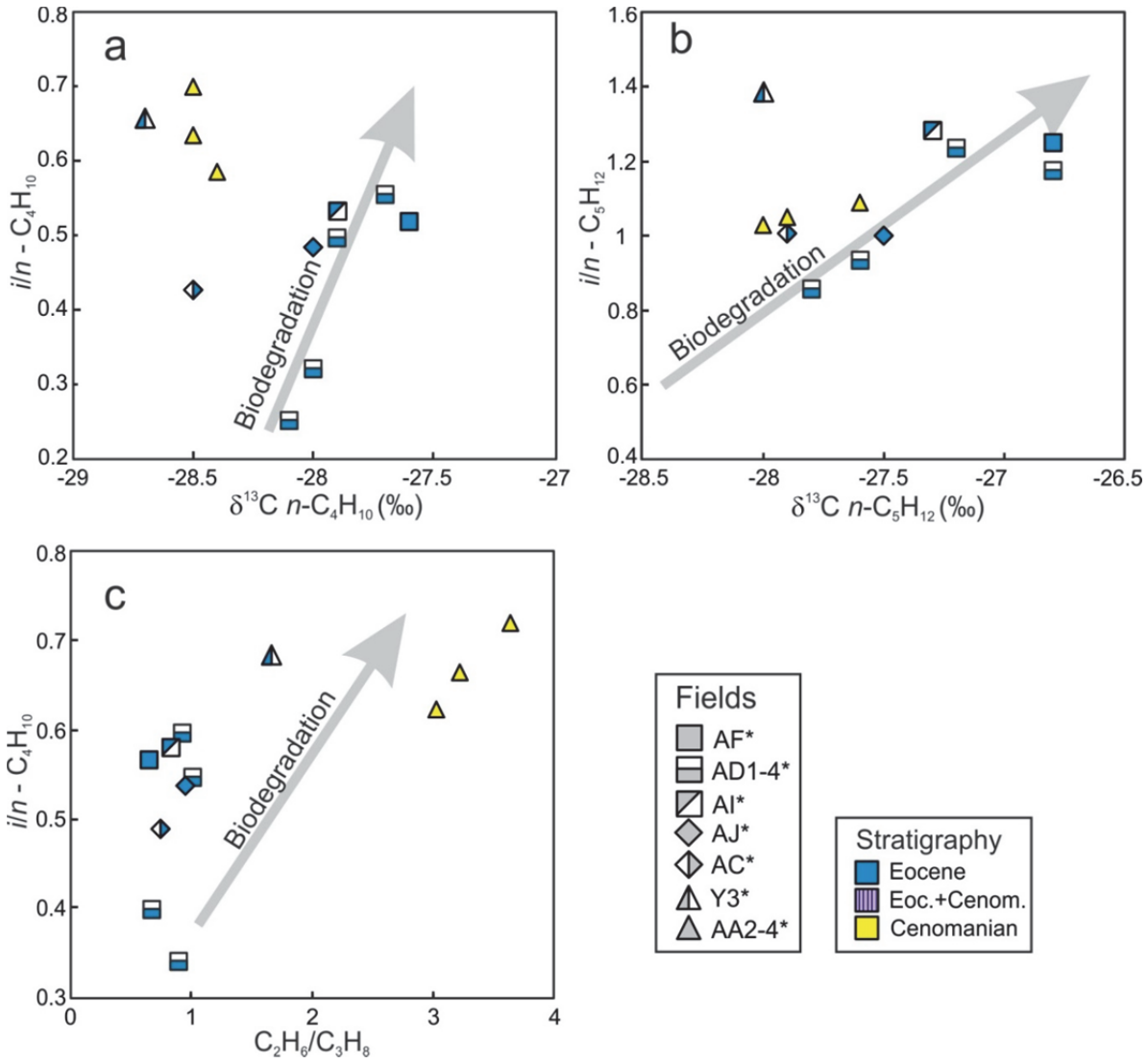

Fig. 16. Geochemical parameters used to assess biodegradation of gas samples. Expected biodegradation trends are marked by grey arrows.

5.7. Primary versus secondary microbial gas

It has been shown that significant amounts of microbial methane exist in oil reservoirs in the study area. In this section, arguments for a secondary microbial origin (methanogenic biodegradation of pre-existing oil) and a primary microbial origin (directly from sedimentary organic matter) are discussed.

Secondary microbial gas

Based on the presence of heavily biodegraded oil and gas, Reischenbacher & Sachsenhofer (2011) postulated that gas from the shallow wells (B*, D*, A1*, A2* and F*) was formed by anaerobic biodegradation of oil. Compared to methane in unaltered oil deposits (e.g. wells I1-6* and J1*, J2*), $\delta^{13}C$ ratios of methane in the wells A1*, A2* (-47.8‰) and B* (-50.2‰) are only slightly reduced. The initial biodegradation of oil and CO_2 reduction would result in isotopically light methane (-65‰ or lower). However, as the proceeding biodegradation of oil will produce progressively heavier CO_2 and CH_4 isotopic compositions (Jones et al., 2008), the methane from wells A1*, A2* and B* is interpreted to have formed during advanced level of biodegradation. However, this interpretation suffers from the lack of CO_2 data.

The same authors also postulated that isotopically light methane in the wells AA2-4* (-70 ‰; Trat field after Schoell, 1984) was formed by incipient biodegradation and argued, that, because of the early stage of biodegradation, microbes could use the lightest carbon isotopes resulting in methane with very negative $\delta^{13}C$ ratios. In the present study, $\delta^{13}C_{methane}$ values in the range of -63 ‰ and an average $\delta^{13}C_{CO2}$ values of -9 ‰ have been determined (Tab. 5). Despite of lack of direct CO_2-CH_4 correlation, slight biodegradation in wells AA2-3* (section 5.6) could indicate that methane may be of secondary microbial origin. Within this context it has to be noted that the wells AA2-4* are characterized by the lowest gas saturation (Fig. 13, Tab. 3) implying the absence of huge amounts of isotopically heavy methane. Thus despite of incipient biodegradation, methane is isotopically very light.

Although microbes may be active at high temperatures, it is commonly accepted that microbial activity relevant for petroleum formation and degradation is restricted to temperatures below 80°C (Head et al., 2003 and references therein). Basin models show that due to uplift and erosion, present day reservoir temperatures (Fig. 17) are probably in the same order, but not higher than during trap charging, which commenced in Early

Miocene time (Gusterhuber et al., 2013). Therefore, biodegradation should be limited to reservoirs with a present-day temperature of less than 80°C. Hence, secondary microbial gas generation is a possible explanation for the presence of isotopically light methane in the shallow fields (e.g. wells AD1-4*, AC* and AA2-4*), but not for deep and hot wells (e.g. wells AH* and Y2*, Fig. 17).

Primary microbial gas

Although it cannot be completely excluded that methanogenic microbes are active at temperatures higher 80°C (Orphan et al., 2000), it is more likely that at least the detected isotopic light methane in deep and hot reservoirs (e.g. AJ* AI*, AF*, AB*, AH*, AE*, O* fields) is of primary microbial origin.

Isotopically light microbial methane also occurs in deep (up to 4410 m) and hot (up to 120°C) Eocene reservoirs in the Bavarian part of the foreland basin (east of Munich, Fig. 1b). Schoell (1977) explained the portion of microbial methane by downward migration from overlying autochthonous Oligo-/Miocene sediments. However, because of normal hydrostatic pressure conditions this model seems unlikely. Moreover, geochemical data from the Austrian part of the North Alpine Foreland Basin provide strong evidence for upward migration of thermogenic hydrocarbons rather than for downward migration of microbial gas (Reischenbacher & Sachsenhofer, 2011; Pytlak et al, 2014).

Imbricated Molasse in the western study area is overpressured (Hinsch, 2013). Hence, downward migration may have occurred from this tectonically displaced unit. The gas from well G2* (currently hydrostatically pressured) in the eastern part of the Molasse Imbricates shows that the imbricated Oligo/Miocene sediments can host primary microbial gas. Moreover, migration of oil from the imbricates into the nearby field (well AE*) is likely (Gratzer et al., 2011; Gusterhuber et al., 2014). Hence, it cannot be excluded that microbial methane detected in fields beneath and along the front of the Molasse Imbricates (e.g. wells AE* and AH*) migrated downwards along faults connecting Molasse Imbricates with underlying autochthonous horizons.

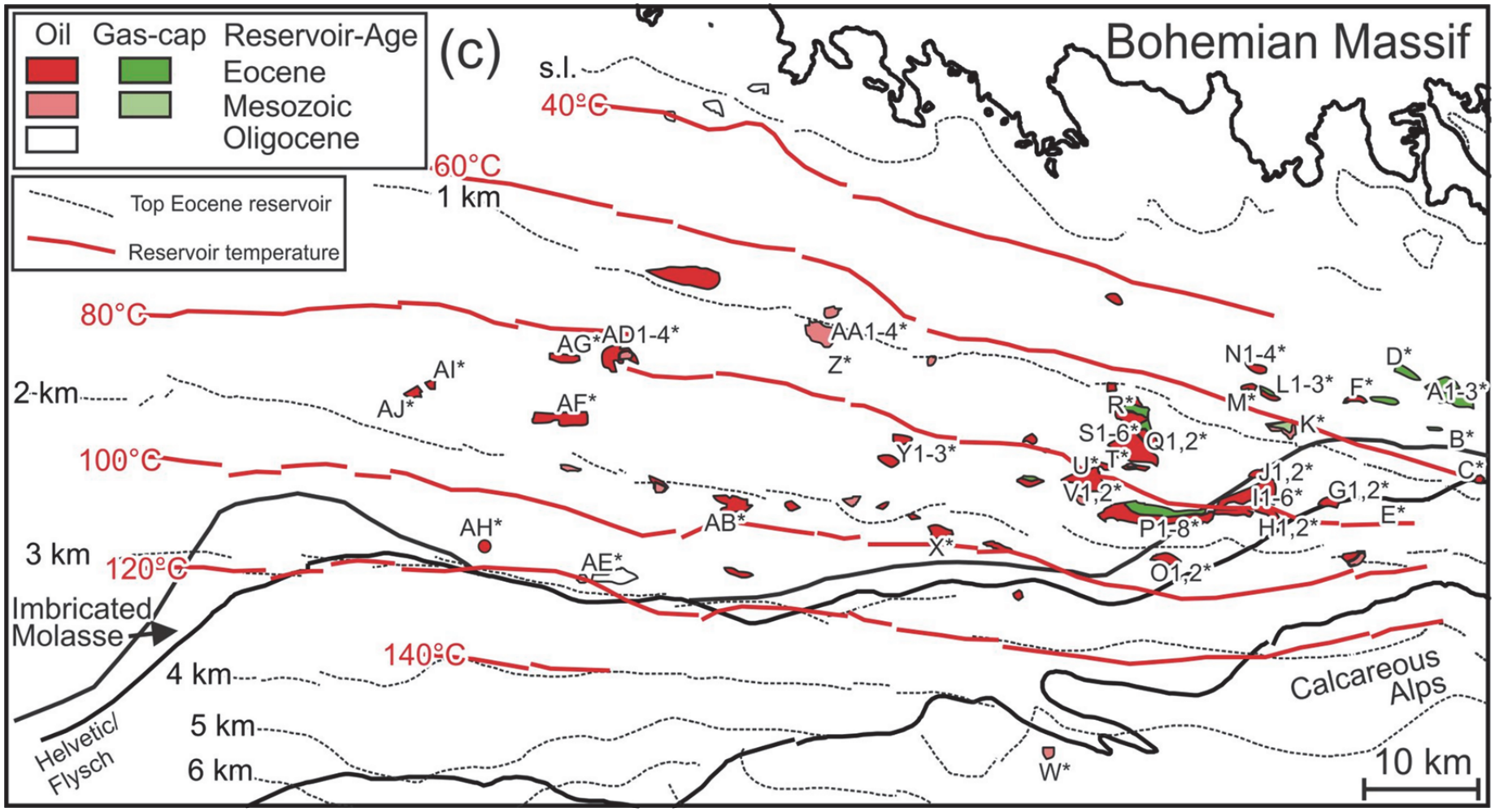

Fig. 17. Position of oil and associated gas fields in Mesozoic and Eocene reservoirs of the Alpine Foreland Basin. Temperatures at the base of the Cenozoic are shown according to Kamyar (2000) and correspond to temperatures in Eocene reservoirs. Temperatures of Cenomanian reservoirs may be slightly higher. Numbers denote the sampled wells. Wells are listed in Tab. 1. Analytical results of sampled wells are given in Tabs. 4 and 5.

However, it is more likely that the microbial portion of the gas has been generated during early basin evolution in underlying (e.g. Eocene Cerithian Beds) and overlying autochthonous horizons (e.g. Rupelian Schöneck and Eggerding fms.). Charging from overlying rocks is closely related to the timing of fault activity (Fig. 18a). Based on seismic interpretation, pre-Eocene, syn-kinematic (Early Oligocene) and post-kinematic fault activities are distinguished. Early Oligocene fault activity, juxtaposed hanging wall Lower Oligocene source rocks and footwall Eocene reservoir units (Fig. 18a). Syndepositional faulting is indicated by thickness variations on the flattened seismic line on the top Eggerding Fm. (Fig. 18b). This process enabled upward migration of microbial gas already during Lower Oligocene time. Support for the presence of early microbial gas east of the Lindach Fault is provided by calcite cement with very light carbon isotope ratios (-28‰) in Eocene reservoir sandstones, which is older than the oil charge (Grundtner et al, 2015; Sachsenhofer et al., 2006). Commencing in early Miocene time, the potential source rocks reached oil window maturity beneath the Alpine nappes and the generated thermogenic hydrocarbons mixed with the pre-existing primary microbial gas (Fig. 19).

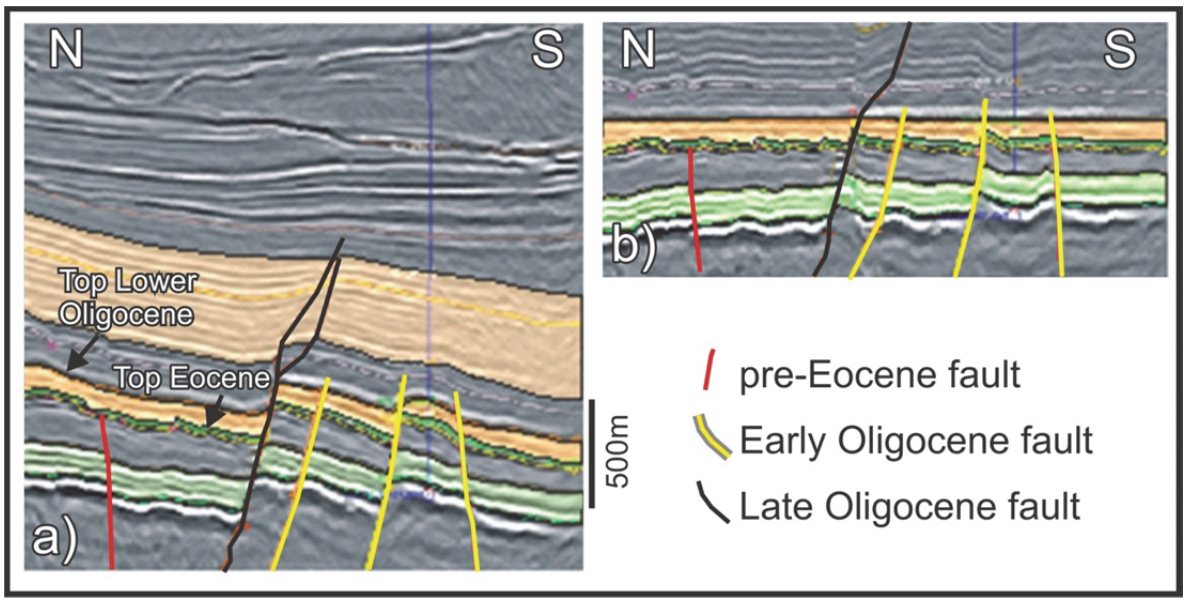

Fig. 18. a) Seismic line east of the S* field with location of faults with different fault activity. b) Seismic line flattened to Top Eggerding Fm. (modified after Linzer & Sachsenhofer, 2010).

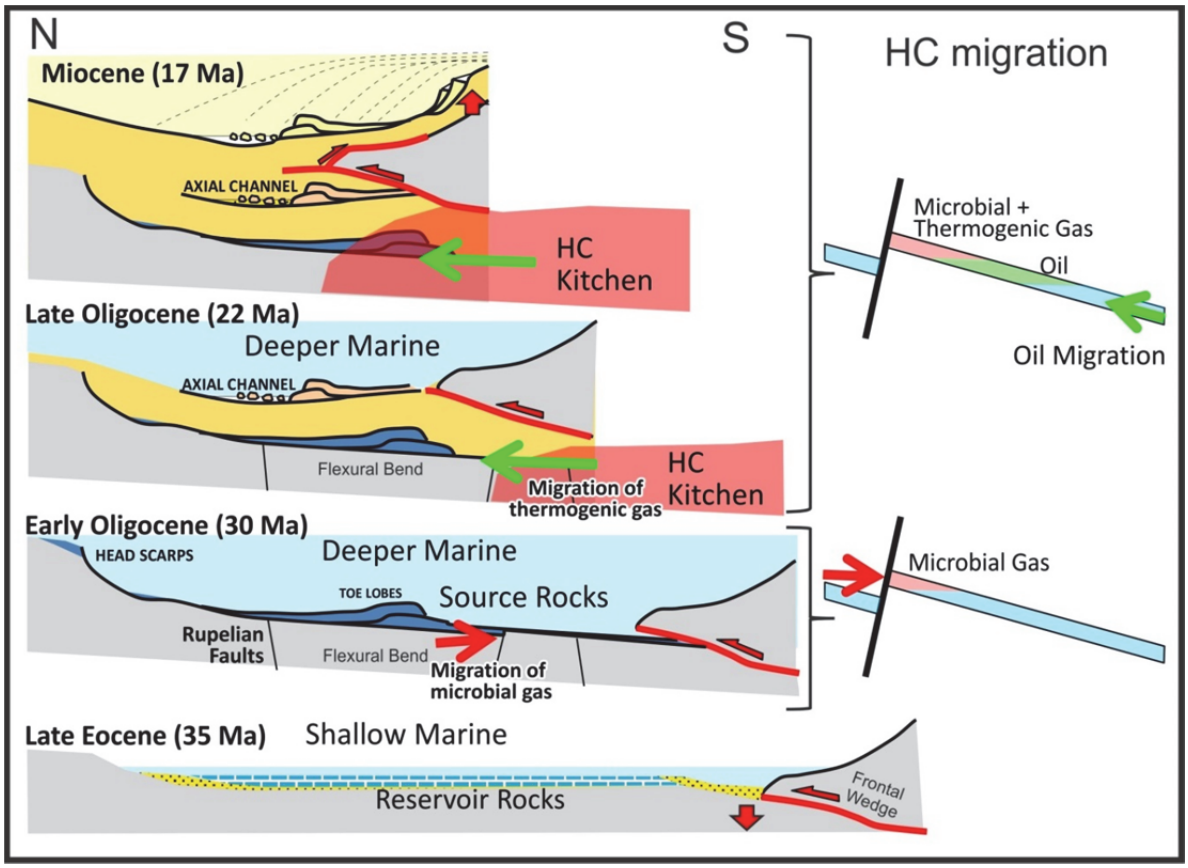

Fig. 19. Cartoon showing evolution of the Alpine Foreland Basin; migration and trapping mechanisms of microbial and thermogenic hydrocarbons (modified after Linzer & Sachsenhofer, 2010)

6. Gas accumulations in Oligocene/Miocene reservoirs: evidence for gas mixing and gas degradation

6.1. Molecular composition

The studied gas samples are dominated by methane (97.2 - 99.4 %) with minor concentrations of C_{2+} hydrocarbons, nitrogen (0.2 - 2.1 %) and carbon dioxide (< 0.5 %). In few samples traces of ethene and/or propene were detected (Fig. 20). Traces of different C_{5+} isomers have been detected, but only some of them have been quantified (Fig. 20). Thus results reported in Table 6 were not normalized to 100%.

Gas dryness, defined by $C_1/(C_2+C_3)$ (Bernard et al., 1978) varies between 96 and 471 with an average value of 228. An exceptional dry gas (~4400) is produced from the KK field (Fig. 21) in the northern part of the basin (see Fig. 6 for location).

Ratios of branched versus straight *n*-alkanes range between 0.9 and 4.4 for butanes and 1.9 and 19.8 for pentanes, respectively.

6.2. Isotopic composition

The stable carbon isotopic composition of methane varies widely from -48.5 to -65.1 ‰ (Tab. 6). Methane, most enriched in ^{13}C has been found in the F-O fields located in the western part of study area (Tab. 6, Fig. 6), whereas methane, most depleted in ^{13}C is from the KK field. δ^2H of methane ranges between -178 and -221 ‰ (Fig. 22). Similarly to $\delta^{13}C$ distribution, methane with elevated ^2H content occurs in the F-O fields. In addition, methane enriched in ^2H is recorded in gas from the X field (Tab. 6).

C_2 (-55.7 to -33 ‰), C_3 (-38.5 to -24.5 ‰) to *n*-C_4 (-33.4 to -17 ‰) hydrocarbons show a decreasing variability in stable carbon isotope ratios (Tab. 6).

Stable isotope ratios of methane obtained in the present study show a wider range of values than carbon (-59.7 to -63.3 ‰) and hydrogen isotope ratios (-197 to -212 ‰) reported by Schoell (1984) and Schulz & van Berg (2009). This is because, these authors coincidently did not sample wells with isotopically heavy methane.

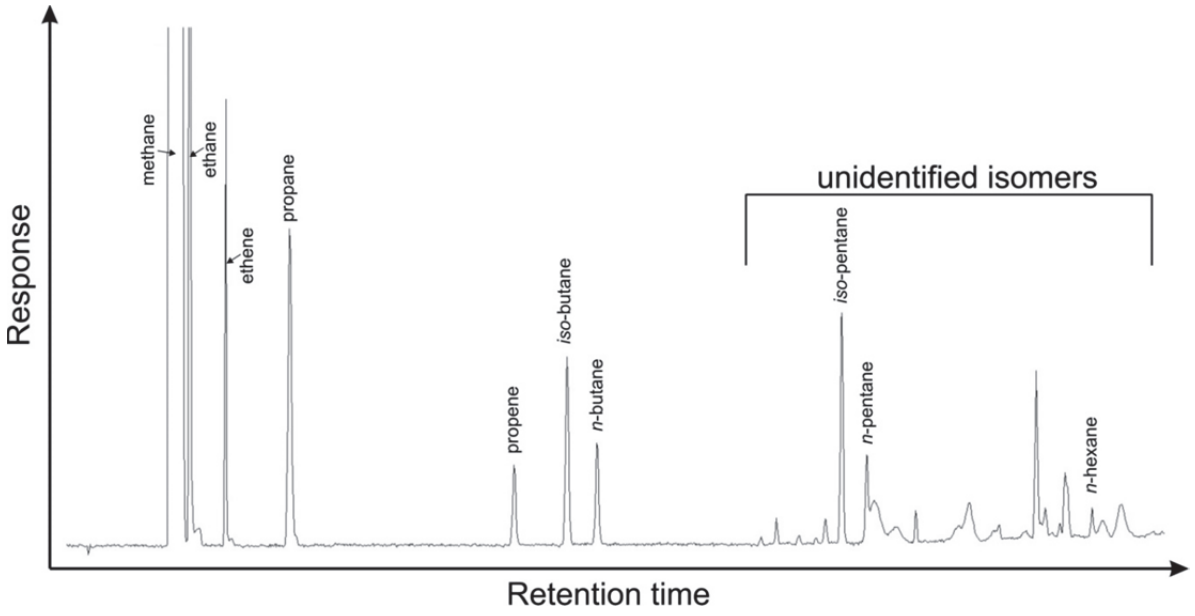

Fig. 20. Flame ionization detector (FID) chromatogram of gas sample from gas field F. For location see Fig. 6.

6.3. Microbial versus thermogenic gas

The driest gas is present in the KK field, where only methane and traces of ethane are observed. Moreover methane from this field is characterized by the most negative carbon isotopic values (Fig. 21, Tab. 6). This suggests a pure microbial origin of the KK gas, located in the shallow northern flank of the basin, and confirms the established models (e.g. Brix and Schultz, 1993; Schoell, 1984). Interestingly, ethane from KK gas is isotopically lighter than that of oil-associated gas from Mesozoic and Eocene reservoirs (Fig. 23, Pytlak et al,. 2016).

All other gas samples contain hydrocarbons up to *n*-hexane and yield significantly lower dryness values. Moreover, a significant number of them display isotope values characteristic for varying contributions of thermogenic hydrocarbons (Figs. 21, 22). Carbon isotope values as positive as -48.5 ‰ (Fig. 21) indicate the presence of the highest amount of thermogenic methane in the F-O fields. Apart from wet gas, some wells produce even liquid hydrocarbons (condensates), another proof for the presence of thermogenic input (Pytlak el al., 2014; Wagner, 1998). Traces of higher hydrocarbons are also visible in total gas composition (Fig. 20). Interestingly, gas dryness in Puchkirchen and Hall reservoirs with liquid hydrocarbons is often relative high (>200; Fig. 21).

Ethane in many samples is strongly depleted in ^{13}C (Fig. 23). This suggests that most of the detected ethane is microbial in origin. Actually, ethane and propane can be generated by microbial activity, although their contribution in total gas composition is typically very low (Hinrichs et al., 2006; Oremland et al., 1988; Rice & Claypool, 1981).

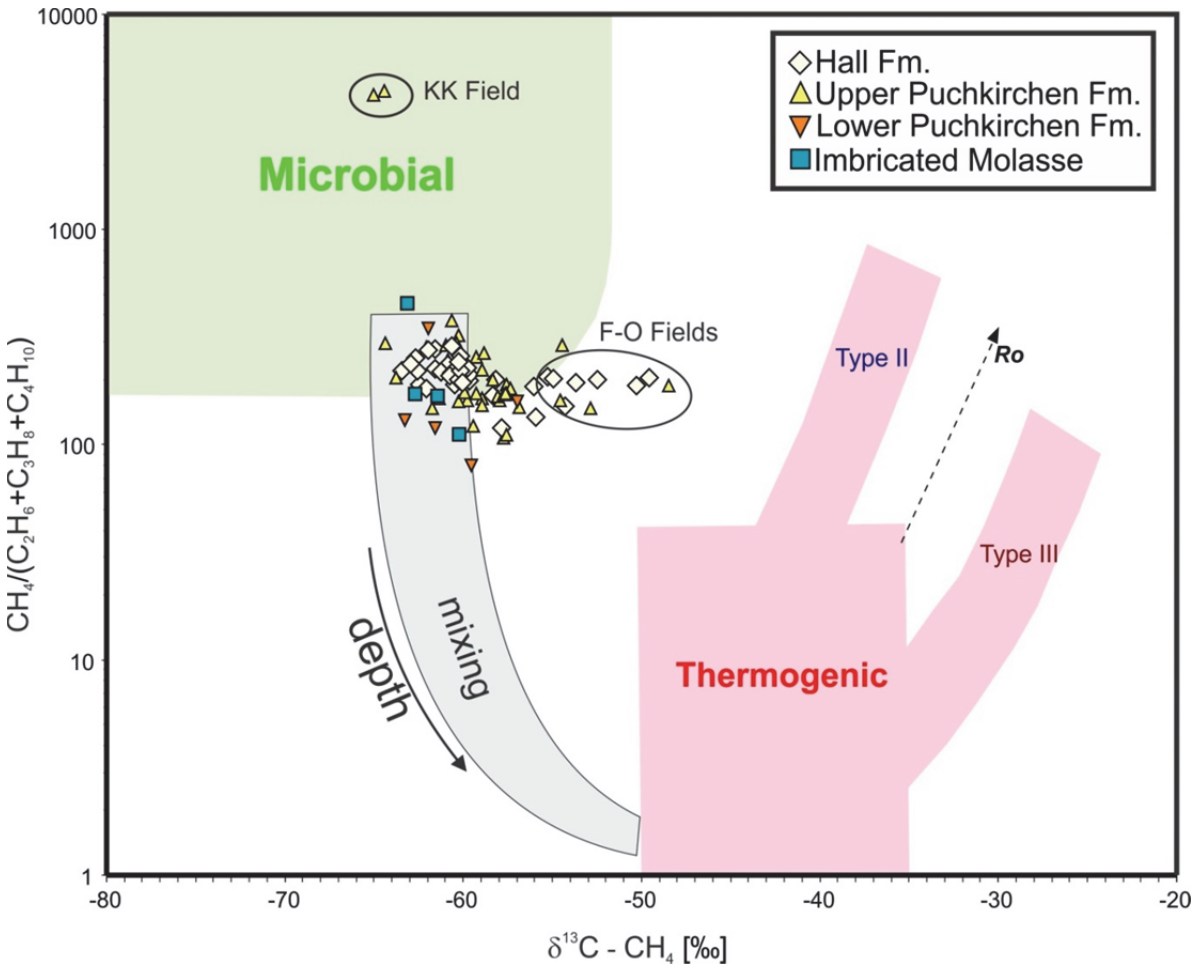

Fig. 21. Genetic characterization of oil associated gas from the Austrian part of the Alpine Foreland Basin (discrimination diagram adopted form Bernard et al., 1978; Whiticar & Suess, 1990). Note that y-axis of original plot is expressed as $CH_4/(C_2H_6+C_3H_8)$. Mixing trend with depth is determined by results of mud gas measurements from a well penetrating Imbricated Molasse (unpublished industrial data, for location see Fig. 6).

Tab. 6. Molecular [% vol] and isotopic composition of gas from wells Oligo/Miocene. Due to confidentiality, in column "Well" true names are substituted by letters corresponding to fields (see Fig. 6), and digits to certain wells.

													$\delta^{13}C$ [V-PDB]						$\delta^{2}H$ [V-SMOW]
Well	**TVDSS**	**Age**	**CH_4**	**C_2H_6**	**C_3H_8**	***i*-C_4H_{10}**	***t*-C_4H_{10}**	***i*-C_5H_{12}**	***n*-C_5H_{12}**	***n*-C_6H_{14}+[a]**	**CO_2**	**N_2**	**CH_4**	**C_2H_6**	**C_3H_8**	***i*-C_4H_{10}**	***n*-C_4H_{10}**	**CO_2**	**CH_4**
A1	1171	UPF	98.55	0.404	0.124	0.046	0.019	0.025	0.006	0.002	0.213	0.489	-59.0	-47.2	-33.8	-25.2	-26.0	-6.0	-205
A2	606	HF	98.34	0.338	0.114	0.045	0.014	0.019	0.004	0.000	0.008	0.482	-62.5	-41.9	-29.3	-22.7	-23.2	-8.2	-198
A3	1182	UPF	97.99	0.416	0.123	0.043	0.020	0.026	0.006	0.002	0.073	0.497	-58.0	-48.8	-35.0	-26.0	-26.5	-5.9	-207
A4	1165	UPF	98.20	0.482	0.202	0.081	0.029	0.041	0.009	0.002	0.131	0.602	-59.5	-45.7	-34.5	-27.5	-27.9	-5.7	-205
A5	1169	UPF	98.37	0.424	0.147	0.049	0.021	0.027	0.007	0.002	0.160	0.507	-59.0	-47.0	-35.0	-26.3	-26.4	-5.7	-206
A6	1167	UPF	98.57	0.405	0.131	0.045	0.024	0.027	0.007	0.003	0.106	0.511	-59.8	-45.9	-35.3	-25.8	-24.5	-6.7	-205
A7	1399	UPF	97.86	0.545	0.220	0.103	0.031	0.041	0.008	0.002	0.103	0.674	-57.8	-45.8	-34.6	-31.1	-30.3	-5.7	-202
B1	802	HF	98.29	0.349	0.162	0.046	0.018	0.020	0.005	0.001	0.020	0.617	-58.4	-48.6	-33.0	-21.9	-22.0	18.0	-210
C1	749	UPF	98.40	0.206	0.052	0.017	0.005	0.007	0.002	0.001	0.009	0.393	-62.0	-55.7	-36.0	-25.0	-24.2	-6.5	-221
D1	1021	UPF	98.19	0.358	0.106	0.032	0.018	0.021	0.005	0.001	0.041	0.430	-57.6	-49.2	-24.7	-26.2	-22.0	5.0	-204
E1	33	HF	98.92	0.277	0.081	0.022	0.007	0.006	0.001	0.000	0.035	0.653	-62.7	-38.0	-26.8	-24.0	-22.0	-38.0	-204
F1	1093	UPF	98.61	0.332	0.160	0.058	0.048	0.033	0.016	0.004	0.076	0.777	-61.4	-42.8	-31.0	-26.0	-24.7	-4.0	-201
F2	690	HF	98.80	0.327	0.124	0.044	0.018	0.020	0.005	0.001	0.072	0.560	-60.5	-46.3	-31.9	-26.0	-24.2	3.0	-202
F3	1694	UPF	97.68	0.687	0.335	0.126	0.064	0.072	0.016	0.004	0.298	0.766	-59.6	-43.5	-35.5	-30.9	-30.2	-1.3	-203
F4	1061	UPF	98.28	0.356	0.106	0.033	0.022	0.018	0.006	0.002	0.069	0.516	-48.5	-38.0	-29.4	-27.2	-25.4	0.1	-185
F5	702	HF	98.40	0.363	0.108	0.033	0.020	0.023	0.007	0.002	0.098	0.459	-56.1	-43.2	-33.5	-28.8	-23.5	-1.4	-180
F6	691	HF	98.54	0.327	0.126	0.044	0.019	0.019	0.005	0.001	0.007	0.616	-50.3	-41.1	-31.6	-29.4	-26.3	-0.3	-193
G1	234	HF	98.94	0.304	0.100	0.029	0.012	0.013	0.003	0.000	0.062	0.516	-63.5	-38.5	-25.7	-25.8	-24.7	-7.1	-202
H1	305	HF	98.65	0.253	0.074	0.018	0.006	0.007	0.002	0.001	0.057	0.471	-61.6	-36.4	-24.5	-17.0	-17.8	-3.8	-199
I1	627	HF	98.73	0.330	0.113	0.035	0.014	0.015	0.004	0.001	0.063	0.420	-60.0	-49.6	-32.0	-26.0	-25.2	4.5	-201
I2	695	UPF	98.82	0.272	0.082	0.019	0.010	0.009	0.003	0.001	0.030	0.373	-59.3	-50.8	-34.1	-26.0	-25.0		-212
I3	689	UPF	98.42	0.263	0.075	0.019	0.010	0.010	0.003	0.002	0.036	0.376	-58.9	-51.3	-33.2	-25.5	-22.0	4.0	-211
J1	1410	UPF	97.24	0.484	0.221	0.071	0.027	0.043	0.009	0.004	0.261	0.725	-61.6	-38.8	-35.7	-25.2	-23.6	-7.4	-204
K1	1151	UPF	98.29	0.371	0.113	0.033	0.017	0.022	0.006	0.002	0.407	0.422	-57.4	-50.8	-33.7	-28.0	-27.7	-7.0	-205
L1	398	HF	99.41	0.273	0.125	0.029	0.011	0.012	0.003	0.005	0.046	0.464	-60.2	-45.1	-30.5	-25.3	-23.5	-7.9	-206
M1	714	UPF	98.46	0.169	0.067	0.016	0.007	0.006	0.001	0.000	0.029	0.447	-60.7	-51.6	-34.2	-31.9	-30.8	-10.0	-212
M2	629	UPF	98.71	0.311	0.065	0.013	0.005	0.005	0.002	0.000	0.114	0.493	-60.9	-54.1	-33.6	-26.0	-23.4	-16.0	-216
M3	742	UPF	98.77	0.267	0.052	0.013	0.005	0.006	0.002	0.001	0.064	0.480	-61.0	-53.4	-35.6	-26.0	-24.6	-17.0	-218
M4	763	UPF	98.92	0.254	0.070	0.016	0.007	0.007	0.002	0.000	0.038	0.407	-62.1	-52.2	-34.7	-33.4	-29.9	-9.1	-202

M5	571	UPF	98.39	0.226	0.054	0.014	0.008	0.006	0.002	0.000	0.085	0.391	-60.3	-52.2	-33.9	-30.9	-29.3	-10.8	-205
M6	577	UPF	97.75	0.262	0.049	0.012	0.005	0.006	0.002	0.001	0.119	0.468	-60.4	-46.0	-34.0	-26.0	-22.4	-15.5	-221
N1	446	HF	98.33	0.318	0.102	0.036	0.010	0.013	0.001	0.003	0.166	0.401	-60.0	-47.5	-28.7	-27.0	-24.0	-8.6	-203
N2	335	HF	99.05	0.317	0.097	0.019	0.006	0.008	0.000	0.000	0.026	0.480	-60.5	-47.2	-31.0	-25.5	-22.0	-8.9	-202
N3	360	HF	98.83	0.302	0.090	0.019	0.006	0.018	0.001	0.000	0.038	0.693	-60.9	-49.6	-30.4	-25.5	-25.0	-4.0	-200
O1	690	HF	97.97	0.319	0.127	0.032	0.011	0.014	0.003	0.000	0.154	0.471	-59.7	-49.9	-33.6	-31.0	-29.9	-9.2	-189
O2	673	HF	98.00	0.319	0.099	0.036	0.015	0.015	0.003	0.001	0.102	0.566	-55.3	-39.4	-30.6	-27.8	-26.7	-6.4	-187
O3	744	HF	97.84	0.326	0.101	0.032	0.013	0.014	0.003	0.001	0.034	0.485	-49.6	-40.8	-31.8	-29.5	-26.0	-6.9	-200
O4	776	HF	98.47	0.427	0.144	0.054	0.022	0.027	0.006	0.002	0.127	0.506	-54.3	-43.3	-32.1	-28.3	-27.2	-8.2	-189
O-5	700	HF	98.76	0.326	0.116	0.034	0.011	0.013	0.002	0.000	0.024	0.480	-52.5	-43.4	-33.9	-28.9	-26.4	-10.8	-205
O6	698	HF	97.89	0.328	0.123	0.034	0.014	0.015	0.004	0.001	0.054	0.488	-53.7	-42.1	-29.9	-27.8	-25.7	-8.2	-192
O7	679	HF	97.56	0.317	0.120	0.030	0.009	0.011	0.002	0.000	0.082	0.580	-55.0	-44.9	-31.3	-28.7	-27.3	-8.0	-197
P1	797	UPF	98.47	0.281	0.040	0.011	0.004	0.005	0.002	0.002	0.072	0.241	-54.5	-42.9	-31.2	-29.3	-28.5	1.8	-187
P2	1045	UPF	98.77	0.282	0.042	0.005	0.003	0.002	0.001	0.000	0.052	0.219	-64.4	-55.1	-31.6		-27.9	-7.1	-178
Q1	1610	UPF	98.45	0.408	0.140	0.046	0.018	0.018	0.003	0.000	0.004	0.578	-60.3	-47.9	-34.7	-27.8	-28.0		-207
R1	273	HF	97.96	0.326	0.083	0.023	0.013	0.011	0.005	0.004	0.035	0.558	-61.3	-42.7	-28.8	-23.2	-22.0	-6.5	-202
R2	254	HF	97.99	0.325	0.077	0.021	0.010	0.008	0.002	0.000	0.021	0.561	-61.6	-42.9	-28.5	-21.8	-20.2	-7.7	-202
R3	317	HF	97.56	0.329	0.080	0.025	0.011	0.011	0.002	0.000	0.000	0.504	-61.3	-43.0	-28.4	-20.6	-22.3		-202
R4	275	HF	98.74	0.322	0.088	0.025	0.011	0.012	0.003	0.000	0.016	0.613	-62.6	-43.5	-29.5	-23.1	-23.5	-7.0	-202
R-5	284	HF	97.33	0.293	0.080	0.022	0.010	0.010	0.002	0.000	0.024	0.596	-63.0	-43.2	-28.4	-18.3	-21.1	-3.0	-201
S1	447	HF	98.95	0.295	0.121	0.028	0.010	0.010	0.002	0.000	0.018	0.557	-60.7	-44.5	-28.8	-21.0	-21.0	-5.0	-203
S2	1184	UPF	98.40	0.371	0.146	0.043	0.023	0.024	0.008	0.003	0.252	0.446	-58.1	-48.1	-34.6	-27.5	-27.5	-3.4	-207
S3	1180	UPF	97.70	0.363	0.142	0.040	0.019	0.026	0.006	0.000	0.075	0.438	-57.8	-48.9	-34.2	-23.8	-24.4	4.2	-206
S4	604	HF	98.99	0.333	0.110	0.028	0.018	0.018	0.006	0.002	0.038	0.439	-58.2	-51.0	-34.0	-28.0	-25.0	-11.0	-205
T1	795	UPF	98.05	0.324	0.109	0.028	0.013	0.016	0.004	0.001	0.045	0.455	-63.8	-49.0	-27.3	-25.3	-22.8	0.0	-190
U1	814	UPF	98.19	0.339	0.165	0.036	0.025	0.021	0.007	0.001	0.021	0.412	-59.3	-49.2	-34.0	-26.8	-26.4	-6.5	-204
U2	739	UPF	98.48	0.334	0.161	0.036	0.026	0.022	0.008	0.002	0.064	0.399	-60.0	-46.5	-31.3	-25.0	-23.4	-7.3	-203
U3	1037	UPF	98.44	0.363	0.222	0.044	0.034	0.030	0.009	0.002	0.044	0.725	-61.8	-49.7	-33.9	-25.7	-26.0	-6.0	-197
V1	375	HF	98.88	0.260	0.087	0.024	0.007	0.010	0.002	0.000	0.054	0.498	-60.2	-33.0	-26.0	-25.8	-25.7	-6.0	-209
V2	228	HF	98.82	0.323	0.148	0.037	0.029	0.019	0.010	0.008	0.055	0.547	-62.1	-36.0	-27.3	-27.2	-27.4	-8.0	-201
W1	489	HF	97.46	0.503	0.195	0.086	0.026	0.038	0.007	0.002	0.068	0.633	-57.9	-45.8	-34.2	-25.8	-28.9	-9.0	-202
W2	498	HF	97.85	0.472	0.151	0.071	0.029	0.040	0.010	0.003	0.394	0.511	-56.0	-46.0	-34.8	-28.9	-29.2	-2.6	-208
W3	1156	UPF	97.61	0.537	0.209	0.096	0.029	0.037	0.007	0.002	0.131	0.656	-57.6	-45.4	-34.6	-28.4	-28.7	-7.8	-202
W4	1162	UPF	97.99	0.448	0.128	0.051	0.021	0.025	0.006	0.002	0.235	0.490	-56.9	-46.3	-34.7	-28.2	-28.6	-6.0	-210
X1	30	Imbr	98.46	0.534	0.010	0.017	0.004	0.001	0.001	0.000	0.037	0.631	-62.8	-38.0	-25.2	-25.5	-20.4	-3.4	-187

X2	190	Imbr	98.01	0.678	0.135	0.036	0.015	0.014	0.003	0.000	0.022	0.567	-60.3	-43.3	-33.0	-26.9	-27.3	-3.0	-184
X3	193	Imbr	98.36	0.458	0.097	0.014	0.005	0.004	0.001	0.000	0.018	0.629	-61.5	-48.9	-36.0	-26.5	-25.5	-4.1	-180
X4	-21	Imbr	98.41	0.182	0.026	0.004	0.001	0.000	0.000	0.000	0.019	0.666	-63.2	-55.5	-38.5	-26.0	-21.5	-1.2	-182
Y1	2026	LPF	98.07	0.432	0.215	0.078	0.024	0.028	0.008	0.002	0.152	0.427	-63.3	-51.8	-37.3	-33.1	-31.7	-10.9	-187
Z1	544	HF	98.11	0.301	0.113	0.031	0.014	0.014	0.003	0.001	0.032	0.428	-59.7	-46.0	-30.0	-24.0	-27.0	-2.0	-204
AA1	628	HF	98.17	0.281	0.103	0.033	0.011	0.013	0.002	0.001	0.074	0.523	-59.8	-47.7	-31.0	-23.0	-22.0	-0.4	-209
BB1	463	HF	98.66	0.294	0.129	0.031	0.013	0.015	0.003	0.000	0.004	0.480	-60.8	-44.3	-29.7	-19.2	-20.8	-6.2	-201
CC1	335	HF	99.45	0.314	0.124	0.037	0.014	0.012	0.002	0.002	0.010	0.522	-60.3	-48.8	-31.0	-23.0	-23.0	-11.1	-201
DD1	1454	LPF	97.95	0.416	0.133	0.041	0.018	0.024	0.006	0.001	0.217	0.393	-57.0	-46.8	-32.4	-30.6	-29.8	-6.7	-186
DD1	1278	UPF	98.50	0.341	0.065	0.014	0.017	0.022	0.006	0.001	0.013	0.457	-59.0	-50.2	-35.1	-31.6	-30.0	-13.1	-189
EE1	594	HF	98.47	0.291	0.101	0.039	0.012	0.014	0.003	0.000	0.079	0.448	-60.2	-43.6	-29.0	-21.0	-22.0	-2.0	-200
FF1	1185	UPF	98.50	0.441	0.109	0.040	0.016	0.032	0.006	0.024	0.039	0.597	-54.6	-49.1	-32.4	-27.0	-28.0	-13.0	-199
GG1	493	HF	99.11	0.262	0.102	0.032	0.010	0.011	0.001	0.001	0.087	0.367	-60.3	-48.4	-30.9		-24.8	-9.8	-198
GG2	505	HF	98.76	0.325	0.131	0.032	0.014	0.013	0.003	0.003	0.052	0.655	-60.1	-43.8	-29.8	-24.0	-23.0	-9.3	-200
HH1	1261	UPF	98.09	0.326	0.109	0.035	0.016	0.020	0.005	0.001	0.117	0.513	-58.4	-46.1	-32.1	-26.0	-26.7	1.2	-205
II1	419	HF	98.53	0.321	0.026	0.006	0.001	0.002	0.000	0.000	0.000	0.536	-62.0	-49.6	-27.0				-195
II2	623	HF	97.99	0.302	0.028	0.006	0.002	0.002	0.000	0.000	0.000	0.539	-60.7	-50.0	-27.3				-195
JJ1	1201	UPF	97.81	0.390	0.118	0.035	0.019	0.024	0.006	0.002	0.239	0.463	-57.6	-49.7	-35.4	-26.0	-26.0	-4.1	-206
JJ2	1181	UPF	97.71	0.387	0.121	0.036	0.019	0.024	0.006	0.003	0.335	0.448	-57.7	-48.9	-35.1	-26.0	-26.4	-5.5	-207
JJ3	1180	UPF	97.58	0.391	0.115	0.034	0.019	0.025	0.006	0.000	0.456	0.463	-57.7	-49.7	-35.0	-24.5	-24.0	-6.2	-207
JJ4	1186	UPF	97.21	0.390	0.110	0.036	0.019	0.025	0.007	0.002	0.271	0.461	-57.7	-49.1	-35.3	-26.9	-27.2	-4.6	-208
KK1	102	UPF	97.47	0.023	0.000	0.000	0.000	0.000	0.000	0.000	0.002	1.806	-65.1	-47.9					-214
KK2	116	UPF	97.93	0.022	0.000	0.000	0.000	0.000	0.000	0.000	0.002	2.106	-64.5	-42.3					-211

TVDSS – True Vertical Depth Subsea, HF – Hall Formation, UPF – Upper Puchkirchen Formation, LPF – Lower Puchkirchen Formation, Imbr – Imbricated Molasse, [a] fraction of *n*-hexane and undefined or unresolved isomers

6.4. Origin of thermogenic gaseous components

Fig. 25a shows that gas dryness decreases with reservoir depth implying a downward increase in thermogenic hydrocarbons (see also Reischenbacher & Sachsenhofer, 2011). Potentially these hydrocarbons may have been generated locally in pelitic rocks within the studied succession (or below), or may have been derived from oil-bearing deeper horizons (e.g. Eocene reservoir rocks).

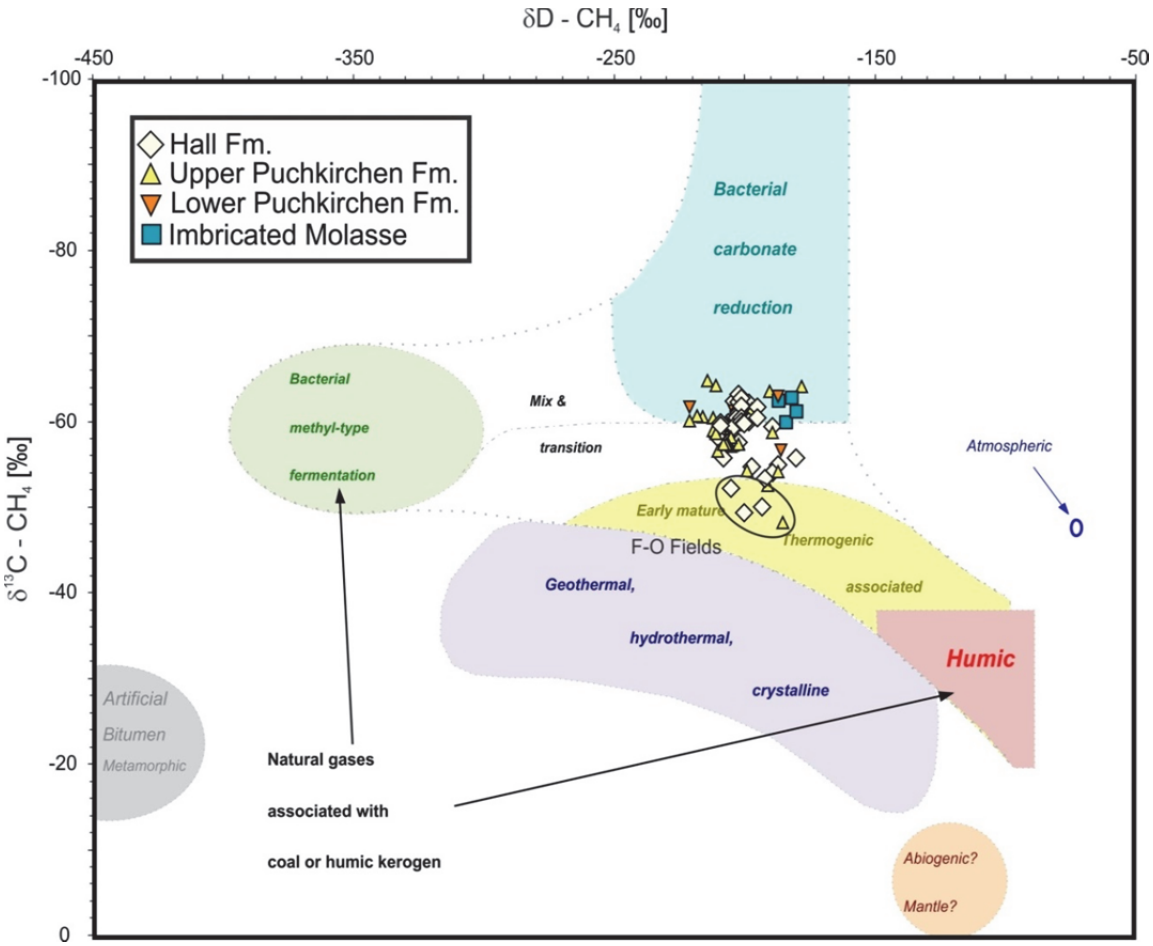

Fig. 22. Genetic characterization of gas from Oligocene-Miocene reservoirs in the Austrian part of the Alpine Foreland Basin (plot modified after Whiticar et al., 1986).

The Cenozoic succession includes potential source rocks. However, these are immature north of the Alpine front (e.g. Gusterhuber et al., 2013, 2014). This is not only valid for Lower Oligocene source rocks, but also for “fish shales” near the top of the Upper Puchkirchen Formation containing up to 3.5 % TOC (Belaed, 2007).

Therefore, it is likely that the thermogenic hydrocarbons migrated upwards from Eocene carrier beds and reservoir rocks (e.g. Wagner, 1998). Although commercial oil deposits in the western part of the study area are missing, industry data show that wet gas and oil stains within Eocene horizons have been detected in the entire study area.

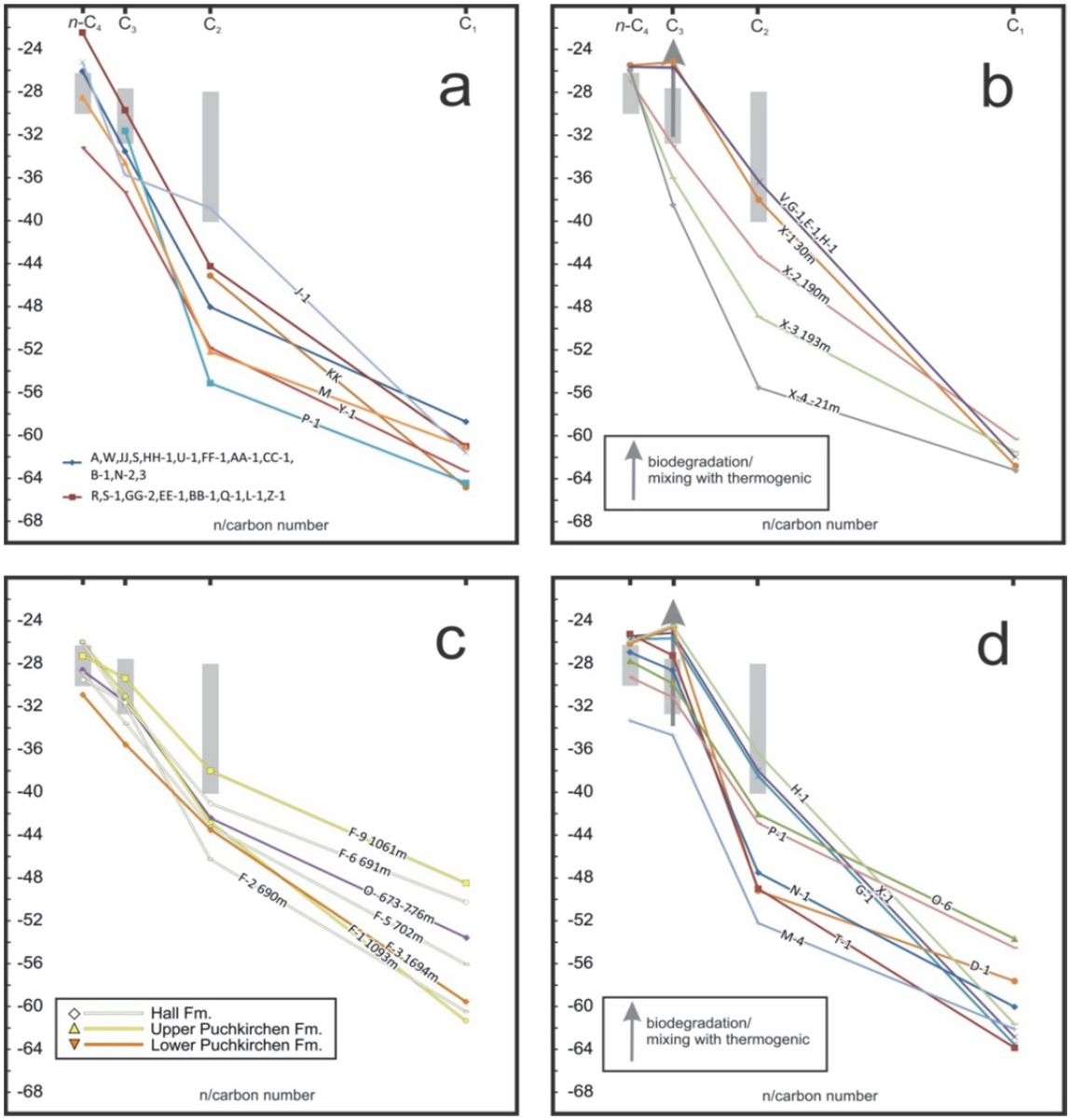

Fig. 23. The natural gas plots (Chung et al., 1988) showing the carbon isotopic compositions of individual hydrocarbons as a function of the carbon number. Depths are True Vertical Depths SubSea (TVDSS) expressed in meters. Gray bars indicate isotopic signature of hydrocarbons associated with oil deposits in the Austrian part of Alpine Foreland Basin (Pytlak et al., 2016 and section 5 in this thesis).

The plot of $\delta^{13}C$ of ethane versus $\delta^{13}C$ of propane (Berner & Faber, 1996; Fig. 25) is often used to determine the maturity of gases. The data from Oligocene-Miocene reservoirs are generally shifted towards light $\delta^{13}C$ values of ethane (Fig. 25). This may indicate a contribution of microbial ethane. Moreover, propane may be enriched in ^{13}C due to biodegradation (see chapter 6.6). Nevertheless propane and *n*-butane isotope ratios are similar to those measured in oil-associated gas from Mesozoic and Eocene reservoirs (Pytlak et al., 2016; Fig. 23), suggesting oil window maturity.

6.5. Controls of mixing of thermogenic and microbial gas

Whereas the microbial component of the gas has been generated locally within the Upper Oligocene to Lower Miocene succession (Schulz & van Berg, 2009), the thermogenic fraction migrated vertically upward from Mesozoic and Eocene carrier beds and/or reservoirs. Migration may have occurred (1) along relative permeable faults or (2) within low permeability rocks along sub-seismic fractures.

(1) Samples G-1, E-1, H-1 and gas from a V field produce methane from Hall reservoirs in the eastern part of the study area. $\delta^{13}C$ values of methane in these fields are characteristic for microbial origin, while those of C_2 to C_4 hydrocarbons are characteristic for thermogenic, oil-associated gas (Fig. 23b). The producing Hall horizons in the above fields are located above or close to oil deposits in Eocene strata. Faults were active in the Alpine Foreland Basin during different times. In some areas fault activity stopped already during deposition of the Lower Puchkirchen Formation, whereas in others it continued till Eggenburgian time. These long-lived faults, provided potential migration pathways connecting Eocene reservoirs and the Hall Formation (Wagner, 1998).

(2) In areas without distinct faults, migration may have occurred through low-permeability caprocks along sub-seismic fractures, silty intervals and/or by diffusion. It is likely that upward migration may be facilitated in areas where lower Oligocene fine-grained rocks are eroded and along the Puchkirchen Channel system, where a high percentage of permeable clastic rocks have been deposited. Within this context, it is remarkable to observe that the F-O fields containing isotopically methane enriched in ^{13}C (-48 to -61.4‰) testifying to a high amount of thermogenic gas, is located both, along the axis of the Puchkirchen Channel and above an area where more than 60 m of lower Oligocene fine-grained rocks have been removed by submarine erosion

(Sachsenhofer & Schulz, 2006). In contrast, the KK field hosting no thermogenic hydrocarbons, but pure microbial gas is located far north of the Puchkirchen Channel and in an area with thick pelitic Lower Oligocene deposits.

Migration through low-permeability caprocks may involve diffusion. Diffusion processes lead to molecular and isotopic fractionation due to differences in the effective diffusion coefficients (e.g. Krooss et al., 1988; Leythaeuser et al., 1983; Xia & Tang, 2012; Zhang & Kross, 2001). Prinzhofer & Pernaton (1997) proposed a plot of the C_2/C_1 ratio versus $\delta^{13}C$ of methane (Fig. 24) to distinguish diffusive fractionation from simple mixing of two end-member gases. Because the Prinzhofer plot may be used for gases in seal rocks, but not for reservoir gases (Zhang & Krooss, 2001) and because the thermogenic end-member gas in the case of the Alpine Foreland Basin is a gas mixture itself (Pytlak et al., 2016), we do not plot reservoir gas data, but mud gas data from a recently drilled well, which penetrated shaly units, several hundred meters thick. The mud gas data show a strong linear relationship between the C_2/C_1 ratio and $\delta^{13}C$ of methane (in the plot with linear axis) suggesting that mixing processes are dominant, whereas fractionation associated with diffusion does not appear to have influenced gas compositions significantly. Obviously diffusive fractionation cannot be completely ruled out, but its effect on the governing molecular and isotopic gas composition may have been overprinted by other processes (mixing, alteration; see below).

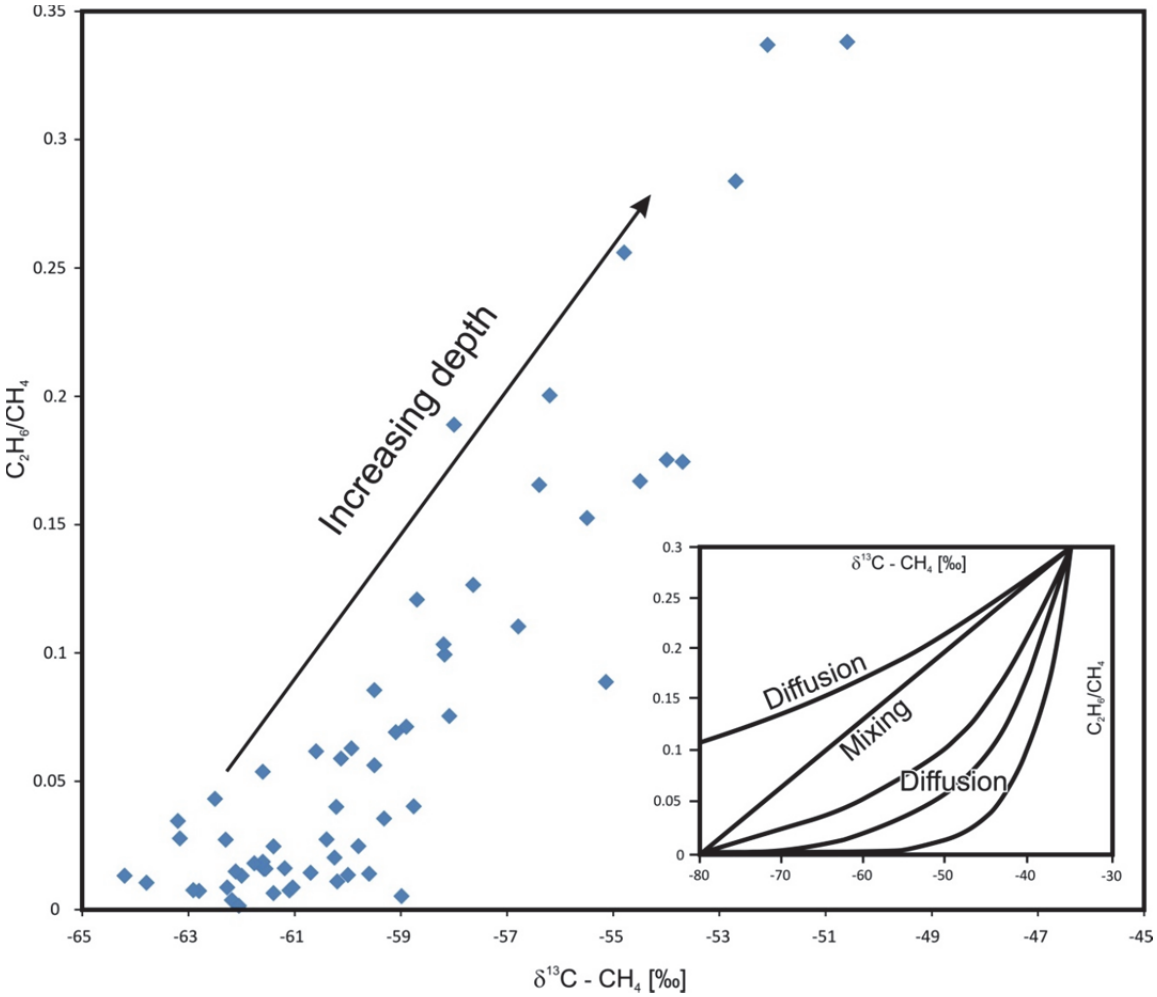

Fig. 24. Cross-plot of C_1/C_2 molecular ratio versus $\delta^{13}C$ of methane (after Prinzhofer and Pernaton, 1997) of mudgas from a well near the southern margin of the Alpine Foreland Basin. Inset presents theoretical mixing and diffusion trends. Diffusion trends depend on ratios of the diffusive permeabilities for ethane over methane.

6.6. Gas biodegradation and secondary microbial methane

During microbial alteration of gaseous hydrocarbons propane is primarily degraded (Head et al., 2003; Kniemeyer et al., 2007). In addition, straight chain alkanes are preferentially removed compared to branched ones (James & Burns, 1984; Palmer, 1993) resulting in increasing *i*/*n*-C_4 ratios. Although *i*/*n*-C_4 ratio can depend on maturity (Alexander et al., 1981), those of non-degraded gases are usually below 0.8 (Huang & Larter, 2014). In most cases microbial activity leads to enrichment in ^{13}C isotope of remaining molecules (e.g. C_3, *n*-C_4).

To visualize gas alteration trends, *i*/*n*-C_4 ratios and stable carbon isotopic composition of propane are plotted versus depth in Figs. 25c, d. *i*/*n*-C_4 ratios significantly above 0.8 indicate that all gases are biodegraded. *i*/*n*-C_4 ratios show a weak, $\delta^{13}C$ ratios of propane a strong downward decreasing trend providing evidence that the effect of in-reservoir biodegradation decreases downwards with increasing formation temperature. Although microbes may be active at high temperatures, it is commonly accepted that microbial activity relevant for petroleum formation and degradation is restricted to temperatures below 80°C (Head at al., 2003 and references therein). This observation agrees with the fact that in the study area a formation temperature of 80°C is reached between 1500 and 2000 m depth subsea (Kamyar, 2000). However, it is important to note that regional uplift after Late Miocene maximum burial resulted in cooling of about 20°C (Gusterhuber et al., 2012). This argues for biodegradation, at least in deep reservoirs, before or after maximum burial.

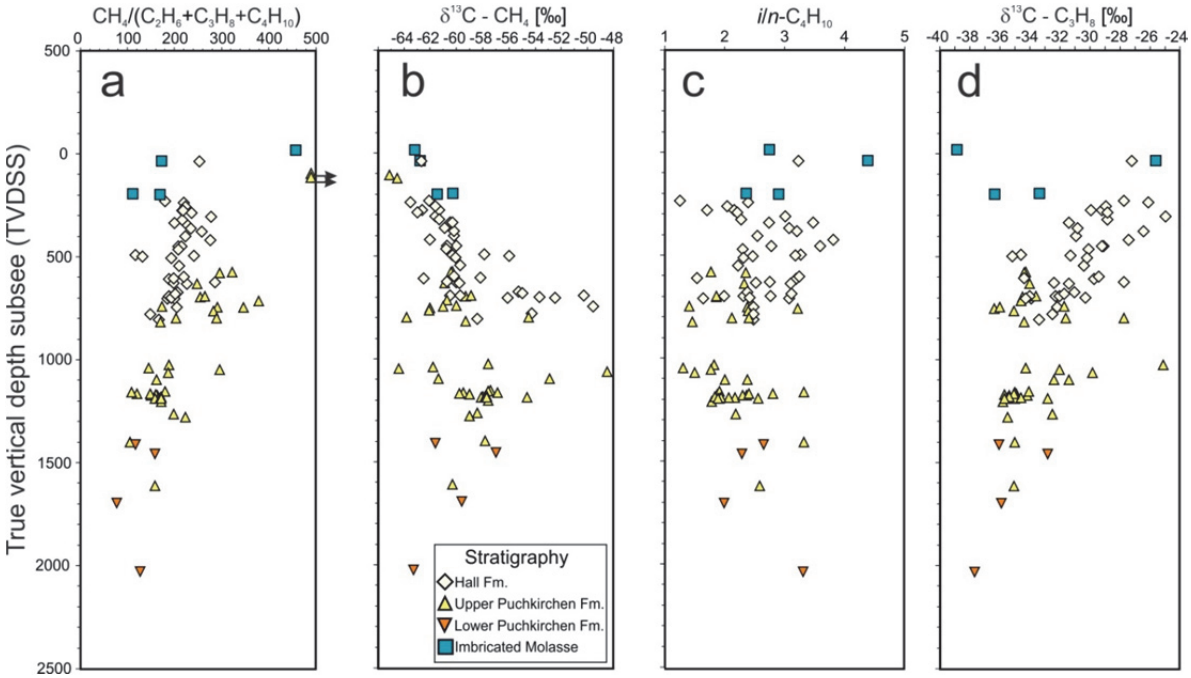

Fig. 25. Depth distribution of selected geochemical parameters. *i*/*n*-C_4H_{10} ratios >1 indicate that all gases are biodegraded. However, dryness and $\delta^{13}C$ - C_3H_8 trends indicate that biodegradation decreases with depth.

The natural gas plot (Chung et al., 1988) shows that a significant number of samples shows deviations from typical $\delta^{13}C$ distribution patterns ($\delta^{13}C_{C2H6} < \delta^{13}C_{C3H8} < \delta^{13}C_{C4H10;}$ Schoell, 1984; Tang et al., 2000) (Figs. 23b, d). This is caused mainly by an enrichment of ^{13}C in propane and reflects the selective microbial removal of this compound.

Some samples contain ethene and propene (Fig. 20), which are considered instable over geological time-scales. Although microbial processes yielding unsaturated hydrocarbons are poorly understood, their presence may indicate recent bacterial activity (Whiticar, 1994). Microbial activity is also confirmed by the presence of metabolites in reservoir rocks (Gruner, pers. comm.). Drill bit metamorphism as source for unsaturated hydrocarbons in reservoirs, which are in production since several years, can be ruled out. Whereas (ongoing) biodegradation is well confirmed, only a weak correlation is observed in the cross-plot of *i*/*n*-C_4 vs $\delta^{13}C$ of propane (Fig. 27a).

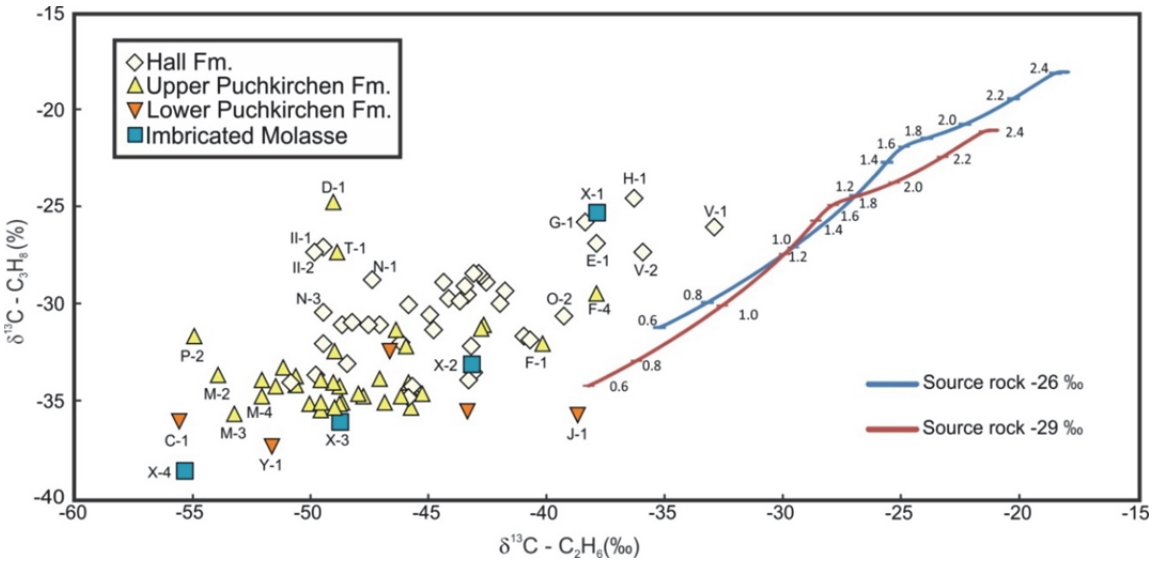

Fig. 26. Relative gas maturity base on $\delta^{13}C$ distribution in ethane and propane (plot modified after Berner & Faber 1996).

A general positive relation exists between the difference of $\delta^{13}C$ of methane and ethane and the $\delta^{13}C$ of propane (Fig. 27b). This may result either from gas mixing or biodegradation. A cross plot of $\delta^{13}C$ of methane versus $\delta^{13}C$ of propane shows two separate trends indicative for mixing and biodegradation of propane, respectively (Fig. 27c).

Recently, biodegradation of hydrocarbons followed by methanogenesis has been recognized as a significant source of (secondary microbial) gas (e.g. Head et al., 2003; Jones et al., 2008; Milkov, 2010; Zengler et al., 1999). The isotopic signature of secondary microbial methane depends on different factors, including the methanogenic community, reaction pathways, progress of alteration, isotopic signature of the substrate, and reservoir temperature (Brown, 2011; Jones et al., 2008). Frequently, secondary microbial methane is accompanied by CO_2 enriched in the ^{13}C isotope (up to 20 ‰) (Milkov, 2011and references therein). Methane depleted in ^{13}C (-65 ‰ or lower) is produced when CO_2 reduction commences, while CO_2 is moderately enriched in ^{13}C isotope (Jones et al., 2008). However, as CO_2 reduction progresses, carbon in both, CO_2 and methane, become heavier. CO_2 concentrations in total gas volume are not necessarily high, since CO_2 can be transformed into calcite cement (Dimitrakopoulos & Muehlenbachs, 1987; Wiggins et al., 1993). Actually, Grundtner et al. (2014) could show that organic matter-derived CO_2 triggering calcite precipitation plays an important role in the diagenetic history of the Alpine Foreland Basin. In the present study, measured $\delta^{13}C$ of CO_2 reaches values up to 18 ‰ with an average value of -5.9 ‰ (Tab. 6, Fig. 27d). Moreover, a general positive relation between $\delta^{13}C$ of CO_2 and C_3H_8 points to methanogenesis (Tab. 6, Fig. 27d). Therefore biodegradation and formation of secondary microbial gas is considered at least as a minor additional source of methane.

Generation of secondary microbial methane results in gas drying. This may explain the relative high dryness values of gas samples with high $\delta^{13}C$ ratios.

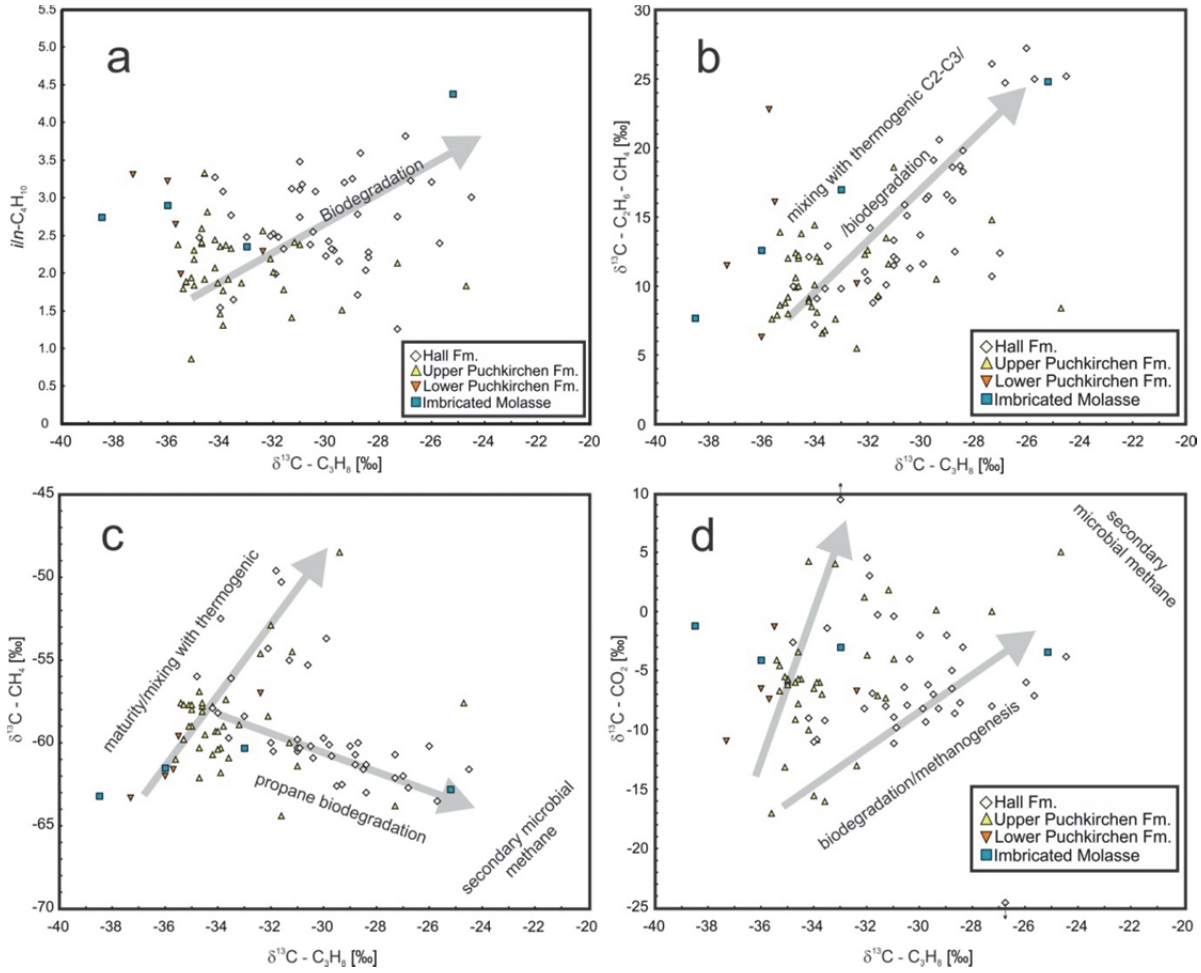

Fig. 27. Correlation of molecular and isotopic composition. Grey arrows indicate possible selective components removal and mixing with thermogenic hydrocarbons.

7. Impact of geothermal fluids on the thermogenic petroleum system

7.1. Chemistry of water samples

Total mineralization (total dissolved solids) of samples measured in the frame of this study varies between 1893.1 mg/l (sample AA2*; Cenomanian reservoir) to 18103.3 mg/l (sample S6*; Eocene reservoir; Tab. 7). To increase the regional coverage of the sample set, selected chemistry/isotope data from industry and Andrews et al. (1987) are included in the interpretation (Tab. 8). Notably, the average salinity of waters from Eocene reservoirs is higher than that of Cenomanian waters (present study: 10559.7 mg/l and 2958.5 mg/l for Eocene and Cenomanian, respectively; industry data: 14164.5 mg/l and 6222 mg/l; published data: 11738.1 mg/l and 2333.5 mg/l; Tabs. 7, 8). However, unusually low salinity water is found in the Eocene reservoir from oil field N* (Tabs. 7, 8), located in the northeastern part of the study area.

The most important dissolved ions are Na^+ and Cl^-. In connate brines these constituents are mainly derived from dissolved halite. To control the quality of samples with respect to possible influence of any reservoir additives used during oil production, the Na^+ and Cl^- concentrations are cross-plotted in Fig. 28. No significant deviation from the sea water dilution line is observed suggesting no influence form reservoir additives. Chlorine which is considered as a conservative constituent is used in further interpretation.

Stable hydrogen and oxygen isotope ratios of water (measured in the frame of this study) from Eocene reservoirs range from -48.3‰ to -12.9‰ and -7.1‰ to 0.6‰ for hydrogen and oxygen, respectively (Tab. 7). The isotopic composition of water from Cenomanian reservoirs range from -51.4‰ to -41.4‰ and -5.8‰ to -4.8‰ for hydrogen and oxygen, respectively.

7.2. Chemistry of oil samples

Oil samples are characterized by abundant *n*-alkanes up to C_{36} (Fig. 29). Because detailed information on biomarkers and stable isotopes based on the C_{15+} fractions has already been presented by Grazer et al. (2011) and Bechtel el al. (2013), the present paper focuses on light hydrocarbons. The dominant light hydrocarbons are *n*-alkanes, albeit cycloalkanes and aromatics are also abundant (Fig. 29a). However, some oils are characterized by progressive depletion or almost entire removal of benzene, toluene, ethylbenzene and xylenes (BTEX) (Fig. 29b). To illustrate this phenomenon, the methylcyclohexane/toluene (Mch/Tol) and cyclohexane/benzene (Ch/B) ratios have been calculated (Tab. 7). Both ratios are cross-plotted in Fig. 30 showing the significant variations of these parameters. Possible primary and secondary processes that govern the mentioned ratios are discussed in the following section.

Tab. 7. Selected hydrocarbon ratios of oil and chemical and isotopic composition of connate water.

Well	Mch/Tol	Ch/B	C15-/C15+	Water chemistry [mg/l]											Water [V-SMOW]	
				Li^+	Na^+	K^+	Mg^{2+}	Ca^{2+}	F^-	Cl^-	Br^-	J^-	NO_3^-	SO_4^{2-}	δ^2H	$\delta^{18}O$
E*	8.3	11.4	4.5													
F*	85.7	257.1	2.6													
G1*	4.5	6.3	3.6													
G2*	3.3	3.8	3.4													
H1*	3.3	4.2	4.2													
H2*	3.8	5.2	4.0													
I1*	5.1	8.9	3.5													
I6*	2.4	2.6	4.0													
J2*	3.3	3.3	3.3													
L1*	19.1	72.1	4.2													
L2*	23.3	174.2	3.3													
L3*	15.5	98.4	3.5													
M*	10.2	28.2	4.3	0.2	1965	12	12	44	8.5	2910	22.2	5.2	0	11		
N1*	83.7	904	2.7													
N2*	79.9	517.3	3.3	0.2	1335	7	7	36	10	1945	13.1	2.2	1	5		
N3*	98.2	40.1	2.2													
N4*	82.7	209.7	2.8	0.6	1626	12	9	25	9	2104	15.2	3.7	0	1		-7.1
O1*	2.4	3.2	3.4	3.2	4357	47	25	215	2.7	6862	59.8	9.9	3	45	-24.6	-0.6
O2*	2.8	3.6	4.2													
P1*	1.7	3	3.8	1.3	6337	51	38	472	6.1	9498	102.4	24.3	0	75		
P2*	1.8	2.3	0.5													
P3*				1.2	4002	58	24	194	2.1	6562	50.4	9.3	1	1	-39.6	-4.3
P4*				0.9	4073	53	20	168	2.3	6769	38.2	7.1	1	22	-39.5	-2.7
P5*	1.9	3	3.9													
P6*	1.9	2.4	4.0													
P7*				1.2	5028	74	29	365	2.8	8804	43	7.6	1	128	-29.1	-3.45
Q2*	3	4.4	5.3													
R*	2.5	5.2	8.1													
S1*	2.1	3.6	3.2													
S2*	2.6	3.4	4.7													
S3*	2.7	3.5	4.8													
S4*	2.4	3.3	5.6	2.4	5926	45	53	212	1.5	9299	74.6	18.2	2		-30.6	-2.2

S5*	2.3	3.7	3.6													
S6*	2.4	3.3	4.9	3	6758	47	84	338	2.1	10748	96.5	24.7	1	2	-23	-0.4
T*	3	6.4	3.1													
U*	6.8	6.4	3.4													
V1*	2.8	4.1	3.5													
V2*	2	2.7	4.9												-23.1	-1.3
V3*	2.2	2.7	5.2												-12.9	0.6
W*	5.8	9.4	3.8													
X*	3.8	6	3.0													
Y1*	6.5	15.7	3.0													
Y2*	6.4	4.4	2.6													
Y3*	9.6	7.7	3.4													
Z*	50.4	88.8	1.9													
AA1*	59.3	130.2	1.6													
AA2*	45.9	30.2	2.1	0.2	929	19	5	17	8.4	888	4.7	1.2	1	19		
AA3*	56.5	38.9	2.4												-51.4	-5.8
AA4*	43.1	30.6	2.2	0.5	1990	30	5	24	0.6	1821	5	1.7	116	30	-41.4	-4.8
AB*	1.7	2.7	3.0								51.2	6.5		159		
AC*	4.5	15	3.0	1.1	4143	83	55	139	2	5823	54	15.1	1	3		
AD1*	3.3	9.8	3.4	2	2681	40	18	49	4.1	3433	26.1	6.8	3	192		
AD2*	2.8	4.9	3.1												-36.5	-2.5
AD3*	3.3	10.3	4.1	2	3117	33	12	20	4.7	4155	31.8	9.1	18	76	-48.3	-4.2
AD4*	6.1	18.5	2.6													
AF*	3.5	4.4	2.7	1.7	4994	41	30	70	1.8	7557	51.2	6.5		159		
AG*	4.6	15.1	4.1													
AH*	2.2	2.9	3.3													
AI*	3.1	9.3	4.3													
AJ*	2	4.9	4.1													

Mch - Methylcyclohexane, Tol - Toluene, Ch - Cyclohexane, B – Benzene, C_{15-}/C_{15+} - ratio of the sum of hydrocarbons with less than 15 carbon atoms over the sum of hydrocarbons with more than 15 carbon atoms

Tab. 8. Chemistry and isotopic composition of reservoir water (industry and literature data).

Well	Water chemistry, industrial data [mg/l]							Water chemistry [mg/l][a]									Water [V-SMOW][a]	
	Na^+	K^+	Mg^{2+}	Ca^{2+}	Cl^-	SO_4^{2-}	HCO_3^-	Na^+	K^+	Mg^{2+}	Ca^{2+}	NH_4^+	Cl^-	HCO_3^-	SO_4^{2-}	SiO_2	δ^2H	$\delta^{18}O$
I1*	6020	186	20	237	9490	397	668											
M*	2660	23	10	67	3673	29	669											
N1*	1160	11	3	18	2011	13	436	1130	11	3	16	4	1570	421	5		-57	-6.5
N2*	1310*	12*	4*	24*	1836 *	11*	479*											
O1*	4600	186	18	295	6730	18	735											
P1*	4790*	75*	31*	383*	7867*	101*	429*											
P2*	2400	2100	22	309	6027													
P3*								3920	68	28	220	9	6494	729	55		-42	-4.4
P5*	4656*	2958*	32*	342*	8456*	102*	521*											
P6*	6300			369	9329													
R*	5622*	76*	62*	325*	8216*	47*	626*	3360	27	20	68	13	4680	1404	110	35	-30	-1.6
S1*	5211*	3874*	63*	720*	11234*	97*	533*											
S2*	7700	66	113	449	12840	9	201											
S3-4*	5211*	3874*	63*	720*	11234*	97*	533*											
S5*	4675	42	34	140	6576	140	647											
S6*	7300	73	45	432	11585	53	273											
T*	4950	54	51	390	7473	153	359											
U*	3562	70	30	271	5388	424	249											
V3*	5450	63	31	242	7764	235	408											
X*	12669	102	112	922	20551	117	414											
Y1*	11117	71	115	731	18124	18	502											
AA1-4*	1081*	394*	3*	21*	1499*	249*	800*	690*	15*	2*	8*	23*	462*	1042*	93*		-63.0*	-8.3*
AB*	3606*	59*	23*	141*	4747*	535*	1142*	2160	62	20	150	11	2720	1019	678	60	-38	-2
AC*	3938	42	31	154	5362	7	761											
AD1*	6200	86	71	469	9182	132	448											
AD3*	6800	96	73	481	9731	79	494											
AD4*	2870	55	19	110	3390	324	1260											
AD1-4*								5744*	93*	67*	320*	123*	9260*	1444*	102*		-20.5*	-1.5*
AF*	6764	67	45	347	10581	111	440	6548	187	41	209	95	10578	954	55		-21	0.2
AI*	1794*	86*	30*	185*	2204*	574*	641*	1410	33	7	31	6	1600	1086	14	56	-57	-6.1
AJ*	1800*	38*	8*	27*	1872*	17*	119*											

[a] data from Andrews et al. (1987), *average salinity and isotopic data from adjacent wells producing from the same formation

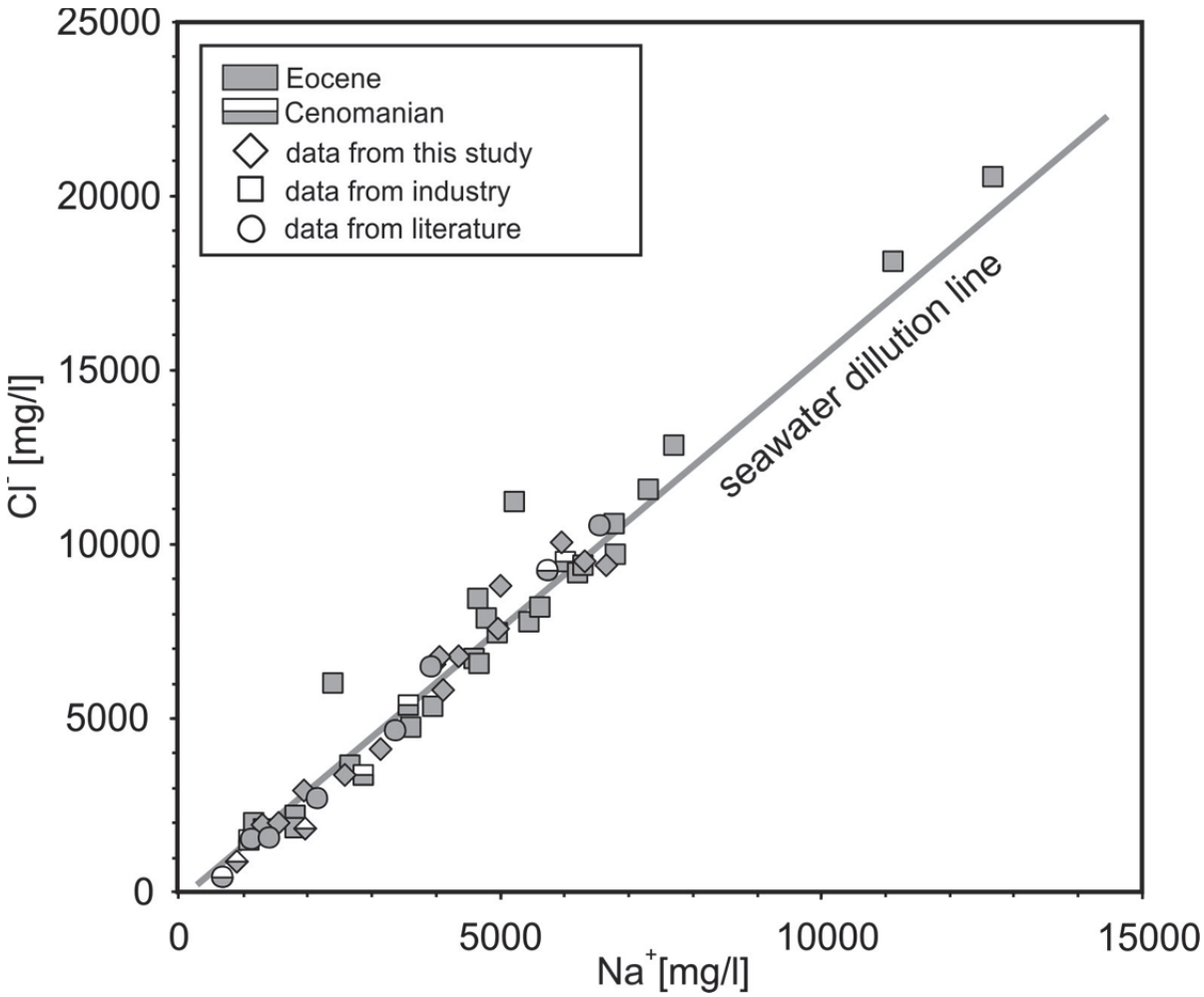

Fig. 28. Cross plot of Na^+ against Cl^- dissolved in the water co-produced with oil. For comparison data from this study are plotted together with industry and literature data. Deviation of the water from the seawater dilution line is probably caused by reservoir additives.

7.3. Possible processes influencing the light hydrocarbon fraction

The observed differences between the light hydrocarbons from different oils (Figs. 29, 30) may originate from natural primary and secondary processes as well as from poor sample handling (e.g. evaporation losses). Therefore it is critical to determine the consequences of each process that can generate compositional differences.

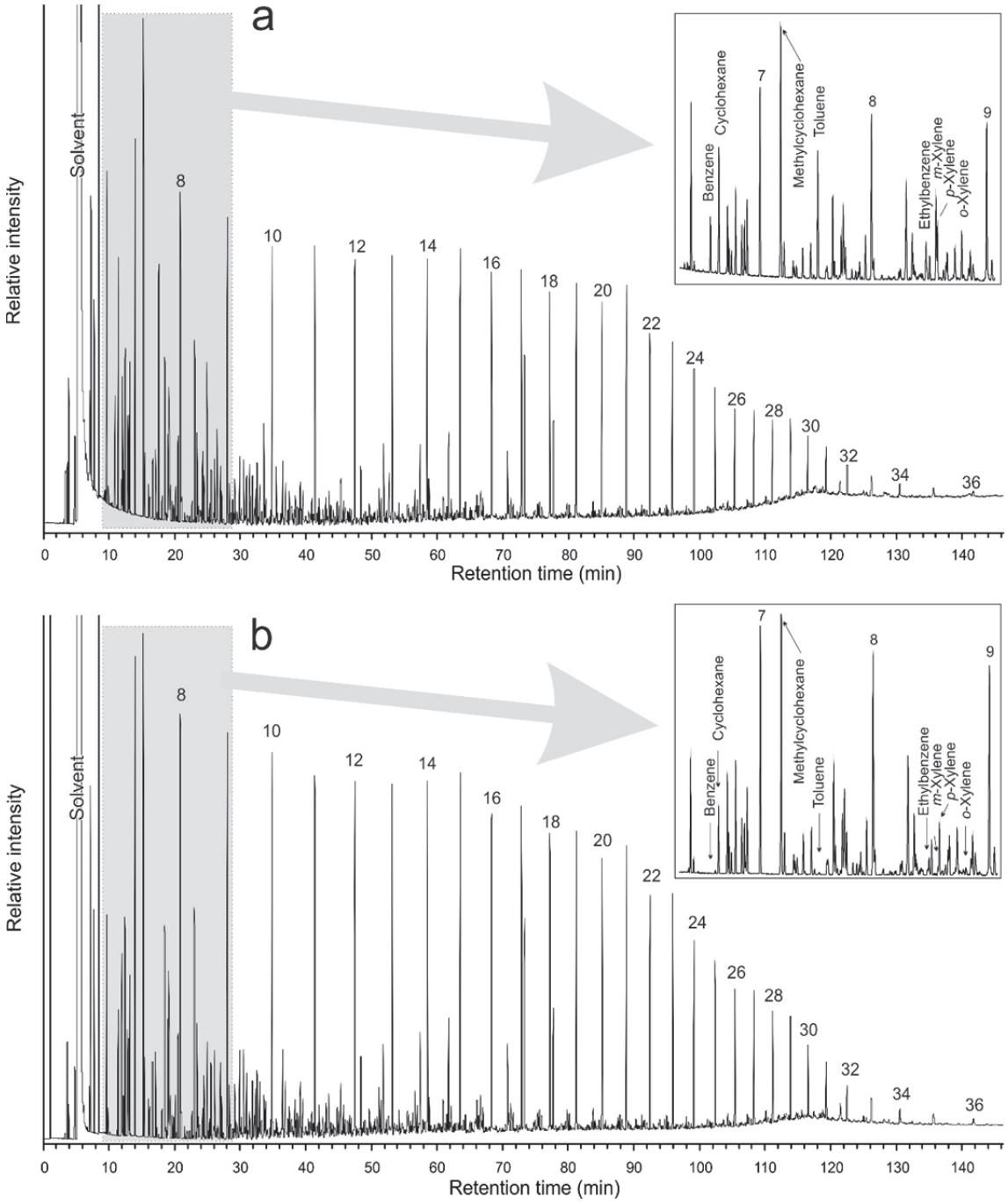

Fig. 29. Gas chromatograms of crude oil samples (a) with abundant BTEX hydrocarbons and (b) with removed or depleted BTEX. *n*-alkanes are labelled according to their carbon number.

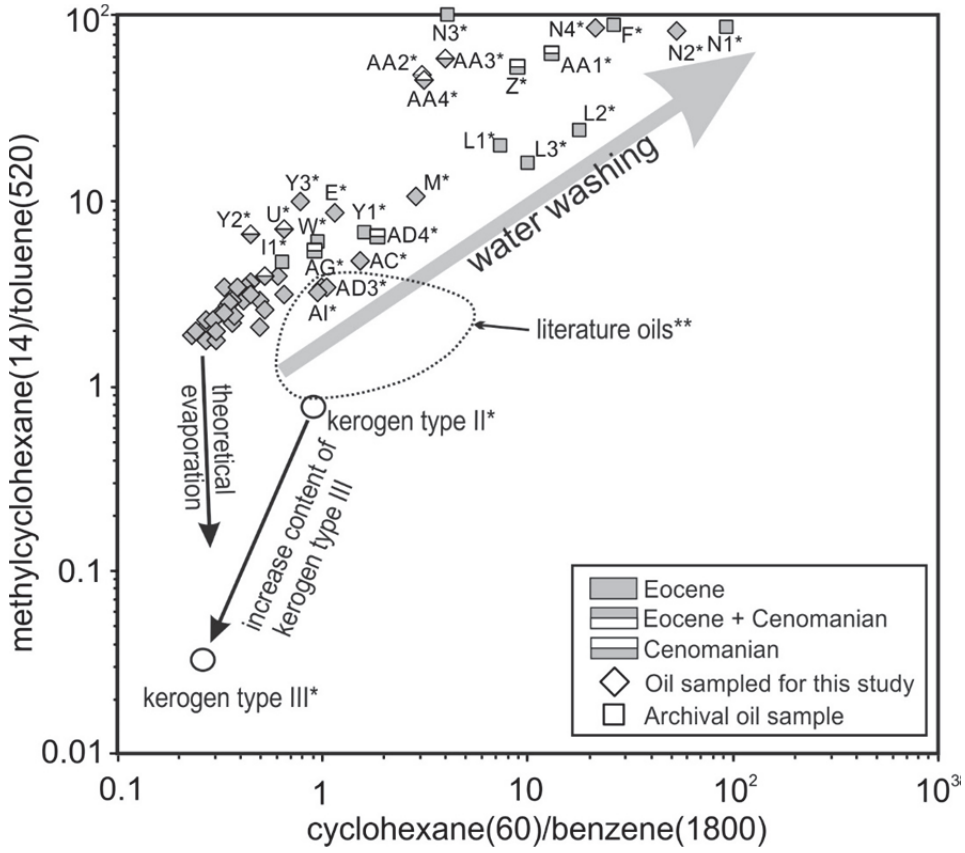

Fig. 30. Cross-plot of the methylcyclohexane/toluene ratio versus the cyclohexane/benzene ratio. Solubilities (mg/l) of different compounds in water are given in brackets. Ratios are calculated from chromatographic peak areas. The theoretical evaporation trend assuming simple mixtures of two compounds is indicated (vapor pressure at 20°C for Mch: 48.3 hPa, Tol: 29.1 hPa, Ch: 104 hPa, B: 100 hPa after GETIS Substance Database). * signature for kerogen type after Schaefer et al. (1983). ** values reported for unaltered oils (Erdman and Morris; 1974; Thompson, 1979; Masterson et al., 2001; Cañipa-Morales et al., 2003; Sharaf & El Nady, 2006; Murillo et al., 2016). For sample location see Fig. 5.

7.3.1. Evaporation losses of light fraction

The current study is based on the quantification of relative volatile hydrocarbons. Therefore, it is critical to discuss the effect of possible losses caused by evaporation during sampling, storage or laboratory handling. Evaporation of hydrocarbons depends on different factors like group type (linear, branched, cyclic, aromatic), isomeric structure, molecular weight and the bulk composition of the sample (Thompson, 1988). However, laboratory controlled evaporation of crude oil showed that this process is primary controlled by differences in boiling points (Cañipa-Morales et al., 2003). Consequently, based on differences in vapor pressure of mixtures of two components (Mch/Tol; Ch/B), it is possible to estimate general evaporation trends. Thus, incidental

loss of light hydrocarbons will result in a strong decrease of the Mch/Tol ratio and a small increase in the Ch/B ratio (see Fig. 30). Hence, evaporation cannot explain the observed strong increase in Mch/Tol and Ch/B ratios, although a minor effect on samples, which have been stored for a long time (archive samples), cannot be ruled out completely.

7.3.2. Influence of source rock facies

Significant differences are observed in generation of hydrocarbons from marine and terrestrial organic matter. Type III kerogen yields predominantly aromatic hydrocarbons (e.g. benzene, toluene) while type I/II kerogen produces more *n*-, iso- and cyclo-alkanes (e.g. Leythaeuser et al., 1979). Moreover, Odden et al. (1998) showed that increasing contents of terrigenous organic matter in source rocks result in higher concentration of aromatics, cyclohexane and methylcyclohexane compared to cyclopentanes and acyclic hydrocarbons. Because the observed trend leads towards higher Mch/Tol and Ch/B ratios, increasing content of coaly facies in source rock can be ruled out (Fig. 30).

7.4. Impact of geothermal fluids on the petroleum system

Light aromatics are more soluble in water than paraffinic hydrocarbons (e.g. Palmer, 1984). Therefore, the obtained positive trend in Fig. 30 is interpreted as selective removal of aromatics during contact with reservoir water. The oil-water interaction can occur during the migration from the source rock to the reservoir and/or after oil accumulation in the reservoir. The longer the migration distance, the higher the potential interaction between oil and water. The lateral migration distance of oil in the Austrian part of the Alpine Foreland Basin varies from less than 20 to more than 50 km (Gratzer et al., 2011; Bechtel et al., 2013). Interestingly, there is no correlation between migration distance and BTEX depletion. For example, samples F* and R* experienced similar migration (~35 km according to Bechtel et al., 2013), but only sample F* is heavily water washed. The same is true for the strongly altered AA1-4* samples and the less affected AC* sample (e.g. Fig. 5). Therefore, the observed water washing phenomenon is probably not a result of longer migration distance. This interpretation is supported by Lafargue & Thiez (1996) and Larter & Alpin (1994), who concluded that migrating oil is in limited contact with water.

A correlation of the degree of water washing with the chemical composition of the reservoir water can be observed in Fig. 31 where the sum of the Mch/Tol and Ch/B ratios is plotted against Cl^- content (Fig. 31a) and stable oxygen and hydrogen isotope values of formation waters (Fig. 31b). Removal of BTEX components increases with decreasing water salinity and isotope ratios of water. The relation between water chemistry and oil properties are discussed in details in section 7.4.1.

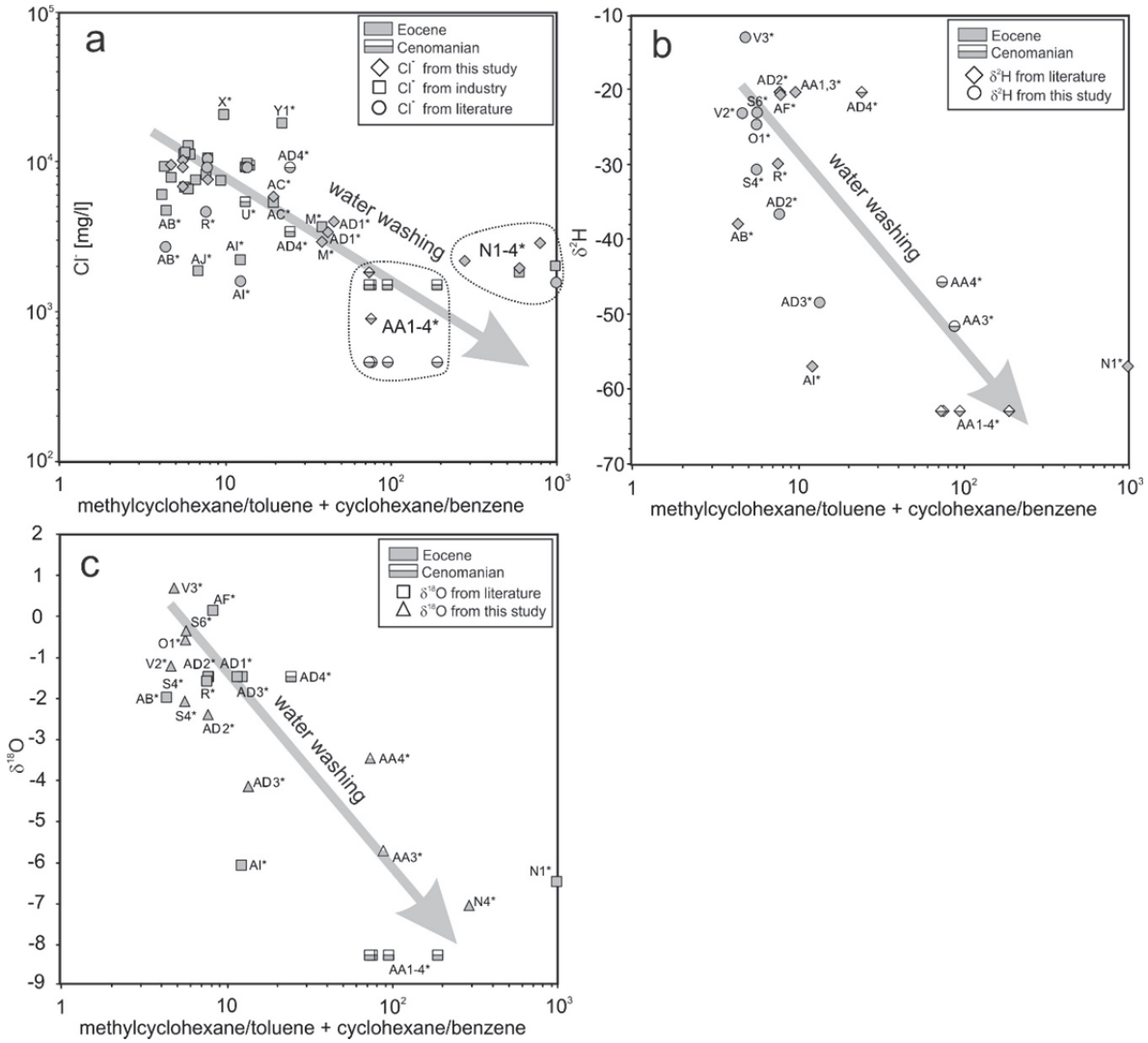

Fig. 31. Cross-plots of the sum of two ratios between cycloalkanes and aromatic hydrocarbons versus (a) chlorine (Cl^-) content in reservoir waters, (b) stable hydrogen isotope ratios of reservoir waters, and (c) stable oxygen isotope ratios of reservoir waters. For sample location see Fig. 5.

7.4.1. Impact of water washing on oil characteristic

Water washing can significantly change oil properties. For example, water washing reduces API gravity, because it is particularly effective for C_{15-} hydrocarbons (Lafargue & Barker, 1988). To test this hypothesis, the ratio of hydrocarbon fractions with less and more than 15 carbon atoms, respectively (C_{15-}/C_{15+}), is cross-plotted versus the sum of two ratios between cycloalkanes and aromatic hydrocarbons in Fig. 32a. It shows that decreasing concentrations of aromatic hydrocarbons correlate fairly well with decreasing contents of light hydrocarbons. This indicates that, to some extent, API gravity of oils form AFB is controlled by water washing. To exclude any effect of losses

of light hydrocarbons during sampling or handling, the C_{15-}/C_{15+} ratio is plotted against industrial API gravity data, obtained during decades of production (Fig. 32b).

In addition, the C_{15-}/C_{15+} ratio is cross-plotted versus the concentration of Cl^- dissolved in co-produced reservoir waters and stable oxygen and hydrogen isotopes of these waters in Fig. 32c, d. Fig. 32c, d shows that oil samples with depleted C_{15-} hydrocarbons are found in reservoirs with low salinity water, characterized by isotopically light hydrogen and oxygen. This clearly indicates a stripping effect of low saline water.

Beside of changes in bulk composition (API gravity) water washing can effectively change the concentration of single compounds. Laboratory experiments showed that the methylphenanthrene index (MPI, Radke et al., 1983), commonly used as maturity indicator, is strongly elevated by water washing (Kuo, 1994). Samples from a field with the lowest API values (AA1-4*) are characterized by a very high MPI value (Gratzer et al., 2011). Therefore, maturity estimates based on MPI values of samples suspected to be water washed have to be used with caution.

Substantial depletion of dibenzothiophene (DBT) during contact with water is emphasized by Lafargue & Barker (1988) and Kuo (1994). Oils from fields located in the western part of study area are typically more sulfur-rich than oils in the eastern part (Gratzer et al., 2011). However oil samples AA1-4*, located in the western part, contain relatively low DBT, compared to other western oil fields. Therefore, water washing may result in a wrong classification of oil families based on sulfur contents and biased interpretations of the source rock facies.

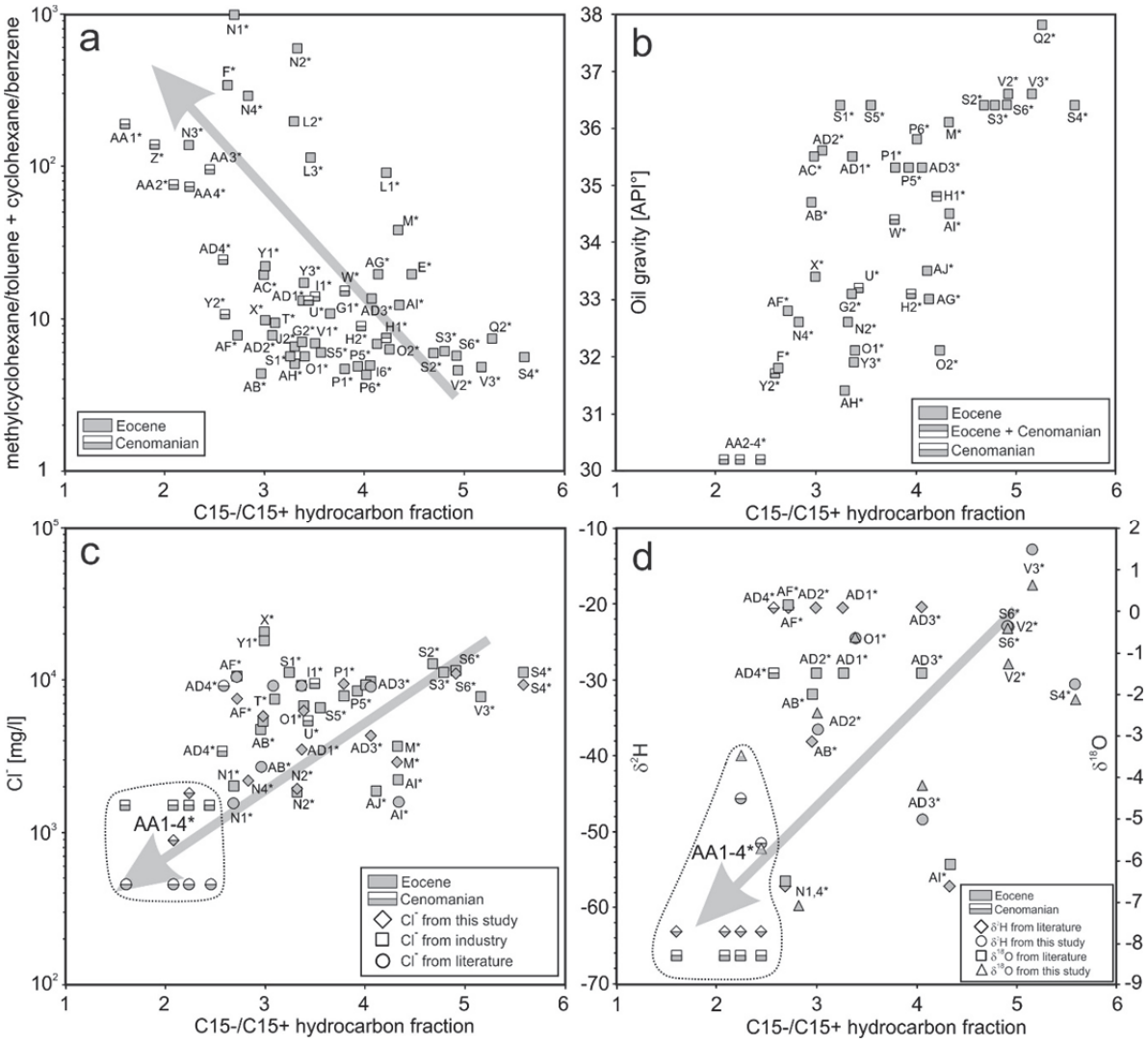

Fig. 32. Cross plots of the ratio of the sum of hydrocarbons with less than 15 carbon atoms over the sum of hydrocarbons with more than 15 carbon atoms (C_{15-}/C_{15+}) versus (a) the sum of two ratios between cycloalkanes and aromatic hydrocarbons, (b) API oil gravity, (c) chlorine content, (d) stable hydrogen and oxygen isotope ratios of reservoir waters. Grey arrows indicate the effect of water washing. For sample location see Fig. 5.

7.4.2. Biodegradation

Water washing requires substantial flow of fresh water. Fresh meteoric water can also introduce microbial communities into oil reservoir, provide oxygen or electron acceptors and inorganic nutrients necessary for microbial activity. Therefore, under favorable geological conditions, both processes are concomitant (e.g. Bailey et al., 1973, Palmer, 1984). Initial biodegradation typically removes C_6-C_{12} *n*-alkanes (Head et al., 2003; Peters et al., 2005), while with proceeding biodegradation aromatic hydrocarbons are utilized in which BTEX are in the first order (Wenger et al., 2002).

The investigated samples are abundant in low molecular *n*-alkanes, but simultaneously depleted in BTEX. Moreover Gratzer et al. (2011) showed that higher *n*-alkanes are major oil constituents. Thus, the selective removal of BTEX components is primarily a result of water washing due to their relatively high solubility in water. However, Gruner et al. (2015) detected intermediate metabolites of hydrocarbon degradation in reservoir water produced from the same fields investigated in the present study. Their results point out that water samples from oil fields affected by water washing contain among others products of BTEX biodegradation. The detected pattern of metabolites is characteristic for those found in initially biodegraded oils under sulphate-reducing conditions (Reuter et al., 1994; Wilkes et al., 2000; internal report). In addition, methane in water washed fields is characterized by unusual stable carbon and hydrogen composition, different to the rest of fields from the study area (Pytlak et al., 2016). Thus, the flow of meteoric water may have triggered very initial biodegradation.

8. Composition of diamondoids in oil samples: potential as indices of source rock facies, maturity and biodegradation

Diamondoids are stable saturated hydrocarbons whose simplest unit is a ten-carbon fused ring cycloalkane molecule known as adamantane (Fig. 33) (Mansoori et al., 2012). The carbon-carbon framework of adamantane can be superimposed on a diamond lattice, and the molecule consists of four connected cyclohexane rings in a "chair" configuration (Fig. 33). A diamondoid with two such fused-ring structures (n = 2) is known as diamantane (Fig. 33), and molecules in which n is up to 11 have been shown to exist in petroleum (Dahl et al., 2003).

Diamondoid hydrocarbons have been found in petroleum (e.g. Landa & Machacek, 1933; Wingert, 1992; Zhang et al., 2015) and also in organic-rich sedimentary rocks including coals (Schulz et al., 2001; Wei et al., 2006b). Due to their cage structure, diamondoids are relatively stable molecules and may therefore become concentrated in an oil during thermal cracking (e.g. Dahl et al., 1999) or as a result of biodegradation (Grice et al., 2000; Wei et al., 2007a). However, diamondoids begin to be destroyed at thermal maturities above 2 %Rr (Fang et al., 2015). It is assumed that diamondoids are products of the thermal alteration of organic matter as they are absent from fresh unconsolidated sediments (Schulz et al., 2001; Wei et al., 2006c).

Experimental studies show that diamondoids can be generated from immature organic-rich material such as peat (Wei et al., 2006c), from kerogen (Wei et al., 2006a), and from crude oils (Fang et al., 2012; Fang et al., 2013) and also from component groups such as saturated, aromatic, resin and asphaltene fractions (Giruts et al., 2006; Giruts and Gordadze, 2007; Fang et al., 2013). They can also be generated from single compounds such as n-alkanes or β-ionane (Gordadze & Giruts, 2008; Berwick et al., 2011). However, the mechanisms of diamondoid generation in sedimentary rocks are not fully understood. Suggested generation pathways include: superacid-catalyzed carbocation rearrangement reactions, i.e. the rearrangement of a carbocation (a molecule in which a carbon atom bears three bonds and a positive charge) from an unstable state to a more stable state via various structural reorganizational "shifts" within the molecule (e.g. Petrov et al., 1974; Sorenson & Whitworth, 1990); carbon surface reactions (Berwick et al., 2011); high temperature cracking of high molecular mass fractions (Giruts et al., 2006; Giruts & Gordadze, 2007); and synthesis of higher diamondoids from lower diamondoids (Dahl et al., 2010). Carbocation rearrangement reactions occur in nature only in the presence of aluminosilicates (Petrov, 1987). Wei et al. (2006a;

2006c) concluded that clay minerals have a catalyzing effect on diamondoid formation, whereas calcite has inhibiting properties. However, diamondoid hydrocarbons have been detected in crude oils sourced from carbonate rocks (Schulz et al., 2001).

Based on the assumption that bridgehead-alkylated diamandoids (i.e. those with an alkyl substituent at the bridgehead carbon atom: see Fig. 33) are thermodynamically more stable than diamandoids with a substituent at a secondary position (Clark et al., 1979), a number of diamondoid-based isomerization indices have been proposed to determine the maturity of a petroleum (e.g. Chen et al., 1996; Zhang et al., 2005). By contrast, other authors have found that diamondoids are of limited applicability as a maturity parameter, and have proposed that diamondoid composition is controlled by the mineral composition and depositional environment of the source rocks (e.g. Li al., 2000; Schulz et al., 2001; Wei et al., 2006a, 2006c, 2007b; Fang et al., 2013, 2015).

The aim of this chapter is to investigate the applicability of diamondoids as a maturity or source rock parameter, with reference to the analysis of oil samples derived from the Austrian sector of the Alpine Foreland Basin (Fig. 34). This basin was chosen because an abundance of geochemical data is available which has been used in previous studies to define oil families (Fig. 34a), for maturity assessments, and for oil-source rock correlations (Gratzer et al., 2011; Bechtel et al., 2013) (Fig. 35).

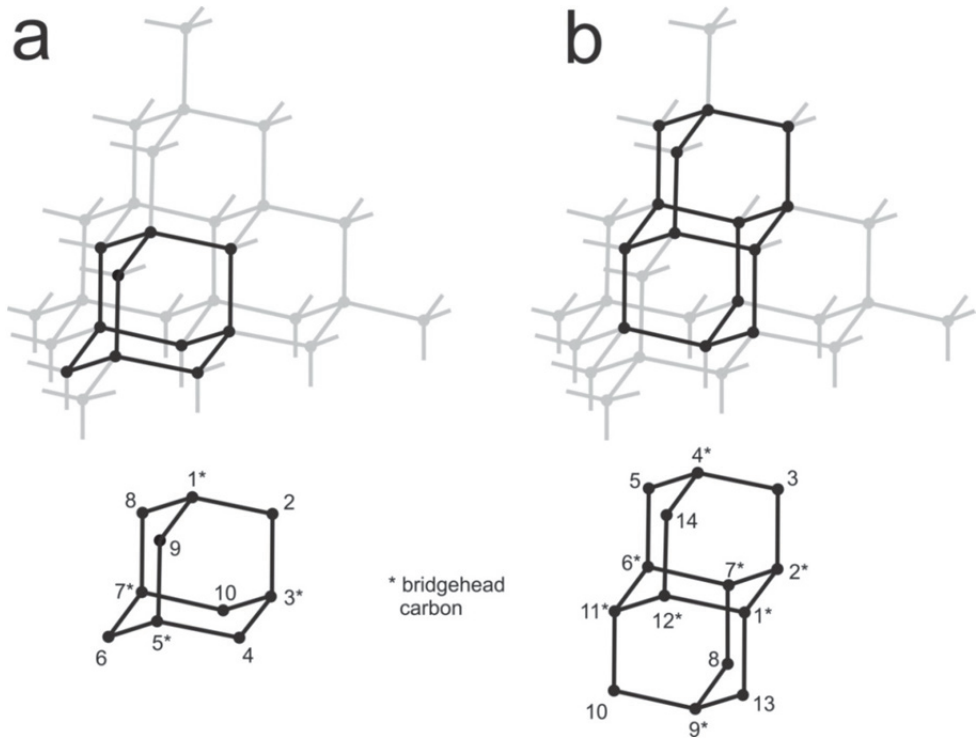

Fig. 33. Schematic diagrams showing the relationship between the lattice diamond structure and the molecular structures of (a) adamantane and (b) diamantane.

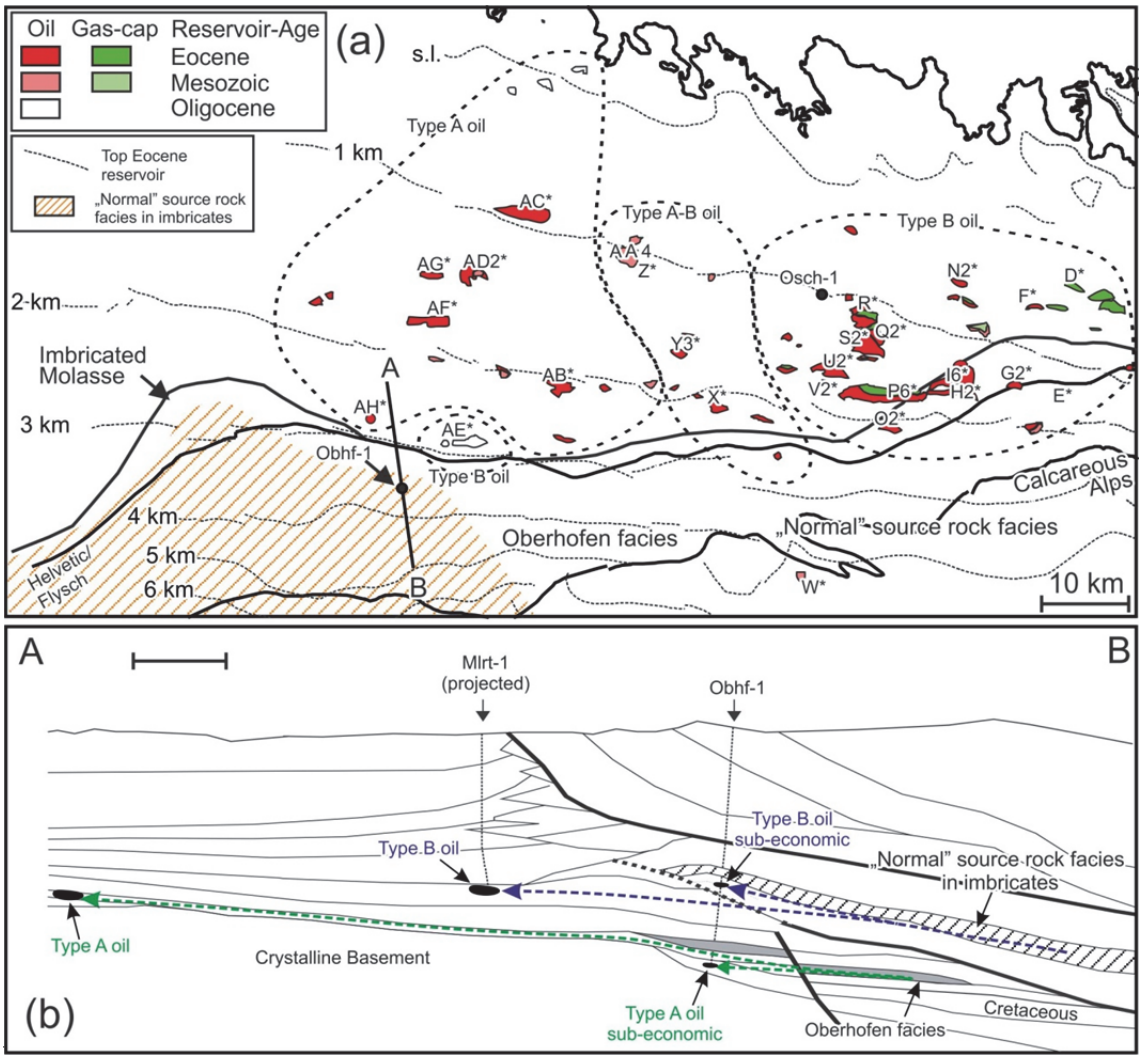

Fig. 34. (a) Distribution of oil fields in the study area together with the locations from which samples were collected. Types of petroleum and source rock facies are after Sachsenhofer & Schulz (2006) and Gratzer et al. (2011), respectively. Cross section A-B is shown in Fig. 34b. (b) North-south cross section through the Alpine foldbelt and adjacent foreland basin illustrating source rock facies, oil types and migration pathways (after Gusterhuber et al., 2014).

8.1. Molecular composition

Diamondoid hydrocarbons are present in all the saturated fractions of the fresh oils analysed (Tab. 9, Fig. 36). Concentrations of adamantanes and diamantanes range between 1.3 and 15.7 ppm and 0.2 and 5.3 ppm, respectively (Tab. 9). In sample W* from the far south of the study area (Fig. 34a), only three types of diamantane were detected. By contrast diamondoids were enriched in sample D* from the NE of the study area (Fig. 34a) (sum of adamantanes and diamantanes = 17.8 ppm, Tab. 9), which is heavily biodegraded (Gratzer et al., 2011) as indicated by almost complete removal of

saturated and aromatic compounds (Fig. 37), and the relatively low API gravity (Tab. 3). Enrichment of diamondoids during biodegradation has previously been described by Grice et al. (2000) and Wei et al. (2007a). Diamondoids are also enriched in sample AJ*, but because this sample is not biodegraded, the process of diamondoid enrichment in this case is not understood.

The stigmastane (5,14α,17α,(H)-24- ethylcholestane 20R) concentration in the samples analysed ranges between 1.41 ppm and 25.83 ppm (average 8.91 ppm; Tab. 9), and the Ts/Tm ratio between 0.66 and 4.74 (average 1.29; Tab. 9). These values are slightly higher than those reported by Gratzer et al. (2011), probably caused by differences in analytical methods.

8.2. Isomerization indices

Chen et al. (1996) and Zhang et al. (2005) proposed various isomerization indices for diamondoids (Tab. 10). These indices are ratios in which diamondoids with different numbers of alkyl substituents at the bridgehead position are both numerators and denominators (Tab. 10, Fig. 33). The values of the indices vary over a wide range, but different indices are correlated when plotted against each other (Fig. 38). Isomerization indices where numerators and denominators are diamondoids with the same number of alkyl substituents at the bridgehead position (e.g. TMAI-3, TTMAI: see Tab. 10 for formulae) show close correlation with each other and with the indices of Chen et al. (1996) and Zhang et al. (2005), which have substituents attached to a secondary position. Therefore, the ratios of diamondoids with alkyl groups attached to a bridgehead position versus those with substituents attached to a secondary position are controlled by the same factors as the ratio of diamondoids with the same number of secondary or bridgehead substituents but at different positions (TMAI-3, TTMAI, Fig. 33).

8.3. Molecular ratios

The studied samples show positive correlations when individual isomerization indices such as MAI, DMAI- 2, TMAI-1, DMD1-2 and EAI-1 are plotted versus total diamondoids yields in ppm (Fig. 39a), and also versus the ratio of diamantanes / adamantanes (Fig. 39b).

Previous studies (Wei et al., 2007b; Gordadze, 2008; Fang et al., 2012, 2013, 2015) have interpreted this observation to reflect increasing thermal stress over the maturity interval <2%Rr, and the generation of diamantanes at generally higher maturities than adamantanes. At maturity levels >2%Rr, the thermal destruction of diamondoids will result in a decrease of the diamondoid yield (Fang et al., 2015).

Values of diamondoid ratios proposed by Fang et al. (2013) and Fang et al. (2015) (e.g. methyladamantane/methyldiamantane, dimethyladamantane/dimethyldiamantane, trimethyladamantane/dimethyldiamantane) have a negative correlation with the isomerization indices (Fig. 39c, d). Laboratory experiments performed by the above-mentioned authors showed that this may indicate high thermal maturities (>2%Rr), at which non-bridgehead substituted diamondoids are destroyed leading to the enrichment of more stable, bridgehead-substituted diamondoids. However, this is not the case in the current sample set where the positive correlation between isomerization indices and diamondoids yields (Fig. 39a) indicates a maturity of <2%Rr.

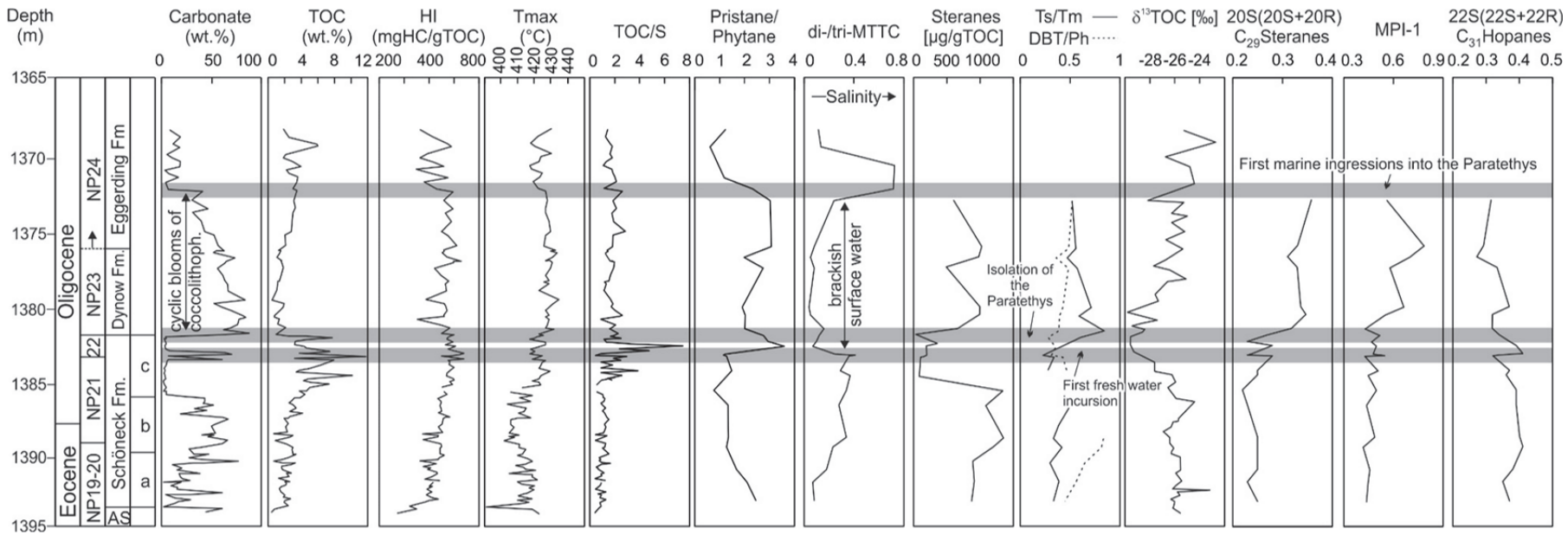

Fig. 35. Bulk geochemical and palaeogeographic proxy data (biomarkers, stable isotopes) in the Lower Oligocene succession in borehole Osch-1 after Schulz et al. (2002; borehole location in Fig. 34a). Inferred palaeogeographic changes are shown after Schulz et al. (2005). TOC – total organic carbon content (after acidification of sample to remove the carbonate), S – total sulphur, HI – hydrogen index, Tmax – temperature at which the maximum rate of hydrocarbon generation occurs, inferred from Rock-Eval pyrolysis, MTTC – methyltrimethyltridecylchroman. Dibenzothiophene/phenanthrene (DBT/Ph), Ts/Tm, C29 steranes isomerization, MPI-1 and C31 hopane isomerization ratios have been added. AS, Ampfing Sandstone.

Tab. 9. Concentration of diamondoids and geochemical parameters of oil from wells producing oil and associated gas. For location see Figs. 5, 34a. For diamondoids assigments see Fig. 36.

Well	DBT / Ph[1]	Stigm.[2]	Ts/Tm[3]	$\delta^{13}C$ *n*-C_{15-31}[4]	Adamantanes [ppm]																
					1	2	3	4	5	6	7	9	10	11	12	13	14	15	16	18	19
D*	0.21	4.76	1.71	n.a.	0.659	1.584	3.096	0.985	1.163	1.256	1.241	0.252	0.584	0.644	0.586	1.070	0.271	0.076	0.432	0.254	1.506
E*	0.22	4.45	1.35	n.a.	0.795	1.183	2.524	0.538	0.701	0.740	0.858	0.115	0.280	0.305	0.282	0.506	0.122	0.036	0.213	0.147	1.080
F*	0.16	5.43	1.36	-31.33	0.372	0.547	1.463	0.261	0.427	0.488	0.562	0.057	0.165	0.194	0.165	0.330	0.068	0.021	0.147	0.079	0.656
G2*	0.20	10.28	1.08	-31.22	0.335	0.499	1.142	0.237	0.329	0.365	0.408	0.052	0.136	0.148	0.133	0.269	0.055	0.018	0.113	0.059	0.474
H2*	n.a.	16.44	1.08	-31.06	0.303	0.383	1.080	0.168	0.310	0.374	0.471	0.037	0.120	0.139	0.114	0.262	0.045	0.015	0.117	0.047	0.487
I6*	0.17	10.36	1.49	-31.15	0.288	0.514	1.250	0.275	0.381	0.399	0.479	0.069	0.161	0.179	0.156	0.309	0.076	0.022	0.130	0.075	0.568
N2*	0.21	8.66	1.30	-30.91	0.278	0.516	0.965	0.294	0.316	0.355	0.393	0.073	0.153	0.156	0.148	0.266	0.066	0.019	0.108	0.064	0.424
O2*	n.a.	10.68	1.51	-31.69	0.184	0.197	0.613	0.086	0.167	0.208	0.258	0.018	0.064	0.073	0.059	0.166	0.022	0.008	0.065	0.022	0.286
P6*	n.a.	2.72	1.52	-31.07	0.100	0.160	0.298	0.078	0.093	0.101	0.106	0.020	0.040	0.043	0.038	0.075	0.019	0.005	0.032	0.018	0.123
Q2*	0.21	6.85	1.32	-31.30	0.799	1.574	2.248	0.808	0.772	0.781	0.858	0.192	0.343	0.363	0.332	0.521	0.159	0.042	0.198	0.153	0.788
R*	0.19	5.62	1.37	-30.92	0.865	1.670	2.270	0.825	0.750	0.787	0.889	0.188	0.334	0.351	0.318	0.496	0.149	0.040	0.188	0.142	0.769
S2*	0.19	6.97	1.21	-30.32	0.626	1.205	1.737	0.618	0.566	0.597	0.614	0.142	0.256	0.270	0.247	0.395	0.122	0.030	0.157	0.119	0.610
U*	0.20	11.28	1.15	n.a.	0.649	1.295	1.970	0.696	0.698	0.700	0.764	0.166	0.312	0.325	0.292	0.488	0.150	0.039	0.199	0.143	0.749
V2*	0.21	8.15	1.20	-30.55	0.735	1.333	2.094	0.661	0.637	0.686	0.722	0.152	0.288	0.298	0.278	0.483	0.131	0.034	0.185	0.139	0.729
W*	0.29	1.57	4.74	-31.72	0.404	0.480	1.354	0.213	0.408	0.410	0.514	0.046	0.134	0.157	0.134	0.291	0.053	0.018	0.115	0.067	0.602
X*	0.28	23.97	0.79	-30.51	0.314	0.459	0.979	0.236	0.275	0.344	0.389	0.062	0.118	0.113	0.099	0.224	0.046	0.013	0.084	0.038	0.439
Y3*	n.a.	25.83	0.74	-30.31	0.240	0.381	0.645	0.210	0.187	0.256	0.257	0.059	0.091	0.085	0.078	0.157	0.036	0.009	0.063	0.022	0.284
Z*	0.40	7.69	1.30	n.a.	0.380	0.867	1.359	0.515	0.439	0.496	0.518	0.133	0.233	0.251	0.223	0.382	0.118	0.033	0.160	0.099	0.566
AA4*	n.a.	6.84	1.19	-30.27	0.341	0.756	1.153	0.432	0.409	0.436	0.464	0.110	0.188	0.194	0.180	0.291	0.090	0.023	0.116	0.076	0.473
AB*	0.37	1.41	1.08	-30.42	0.449	0.576	1.409	0.268	0.401	0.441	0.521	0.066	0.154	0.164	0.135	0.289	0.062	0.019	0.124	0.070	0.599
AC*	0.44	4.91	1.10	-30.40	0.326	0.548	1.108	0.302	0.320	0.353	0.441	0.081	0.142	0.139	0.128	0.253	0.065	0.017	0.110	0.061	0.478
AD2*	n.a.	7.75	0.81	-30.32	0.564	0.963	1.533	0.506	0.443	0.487	0.544	0.128	0.193	0.173	0.169	0.307	0.088	0.021	0.123	0.080	0.574
AF*	0.41	4.90	0.66	-29.71	0.244	0.394	0.690	0.202	0.220	0.232	0.267	0.056	0.089	0.091	0.076	0.161	0.039	0.011	0.065	0.034	0.287
AG*	0.49	6.57	1.03	-30.61	0.446	0.722	1.103	0.369	0.335	0.367	0.337	0.097	0.133	0.121	0.108	0.206	0.058	0.015	0.081	0.053	0.388
AH*	0.21	10.82	0.99	n.a.	0.702	1.033	1.729	0.532	0.500	0.609	0.739	0.133	0.191	0.175	0.153	0.343	0.073	0.020	0.124	0.060	0.750
AI*	0.50	8.70	1.07	-29.85	0.775	1.492	1.742	0.817	0.590	0.658	0.600	0.215	0.294	0.246	0.219	0.331	0.135	0.027	0.131	0.089	0.560
AJ*	0.48	16.89	0.77	n.a.	1.315	2.242	3.320	1.226	1.043	1.139	1.228	0.314	0.426	0.393	0.353	0.598	0.185	0.043	0.223	0.159	1.221

Tab. 9. Continuation

Well	Diamantanes [ppm]						
	22	23	24	25	26	28	29
D*	0.150	0.418	0.171	0.847	0.085	0.116	0.387
E*	0.098	0.216	0.070	0.361	0.035	0.042	0.122
F*	0.061	0.141	0.036	0.212	0.020	0.046	0.091
G2*	0.044	0.112	0.031	0.168	0.015	0.040	0.064
H2*	0.051	0.141	0.064	0.141	0.046	0.052	0.055
I6*	0.110	0.250	0.069	0.319	0.035	0.070	0.129
N2*	0.083	0.192	0.068	0.257	0.035	0.052	0.094
O2*	0.026	0.064	0.011	0.074	0.008	0.038	0.084
P6*	0.025	0.054	0.019	0.075	0.011	0.022	0.029
Q2*	0.202	0.482	0.167	0.609	0.082	0.100	0.225
R*	0.192	0.429	0.157	0.562	0.077	0.108	0.219
S2*	0.158	0.344	0.133	0.476	0.066	0.092	0.189
U*	0.190	0.405	0.180	0.623	0.091	0.085	0.228
V2*	0.200	0.429	0.139	0.567	0.081	0.100	0.212
W*	0.034	0.108	n.d.	0.147	n.d.	n.d.	n.d.
X*	0.117	0.236	0.057	0.212	0.041	0.081	0.086
Y3*	0.092	0.246	0.052	0.170	0.035	0.073	0.079
Z*	0.191	0.453	0.165	0.564	0.116	0.105	0.233
AA4*	0.155	0.380	0.129	0.434	0.086	0.090	0.166
AB*	0.108	0.402	0.061	0.254	0.037	0.068	0.079
AC*	0.178	0.528	0.111	0.392	0.073	0.093	0.133
AD2*	0.260	0.628	0.152	0.493	0.098	0.111	0.178
AF*	0.109	0.276	0.068	0.224	0.044	0.061	0.070
AG*	0.203	0.464	0.121	0.414	0.083	0.104	0.152
AH*	0.311	0.630	0.146	0.507	0.121	0.116	0.215
AI*	0.264	0.580	0.147	0.495	0.100	0.114	0.175
AJ*	0.702	1.687	0.416	1.468	0.284	0.255	0.501

[1] After Gratzer et al. (2011), [2] concentration (ppm) of stigmastane (5α,14α,17α,(H)-24-ethylcholestane 20R) monitored the m/z 400 →217 ion transitions, calculated from m/z 400 → 217 ion transitions of internal standard (5β(H)cholane), [3] Ts/Tm ratio monitored by m/z 370 →191 ion transitions, [4] average values of $\delta^{13}C$ of $C_{16\text{-}31}$ *n*-alkanes after Bechtel et al. (2013), n.a. - not analyzed, n.d. – not detected due to low peak intensity

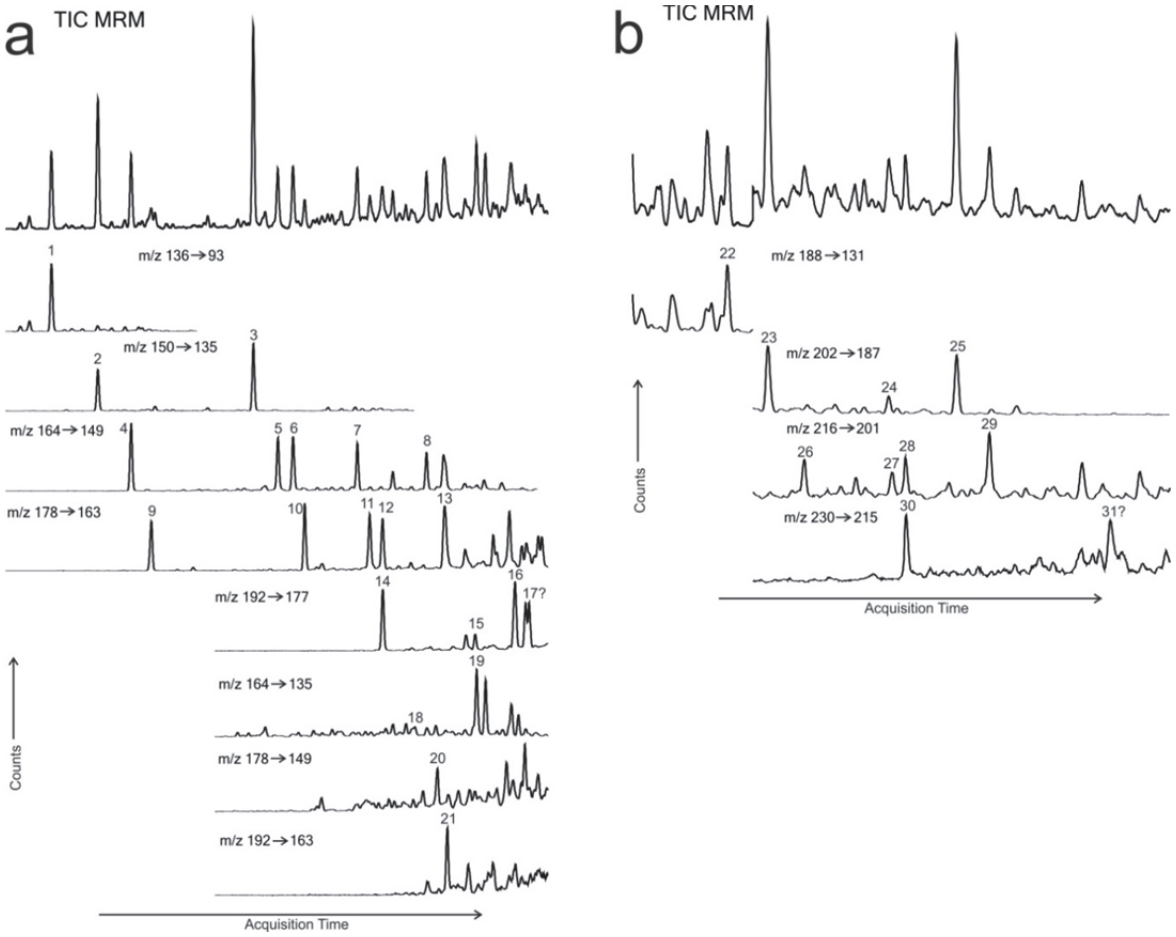

Fig. 36. GC-MS-MS chromatograms of diamondoids in sample V2* from the study in the Alpine Foreland Basin (sample location in Figs. 5, 34a; data in Table. 9): (a) adamantanes, (b) diamantanes. Parent-daughter chromatogrames are autoscaled to the highest peak.

Peak assignments:

1 - Adamantane, 2 - 1-Methyladamantane, 3 - 2-Methyladamantane,
4 - 1,3-Dimethyladamantane, 5 - 1,4-Dimethyladamantane(cis),
6 - 1,4-Dimethyladamantane(trans), 7 - 1,2-Dimethyladamantane,
8 - 2,6+2,4-Dimethyladamantane, 9 - 1,3,5-Trimethyladamantane,
10 - 1,3,6-Trimethyladamantane, 11 - 1,3,4-Trimethyladamantane(cis),
12 - 1,3,4-Trimethyladamantane(trans), 13 - 1,2,3-Trimethyladamantane,
14 - 1,2,5,7-Tetramethyladamantane, 15 - 1,3,5,6-Tetramethyladamantane,
16 - 1,2,3,5-Tetramethyladamantane, 17 - 1-Ethyl-3,5,7-Trimethyladamantane,
18 - 1-Ethyladamantane, 19 - 2-Ethyladamantane,
20 - 1-Ethyl-3-Methyladamantane, 21 - 1-Ethyl-3,5-Dimethyladamantane,
22 – Diamantane, 23 - 4-Methyldiamantane, 24 - 1-Methyldiamantane,
25 - 3-Methyldiamantane, 26 - 4,9-Dimethyldiamantane,
27 - 1,4+2,4-Dimethyldiamantane, 28 - 4,8-Dimethyldiamantane,
29 - 3,4-Dimethyldiamantane, 30 - 1,4,9-Trimethyldiamantane,
31 - 3,4,9-Trimethyldiamantane.

Tab. 10. Isomerization indices of diamondoids determined by GC-MS-MS analyses.

Index	Formula (%)[1]	Reference
MAI	2/(2+3)	Chen et al., 1996
MDI	23/(23+24+25)	Chen et al., 1996
EAI-1	18/(18+19)	Zhang et al., 2005
DMAI-1	4/(4+7)	Zhang et al., 2005
DMAI-2	4/(4+5+6)	Zhang et al., 2005
TMAI-1	9/(9+10)	Zhang et al., 2005
TMAI-2	9/(9+11+12)	Zhang et al., 2005
TMAI-3	10/(10+13)	present study
DMDI-1	26/(26+29)	Zhang et al., 2005
DMDI-2	26/(26+28)	Zhang et al., 2005
TTMAI	14/(14+16)	present study

[1] numbers indicate peaks from Fig. 36For peak assignments see Fig. 36.
Key:
2. 1-Methyladamantane,
3. 2-Methyladamantane,
4. 1,3-Dimethyladamantane,
5. 1,4-Dimethyladamantane(cis),
6. 1,4 Dimethyladamantane(trans),
7. 1,2-Dimethyladamantane,
9. 1,3,5-Trimethyladamantane,
10. 1,3,6 Trimethyladamantane,
11. 1,3,4-Trimethyladamantane(cis),
12. 1,3,4-Trimethyladamantane(trans),
13. 1,2,3 Trimethyladamantane,
14. 1,2,5,7-Tetramethyladamantane,
16. 1,2,3,5-Tetramethyladamantane,
18. 1-Ethyladamantane,
19. 2-Ethyladamantane,
23. 4-Methyldiamantane,
24. 1-Methyldiamantane,
25. 3-Methyldiamantane,
26. 4,9-Dimethyldiamantane,
28. 4,8-Dimethyldiamantane,
29. 3,4-Dimethyldiamantane.

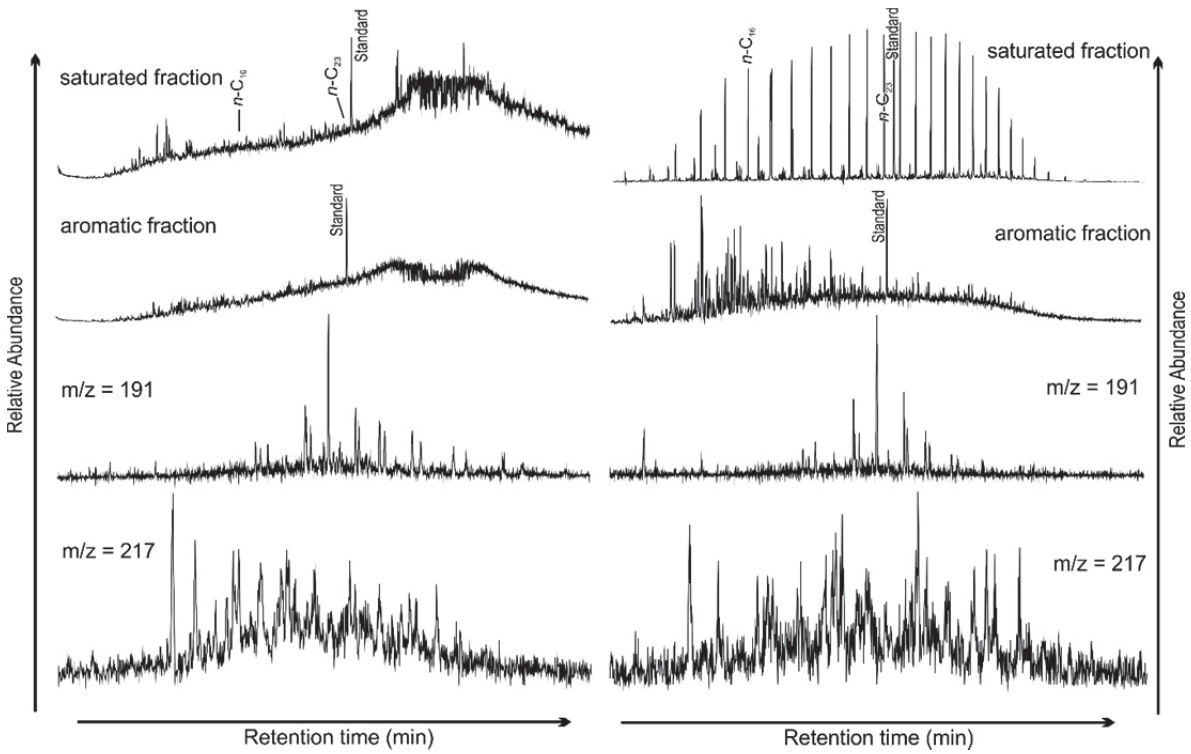

Fig. 37. Chromatograms (Total Ion Current) of the saturated and aromatic hydrocarbon fractions, *m/z* = 191 and 217 of crude oil samples D* (left) and AB* (right) (sample locations in Figs. 5, 32a) *n*-Alkanes are labeled according to their carbon number. Standard for aromatic and saturated fractions = 1,1' binaphtyl and deuterated tetracosane, respectively. Sample D* is interpreted to be highly biodegraded.

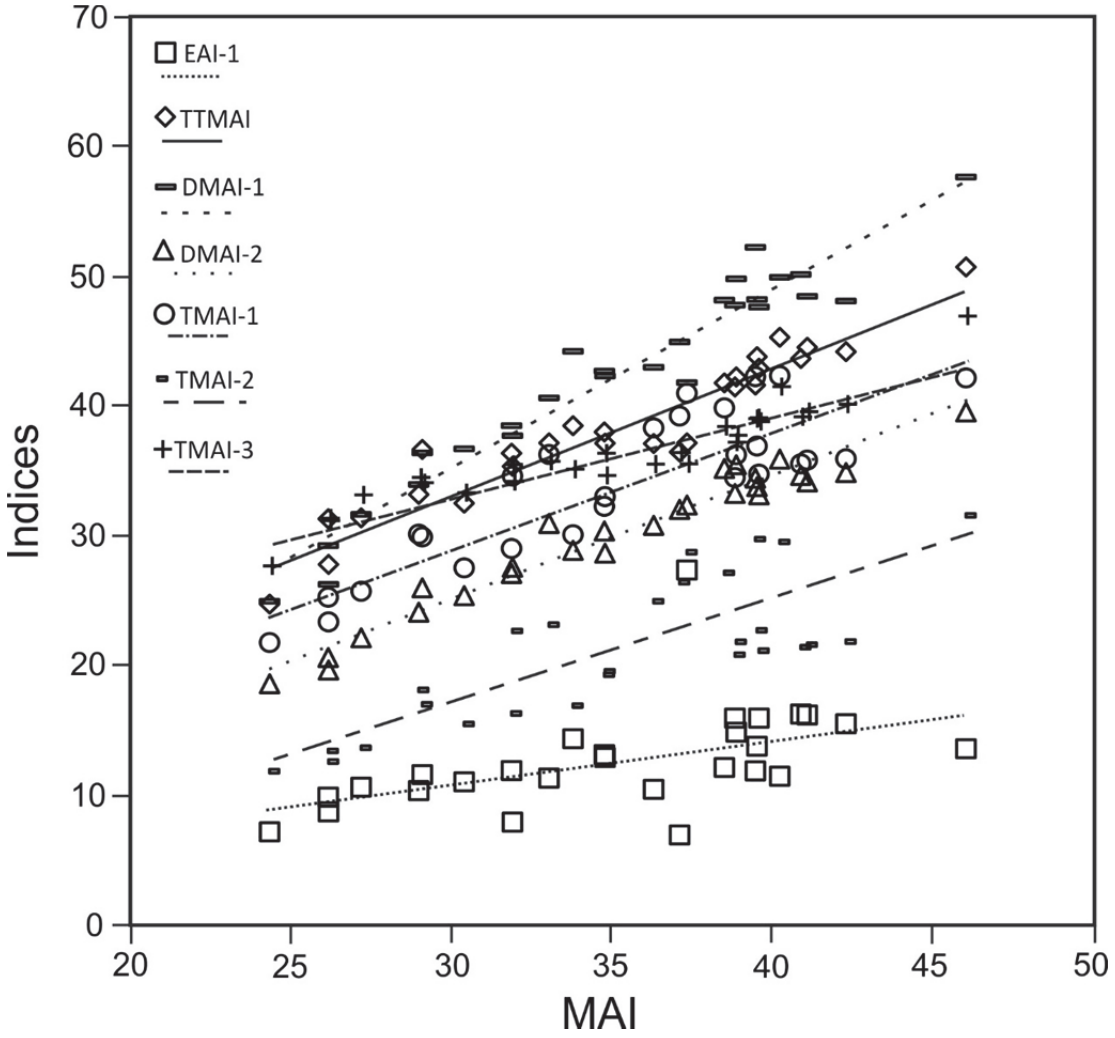

Fig. 38. Cross-plot of the MAI diamondoid index versus other adamantane-derived isomerization indices for the oil samples analysed (see Table 10 for the formulae used to calculate the indices).

8.4. Correlation with maturity-related parameters

In general, diamondoid isomerization indices in the studied samples do not show convincing relationships with either aliphatic nor aromatic maturity parameters (e.g. ratios of C29 sterane and C31 hopane isomerization, hopane/moretane ratio, or MPI-1: Fig. 40a-d). However, Fig. 35 shows that some maturity parameters are also facies dependent. For example, sterane isomerization and MPI-1 in general increase upwards in the borehole succession at Osch-1 (Fig. 35), while hopane isomerization decreases slightly in the same direction. Consequently, with the exception of MPI-1 which shows a slight correlation with the Ts/Tm ratio, aliphatic and aromatic maturity parameters in the oil samples do not show good correlation when plotted against each other. However, EAI-1 shows a reasonable positive correlation with MPI-1 (Fig. 40d).

Laboratory experiments show that diamondoids-related indices do not reflect the thermal stress at maturities up to 1.3%Rr (Wei et al., 2007) or 1.7%Rr (Fang et al., 2012, 2013, 2015). However, higher maturity would lead to cracking of major oil constituents (as well as biomarkers) and enrichment of diamondoids (i.e. the progressive concentration of diamondoids during cracking of less stable hydrocarbons), as described by Dahl et al. (1999) and later observed by Azevedo et al. (2008), Springer et al. (2010) and Zhang et al. (2015). In the present data, no correlation was observed in a cross-plot (Fig. 41) between stigmastane (Tab. 9) and the sum of 3+4-methyldiamantane (Tab. 9). This suggests that the analysed oils have not undergone intense cracking of major substituents.

The specificity of many biomarker-related parameters is limited to early mature/mature stages of organic matter transformation (e.g. hopane isomerization). Therefore, the direct correlation of maturity parameters based on biomarkers or other specific compounds with diamondoid isomerization indices does not show a convincing correlation.

Alternatively, the mature oils may mix with more highly mature oils (condensates) generated by the cracking of kerogen. Source rocks at higher maturity levels would generate oils with progressively higher contents of light (C1-C4) hydrocarbons, increasing the API gravity of the final mixture. In order to investigate this, the API gravities, C7 maturity-related parameters and stable carbon and hydrogen isotopic composition of ethane, propane, *n*-butane and *n*-pentane are plotted versus diamondoid isomerization indices in Fig. 40e-i. Although API gravity can be strongly influenced by vertical/horizontal migration and alteration processes, a notable correlation between API gravity and EAI-1 can be observed in Fig. 40g. There is also a good correlation between EAI-1 and the maturity parameters derived from light hydrocarbons (Fig. 40e,f). It is important to note that EAI-1 correlates very well with the isotopic composition of gaseous hydrocarbons (which are dissolved in the investigated oil samples) (Fig. 40h, i). According to the model of Berner & Faber (1996), the most negative $\delta^{13}C$ values measured from ethane and propane corresponds to a thermal maturity equivalent to a vitrinite reflectance of 1-1.2% Rr. Because EAI-1 correlates with different parameters (including the aromatic and C7 fraction, the isotopic composition of gaseous hydrocarbons, and the API gravities), it appears to be a good maturity indicator.

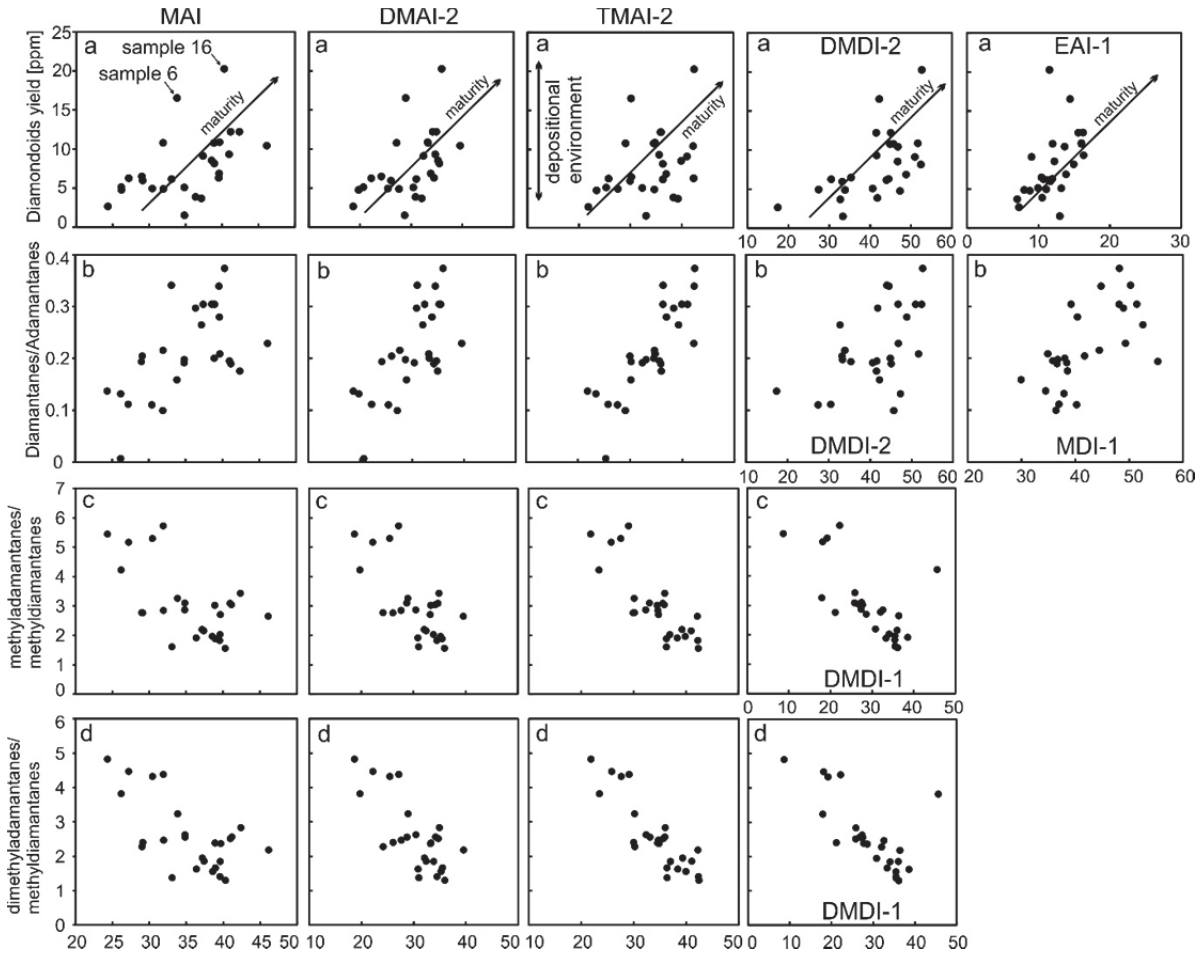

Fig. 39. Cross-plots of diamondoids yield (a) and molecular ratios (b, c, d) versus diamondoid isomerization indices for the oil sampes analysed. The diamondoids yield in the oil samples (cross-plots in row a) depends on the environmental and redox conditions during deposition of the source rock, including the presence of higher-plant organic matter and/or clays (vertical line), as well as increasing thermal maturity (diagonal line) (Gordzadze, 2008). See Table 10 for the formulae used to determine the indices.

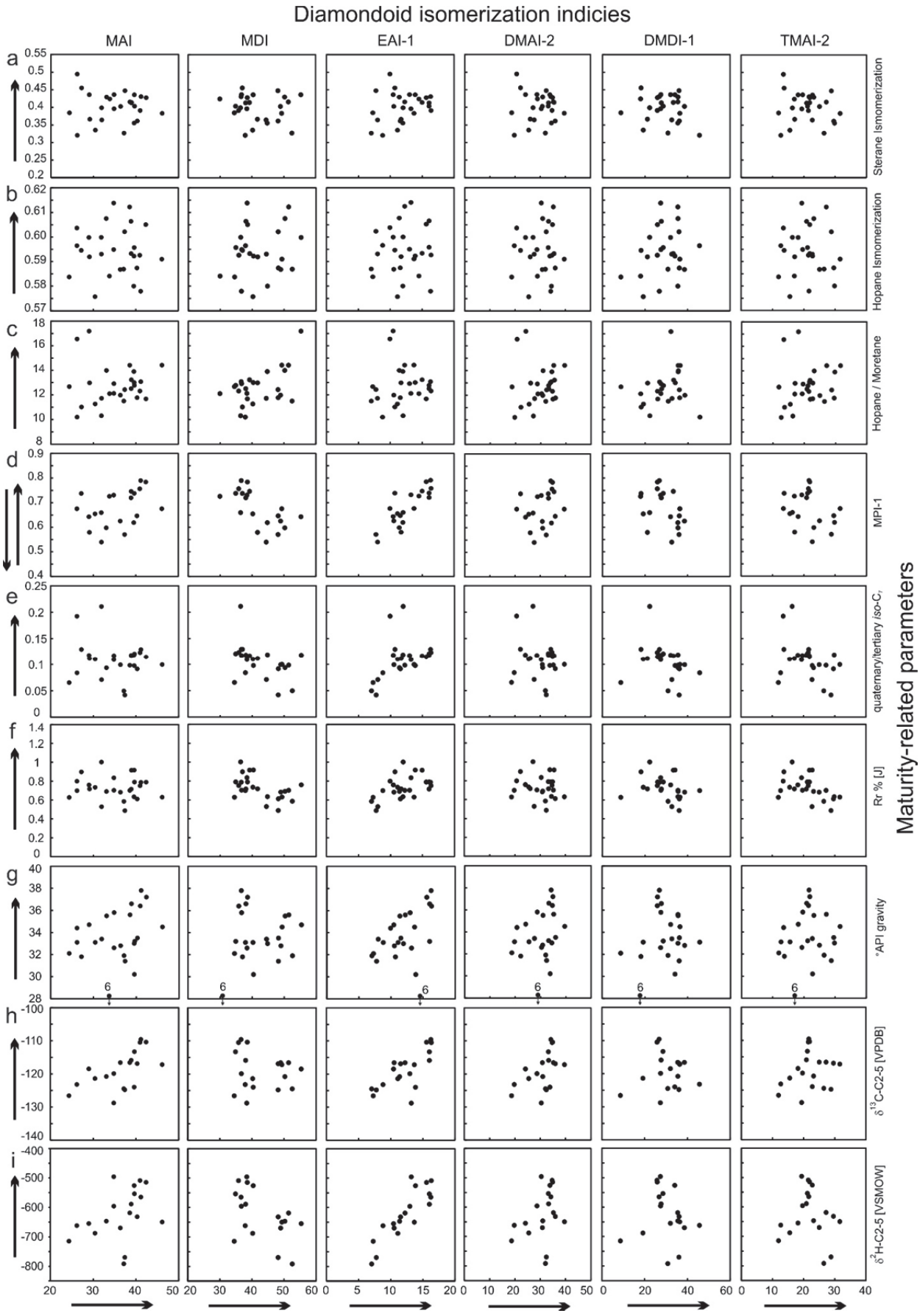

Fig. 40. Cross-plots of isomerization indices versus maturity-related biomarkers/specific compounds. The arrows indicate the theoretical increase of the indices and biomarkers values with increasing oil maturity. MPI-1, the methylphenanthrene

index (Radke & Welte, 1983) decreases with increasing maturity at advance stages of maturation. (a) Sterane isomerization: 20S/(20S+20R)ααα C29 steranes (monitored transition of *m/z* 400-217 in GC-MS/MS parent-daughter mode); (b) hopane isomerization: 22S/(22S+22R) C31 hopanes (monitored transition of *m/z* 426-191 in GC-MS/MS parent-daughter mode); (c) hopane / moretane ratio: αβ C30 hopane / βα C30 hopane (monitored transition of *m/z* 412-191 in GC-MS/MS parent-daughter mode); (d) MPI-1 values from Gratzer et al. (2011); (e) quaternary / tertiary *iso*-C7: ratio of quaternary alkanes (2,2-dimethylpentane + 3,3-dimethylpentane) over tertiary alkanes (3-ethylpentane + 2,3-dimethylpentane + 2,4-dimethylpentane) (after Hunt et al., 1980); (f) Rr % [J]: inferred vitrinite reflectance (Rr %) from parameter J: (2-methylhexane + 3-methylhexane) / (1,cis-3-, + 1,trans-3-, + 1,trans-2-, + 1,cis-2-dimethylcyclopentane), linear regression: Rr % = 0.84 + 1.1 log J (Schaefer & Littke, 1987); (g) API gravity; (h) δ^{13}C-C2-C5: summed δ^{13}C values of ethane, propane, *n*-butane, *n*-pentane (gas associated with investigated oils, after Pytlak et al., 2016a); (i) δ^{2}H-C2-C5: summed δ^{2}H values of ethane, propane, *n*-butane, *n*-pentane (gas associated with investigated oils, after Pytlak et al., 2016a).

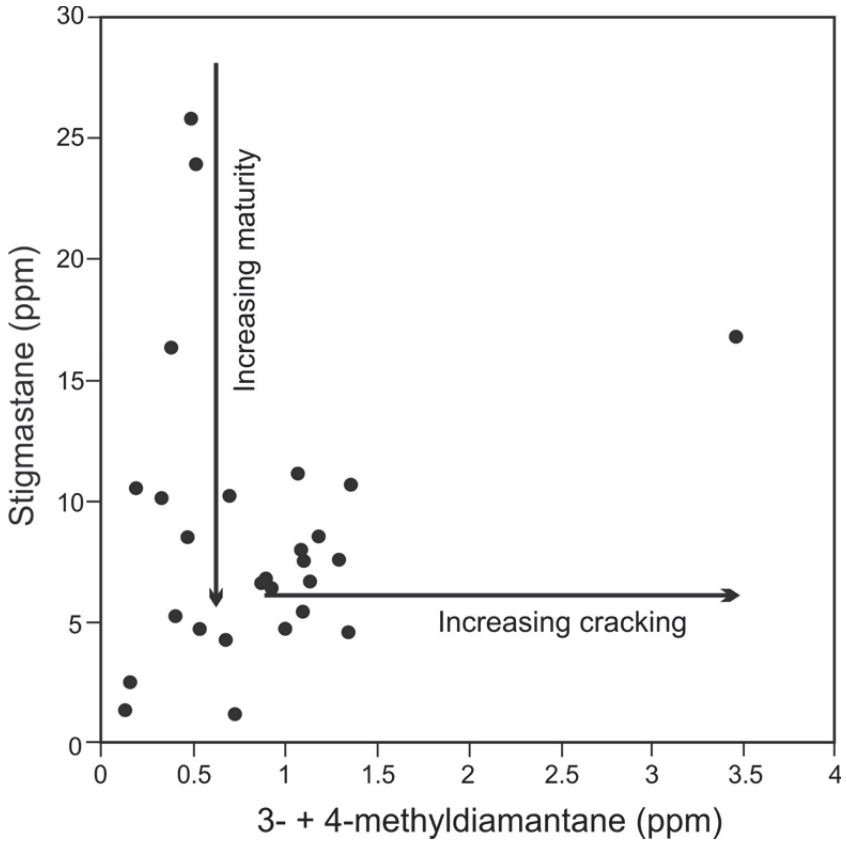

Fig. 41. Cross-plot of the sum of 4- and 3-methyldiamantane versus C_{29}ααα 20R sterane (stigmastane) concentration for the oils analysed from the Alpine Foreland Basin. Predicted lines characterizing the correlation between the concentration of diamondoids and biomarkers in oils of different thermal maturities are given according to Dahl et al. (1999). Decreasing biomarker concentrations with increasing thermal maturity is followed by oil cracking, which results in increased concentrations of diamondoids due to their high thermal stability (Dahl et al., 1999).

8.5. Influence of source rock heterogeneity on diamondoid composition

Apart from EAI-1, most diamondoid isomerization indices show a poor relationship with aliphatic, aromatic and C7 maturity parameters, API gravities and isotopic composition of gaseous hydrocarbons (Fig. 40). This suggests that the diamondoid composition may be influenced by variations of organic matter in the source rock facies. Furthermore, a notable correlation between diamondoid composition and the DBT/Ph and $\delta^{13}C$ values of *n*-alkanes (Fig. 42, Tab. 9) is observed. Clear correlations are also observed between diamondoid isomerization indices and both $\delta^{13}C$ values of *n*-alkanes (Fig. 42a-d) and DBT/Ph ratios (Fig. 42ik), as well as between diamondoid molecular ratios and $\delta^{13}C$ values of *n*-alkanes (Fig. 42e-h) and DBT/Ph (Fig. 42l-o). In addition, Ts/Tm ratios show a good correlation with $\delta^{13}C$ values of *n*-alkanes (Fig. 42e) and the DBT/Ph ratio (Fig. 42l). As discussed above, the DBT/Ph ratio reflects variations in organic matter within the source rocks. $\delta^{13}C$ values of *n*-alkanes in the studied oils vary by more than 2‰. This must be related to facies variations, because variations in maturity would result in a negative trend between $\delta^{13}C$ and the Ts/Tm ratio but the observed trend is positive (Fig. 42e). Thus, it can be assumed that isotopically light oils contain an increased contribution of oil generated from the isotopically light kerogen in the upper part of the Schöneck Formation (unit c) and the lower part of the Dynow Formation (Fig. 35). Because of the close correlation between the Ts/Tm ratio and the $\delta^{13}C$ values of *n*-alkanes (Fig. 42e), it seems that that the Ts/Tm ratio is controlled by source rock facies rather than by maturity. Therefore differences in diamondoid composition may be related to the varying contribution of different source rock units in the Schöneck Formation to the oils sampled, i.e. by the marly “a/b” units as opposed to the shale-rich unit “c” (Fig. 35). The differences in diamondoid composition may also be due to variations in the contribution by the redeposited Oberhofen facies source rocks relative to the non-redeposited source rock (Fig. 34c, d).

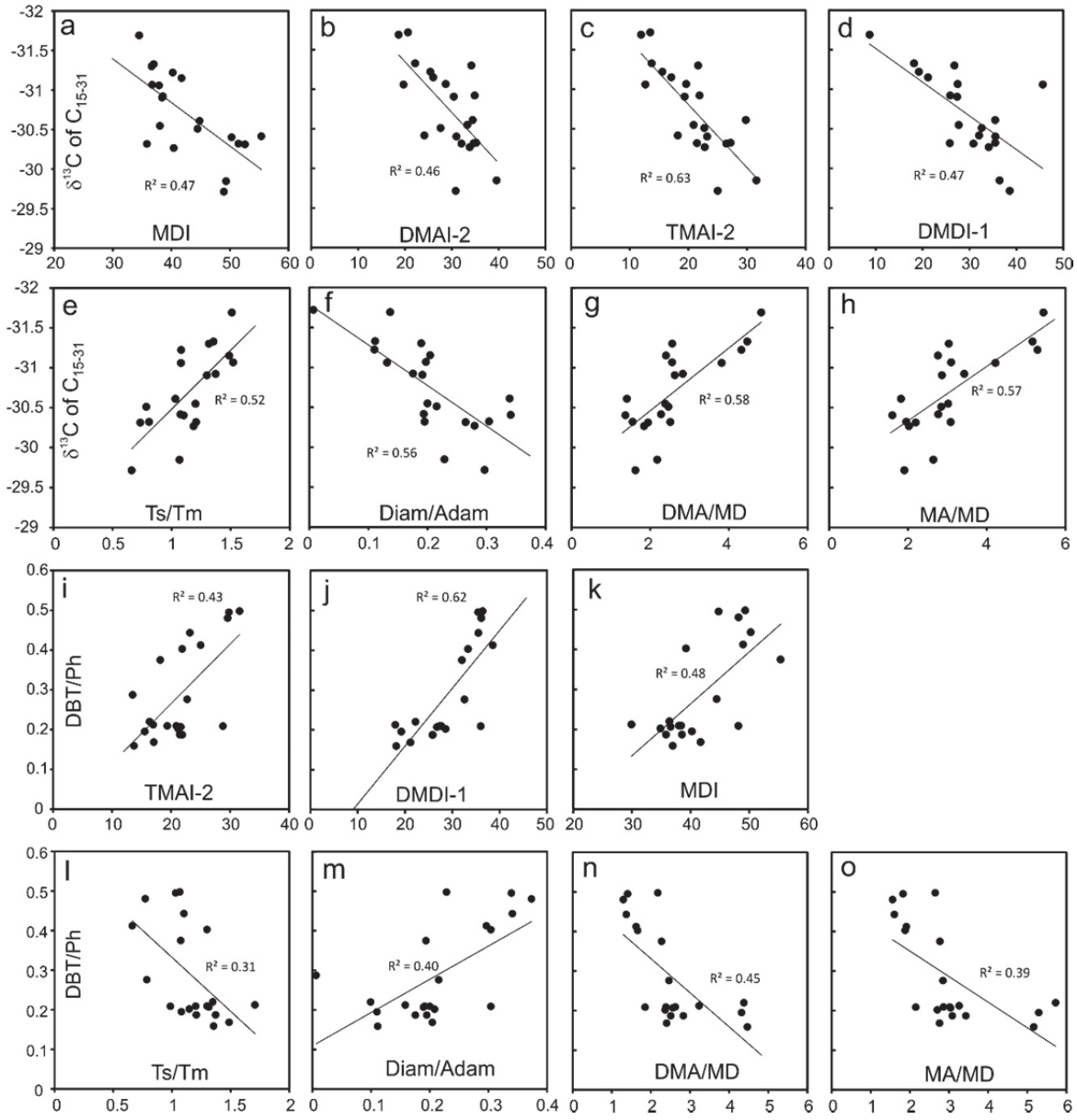

Fig. 42. (a-d) Cross-plots of $\delta^{13}C$ values of $C_{15\text{-}31}$ *n*-alkanes versus diamondoid isomerization indices; (e-h) cross-plots of $\delta^{13}C$ values of $C_{15\text{-}31}$ *n*-alkanes versus Ts/Tm and molecular ratios of diamondoids; (i-k) cross-plots of DBT/Ph ratios versus diamondoid isomerization indices; (l-o) cross-plots of DBT/Ph ratios versus Ts/Tm and molecular ratios of diamondoids. Linear trend lines are indicated. Diam; diamantanes, adam; adamantanes, DMA; dimethyladamantanes, MD; methyldiamantanes, MA; methyladamantanes.

9. Origin of condensates co-produced with microbial gas: lessons learned from ancillary geochemical methods

All previous geochemical studies (e.g. Schulz et al., 2002; Gier, 2000; Sachsenhofer et al., 2010; Gratzer et al., 2011; Bechtel et al., 2013) of oils and source rocks in the Alpine Foreland Basin were based on the C_{15+} hydrocarbon fraction (including biomarkers and stable isotopes). In contrast, light hydrocarbons (C_{15-} fraction) remained uninvestigated, although they are important proxies for facies and maturity of source rocks, migration, biodegradation and especially water washing. Therefore, to answer the question about condensate origin, biomarker (where available) and stable carbon isotopic data are supplemented by light hydrocarbons and diamondoids.

It has to be considered, that all light hydrocarbon parameters may be influenced by the facies and maturity of the source rock, as well as by alteration processes, making the interpretation complex. For this reason, well characterized oil samples from Cenomanian/Eocene reservoirs (Gratzer et al., 2011; Bechtel et al., 2012) are studied together with the condensates. In the interpretation, I also take advantage of a good understanding of source rocks (Sachsenhofer & Schulz, 2006; Sachsenhofer et al., 2010), thermal hydrocarbon generation and uplift histories (Gusterhuber et al., 2012; 2013; 2014) in the study area. Hence, the Alpine Foreland Basin offers a great opportunity to study different mechanisms of hydrocarbon generation and mixing, which may be relevant also in other foreland basins.

9.1. Molecular and isotopic composition

Condensates from Oligocene/Miocene reservoirs are predominantly composed of very light ends (up to $C_{10,}$ Fig. 43). However, in most cases a subordinate heavier oil component is also present, which contains biomarkers (Tab. 11). A notable feature of the condensate samples is near-absence of *n*-alkanes (Fig. 43). Moreover, in all gas chromatograms humps of unresolved components are noticeable. Some samples show a predominant pristane peak without a strong *n*-C_{17} peak nearby. However, the strong phytane peak is not observed.

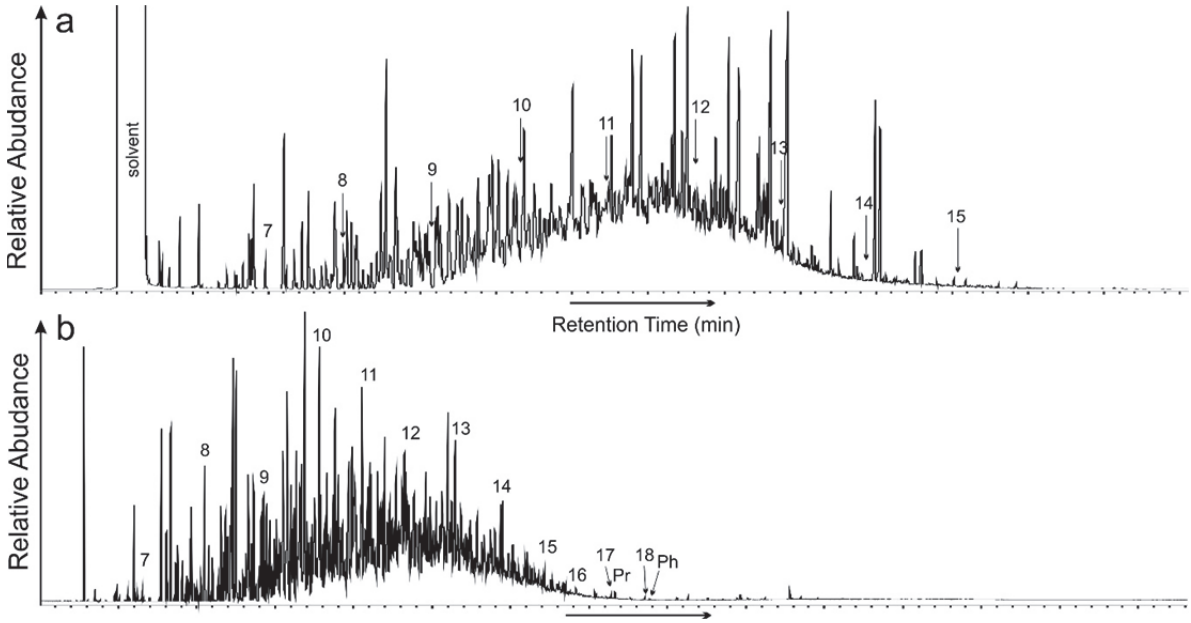

Fig. 43. FID-gas chromatograms of a) JJ2 condensate sample from Upper Puchkirchen Formation (Miocene) and b) A2* condensate sample from an Eocene reservoir. *n*-alkanes are labelled according to their carbon number, Pr-Pristane, Ph-Phytane. See Figs. 5 and 6 for location.

Concentrations of "classical" biomarkers (e.g. hopanes, steranes, diasteranes etc.) in Oligocene/Miocene condensate samples are very low. However, after pre-analysis concentration biomarker fingerprints from 14 samples could be obtained (Tab. 11). In samples Y1 and X2 no steranes were detected. The concentrations of C_{27} and C_{29} steranes are slightly higher that of C_{28} steranes. C_{29} sterane epimer ratios (20S/(20S+20R)) range from 0.11 to 0.56 (median 0.42) (Tab. 11). Samples D1, F4 and JJ3 show no hopane biomarkers. The most abundant compound within terpane biomarkers is $\alpha\beta C_{30}$ hopane. Oleanane is present in all samples that contain terpanes. C_{31} hopane epimer ratios (22S/(22S+22R)) vary between 0.45 and 0.67 (median 0.59) (Tab. 11). Tricyclic terpanes can be identified in samples A1, B1, D1, W1, X2, Y1, II1 and JJ2. Some additional samples show very low traces of biomarkers but results of these samples are not given in Tab. 11. Land plant biomarkers (e.g. primarane) and highly branched isoprenoids (HBIs) are enriched compared to other saturated compounds (see next sections for more details).

Results of the diamondoid analysis show that varying amounts of diamondoid hydrocarbons are present in all condensate samples, but sample X2 contains a very low amount. Generally adamantanes are more abundant (0.41- 63.11 ppm) than diamantanes (0.01-2.76 ppm) (Tab. 11). MAI (methyladamantane index) and EAI-I (ethyladamantane index) range from 28 to 61 and 12 to 29, respectively.

Due to depletion or absence of *n*-alkanes, the determination of their stable carbon isotopic compositions was not possible in some samples (Tab. 13). The $\delta^{13}C$ values of specific *n*-alkanes differ by about 2.5‰ between the samples. It is characteristic that $\delta^{13}C$ values decrease with increasing carbon number of *n*-alkanes (Tab. 13).

Tab. 11. Selected geochemical parameters of condensate samples from Oligocene/Miocene and Eocene reservoirs. Biomarkers are pre-concentrated and have been measured by GC-MS.

Sample	*n*-C_7/MCH	Tol/*n*-C_7	I[a]	H[b]	Diam sum[c]	D/A[d]	MDI[e]	EAI-1[f]	C_{27} Diasterane/ C_{27} Sterane	C_{27} Sterane/ Steranes	C_{28} Sterane/ Steranes	C_{29} Sterane/ Steranes
A1	0.11	0.87	0.12	4.38					0.66	0.33	0.24	0.44
A4	0.11	2.74	0.10	3.71								
A6	0.15	0.92	0.14	6.11								
A7		0.93	0.15	5.29	24.2	0.027	59.9	24.9	0.67	0.41	0.30	0.29
B1	0.30	0.17	0.17	7.55	38.4	0.026	60.6	28.7	1.14	0.39	0.21	0.40
D1		0.52	0.11	5.22	50.9	0.042	58.8	18.2	0.68	0.29	0.21	0.50
F4									0.78	0.42	0.23	0.36
F5	0.19	2.84	0.07	4.78								
J1	0.28	0.51	0.20	9.76	8.0	0.063	58.9	19.5				
M4	0.26	0.42	0.16	9.04								
M5	0.17	0.65	0.12	6.60								
O6	0.30	1.33	0.08	5.69								
O5	0.26	1.57	0.09	6.86								
P2	0.23	0.12	0.16	8.58								
S2	0.09	4.12	0.12	2.52								
T1		0.25	0.26	12.35	36.4	0.015	58.2	12.3	1.42	0.35	0.26	0.38
W1	0.13	0.66	0.11	4.82					0.94	0.37	0.22	0.40
W3	0.09	2.64	0.11	3.29					0.74	0.38	0.18	0.44
X2	2.18	0.20	2.39	3.75	0.4	0.020	43.3	14.9	0.67	0.34	0.32	0.34
Y1	0.21	0.81	0.11	6.07	18.3	0.089	56.3	24.7				
DD1	0.23	2.60	0.14	7.63					0.77	0.40	0.26	0.34
FF1		0.52	0.25	5.15	49.1	0.059	59.6	22.8				
II1									0.51	0.31	0.23	0.47
JJ1	0.08	3.08	0.08	3.21								
JJ2	0.13	0.82	0.14	5.05					0.60	0.31	0.27	0.41
JJ3	0.12	0.92	0.13	4.97					0.85	0.41	0.32	0.27
JJ4					43.5	0.024	60.8	21.2				
A1*	0.47	6.94	0.87	9.43	9.6	0.042	41.9	11.4	1.14	0.37	0.24	0.39
A2*	0.52	22.96	0.50	2.19								
A3*	0.49	14.91	0.48	9.09	64.7	0.026	43.7	14.8	0.35	0.61	0.16	0.23

Tab. 11. Continuation

Sample	20R αββ/20R ααα C_{29}-Steranes	20S/(20S+20R) ααα C_{29}-Steranes	Oleanane / (Oleanane+Hopane)	22S/(22S+22R) C_{31}-Hopanes	C_{29} Hopane/ C_{30} Hopane	C_{35}/(C_{35}+C_{34}) Homohopanes	C_{30} Diahopane/ (C_{30} Diahopane+C_{30} Hopane)	C_{26}/C_{25} Tricyclic Terpanes	C_{31}R Hopane/ C_{30} Hopane
A1	1.21	0.43	0.13	0.58	1.33	0.46	0.03	0.49	0.45
A4									
A6									
A7	0.28	0.11	0.44	0.45	0.64	0.48	0.09		
B1	1.37	0.54	0.15	0.58	0.73	0.37	0.06	0.67	0.24
D1	1.34	0.45	0.11	0.55	1.04	0.40		0.51	0.58
F4	0.38	0.48							
F5									
J1									
M4									
M5									
O6									
O5									
P2									
S2									
T1	0.62	0.21	0.37	0.60	0.72	0.42	0.08		0.27
W1	1.84	0.56	0.17	0.62	0.84	0.42	0.17	0.54	0.32
W3	1.09	0.38	0.19	0.67	0.72				0.31
X2	0.75	0.39	0.07		0.50	0.41	0.05	0.39	0.25
Y1			0.09	0.62	0.81	0.41	0.07	0.38	0.33
DD1	0.95	0.23							
FF1									
II1	1.82	0.49	0.06	0.60	0.79		0.08	0.40	0.34
JJ1									
JJ2	1.15	0.42	0.08	0.54	0.89			0.42	0.48
JJ3	0.91	0.32							
JJ4									

A1*	1.21	0.53	0.10	0.53	0.68	0.11	0.49	0.34
A2*					0.86	0.15		0.34
A3*	1.78	0.65	0.12	0.61	0.86	0.15	0.40	0.34

(a) Isoheptane value (I): (2- + 3-methylhexane) / (1*cis*3- + 1*trans*3- + 1*trans*2-dimethylcyclopentane) (after Thompson, 1979)
(b) Heptane value (H): (100**n*-C_7) / (cyclohexane + 2- + 3-methylhexane + 1,1-dimethylcyclohexane + 1*cis*3- + 1*trans*3 + 1*trans*2-dimethylcyclopentane + methylcyclohexane + *n*-C_7) (after Thompson, 1979)
(c) Sum of diamondoid hydrocarbons [ppm]
(d) Ratio of diamantanes over adamantanes
(e) Methyladamantane index ((1-methyladamantane/(1-methyladamantane + 2-methyladamantane))*100) (after Chen et al. 1996)
(f) Ethyladamantane index ((1-ethyladamantane/(1-ethyladamantane + 2-ethyladamantane))*100) (after Zhang et al., 2005)

Tab. 12. Selected geochemical parameters from oils in Cenomanian/Eocene reservoirs.

Sample	*n*-C_7/MCH	Tol/*n*-C_7	I[a]	H[b]	U[c]	J[d]	Rr % [J][e]	V[f]	Rr %[V][g]	Quater/ Tertiary (iso)[h]	Quater/ Tertiary (cyclo)[i]	20R αββ/20R ααα C_{29}-Steranes	20S/(20S+20R) ααα C_{29}-Steranes
D*												1.49	0.42
E*	0.76	0.16	1.49	24.34	1.32	1.40	1.00	1.59	1.36	0.20	0.14	1.03	0.40
F*	0.82	0.01	1.22	25.14	1.44	1.13	0.90	1.37	1.25	0.13	0.09	1.06	0.46
G1*	0.70	0.32	0.80	19.95	0.55	0.76	0.71	0.94	0.95	0.12	0.07		
G2*	0.83	0.36	0.84	22.43	0.53	0.80	0.73	0.98	0.98	0.11	0.07	0.72	0.34
H1*	0.78	0.39	0.97	22.52	0.83	0.92	0.80	1.09	1.07	0.13	0.10		
H2*	0.72	0.37	0.78	19.57	0.58	0.74	0.70	0.91	0.92	0.08	0.08	0.62	0.32
I1*	0.56	0.35	0.74	16.83	0.76	0.71	0.67	0.85	0.87	0.11	0.09		
I6*	0.62	0.68	0.82	19.79	0.84	0.77	0.72	0.90	0.92	0.11	0.11	0.96	0.37
J2*	0.50	0.59	0.78	17.01	0.86	0.73	0.69	0.88	0.90	0.11	0.11		
L1*	0.67	0.08	0.87	19.64	0.73	0.83	0.75	0.99	0.99	0.11	0.10		
L2*	0.56	0.08	0.81	17.62	0.88	0.76	0.71	0.92	0.94	0.10	0.10		
L3*	0.64	0.10	0.82	20.52	1.01	0.77	0.72	0.93	0.94	0.08	0.10		
M*	0.75	0.13	0.86	21.30	0.67	0.81	0.74	0.98	0.98	0.12	0.09		
N1*	0.87	0.01	1.14	25.02	0.71	1.07	0.87	1.31	1.21	0.12	0.09		
N2*	0.87	0.01	1.05	24.68	0.65	0.99	0.84	1.21	1.15	0.11	0.09	0.88	0.40
N3*	0.60	0.02	1.01	18.96	0.91	0.94	0.81	1.20	1.14	0.12	0.10		
N4*	0.93	0.01	1.15	25.75	0.63	1.09	0.88	1.34	1.23	0.12	0.09		
O1*	0.69	0.60	0.66	19.13	0.57	0.61	0.61	0.75	0.78	0.07	0.08		
O2*	0.69	0.52	0.68	18.86	0.56	0.64	0.63	0.79	0.82	0.07	0.08	0.83	0.38
P1*	0.65	0.92	0.81	19.21	1.43	0.78	0.72	0.98	0.99	0.10	0.10		
P2*	0.69	0.80	0.82	19.43	0.72	0.76	0.71	0.91	0.92	0.10	0.10		
P3*													
P4*													
P5*	0.63	0.82	0.79	25.52	1.11	0.72	0.68	0.85	0.87	0.11	0.09		
P6*	0.68	0.77	0.81	20.12	0.86	0.75	0.70	0.89	0.91	0.12	0.09	1.09	0.44
P7*													
Q2*	0.80	0.41	0.93	22.52	0.70	0.89	0.79	1.05	1.04	0.13	0.10	0.94	0.43
R*	0.88	0.46	1.00	27.33	0.77	0.90	0.79	1.06	1.04	0.11	0.09	1.03	0.43
S1*	0.72	0.65	0.84	23.35	0.91	0.76	0.71	0.90	0.92	0.10	0.09		
S2*	0.78	0.50	0.89	22.28	0.73	0.83	0.75	0.98	0.99	0.12	0.10	0.88	0.39
S3*	0.77	0.49	0.89	21.99	0.71	0.86	0.77	1.02	1.01	0.12	0.10		
S4*	0.79	0.53	1.04	17.31	0.76	1.00	0.84	1.13	1.10	0.09	0.07		

S5*	0.74	0.58	0.87	22.32	0.81	0.82	0.74	0.96	0.97	0.10	0.10		
S6*	0.75	0.54	0.89	21.82	0.74	0.86	0.77	1.01	1.01	0.11	0.10		
T*	0.64	0.51	0.81	20.81	0.90	0.74	0.70	0.87	0.89	0.10	0.09		
U*	0.88	0.17	1.02	23.98	0.87	0.90	0.79	1.08	1.06	0.12	0.10	0.98	0.40
V1*	0.60	0.58	0.72	17.81	0.68	0.67	0.65	0.83	0.85	0.11	0.09		
V2*	0.78	0.65	0.86	21.36	0.69	0.77	0.71	0.93	0.94	0.12	0.09	0.90	0.41
V3*	0.77	0.60	0.88	21.17	0.69	0.84	0.76	1.01	1.00	0.13	0.10		
W*	0.39	0.43	0.97	14.33	1.27	0.92	0.80	1.07	1.05	0.16	0.17	2.24	0.49
X*	0.61	0.43	0.55	17.71	0.53	0.52	0.53	0.66	0.67	0.07	0.06	0.64	0.36
Y1*	0.63	0.25	0.79	20.02	0.76	0.75	0.70	0.92	0.93	0.10	0.09		
Y2*	1.18	0.13	2.32	30.59	1.64	2.16	1.21	2.37	1.67	0.14	0.19		
Y3*	0.83	0.13	0.61	20.31	0.31	0.59	0.58	0.74	0.77	0.05	0.04	0.51	0.33
Z*	1.08	0.02	1.27	28.62	0.83	1.17	0.91	1.41	1.27	0.12	0.10	1.11	0.41
AA1*	0.76	0.02	1.10	24.49	1.05	1.05	0.86	1.26	1.18	0.11	0.09		
AA2*	1.33	0.02	1.33	31.86	0.72	1.26	0.95	1.48	1.31	0.10	0.09		
AA3*	1.23	0.01	1.31	29.67	0.61	1.26	0.95	1.49	1.31	0.11	0.09		
AA4*	1.23	0.02	1.22	30.47	0.64	1.17	0.92	1.40	1.26	0.10	0.08	0.98	0.44
AB*	0.76	0.76	0.90	21.87	0.81	0.84	0.76	1.02	1.01	0.12	0.10	1.65	0.44
AC*	0.76	0.29	0.76	22.81	0.72	0.73	0.69	0.89	0.91	0.09	0.09	1.09	0.43
AD1*	0.74	0.40	0.77	22.43	0.72	0.74	0.70	0.90	0.92	0.10	0.09		
AD2*	0.88	0.40	0.79	25.67	0.80	0.75	0.70	0.91	0.93	0.10	0.07	1.02	0.42
AD3*	0.72	0.43	0.74	24.05	0.67	0.67	0.65	0.82	0.85	0.10	0.08		
AD4*	0.60	0.28	0.71	19.13	0.75	0.66	0.65	0.81	0.84	0.11	0.09		
AF*	0.82	0.35	0.76	22.81	0.63	0.72	0.68	0.89	0.91	0.10	0.08	1.09	0.40
AG*	0.68	0.32	0.70	20.38	0.77	0.65	0.63	0.82	0.84	0.12	0.08	0.84	0.36
AH*	0.64	0.72	0.51	18.00	0.52	0.48	0.49	0.60	0.60	0.04	0.06	1.13	0.45
AI*	0.75	0.43	0.68	20.88	0.63	0.64	0.63	0.80	0.83	0.10	0.08	0.80	0.38
AJ*	0.85	0.60	0.72	23.85	0.74	0.62	0.61	0.77	0.79	0.09	0.07	0.64	0.36

Tab 12. Continuation

Sample	Oleanane / (Oleanane+Hopane)	22S/(22S+22R) C_{31}-Hopanes	C_{29} Hopane/ C_{30} Hopane	$C_{35}/(C_{35}+C_{34})$ Homohopanes[j]	C_{30} Diahopane/ (C_{30} Diahopane+C_{30} Hopane)	C_{26}/C_{25} Tricyclic Terpanes[k]	C_{31}R Hopane/ C_{30} Hopane	C_{29}Ts / C_{30} Diahopane	Ts/αβC_{30} Hopane	DBT / Ph[l]
D*	0.11	0.58	0.50	0.46	0.22			1.20	0.62	0.21
E*	0.10	0.59	0.60	0.44	0.12	0.74	0.26	1.62	0.42	0.22
F*	0.09	0.59	0.50		0.14			1.59	0.44	0.16
G1*				0.50						
G2*	0.08	0.57	0.57	0.46	0.10	0.55	0.32	1.80	0.35	0.20
H1*				0.48						0.16
H2*	0.09	0.59	0.53		0.09			2.17	0.29	
I1*				0.46		0.41				0.66
I6*	0.09	0.59	0.46	0.40	0.11	0.41	0.21	1.87	0.30	0.17
J2*										
L1*				0.48						
L2*				0.45						
L3*				0.44						
M*				0.45		0.55	0.29			0.20
N1*										
N2*	0.08	0.61	0.52	0.42	0.10	0.49	0.28	1.63	0.33	0.21
N3*				0.43						
N4*						0.68	0.29			0.21
O1*				0.47						0.07
O2*	0.09	0.58	0.52		0.08			1.88	0.35	
P1*				0.39		0.32	0.31			0.17
P2*										
P3*				0.40		0.39	0.28			
P4*				0.30						
P5*				0.42		0.61	0.30			0.16
P6*	0.09	0.59	0.50		0.12			1.78	0.40	
P7*				0.42		0.57	0.28			
Q2*	0.07	0.57	0.50	0.41	0.11	0.71	0.31	1.99	0.39	0.21
R*	0.08	0.60	0.53	0.42	0.11	0.51	0.32	1.65	0.38	0.19
S1*				0.43		0.62	0.27			0.18
S2*	0.08	0.59	0.49	0.42	0.11	0.74	0.30	1.81	0.35	0.19
S3*				0.44						0.22
S4*				0.38		0.57	0.29			0.20

S5*				0.45		0.48	0.31			0.19
S6*				0.43		0.64	0.30			0.19
T*				0.45		0.52	0.27			
U*	0.07	0.59	0.57	0.42	0.10	0.53	0.26	1.73	0.36	0.20
V1*										
V2*	0.08	0.60	0.50	0.44	0.10	0.47	0.29	1.90	0.35	0.21
V3*				0.45		0.65	0.28			0.21
W*	0.14	0.60	0.33	0.43	0.26	0.46	0.32	1.08	0.84	0.29
X*	0.05	0.59	0.57	0.43	0.06			2.94	0.23	0.28
Y1*										
Y2*				0.41		0.65	0.20			0.36
Y3*	0.07	0.58	0.60		0.06			2.76	0.24	
Z*	0.07	0.59	0.47	0.38	0.11	0.45	0.22	1.91	0.34	0.40
AA1*				0.40		0.64	0.27			
AA2*				0.42		0.81	0.30			0.19
AA3*				0.43		0.56	0.28			0.23
AA4*	0.07	0.59	0.53		0.10			1.75	0.33	
AB*	0.14	0.59	0.58	0.41	0.18	0.43	0.24	1.10	0.47	0.37
AC*	0.12	0.60	0.59	0.48	0.13	0.48	0.35	1.75	0.41	0.44
AD1*				0.47		0.55	0.33			0.46
AD2*	0.10	0.61	0.65		0.09	0.64		2.13	0.33	
AD3*										0.48
AD4*				0.47						
AF*	0.13	0.58	0.68	0.43	0.10	0.57	0.40	1.67	0.36	0.41
AG*	0.11	0.58	0.64	0.41	0.11			1.92	0.44	0.49
AH*	0.05	0.60	0.53	0.46	0.08	0.56	0.25	2.27	0.25	0.21
AI*	0.10	0.59	0.63	0.44	0.11	0.50	0.27	1.97	0.44	0.50
AJ*	0.09	0.58	0.65	0.43	0.07	0.42	0.24	2.19	0.26	0.48

(Footnote to previous page)

(a) Isoheptane value (I): (2- + 3-methylhexane) / (1*cis*3- + 1*trans*3- + 1*trans*2-dimethylcyclopentane) (after Thompson, 1979)
(b) Heptane value (H): (100**n*-C_7) / (cyclohexane + 2- + 3-methylhexane + 1,1-dimethylcyclohexane + 1*cis*3- + 1*trans*3 + 1*trans*2-dimethylcyclopentane + methylcyclohexane + *n*-C_7) (after Thompson, 1979)
(c) Naphthene branching value (U): cyclohexane/methylcyclohexane (after Thompson, 1979)
(d) maturity-sensitive low molecular-weight hydrocarbon parameter (J): (2- + 3-methylhexane) / (1*trans*3- + 1*cis*3- + 1*trans*2- + 1*cis*2-dimethylcyclopentane)
(e) Inferred vitrinite reflectance (Rr %) from parameter J: Rr = 1.0 + 1.8*log J (after Schaefer & Littke, 1988)
(f) maturity-sensitive low molecular-weight hydrocarbon parameter (V): (2,2- + 2,3- + 2,4- + 3,3-dimethylpentane + 2,2,3-trimethylbutane + 2- + 3-methylhexane + 3-ethylpentane) / (1,1- + 1*cis*3- + 1*trans*3- + 1*trans*2- + 1*cis*2-dimethylcyclopentane) (after Schaefer & Littke, 1988)
(g) Inferred vitrinite reflectance (Rr %) from parameter V: Rr = 0.84+1.1*logV (after Schaefer & Littke, 1988)
(h) Quaternary / tertiary ratio of quaternary alkanes (2,2-dimethylpentane + 3,3-dimethylpentane) over tertiary alkanes (3-ethylpentane + 2,3-dimethylpentane + 2,4-dimethylpentane) (after Hunt et al., 1980)
(i) Quaternary / tertiary ratio of quaternary alkanes (1,1-dimethylcyclopentane) over tertiary alkanes /(1,1- + 1*cis*3- + 1*trans*3- + 1*trans*2- + 1*cis*2-dimethylcyclopentane) (after Hunt et al., 1980)

Biomarkers are measured by GC-MS/MS except of (j, k, l) which are archival data and data from Gratzer et al. (2011)
MCH-methylcaclohexane, Tol-toluene, DBT-dibenzothiophene, Ph-phenanthrene

Tab. 13. Stable carbon isotopic composition of *n*-alkanes and isoprenoids from condensate samples. See Fig. 6 for location.

Sample	$\delta^{13}C$ [V-PDB]								
	***n*-C_{15}**	***n*-C_{16}**	***n*-C_{17}**	***n*-C_{18}**	***n*-C_{19}**	***n*-C_{20}**	**Norpristane**	**Pristane**	**Phytane**
A1	-29.54	-29.72	-30.23	-30.10	-30.27	-30.66	-30.26	-30.75	-31.14
A6	-29.56	-29.89	-30.31	-30.46	-30.55		-30.34	-30.76	-31.20
A7	-28.94	-29.71	-30.33	-30.31	-30.38	-30.61	-30.39	-30.73	-31.01
B1	-28.76	-29.05	-28.82	-29.51	-30.33	-30.69		-29.32	-29.64
D1	-29.80	-29.68	-30.02	-29.83	-30.21			-30.28	-30.15
J1	-29.66	-29.85	-30.06	-29.93	-30.21	-30.72	-30.38	-30.41	-30.93
M3		-29.13	-29.84	-30.36	-30.58	-31.03	-30.05	-30.31	-30.54
M5			-30.07	-30.54	-30.90			-30.22	-30.78
O6			-29.76	-30.28	-30.44			-30.81	-31.26
T1	-28.66	-29.06	-29.50	-29.65	-29.75	-29.92	-29.48	-29.75	-29.94
U3	-28.93	-29.24	-29.76	-30.21	-30.32			-29.95	-30.22
W3	-29.63	-30.17		-30.45	-30.96	-31.21	-29.87	-29.93	-30.29
X2	-30.22	-30.93	-31.07	-31.55	-31.92	-32.14	-31.38	-32.41	-31.93
Y1	-28.83	-29.29	-29.73	-30.07	-30.24	-30.75	-29.83	-30.06	-30.45
DD1	-29.70		-30.51	-30.72			-29.56	-30.24	-30.37
JJ2	-28.75	-29.26	-30.04	-30.29	-30.43	-30.69	-30.47	-30.85	-30.99
FF1	-30.98	-31.27	-31.55	-31.90	-32.22	-32.68	-31.94	-32.43	-32.61
A3*	-30.54	-30.35	-31.17	-31.41	-31.67	-32.06	-31.23	-31.74	-32.01
A1*	-30.85	-31.04	-31.36	-31.83	-32.13	-32.52		-31.57	-31.82

9.2. Biodegradation

Before condensate samples from Oligocene/Miocene reservoirs are examined regarding source rock facies and maturity, the effect of possible biodegradation must be clarified. Biodegradation of crude oils in subsurface resevoirs removes compound classes in a well documented sequence: The most degradable compounds are *n*-alkanes, followed by more resistant branched acyclic and monocyclic hydrocarbons (e.g. Wenger et al., 2002). Thus, the observed strong depleation in *n*-alkanes (Fig. 43a) from condensate samples in Oligocene/Miocene indicates microbial degradation. For this reason, maturity parameters based on low molecular weight alkanes (e.g. heptane and isoheptane values; Thompson, 1983) are strongly influenced by biodegradation (Fig. 44).

Aromatic hydrocarbons are degraded only after significant removal on *n*-alkanes. Wilkes et al. (2000) showed that 1,2,3-trimethylbenzene is more resistant to biodegradation in anaerobic ground waters than other isomers. This trend is also observed in the condensate samples from Oligocene/Miocene reservoirs (Fig. 45). Wilkes et al. (2000) suggest that, selective removal of certain compounds may be caused by sulphate-reducing bacteria. The action of this community is confirmed by concomitant degradation of aromatic hydrocarbons (4-methylbiphenyl/3-

methylbiphenyl) and *n*-alkanes (pristane/*n*-C_{17}) (Jones et al. 2008; Fig. 46) and the presence of framboidal pyrite in Oligocene/Miocene reservoir sandstones (Grundtner et al., 2016).

Other aromatic compounds like phenanthrenes and dibenzothiophenes are absent in most samples. However, it difficult to state whether aromatic compounds are removed by biodegradation or fractionation processes (see below).

In contrast, condensate in Eocene reservoirs in field A* displays only minor biodegradation, although it occurs together with strongly degraded tar and degraded secondary microbial gas (Pytlak et al., 2016a; Fig. 43b).

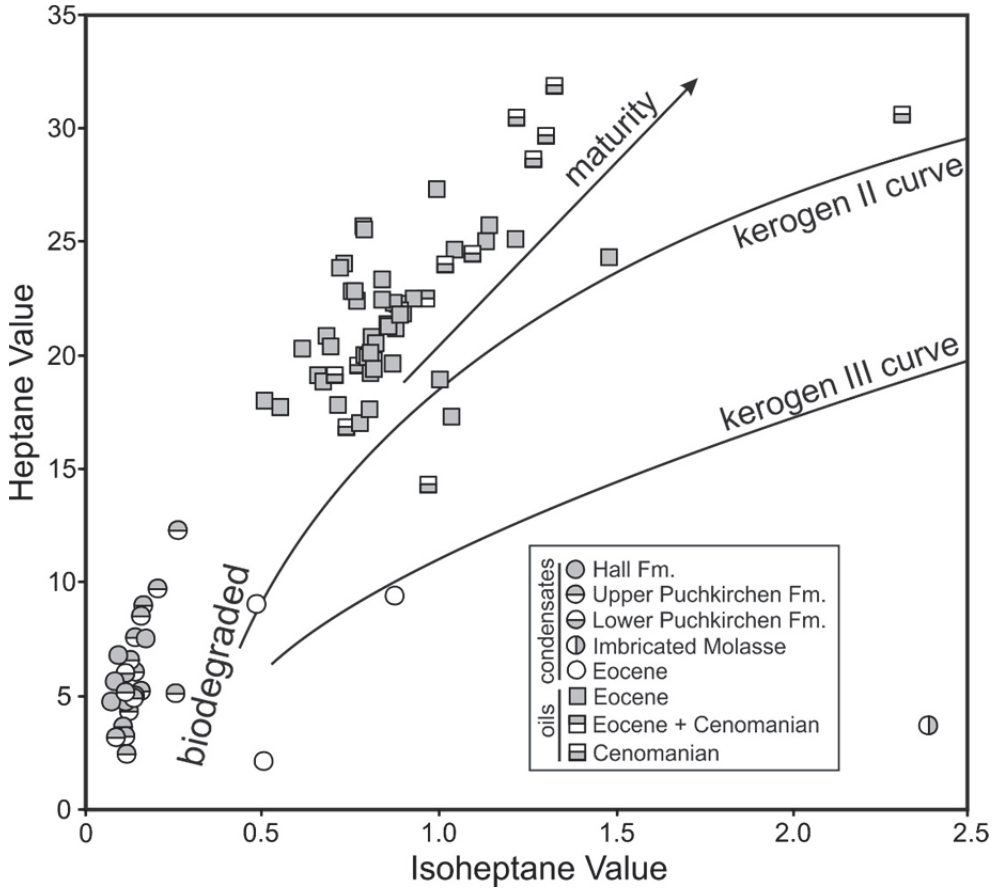

Fig. 44. Cross-plot of isoheptane value ((2- + 3-methylhexane) / (1*cis*3- + 1*trans*3- + 1*trans*2-dimethylcyclopentane) versus heptane value ((100**n*-C_7) / (cyclohexane + 2- + 3-methylhexane + 1,1-dimethylcyclohexane + 1*cis*3- + 1*trans*3 + 1*trans*2-dimethylcyclopentane + methylcyclohexane + *n*-C_7)) (Thompson, 1979).

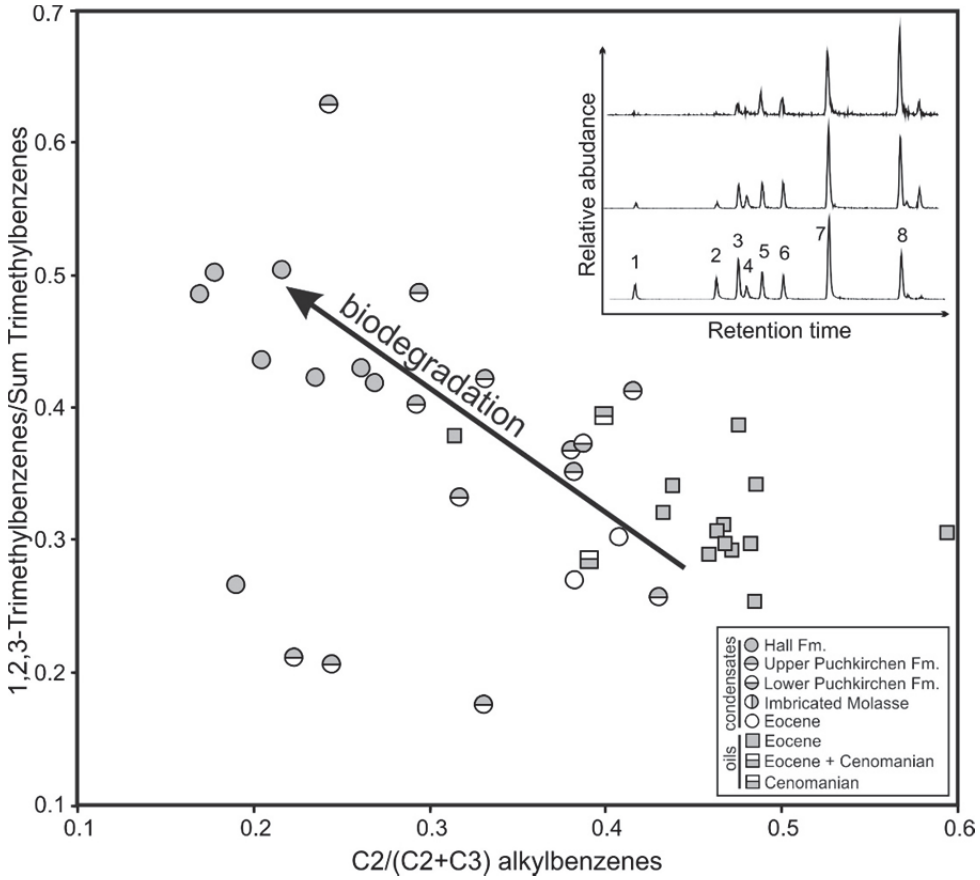

Fig. 45. Cross-plot of 1,2,3-trimethylbenzenes/sum of trimethylbenzenes ratio versus C2/(C2+C3) alkylbenzenes ratio. Partial mass chromatograms of the trimethylbenzenes for three samples are shown. Peak identification: 1- isopropylbenzene, 2- *n*-propylbenzene, 3- 1-methyl-3-ethylbenzene, 4- 1-methyl-3-ethylbenzene, 5- 1,3,5-trimethylbenzene, 6- 1-methyl-2-ethylbenzene, 7- 1,2,4-trimethylbenzene, 8- 1,2,3-trimethylbenzene.

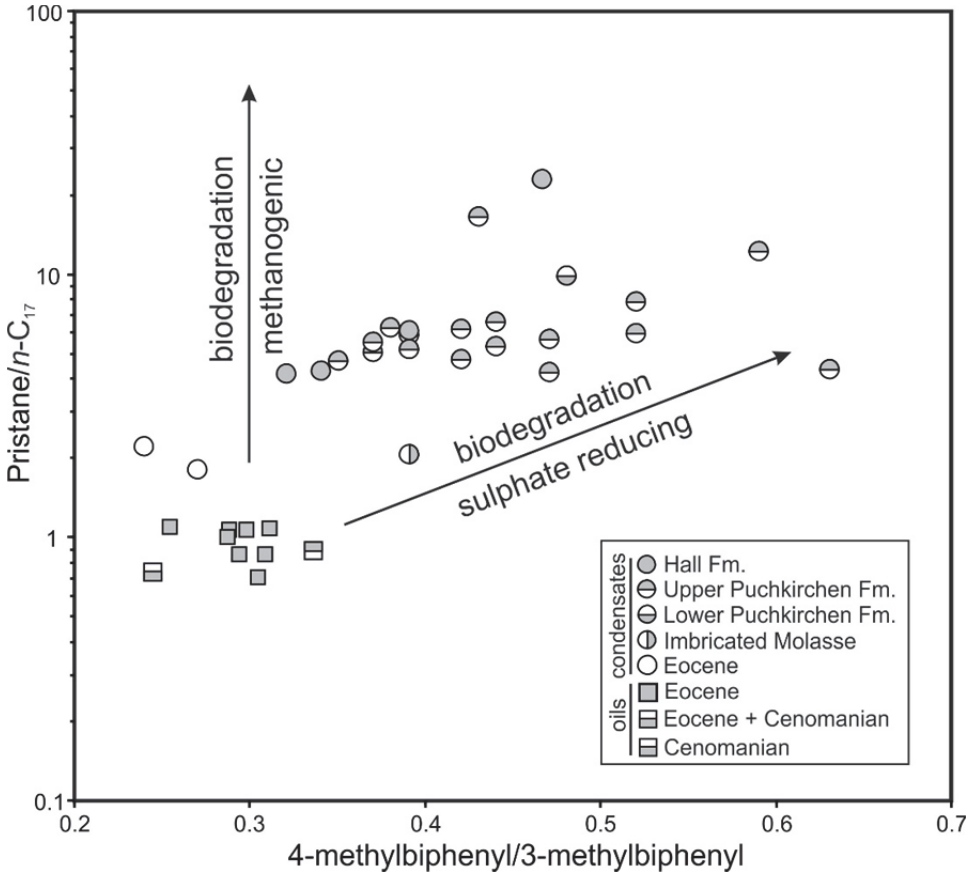

Fig. 46. Cross-plot of pristane/*n*-C_{17} ratio versus 4-methylbiphenyl/3-methylbiphenyl ratio. Concomitant degradation of *n*-alkanes and selective aromatic hydrocarbons points to action of sulphate-reducing bacteria (Jones et al., 2008).

9.3. Maturity

9.3.1. Cenomanian/Eocene oils

Several light hydrocarbon parameters have been proposed to assess oil maturity. Hunt et al. (1980) observed that source rocks yield a maximum of quaternary isoheptanes at greater depths than that of tertiary isoheptanes. Most probably this is due to the greater stability of the intermediate tertiary carbonium ion or free radical (Hunt et al. 1980). Consequently the quaternary/tertiary isoheptanes ratio is applied as a maturity indicator in this section. Heptanes and isoheptane (Thompson, 1983) values can be used as relative maturation indicator (increase of values indicate higher oil maturity). Interestingly, a positive trend is oberved in Fig. 44, suggesting that oils generated at different maturation stages can be distinguished. Thompson (1983) concluded that oils characterized by heptane and isoheptane ratios of around 20 and 0.9, respectively, correspond to maturity of 0.9 % vitrinite reflectance (Fig. 44).

Schaefer & Littke (1988) observed that their parameters “J” (similar to Thompson’s isoheptane value; Tab. 12) and “V” increase with increasing maturity. Applying the equations Ro = 1+1.8*logV and Ro = 0.84+1.1*logJ (Schaefer & Littke, 1988), apparent maturities of oils from Alpine Foreland Basin range from 0.5% to 1.2% (“J) and from 0.6 to 1.7% Ro (“V”), respectively (Tab. 12). Ro values above 1.0%Ro suggest that extensive cracking of major oil costituents should have occurred. However, this is not the case, as higher *n*-alkanes are abundant components of all studied oils. Instead, maturation of source rocks resulted in progressive generation of higher volumes of lighter hydrocarbons as revealed by a parallel increase of light hydrocarbon and biomarker/aromatic maturity-related parameters (Fig. 47).

Progressive generation of light hydrocarbons with increasing maturity should increase API values. To test this, light hydrocarbon maturity-related parameters, diamondoid isomerization index EAI-1 and stable carbon and hydrogen isotopic compositions of gaseous hydrocarbons are plotted against API gravity in Figs. 48 and 49. Although API gravities are strongly influenced by alteration processes, a noticeable correlation with light hydrocarbon fraction maturity-related parameters is observed (Fig. 48). Indeed, samples which deviate from the trend observed in Fig. 48 are known to be affected by water washing (Pytlak et al., submitted) and possible biodegradation (Pytlak et al.,

2016a). Despite of this, a reasonable correlation is also observed between API and gas isotopes and EAI-1 (Fig. 49).

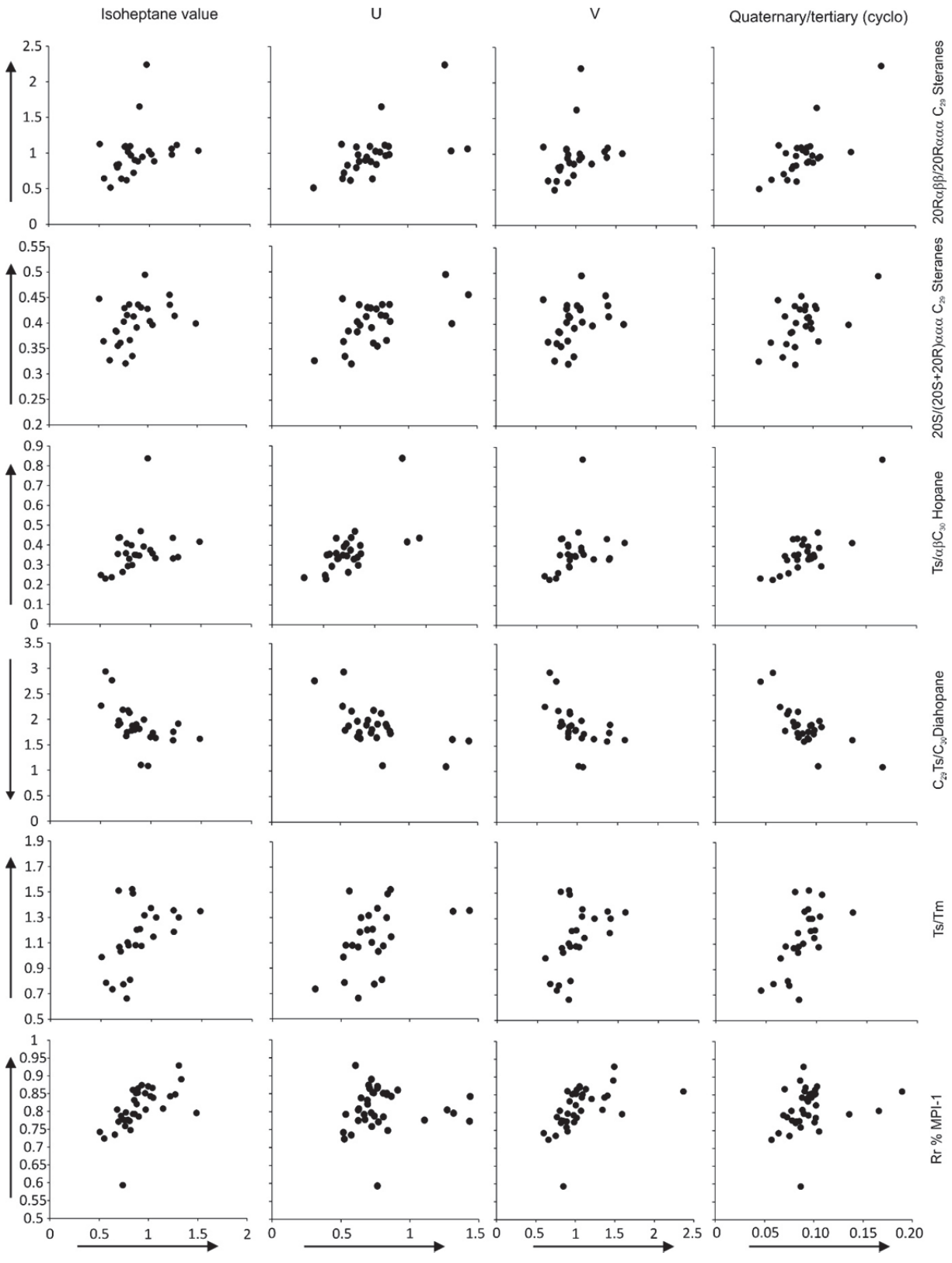

Fig. 47. Cross-plos of maturity-related light hydrocarbon parameters versus maturity-related biomarker ratios. Isoheptane value: (2- + 3-methylhexane) / (1*cis*3- +

1*trans*3- + 1*trans*2-dimethylcyclopentane) (Thompson, 1979), U: cyclohexane / methylcyclopentane (Thompson, 1983), V: (2,2- + 2,3- + 2,4- + 3,3-dimethylpentane + 2,2,3-trimethylbutane + 2- + 3-methylhexane + 3-ethylpentane) / (1,1- + 1*cis*3- + 1*trans*3- + 1*trans*2- + 1*cis*2-dimethylcyclopentane) (Schaefer & Littke, 1988), Quaternary/Tertiary (cyclo): ratio of quaternary over tertiary cyclopentanes: 1,1-dimethylcyclopentane / (1,1- + 1*cis*3- + 1*trans*3- + 1*trans*2- + 1*cis*2-dimethylcyclopentane) (Hunt et al., 1980), 20Rααβ/20RαααC$_{29}$ Steranes: (monitored transition of *m/z* 400-217 in GC-MS/MS parent-daughter mode), 20S/(20S+20R)αααC$_{29}$ steranes (monitored transition of *m/z* 400-217 in GC-MS/MS parent-daughter mode), Ts/αβC$_{30}$ Hopane: ratio of 18α-22,29,30-trisnorneohopane over αβC$_{30}$ Hopane (monitored transition of *m/z* 370-191 and 412-191 in GC-MS/MS parent-daughter mode, respectively), C$_{29}$ Ts/C$_{30}$ Diahopane: ratio of C$_{29}$ Ts over C$_{30}$ Diahopane (monitored transition of *m/z* 398-191 and 412-191 in GC-MS/MS parent-daughter mode, respectively), Ts/Tm: 18α-22,29,30-trisnorneohopane/17α-22,29,30-trisnorneohopane (monitored transition of *m/z* 370-191 in GC-MS/MS parent-daughter mode), (for distribution of terpane components see Fig. 52), Rr % MPI-1: inferred vitrinite reflectance from MPI-1(methylphenanthrene index; Radke & Welte, 1993) (MPI-1 values after Gratzer et al., 2011). The arrows indicate the theoretical change of values with increasing maturity.

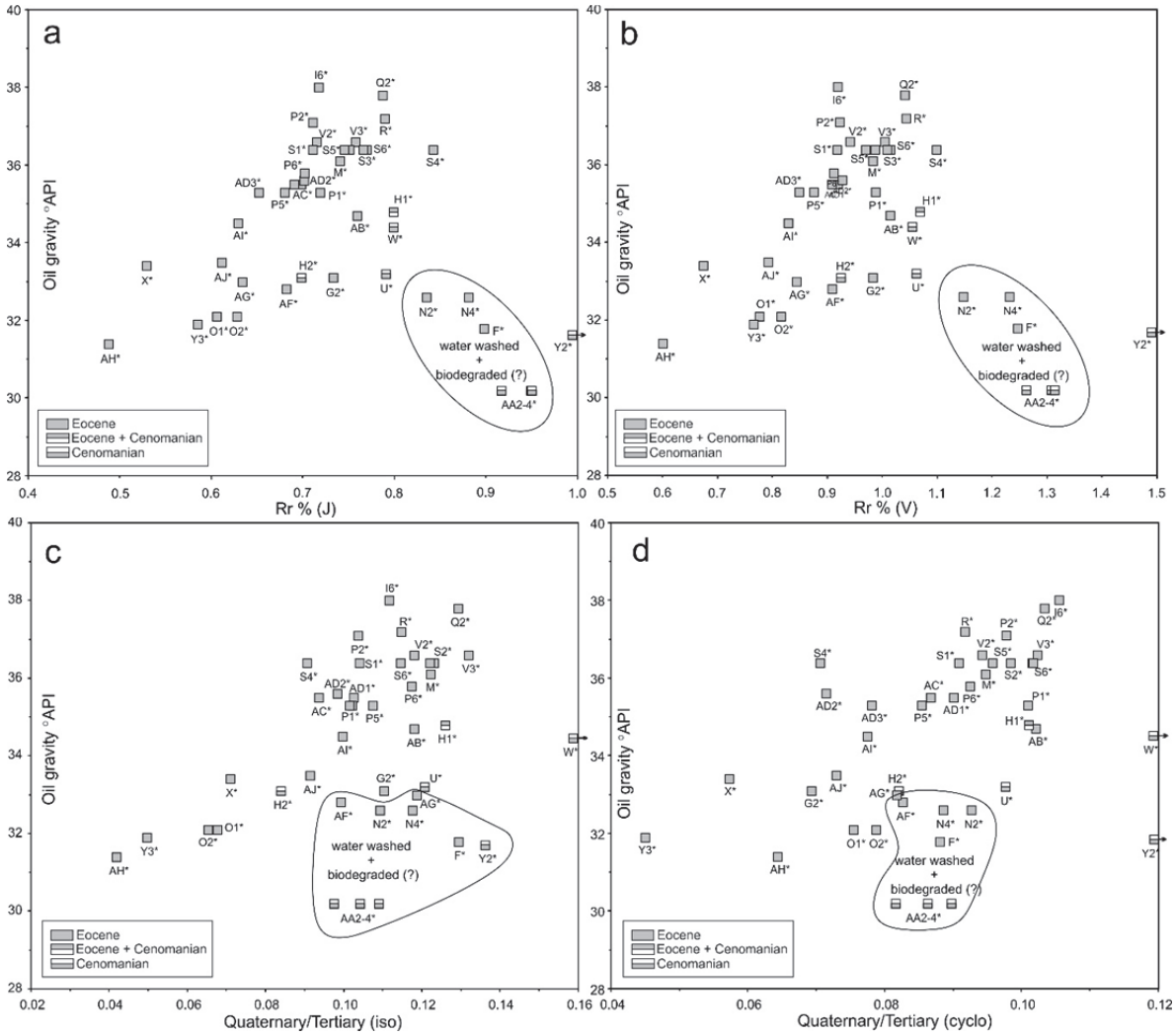

Fig. 48. Cross-plots of oil gravity (°API) versus (a) inferred vitrinite reflectance (Rr %) from parameter J: (2- + 3-methylhexane) / (1*trans*3- + 1*cis*3- + 1*trans*2- + 1*cis*2-dimethylcyclopentane) (Schaefer & Littke, 1988), (b) inferred vitrinite reflectance (Rr %) from parameter V: (2,2- + 2,3- + 2,4- + 3,3-dimethylpentane + 2,2,3-trimethylbutane + 2- + 3-methylhexane + 3-ethylpentane) / (1,1- + 1*cis*3- + 1*trans*3- + 1*trans*2- + 1*cis*2-dimethylcyclopentane) (Schaefer & Littke, 1988), (c) ratio of quaternary over tertiary pentanes: (2,2- + 3,3-dimethylpentane)/(3-ethylpentane + 2,3- + 2,4-dimethylpentane) (Hunt et al., 1980), (d) ratio of quaternary over tertiary cyclopentanes: 1,1-dimethylcyclopentane / (1,1- + 1*cis*3- + 1*trans*3- + 1*trans*2- + 1*cis*2-dimethylcyclopentane) (Hunt et al., 1980).

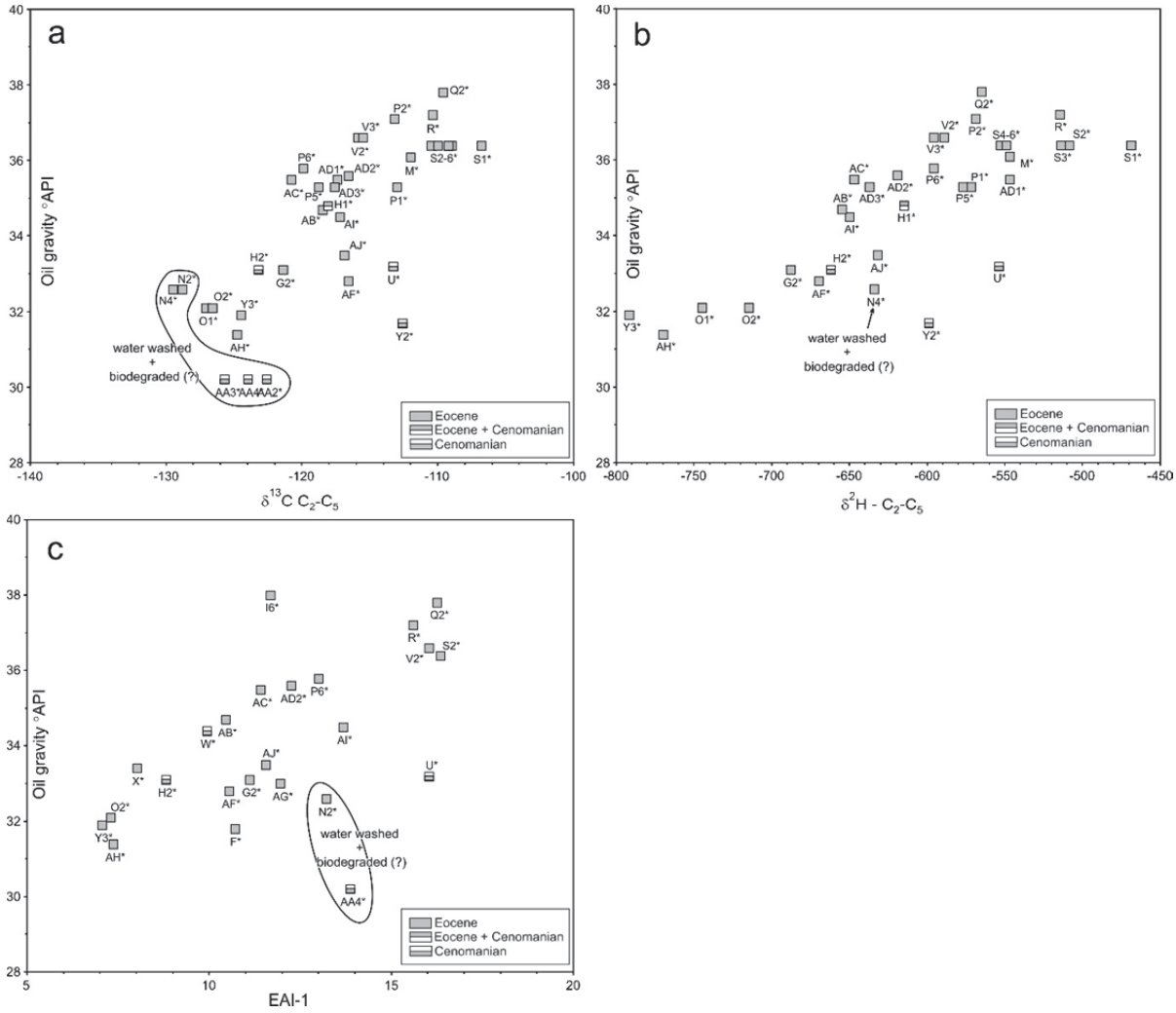

Fig. 49. Cross-plots of oil gravity (°API) versus (a) $\delta^{13}C$-C_2-C_5: summed $\delta^{13}C$ values of ethane, propane, *n*-butane, *n*-pentane (gas associated with investigated oils, after Pytlak et al., 2016a), (b) $\delta^{2}H$-C_2-C_5: summed $\delta^{2}H$ values of ethane, propane, *n*-butane, *n*-pentane (gas associated with investigated oils, after Pytlak et al., 2016a), (c) EAI-1: Ethyladamantane index; diamondoids isomerization index.

Supporting evidence that the stable carbon and hydrogen isotope composition of ethane, propane, *n*-butane and *n*-pentane are controlled by maturity is provided by positive relations with light hydrocarbons maturity parameters (Fig. 50a,b,d,e) and MPI-1 (Fig. 50c,d).

All mentioned cross-correlations show that API gravities of unaltered oils from the Alpine Foreland Basin are primarily governed by maturity.

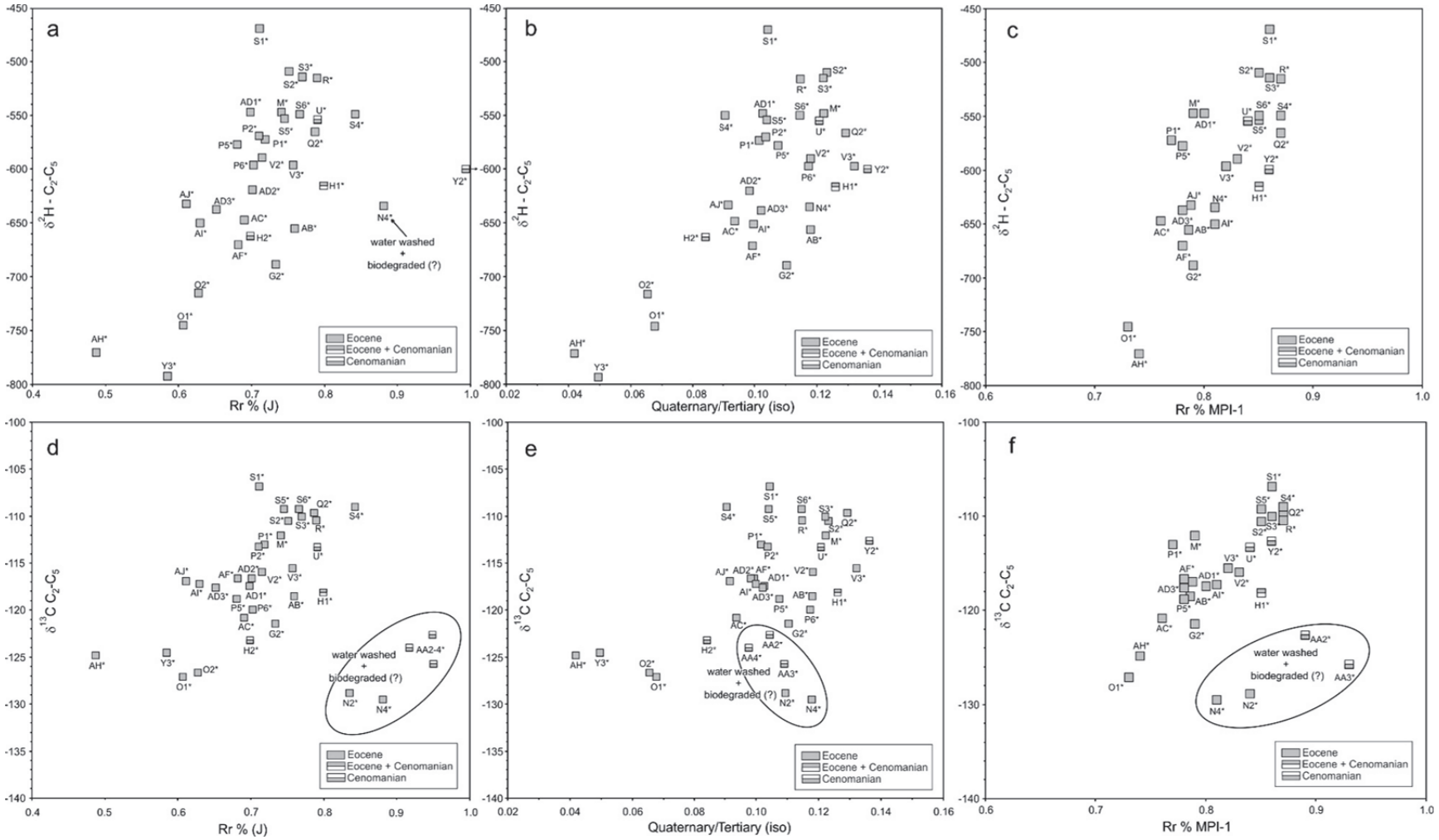

Fig. 50. Cross-plots of (a-c) summed δ^2H and (d-f) $\delta^{13}C$ values of ethane, propane, *n*-butane, *n*-pentane from gas associated with investigated oils (after Pytlak et al., 2016a) over (a, d) vitrinite reflectance (Rr %) from parameter J: (2- + 3-methylhexane) / (1*trans*3- + 1*cis*3- + 1*trans*2- + 1*cis*2-dimethylcyclopentane) (Schaefer & Littke, 1988), (b, e) quaternary/tertiary pentanes ratio: (2,2- + 3,3-dimethylpentane)/(3-ethylpentane + 2,3- + 2,4-dimethylpentane) (Hunt et al., 1980), and (c, f) vitrinite reflectance from MPI-1 (methylphenanthrene index; Radke & Welte, 1993) (MPI-1 values after Gratzer et al., 2011).

9.3.2. Oligocene/Miocene condensates

C_{29} sterane and C_{31} hopane epimer ratios (20S/(20S+20R)) and 22S/(22S+22R)) of condensate samples are close to equilibrium (Tab. 11) suggesting generation at least peak oil window maturity. Some very low biomarker isomerization ratios are most probably caused by extensive biodegradation. To eliminate alteration effects, maturity was also estimated using diamondoid hydrocarbons, which are more resistant to micobial degradation.

Methyladamantane indices (MAI) in condensate samples range from 28 to 60 (Fig. 51b, Tab. 11). According to Chen et al. (1996), this MAI range corresponds to vitrinite reflectance values of about 0.7 to 1.1%Rr.

To the best of my knowledge, the ethyladamantane index (EAI) has not yet been used to estimate vitrinite reflectance. However, a good correlation is observed between EAI and MPI-1 in Cenomanian/Eocene oil samples in the Alpine Foreland Basin (VR_{MPI} = (EAI+32.07)/55.195; $r^2 = 0.72$) (see section 8). The application of this equation for the condensate sample suggests that they have been generated at oil window maturity (0.9-1.1 %Rr).

Similarly, in Cenomanian/Eocene reservoirs EAI correlates with the stable isotopic composition of associated ethane. The fact that the latter can be used to estimate %Rr (see Berner & Faber, 1996) allows an additional calibration of EAI. Applying the model of Berner & Faber (1996) and assuming an average isotopic composition of the source rock of -27‰ V-PDB (Schulz et al., 2002; VR_{C2} = (EAI+10.0817)/25.249; $r^2 = 0.90$), the maturity of source rock for condensate is estimated as 0.9 to 1.6% Rr. However, the vitrinite reflectance values probably are biased due to regional variations of the isotopic signature of the source rock (Bechtel et al., 2013; see also below) and, therefore, are not used in the following. Hence, despite of the EAI-C_2 correlation, I assume that condensates were generated at peak-oil to late oil window maturity (max. 1.1% Rr) and are not products of intense thermal cracking.

The presence of in condensates, including diamondoid hydrocarbons, makes it likely that methane in Oligocene/Miocene reservoirs is partly thermogenic in origin (Tab. 11). Indeed, $\delta^{13}C$ values indicate the presence of varying proportions of thermogenic methane (see section 5.2). Interestingly, there is a weak positive correlation between the percentage of thermogenic methane (estimated based on $\delta^{13}C$ values) in

Oligocene/Miocene reservoirs and concentrations of diamondoids in condensates (Fig. 51a), although diamondoid concentrations may be elevated by biodegradation removing less resistant saturated and aromatic components. In addition, increasing input of thermogenic methane is also correlated with maturity-related diamondoid isomerization indices (Chen et al., 1996; Pytlak et al., 2017; Fig. 51b,c).

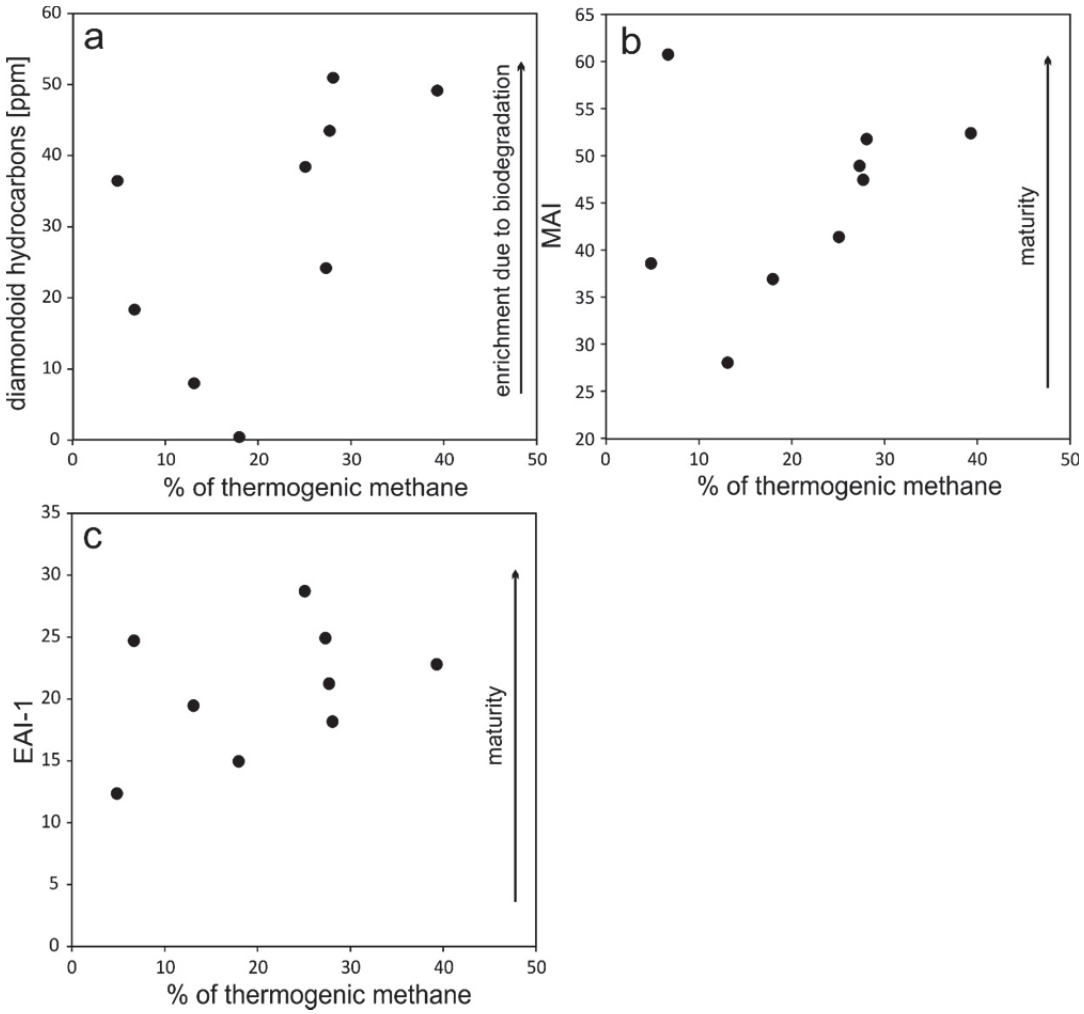

Fig. 51. Cross-plots of (a-c) estimated percentage of thermogenic methane in Oligocene/Miocene reservoirs, based on mixing of two end-members with distinctive stable carbon isotopic compositions: -38.4‰; after Pytlak et al. (2016a) and -65.1‰; after Pytlak et al. (2016b) versus (a, d) concentration of diamondoid hydrocarbons in condensate samples, (b) methyladamantane index; diamondoids isomerization index, (c) ethyladamantane index; diamondoids isomerization index (see Pytlak et al., 2017 and section 8 for more details on diamondoids in oil samples).

9.4. Genetic type and depositional environment of source organic matter

"Classical" biomarkers and compound specific isotopy are used in this section to characterize condensate samples from Oligocene/Miocene reservoirs, to provide information on their source rock and to compare them with Cenomanian/Eocene oils.

High oleanane index values (oleanane/(oleanane+hopane); Tab. 11) show that the source rock of the condensates was deposited during Late Cretaceous or Cenozoic time. Because Upper Cretaceous source rocks are not known from the study area, this is a strong argument for an origin from the organic-matter rich Lower Oligocene succession, which also generated the oil in Cenomanian/Eocene reservoirs (Gratzer et al., 2011). However, the oleanane index of condensates is higher than that of oils, perhaps because of higher maturation.

A common origin of Oligocene/Miocene condensates and Cenomanian/Eocene oils is also supported by similar distribution patterns of regular ααα steranes and αβ hopanes (Figs. 52, 53).

Dibenzothiophene/phenanthrene and Pr/Ph ratios are similar for condensate and oil samples (Fig. 54). Pr/Ph ratios in the range of 1 to 3 indicate dysoxic conditions during source rock deposition. Oxygen-depleted conditions are also supported by relatively high $C_{35}/(C_{34}+C_{35})$ homohopane ratios. High Pr/Ph ratios of samples S2 and A7 (Fig. 54) probably result from fractionation during migration (Napitupulu et al., 2000; see below). The relative distribution of hopanes and tricyclicternapes can be used to distinguish marine shale from lacustrine source rock. Oils derived from marine shale generally have higher C31 22R homohopane/C30 hopane ratio and lower C26/C25 Tricyclic terpane ratio compared to oils derived from lacustrine source rock (Fig. 55; Peters et al., 2005).

Both, Oligocene/Miocene condensates and Cenomanian/Eocene oils contain significant amounts of HBIs (Fig. 56) indicating that diatoms contributed significantly to the organic matter of the source rock. Input of terrestrial organic matter is reflected by land plant-derived biomarkers (e.g. bicylic sesquiterpanes: eudesmane and cadinane, diterpanes: norpimarane, pimarane, abietane, phylocladane). Both HBIs and land plant biomarkers occur in higher concentrations in condensates compared to oils. Probably this is an effect of the removal of *n*-alkanes during biodegradation.

Relatively high C_{27} diasterane/C_{27} sterane ratios and low C_{29}/C_{30} hopane ratios (Tab. 11) point to a clay-rich source rock. In comparison to oil samples, C_{27} diasterane/ sterane and C_{29}/C_{30} hopane ratios of condensate samples are elevated (Fig. 52). As biodegradation can elevate both, the C_{27} diasterane / sterane (Seifert & Moldowan, 1979) and the C_{29}/C_{30} hopane ratio (Peters et al., 2005), this difference may reflect different degrees of degradation.

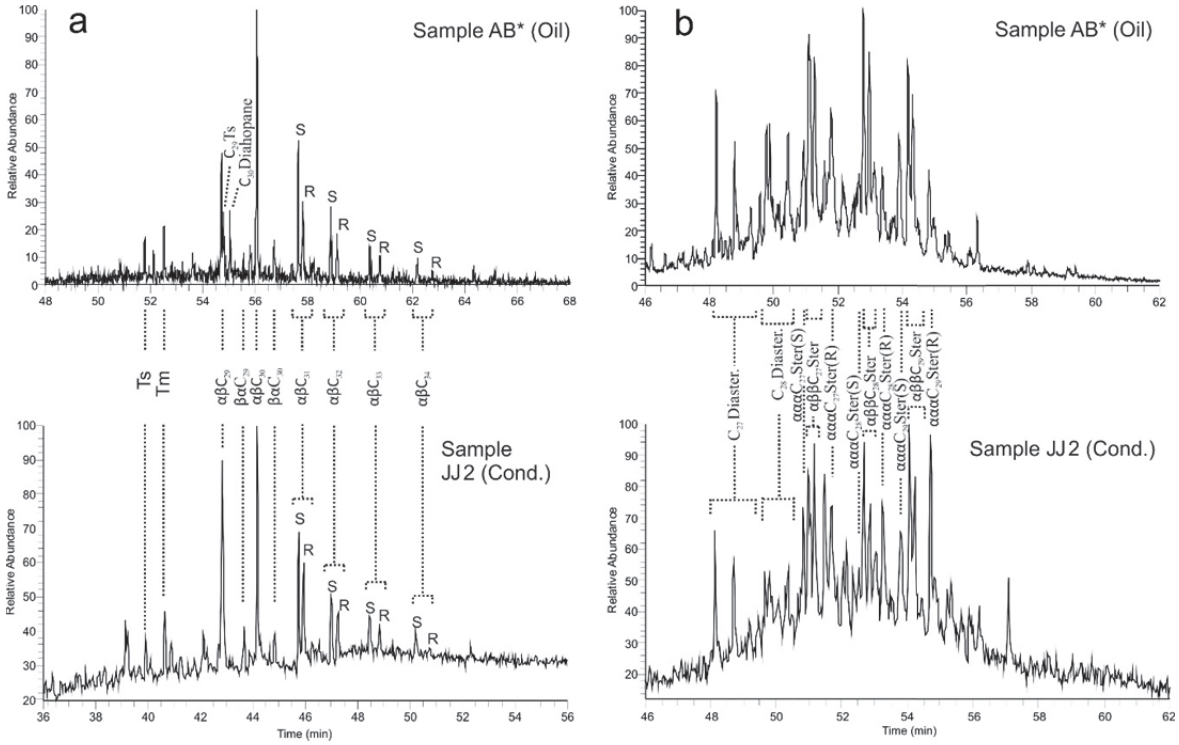

Fig. 52. Comparison of (a) terpanes (*m/z* 191) and (b) steranes (*m/z* 217) biomarker fingerprints in two samples: oil from Eocene reservoir and condensate from Miocene reservoir.

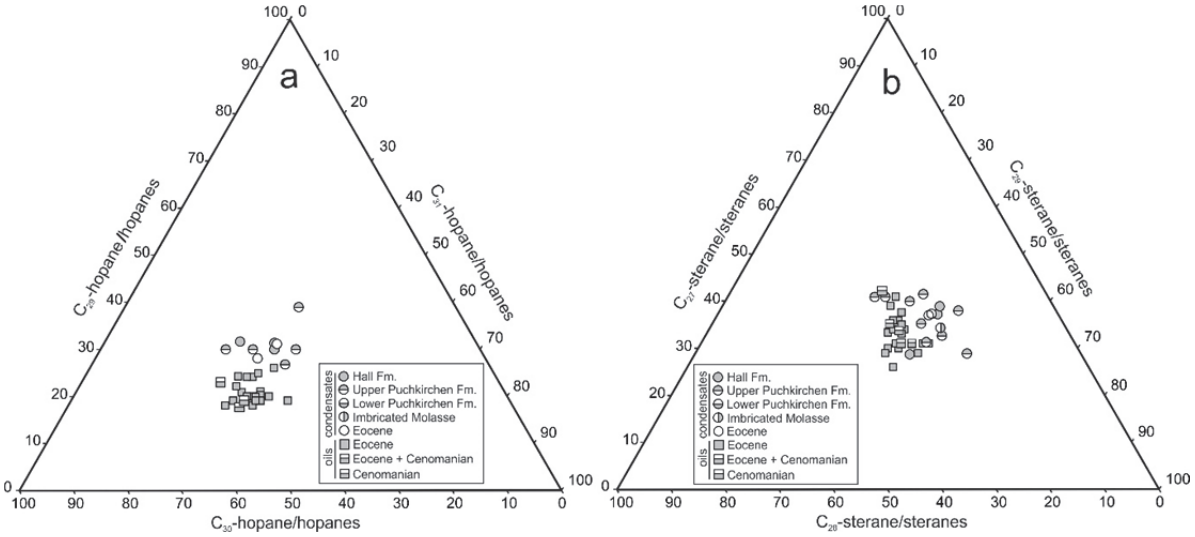

Fig. 53. Tertnary diagram of relative proportions of (a) αβ hopanes and (b) regular ααα steranes in oils samples from Cenomanian/Eocene reservoirs and condensates from Eocene and Oligocene/Miocene resrvoirs.

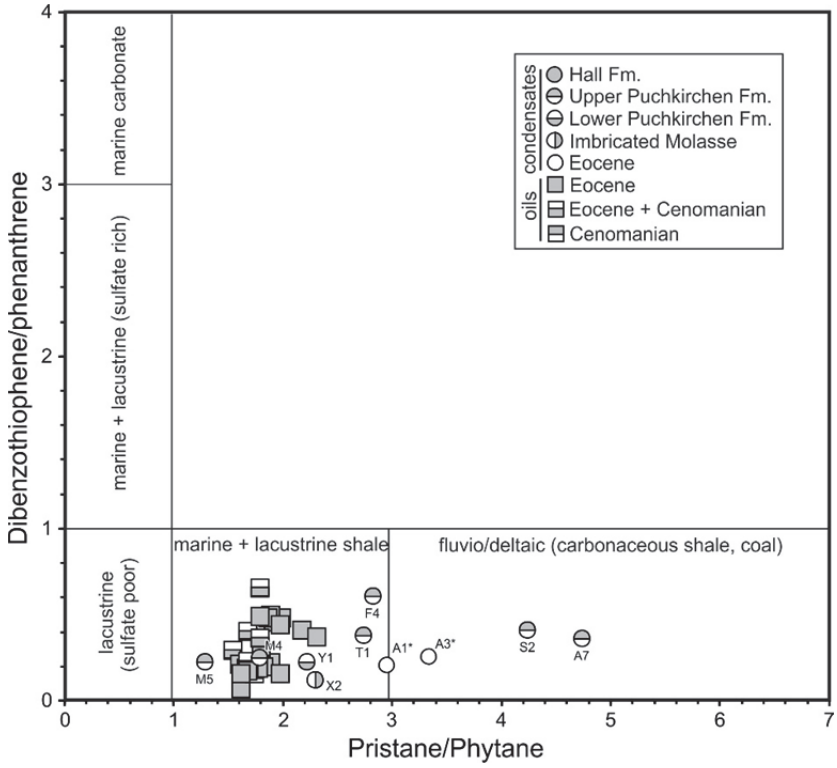

Fig. 54. Cross-plot of the dibenzothiophene/phenanthrene ratio versus pristane/phytane ratio. Classification of source kerogen sedimentation conditions after Hughes et al. (1995).

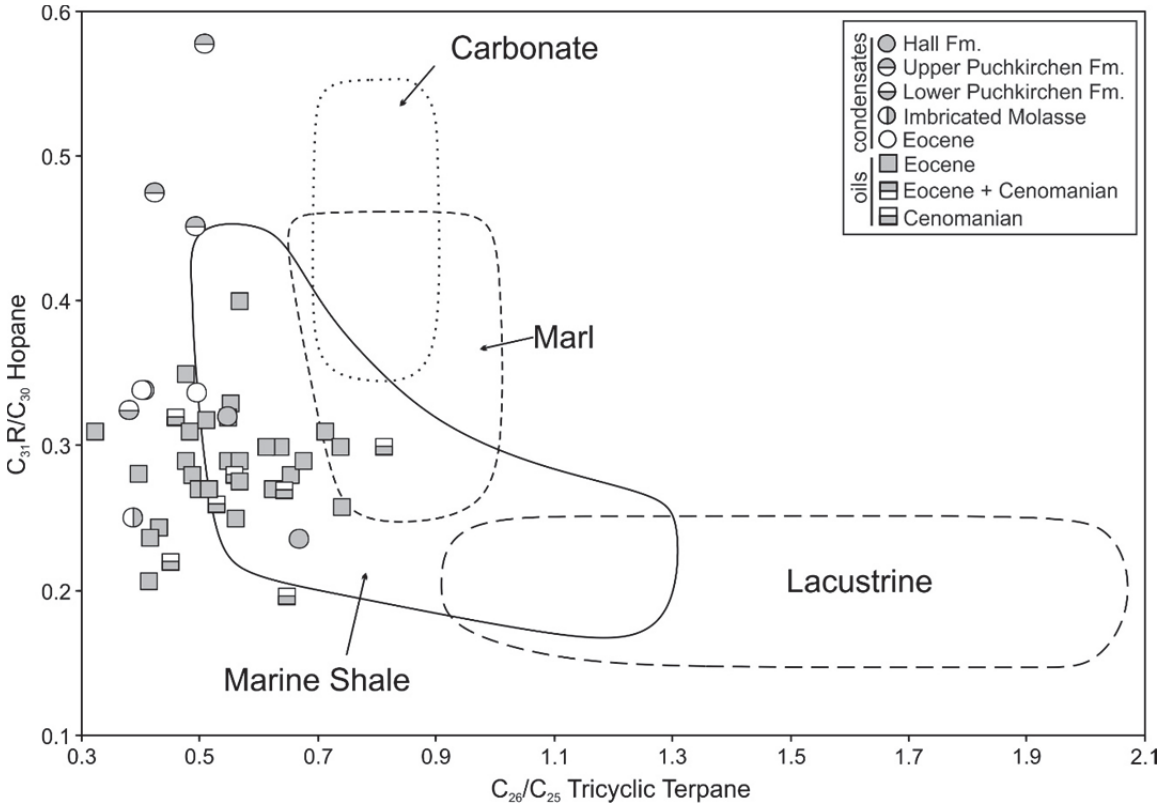

Fig. 55. Cross-plot of C_{26}/C_{25} tricyclic terpane versus C_{31} 22R/C_{30} hopane to predict source-rock depositional environments (modified after Peters et al., 2005).

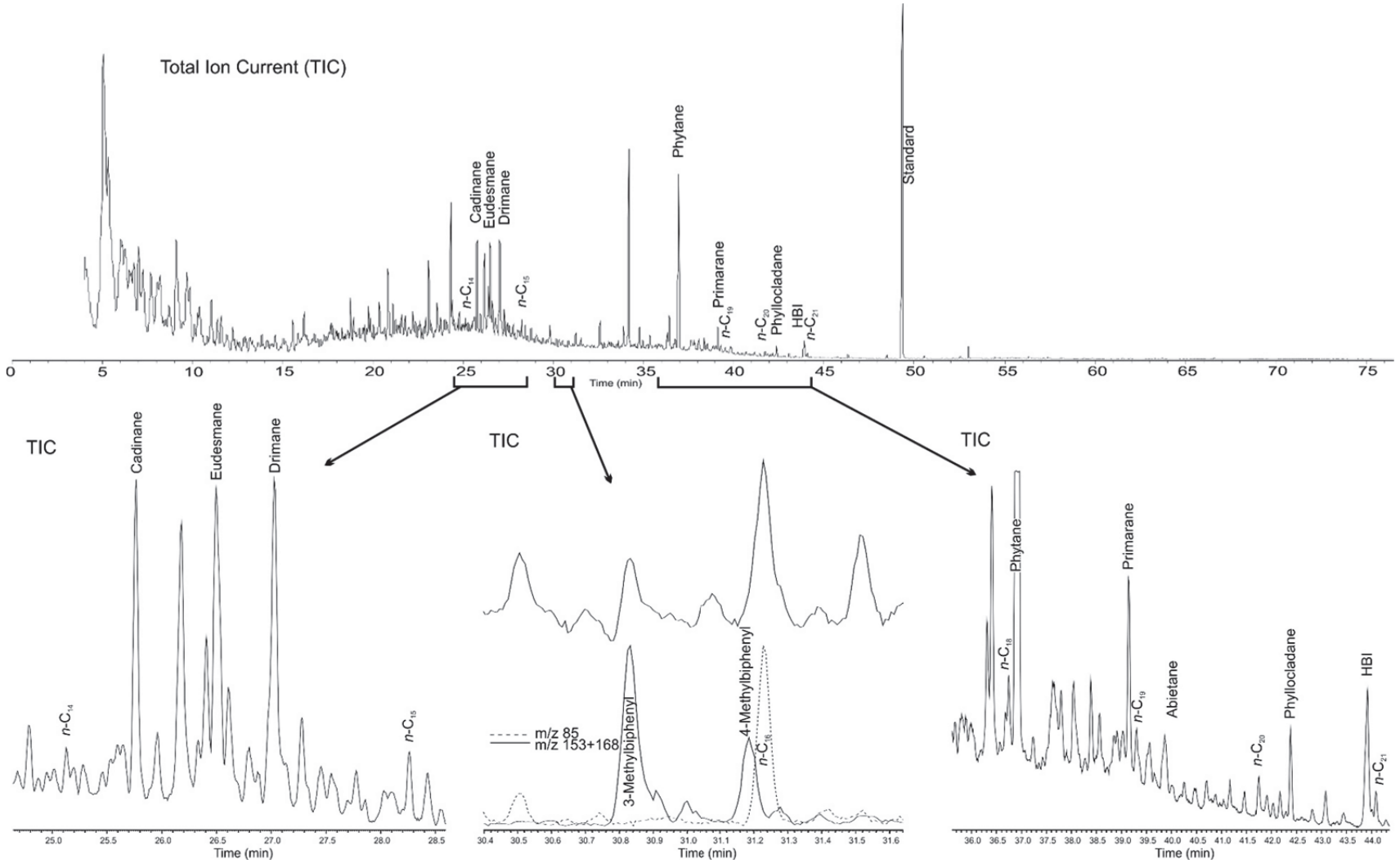

Fig. 56. Mass chromatogram (Total Ion Current, upper section) of condensate sample M5. HBI- Higly branched isoprenoid.

$\delta^{13}C$ values of individual C_{15}-C_{20} *n*-alkanes and isoprendoids of Oligocene/Miocene condensate samples and two condensate samples from Eocene reservoir are displayed in Fig. 57. They show a decrease of $\delta^{13}C$ values with increasing number of carbon atoms and a clear regional trend with an depletion of ^{13}C in the eastern part of the study area.

The same trends have been observed for oils in Cenomanian and Eocene reservoirs by Gratzer et al. (2011) and Bechtel et al. (2013). According to these authors, the east-west trend reflects differences in the isotopic composition of the upper and lower part of the source rock. The organic matter of black shales in the upper part of the Schöneck Formation shows isotopically lighter $\delta^{13}C$ values (depletion of ^{13}C) than the organic matter in its marly lower part (Schulz et al., 2002). Hence, a higher contribution of the upper unit of Schöneck Formation to eastern oils is in agreement with a higher thickness of this unit in this area (Sachsenhofer & Schulz, 2006).

$\delta^{13}C$ values of condensates from fields located in the western part of study area exceed the maximum values of oils. Most probably this is caused by extensive biodegradation which leads to enrichment of ^{13}C in residual *n*-alkanes (Boreham et al., 1995). On the other hand, the isotopically heaviest condensates are produced from fields located westwards from the westernmost oil fileds. Consequently, the observed values simply my reflect the continuation of the east-west trend. In any case, the described observations show that condensate samples from Oligocene/Miocene reservoirs are genetically related with oils from Cenomanian/Eocene reservoirs.

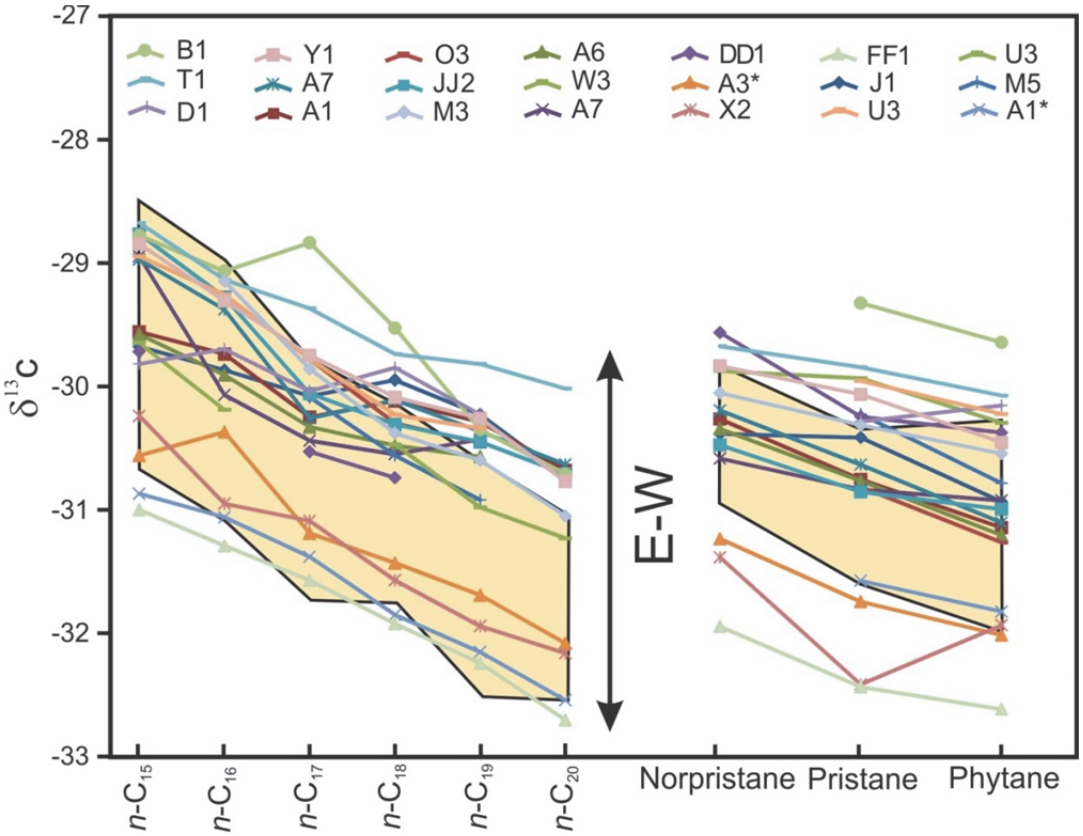

Fig. 57. Carbon isotopic composition of individual *n*-alkanes and acyclic isoprenoids from condensate samples produced from Oligocene/Miocene and Eocene reservoirs. Yellow background area represents minimum and maximum carbon isotopic composition of individual *n*-alkanes and acyclic isoprenoids from oil samples (Cenomanian and Eocene reservoirs, after Bechtel el al., 2013). Both isotopic composition of condensates and oils displays an E-W trend.

9.5. Evaporative fractionation

As shown above, condensates from Oligocene/Miocene and Eocene reservoirs are genetically related with oils from Cenomanian/Eocene reservoirs. Moreover, all applied maturity parameters argue against an overmature source rock and/or cracking of oil in high-temperature reservoirs. This implies that the condensates are not generated from a deep, highly mature source in which heavier hydrocarbons and/or kerogen have undergone extensive cracking.

An alternative process, which leads to the formation of a condensate is called evaporative fractionation (Thompson, 1987) and describes the loss of light hydrocarbons from a deeper oil reservoir resulting from a later gas charge. During this process, the gas phase of a gas-saturated oil escapes from the oil, leaving behind residual oil enriched in compounds like toluene and cycloalkanes, while other

compounds (e.g. heptane), are preferentially dissolved in the escaping gas phase (Thompson, 1987).

9.5.1. Condensates and oils from Cenomanian/Eocene reservoirs

Three condensate samples from Eocene reservoirs in the A* field, located in the eastern part of study area (Fig. 5), follow the evaporative fractionation trend described by Thompson (1987) (Fig. 58). This indicates that a pre-existing oil accumulation, either in underlying Cenomanian reservoirs or in Eocene reservoirs south of the A* field, was affected by a later gas charge, when thrusting continued (e.g. Schmidt and Erdogan, 1993).

A similar scenario was described by Sachsenhofer et al. (2006), who explained the presence of asphaltene-rich, non-producible petroleum (tar) in Eocene reservoir sandstones in the J* field (see Fig. 59 for location) by asphaltene precipitation caused by a later gas charge (and the adsorption of asphaltenes onto kaolinite).

In addition, the effect of evaporative fractionation can be observed regionally and even in single fields in the eastern part of the study area (inset in Fig. 59), which in contrast to western fields contain extensive gas caps (Malzer, 1993; fields I, J, P, S, V). The gas cap reflects a higher percentage of thermogenic gas and is in agreement with isotope data, which show that the gas was generated at slightly higher maturity than the oil (Fig. 11b). In addition to fractionation within traps, fractionation may have occurred also during the migration.

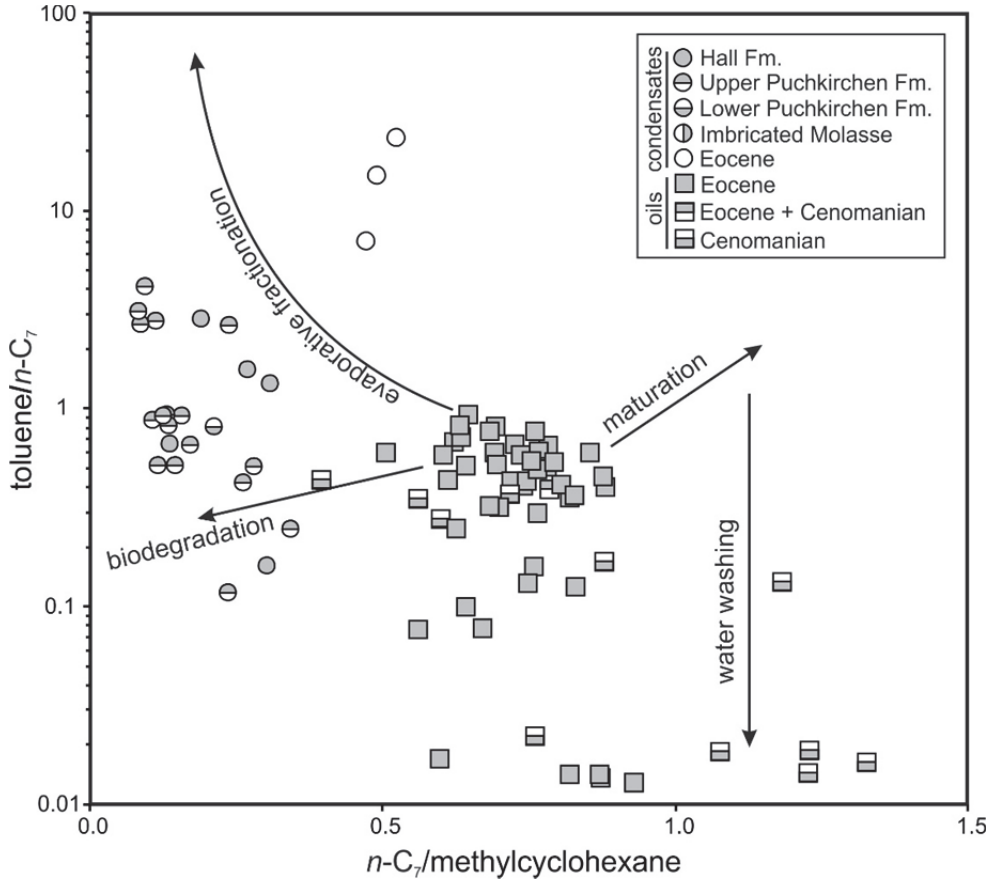

Fig. 58. Cross-plot of toluene/*n*-C_7 and *n*-C_7/methylcyclohexane ratios (after Thompson, 1987).

9.5.2. Condensates from Oligocene/Miocene reservoirs

Condensates in Oligocene/Miocene reservoirs are probably also products of evaporative fractionation. However, it is difficult to separate the effects of evaporative fractionation and extensive biodegradation (Fig. 58).

Positive relations exist between fractionation (toluene/*n*-C_7) of the condensates and both, the percentage of thermogenic methane in Oligocene/Miocene reservoirs (Fig. 59a) and the maturity, established based on diamondoid hydrocarbons in condensates (Fig. 59b-d). I consider that higher amounts of thermogenic methane and stronger fractionation reflect that thermogenic gas repeatedly stripped the original oil in Cenomanian/Eocene reservoirs. Obviously, increasing gas volumes, which cause stronger fractionation when passing through the oil deposit, are expected at higher maturity.

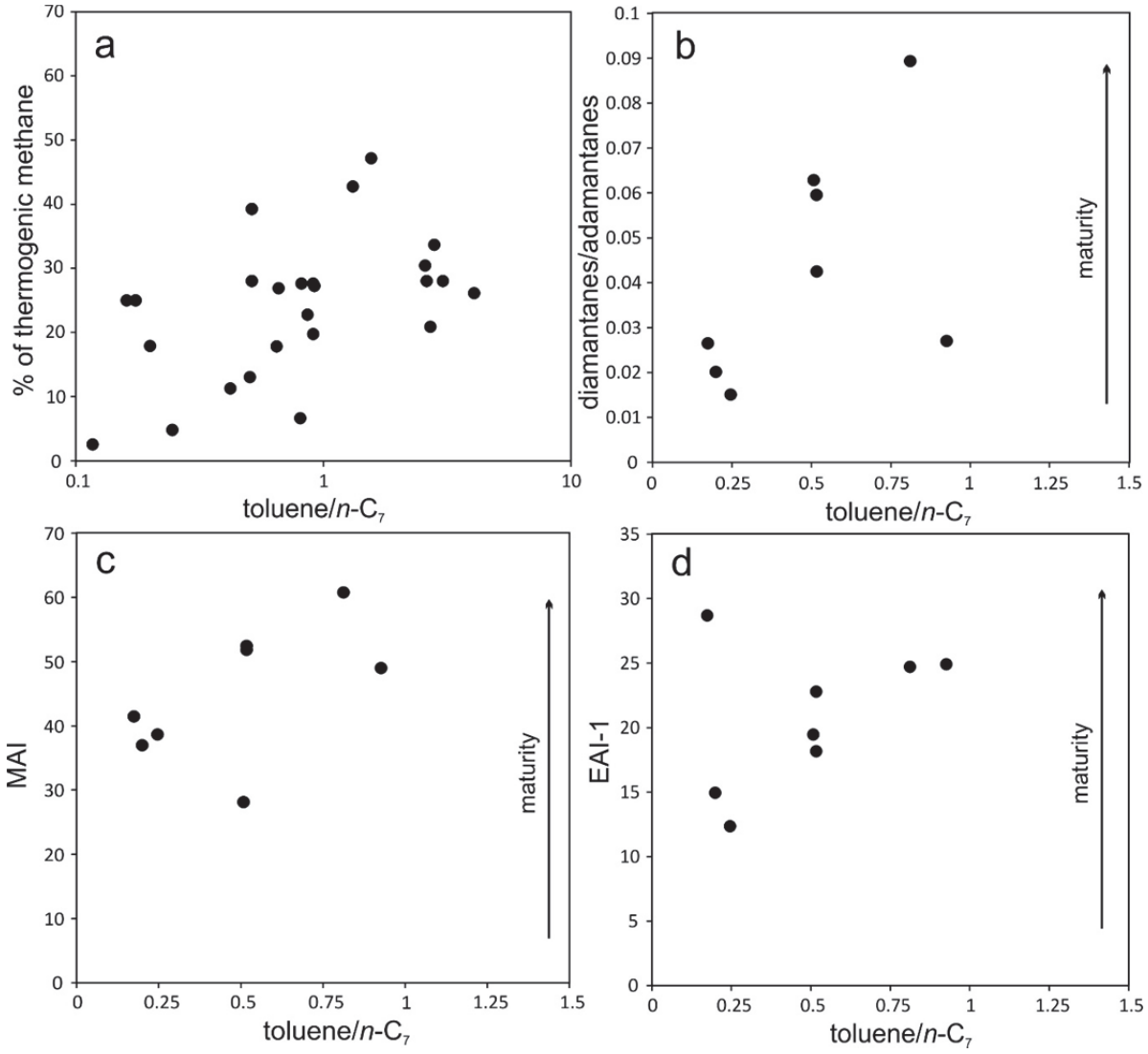

Fig. 59. Cross-plots of toluene/*n*-C_7 ratio (parameter derived from condensates co-produce with microbial methane) versus (a) estimated percentage of thermogenic methane in Oligocene/Miocene reservoirs, based on mixing of two end-members with distinctive stable carbon isotopic compositions: -38.4‰; (Pytlak et al., 2016a) and -65.1‰ (Pytlak et al., 2016b), (b) sum of diamantane hydrocarbons over sum of adamantane hydrocarbons (diamondoids from condensates co-produce with microbial methane), (c) methyladamantane index; diamondoids isomerization index, (d) ethyladamantane index; diamondoids isomerization index.

10. Implications for energy exploration and production

10.1. Hydrocarbon deposits

The study shows that in a single petroleum system hydrocarbons of different origin may be present: thermogenic, primary and secondary microbial.

10.1.1. Cenomanian/Eocene reservoirs

Geochemical data (e.g. isotopic composition of gaseous hydrocarbons, light hydrocarbons parameters, diamondoids) clearly shows that Cenomanian/Eocene reservoirs in eastern part of the basin are filled with mixture of hydrocarbons expelled from source rock at different maturation stages. According to parameters presented in this study, gaseous hydrocarbons have been generated at 0.7 to 1.2 %Rr. This is higher than estimates for oil (0.7-0.9 %Rr; Gratzer et al., 2011). In addition, no cracking trend (high temperature zone) based on biomarkers and diamondoids concentration was observed. This has certain consequences on understanding of the basin history.

Firstly, the north-south extension and burial depth of the active source rock (hydrocarbon kitchen) is higher than it has been assumed. Numeric models from Gusterhuber et al. (2013) show that a vitrinite reflectance of 1.2% is reached only at ~6 km depth subsea.

Secondly, the different source rock maturities control the physical properties of accumulated oil (excluding those reservoirs that have undergone secondary alteration processes). Deposits which received a high amount of late oil window hydrocarbons are characterized by elevated API values and developed gas caps (Fig. 60). Further, the geographical distribution of API gravities suggests, that a classic fill-spill migration sequence (Schmidt and Erdogan, 1996) seems to be invalid for the Alpine Foreland Basin. For example, oil fields R*, S*, Q* are characterized by higher API values than fields P* and O* located closer to the oil kitchen (Tab. 3).

In addition, the presence of highly fractionated hydrocarbons may result in the detection of new oil fields. An example is provided by field A* (see Fig 5 for location), which produced secondary microbial gas resulting from the degradation of oil, forming now a thin tar rim (Pytlak et al., 2016a). Between the tar rim and the gas, non- (or weakly) biodegraded, but strongly fractionated condensate (Fig. 58) was observed. In

total only about 5000 t of the condensate were produced (Kreutzer, 1993). However, I assume that the fractionated condensate may indicate an oil accumulation either below the Eocene reservoir (e.g. in Cenomanian), or along the migration pathway, which has not been detected yet. The differences in the degree of degradation indicate that evaporative fractionation post-dated biodegradation.

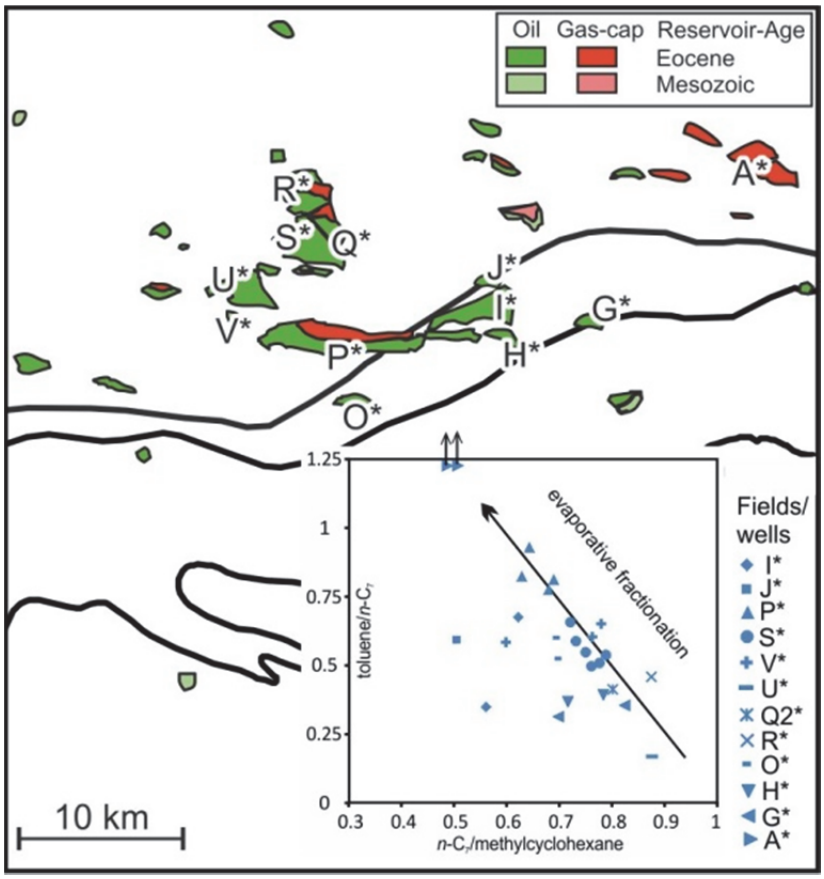

Fig. 60. Location of oil and associated gas fields in eastern part of study area. The inset illustrates the evaporative fractionation process within the oil and gas-condensate fields.

The co-existence of primary microbial and thermogenic hydrocarbons has been described in literature (e.g. Lillis, 2007; Penteado et al., 2014; Prinzhofer et al., 2000), but, to the best of my knowledge, reports on primary microbial gas in deep and hot reservoirs (>100°C), as observed in the Alpine Foreland Basin (Schoell, 1977; this study), are very rare. Partly this may be due to the fact that the subsequent charge of thermogenic oil and gas masks the preexisting microbial gas accumulations (Lillis, 2007). However, the correct identification of primary microbial gas is important as the

pre-existing primary microbial gas contributes to the total volume of accumulated hydrocarbons and, thus, may have a positive impact on the hydrocarbon potential. This is especially important in undercharged basins characterized by a low SPI, like in the Alpine Foreland Basin (Sachsenhofer et al., 2010). Additional quantitative information may be provided by petroleum systems modeling. Unfortunately existing models for the thermogenic petroleum system in the Alpine Foreland Basin consider the biodegradation risk, but not primary microbial gas generation (e.g. Gusterhuber et al., 2013).

Secondary microbial methane results from biodegradation of oil (e.g. Milkov, 2011) and, hence, is often associated with heavy oil, like in the wells A1* and A2* in the eastern part of the study area (Fig. 5), or tar mats. Therefore, the correct designation of the type of microbial gas (secondary vs. primary) is important for the exploration risk assessment in terms of oil quality.

The recognition of field compartmentalization is an important issue in hydrocarbon production. Geochemical data may contribute to delineate different compartments, but are useless in fields with geochemically similar oils. This thesis shows that in cases where oil composition is the same, gas composition may provide a convenient tool to prove field compartmentalization (see wells I1-6*, J1*, J2*, H1*, H2*, Y2* and Y3*, Tab. 5).

10.1.2. Oligocene/Miocene reservoirs

Dryness and the most negative $\delta^{13}C$ values of methane suggest a pure primary microbial origin of gas in Oligocene-Miocene reservoir horizons in the KK field, confirming the traditional model. In all others samples heavier hydrocarbons are present. The amount of C_{2+} hydrocarbons increases with reservoir depth, indicating a downward increasing contribution of thermogenic hydrocarbons. Varying contributions of thermogenic hydrocarbons are also reflected by strongly varying $\delta^{13}C$ values of methane. Based on $\delta^{13}C$ values of methane, gas from the F-O field in the western part of the study area contains the highest contribution of thermogenic hydrocarbons. The geochemical data suggest that Oligocene/Miocene condensates are derived from the same source rock than Cenomanian/Eocene oils. However, in the western part of the basin, the Schöneck Formation (the main source rock units) is missing in autochthonous sediments, but is present in Molasse imbricates (Sachsenhofer & Schulz, 2006). In addition, slid and re-deposited Schöneck Formation (Oberhofen facies; Fig. 34a, b) may form a potential source rock (Sachsenhofer & Schulz, 2006).

The gaseous hydrocarbons display an oil-window maturity. Based on biomarkers isomerization, the condensates formed at peak oil window maturity. In contrast, according to diamondoid isomerization index (MAI) maturities of condensates can reach 1.2 % Rr. Models of the thermal evolution of the frontal part of the Alps show that these maturities have not been reached in the Molasse Imbricates (Gusterhuber et al., 2014). This implies generation of the condensates form deeply buried autochthonous source rocks. In any case, the condensates from Oligocene/Miocene reservoirs are in fact the mixture of oil window products (representing biomarkers) and more mature hydrocarbons (high diamondoid isomerization indices).

Upward migration of hydrocarbons from autochthonous strata along faults is likely (e.g. fields in the eastern part of the study area) (Figs. 61, 62). Migration also occurred through low-permeability seal rocks (e.g. along sub-seismic fractures). Migration may have been facilitated in areas where lower Oligocene pelitic rocks are eroded and along the Puchkirchen Channel system, where a high percentage of permeable clastic rocks have been deposited. An effect of diffusion on molecular and isotopic composition of the gas cannot be observed.

“Bulk volume flow” rather than diffusion is supported by the fact that condensates show signs of evaporative fractionation. This process requires the passing of gas

through pre-existing oil deposits. This implies some possible oil deposits along the gas migration pathway (Fig. 62). Although oil stains are known from the Molasse Imbricates (Gusterhuber et al., 2014), low maturity of source rocks within the imbricates argues against generation of the late oil window-gas within them. Therefore, it is more likely that the oil has to be searched for in the deeper part of the autochthonous strata (Fig. 62).

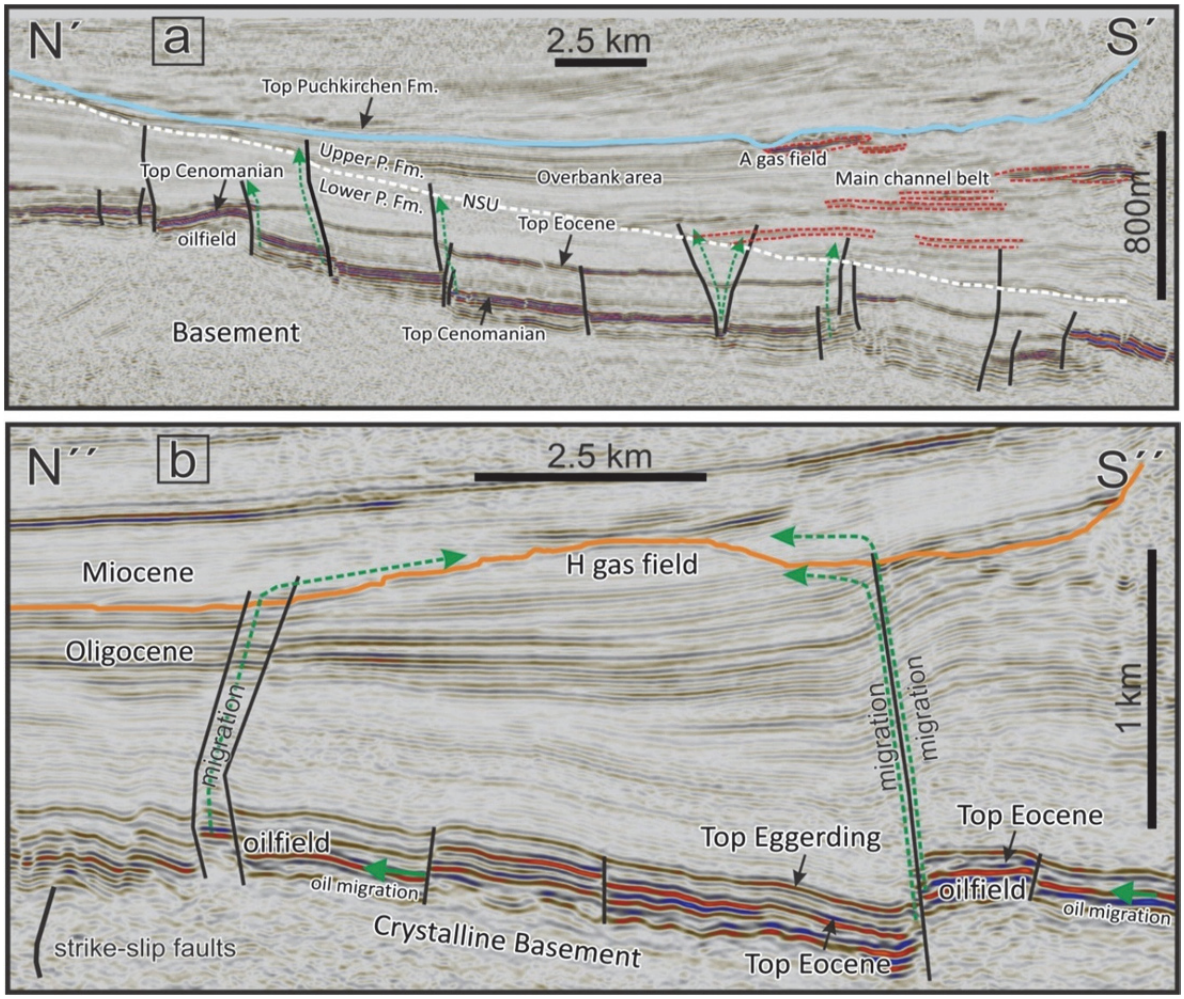

Fig. 61. Seismic examples of the Alpine Foreland Basin (for location see Fig. 6). (a) Cross-section across gas field A. Location of Puchkirchen channel belt and adjacent overbank deposits (both are the main gas reservoirs) are indicated with dashed red lines. Northern Slope Unconformity (NSU, Masalimova et al., 2015) separates Lower Puchkirchen Formation (Lower P. Fm.) from Upper Puchkirchen Formation (Upper P. Fm.). The NSU is cross-cut by faults active during deposition of Upper Puchkirchen Formation providing potential migration pathways for thermogenic hydrocarbons (dashed green lines). (b) Cross-section across gas field H and oil fields. Majority of oil and thermogenic gas in the Alpine Foreland Basin are trapped in Cenomanian and Eocene reservoirs in fault-related structures.

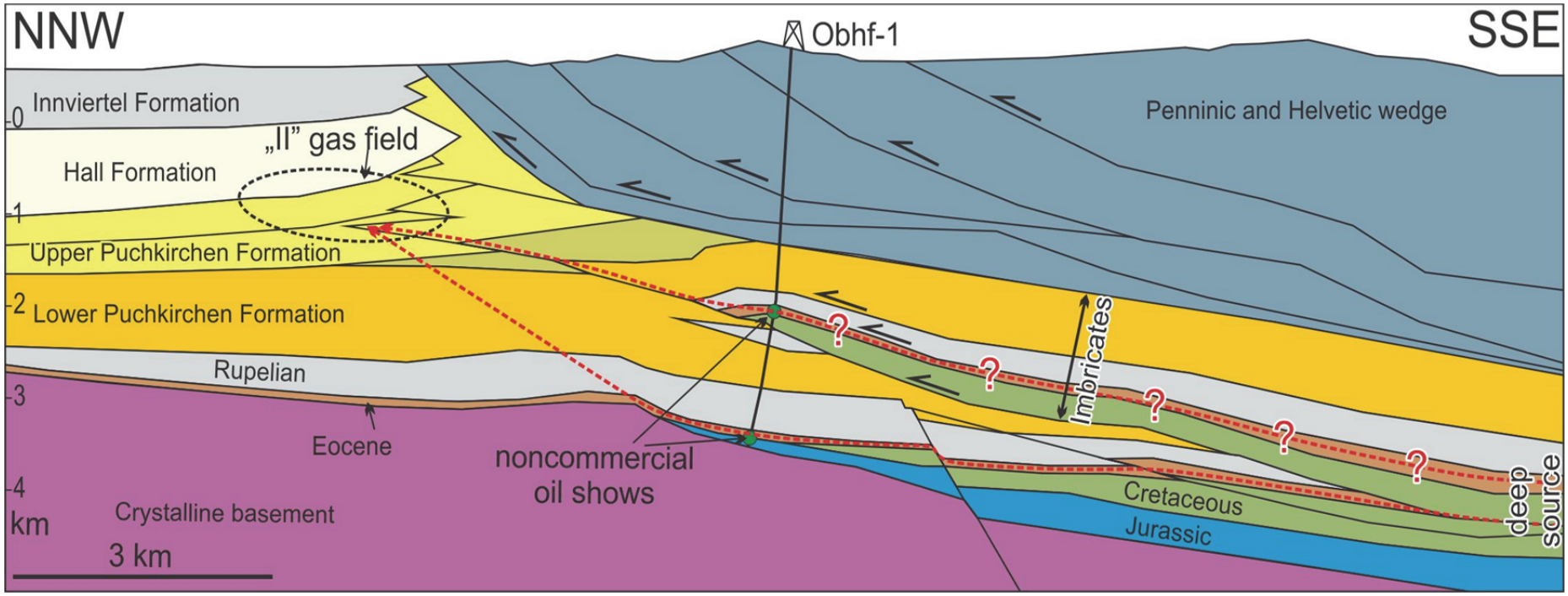

Fig. 62. Interpreted three-dimensional reflection seismic profile of the imbricated Molasse (after Hinsch, 2013). Deep faults that spans from Cenomanian/Eocene and Oligocene/Miocene reservoirs are shown in Fig. 61.

10.2. Fluid flow in deep aquifers

Significant removal of aromatics from bulk oil composition requires a sufficient volume of BTEX-undersaturated water. Knowing the relative solubility of individual oil components, the volume of water required to diminish its concentration can be estimated. Based on this and diffusion phenomenon, Lafargue & Barker (1988) and Lafargue & Thiez (1996) used a simple numerical approach to model natural water washing. The models of Lafargue & Thiez (1996) show that the removal of BTEX is limited by water velocity, if the water flow beneath the oil-water-contact is below 10 cm/year, but by rate of diffusion if water flow is higher.

In the following two oil fields (AA*, N*) affected by major water washing are described and implications for hydrogeological models are discussed.

In the AA* field Cenomanian reservoir rocks of water washed samples AA1-4* and Z* directly overlie fresh water bearing Malmian carbonates. In order to test, if mixing between Malmian and Cenomanian/Eocene brines occurs, the Cl^- concentration and stable isotope ratios in water co-produced with oil are cross-plotted in Fig. 63. The correlation line between δ^2H and $\delta^{18}O$ values (Fig. 63c) shows slight deviation of Malmian water from the global meteoric water line (GMWL). The Malmian aquifer was charged during Pleistocene to Early Holocene time, at temperatures of about 1.4°C to 3.4°C (Andrews et al., 1985; 1987, Goldbrunner, 2012). The position of the water samples in Fig. 63a-c suggests different degrees of mixing of original connate brines and Malmian water. Within this context, connate brines in the Cenomanian reservoir in field AA* experienced extensive, but not complete replacement by meteoric Malmian water (Fig. 63) indicating that a significant volume of relatively stagnant connate brine remained in the reservoir. Considering hydrostatic conditions, it is unlikely that the concentration gradient would be high enough to explain the strong observed BTEX depletion. This implies that water in the Malmian aquifer below the Cenomanian horizon (Fig. 64) is under dynamic condition, thus, providing sufficient undersaturated water that drives diffusion and removes BTEX from the reservoir area. The high permeability of the Malmian carbonate, a pre-requisite for significant water flow, is proven by losses of drilling mud (industry data) and allows the reinjection of thermal water in field AA* (Fig. 64, Elster et al., 2016).

The strongest water washing effect is observed in the Eocene reservoir of field N*, located in the eastern part of the basin (Fig. 5). Strong support for mixing of meteoric water and connate brine in this field is provided by Cl^- and isotope data. Moreover, water sample N1* plots close to Malmian water in Fig. 63c. Within this context it is noteworthy, that an extensive aquifer is indicated by a strong water drive keeping the reservoir pressure constant, despite of decades of oil production. A relative high reservoir temperature of field N* (50°C) despite of shallow depth (~1000 m $TVD_{subsurfce}$; Kamyar, 2000) provides further evidence of upward directed fluid flow. However, field N* is located east of the pinchout of Malmian rocks and the Eocene reservoir directly overlies crystalline basement (e.g. Wessely et al., 1981; Kröll et al., 2006). This suggests that the crystalline basement itself forms an important aquifer. Similarly, crystalline basement rocks are considered an important aquifer in the recharge area (Fig. 3, Goldbrunner 2000) and along faults separating Malmian carbonates (Fig. 4, Goldbrunner, 2012). Furthermore, in the discharge area east of the limit of the Malmian aquifer (Figs. 3, 4) water flow takes place in Cenozoic sandstones, including Eocene horizons (Fig. 4; Schubert, 1996). Fig. 3 shows that field N* is located outside the boundaries of the regional thermal water system, considered by the Bayrisches Landesamt für Wasserwirtschaft (1999). Hence, the study results inply that the boundaries of established flow models need modifications.

Whereas oils from the northern part of study area are heavily water washed, oils from the southern part typically show no evidence of water washing (e.g. G*, O*, P*, and E* fields; Fig. 3). This is in agreement with stagnant conditions in the reservoir and the Malmian aquifer in this area (Fig. 3).

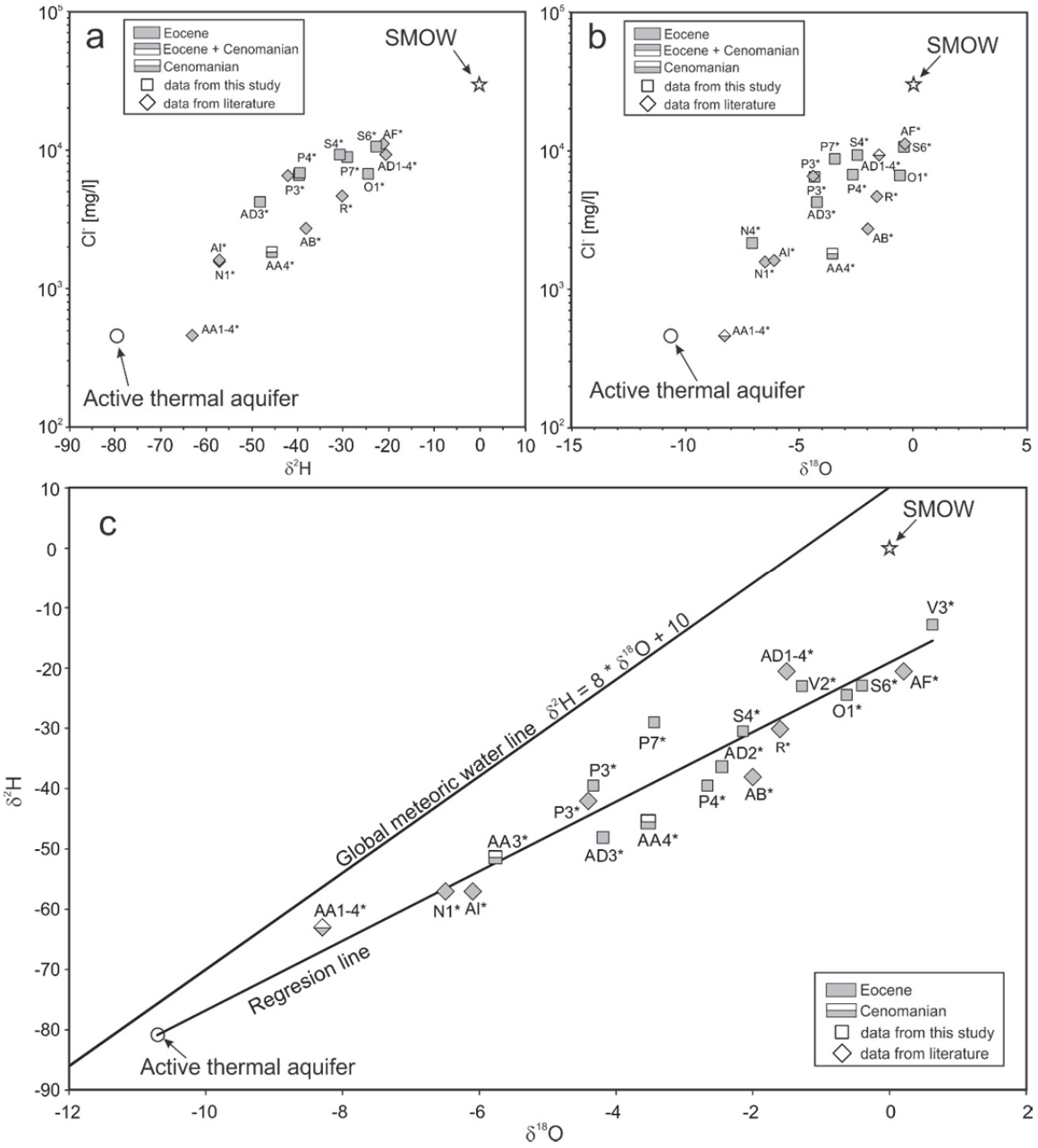

Fig. 63. Cross-plots of chlorine content and isotopic composition of deep ground and formation waters of the Alpine Foreland Basin; (a) δ^2H values versus Cl^- content, (b) $\delta^{18}O$ values versus Cl^- content, (c) δ^2H versus $\delta^{18}O$ values. Note that industry salinity data are plotted against isotopic composition of samples measered in the frame of this study (Figs. a,b). Average isotopic and salinity values of active thermal water (Malmian aquifer) are indicated after Andrews et al. (1987); Goldbrunner (2012); Elster et al. (2016). For sample location see Fig. 5.

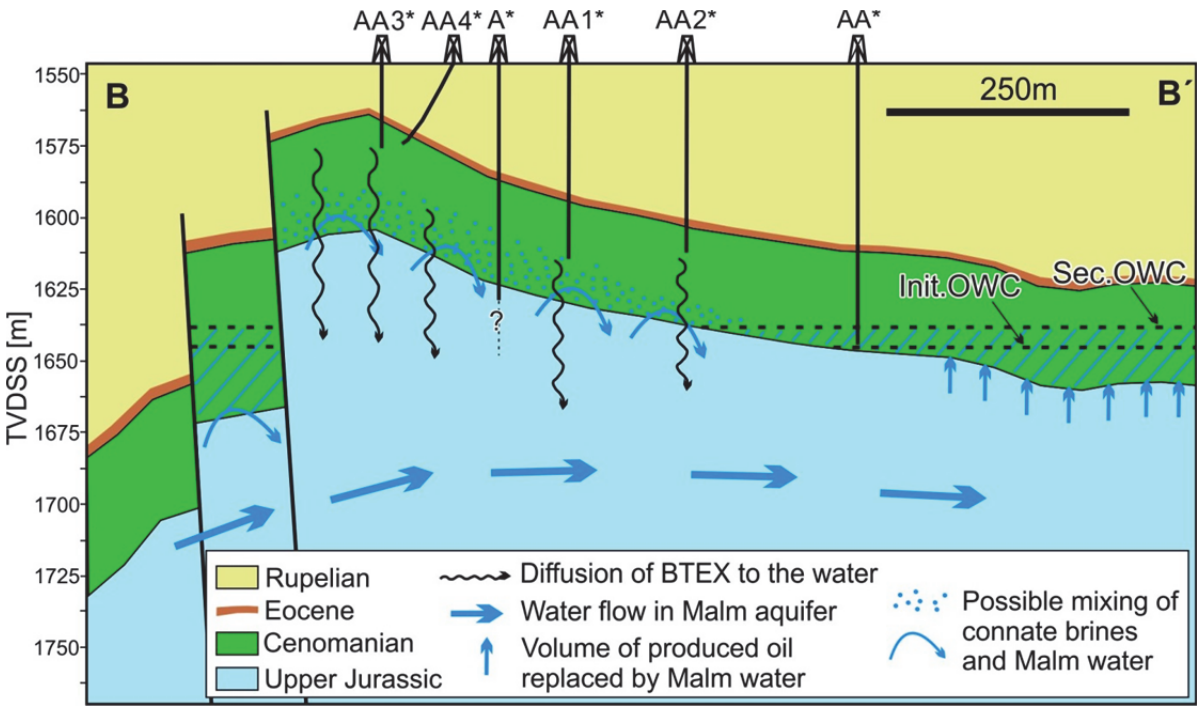

Fig. 64. Simplifed cross section of oil field and location of AA1-4* samples. Well A* is used for re-injection of thermal water produced form Malmian horizon by a well located 3 km west of the section. Well AA* is used as re-injector for reservoir brines co-produced with oil. Init. OWC – initial oil-water-contact at the beginnnig of oil production, Sec. OWC – secondary oil-water-contact estimated after 40 years of production, TVDSS – true vertical depth subsurface.

11. Conclusions

Generation, mixing, and alteration of thermogenic and microbial gas in oil deposits:

Based on stable carbon and hydrogen isotopic variations several gas families are defined, which are the result of various processes active during hydrocarbon generation and degradation:

- Gas samples from P1-8*, I1-6*, J1*, J2*, H2* (Group I) show signatures of "typical" thermogenic gas generated within the oil window. Gas in the N* field is unique in comprising isotopically light methane and C_{2+} hydrocarbons. Despite of low carbon isotope ratios of methane (-60 ‰), the N* gas is interpreted as low maturity.
- Gas samples along the southern margin of the Alpine Foreland Basin (Group IIa) and samples between P*, I*, J* and N* (Group IIb) are characterized by mixing of thermogenic gas and varying amounts of microbial methane.
- Gas samples from the shallow northeastern part of the study area (e.g. A* Field) are associated with heavily biodegraded oil (Group IV). Their origin is explained by secondary microbial origin (methanogenesis during in-reservoir oil degradation).
- Methane in gas samples from the western part of the study area (Group III) is mainly of microbial origin. Relative heavy hydrogen isotopes indicate a different source for the microbial methane compared to that of Group I and II gases.

Gas maturity varies from 0.6 to 1.2 %Rr. In general there is a good accordance with oil maturity. According to ethane and propane isotope data, the highest maturity of wet gas occurs in the S*, Q*, R* area. In those fields the thermogenic methane signature is masked by microbial input. The isotopically heaviest methane is trapped in the P* field.

Whereas a secondary microbial origin is likely for methane in Group IV and some Group III gases, a primary microbial origin is probable for gas samples from fields, which are now at temperatures exceeding 80°C (part of Group IIa and III samples). Although Group III gases do not show signs of advanced biodegradation, methane may be of secondary microbial origin. Because GOR of these gases are typically low, implying a small methane volume, even very slight in-reservoir hydrocarbon biodegradation may result in isotopically light methane.

Potential source rocks for primary microbial gas include adjacent Eocene Cerithian Beds and Lower Oligocene pelitic rocks (Schöneck, Eggerding fms.). Gas from the latter may have migrated into the reservoirs across E-W trending normal faults, which juxtaposed both already during Early Oligocene time. During Early Miocene time, the main source rocks reached the oil window beneath the Alpine nappes and generated oil and thermogenic gas, which mixed with the pre-existing primary microbial gas.

Microbial methane generated within the Molasse Imbricates is a speculative additional source for isotopically light methane in autochthonous Eocene reservoirs near the northern margin of the Alps. As the Oligo/Miocene rocks in the Molasse Imbricates are (partly) overpressured, lateral and downward migration seems to be possible.

Apart from the local implication, the study results show that:

- The presence of pre-existing primary microbial gas may increase the hydrocarbon potential in undercharged basins.
- The identification of secondary microbial gas supports exploration risk assessment.
- Gas composition may help to prove oil field compartmentalization.

Gas accumulation in Oligocene/Miocene reservoirs: evidence for gas mixing and gas degradation:

Gas trapped in Oligocene-Miocene reservoir rocks in the Alpine Foreland Basin has traditionally been considered (primary) microbial in origin. A detailed investigation of samples from all producing gas fields provides a more differentiated picture, which contributes significantly to the understanding of the petroleum system.

- Dryness and the most negative $\delta^{13}C$ values of methane suggest a pure primary microbial origin of gas in Oligocene-Miocene reservoir horizons in the KK field, confirming the traditional model.
- In all others samples heavier hydrocarbons are present. The amount of C_{2+} hydrocarbons increases with reservoir depth, indicating a downward increasing contribution of thermogenic hydrocarbons. Varying contributions of thermogenic hydrocarbons are also reflected by strongly varying $\delta^{13}C$ values of methane. Based on $\delta^{13}C$ values of methane, gas from the F-O field in the

western part of the study area contains the highest contribution of thermogenic hydrocarbons.

- The thermogenic hydrocarbons display an oil-window maturity and are derived from the deeper Mesozoic and Eocene oil-bearing reservoir and carrier beds. Upward migration along faults is likely (e.g. fields in the eastern part of the study area). Migration also occurred through low-permeability seal rocks (e.g. along sub-seismic fractures). Migration may have been facilitated in areas where lower Oligocene pelitic rocks are eroded and along the Puchkirchen Channel system, where a high percentage of permeable clastic rocks have been deposited. An effect of diffusion on molecular and isotopic composition of the gas cannot be observed.
- All gas samples in Oligocene-Miocene reservoirs are biodegraded, but the degree of biodegradation decreases downwards. Biodegradation results in an increase in the i/nC_4 ratio, a selective removal of propane, an increase in $\delta^{13}C$ of propane, and gas drying.
- Biodegradation is accompanied with the generation of secondary microbial methane (and ^{13}C enriched CO_2) resulting in further drying of the gas. Hence gas dryness is high even in samples with high contributions of thermogenic hydrocarbons.
- The presence of alkenes suggests that biodegradation is an ongoing process.

Impact of geothermal fluids on the thermogenic petroleum system:

- Strong depletion of BTEX compounds in some oils proves water washing. Additional observed features of water washing include a decrease in API gravity related to depletion in low molecular saturated components.
- Water co-produced with water washed oil shows progressive reduction in chlorine content and depletion in ^{2}H and ^{18}O isotopes indicating that connate brines have been partly replaced by meteoric water characteristic for the underlying Malmian carbonates, the main aquifer for geothermal water in the basin.
- Most strongly affected oils are located in the shallow northern and northeastern part of study area (fields F*, N*, AA*, Z*). In case of the AA* and Z* fields producing from Cenomanian reservoirs, directly overlying the active Malmian aquifer, a hydraulic connectivity between the reservoir and the aquifer is

obvious. The F* and N* fields are located east of the extension of the Malmian aquifer and produce from Eocene reservoirs. In case of the N* field, the Eocene rocks directly rest on crystalline basement. This suggests that Malmian water is discharged (north-eastwards) through crystalline basement rocks and that previous flow models of the regional geothermal aquifer have to be modified.

- In contrast to shallow northern fields, fields located in the deep southern part of the basin (e.g. G*, P*, V*, R*, X*, AB*, AG*, AJ*) are virtually not affected by water washing. Water in these fields typically has a relatively high salinity.
- The results emphasize the importance of combining data from petroleum and geothermal industry, which are often handled separately: Recognition of active water flow may help to predict gravity and viscosity anomalies, biodegradation risk and the presence of hydrodynamic traps. Otherwise recognition of water washing helps to improve flow models of the underlying geothermal aquifer.

Composition of diamondoids in oil samples: potential as indices of source rock facies, maturity and biodegradation:

- Diamondoid hydrocarbons have been detected in all 27 analyzed crude oil samples from the Austrian part of the Alpine Foreland Basin; the oils were generated by Oligocene source rocks at the peak of the oil window and were obtained from Cretaceous, Eocene and Rupelian reservoir rocks.
- Biodegradation of oil sample D* from a location in the shallow NE part of the basin resulted in a significant enrichment of diamondoids due to the molecule's high resistance to microbial degradation. The enrichment of diamondoid hydrocarbons can be used to assess biodegradation.
- A number of different isomerization indices based on the number of alkyl substituents in the adamantane and diamantane structure, and based on the position (bridgehead or secondary) of substitution, are positively correlated with each other, suggesting that all the indices are controlled by the same processes.
- Correlations of molecular ratios and isomerization ratios indicate that extensive thermal cracking (>2%Rr) of the oil samples has occurred. However according to published models, high maturity should lead to the destruction of diamondoids, but this is not consistent with the observed positive correlation between diamondoid yields and isomerization indices. Therefore, the

diamondoid ratios (molecular and isomerization) should be used with caution as maturity indicators.

- Maturity parameters based on biomarkers or specific compounds in general do not show convincing correlations with the diamondoid isomerization indices.
- Of the diamondoid isomerization indices investigated, only the EAI-1 index correlates with biomarker maturity parameters; EAI-1 may therefore be a good maturity indicator.
- Oils from the Austrian part of the Alpine Foreland Basin have not undergone extensive cracking.
- Some of the diamondoid indices correlate with Ts/Tm ratios, DBT/Ph ratios and $\delta^{13}C$ values of *n*-alkanes, which reflect heterogeneities in the composition of the organic matter within the source rocks. Hence, the composition of diamondoids in the Austrian part of the Alpine Foreland Basin is influenced by organic matter variations in the source rock facies.

Cross-correlation of EAI-1 and the isotopic composition of gaseous hydrocarbons suggest that source rocks at a maturity of about 1.0-1.2% vitrinite reflectance contributed to the mature oils. The applicability of the EAI-1 index needs to be verified in another, well understood petroleum basin.

Origin of condensates co-produced with microbial gas: lessons learned from ancillary geochemical methods:

Geochemical investigations of condensate (and oil) samples form Cenomanian/Eocene reservoirs and condensate samples from Oligocene/Miocene reservoirs pointed out several conclusion regarding source, maturity and migration mechanisms.

- Maturity parameters based on the light hydrocarbons fraction (J, V), as well as diamondoid isomerization indices and $\delta^{13}C$ of ethane and propane show that light hydrocarbons in oils from Cenomanian/Eocene reservoirs have been generated from a source rock with late oil window maturity (1.1-1.2% Rr). This is a higher maturity level than indicated by biomarker isomerization ratios and MPI-1 (0.6-0.9 %Rr; Gratzer et al., 2011) and points to mixing of two end-member oil phases, both generated from the same source rock, but at different maturity levels. Mixing of fluids with different maturities is also supported by presence of evaporative fractionation (see Fig. 59).

- API gravity of (non-altered) oils and the development of gas caps in the eastern part of the study area are controlled by the relative percentage of the oil fraction with higher maturity.
- Despite strong biodegradation, a similar mixing of two end-member hydrocarbon phases with different maturity can be observed in condensates from Oligocene/Miocene reservoirs.
- The same (Lower Oligocene) source rock for condensates in Oligocene/Miocene reservoirs and oils in Cenomanian/Eocene reservoirs is proven by geochemical features (incl. presence of oleanane, $\delta^{13}C$ of n-alkanes, C_{27-29} sterane and C_{29-31} hopane patterns, DBT/Ph and Pr/Ph ratios).

Condensates in Oligocene/Miocene reservoirs (and A* field condensates) are characterized by high toluene/*n*-C_7 ratios. Moreover concentration of diamondoids (and their isomerization indices) in the condensates are positively correlated with percentages of thermogenic methane in co-produced (microbial) gas. Consequently, the condensates are explained as products of evaporative fractionation of oils in Cenomanian/Eocene reservoirs.

12. References

http://gestisen.itrust.de/nxt/gateway.dll/gestis_en/000000.xml?f=templates$fn=default.htm$vid=gestiseng:sdbeng$3.0

Alexander R., Kagi, R.I., Woodhouse, G.W., 1981. Variation in the Ratio of Isomeric Butanes with Sediment Temperature in the Carnarvon Basin of Western Australia. In Bjorøy, M. et al. (eds.), Advances in Organic Geochemistry. Wiley, Chicester, pp. 76-79.

Andrews, J.N., Goldbrunner, J.E., Darling, W.G., Hooker, P.J., Wilson, G.B., Youngman, M.J., Eichinger, L., Rauert, W., Stichler, W., 1985. A radiochemical , hydrochemical and dissolved gas study of groundwaters in the Molasse basin of Upper Austria. Earth and Planetary Science Letters 73, 317-332.

Andrews, J.N., Youngman, M.J., Goldbrunner, J.E., Darling, W.G., 1987. The Geochemistry of Formation Waters in the Molasse Basin of Upper Austria. Environmental Geology and Water Sciences, 10, 43-57.

Azevedo, D.A., Tamanquiera, J.B., Dias, J.C.M., Carmo, A.P.B., Landau, L., Goncalves, F.T.T., 2008. Multivariate statistical analysis of diamondoid and biomarker data from Brazilian basin oil samples. Fuel, 87, 2122-2130.

Bailey, N.J.L., Krouse, H.R., Evans, C.R., Rogers, M.A., 1973. Alteration of crude oil by waters and bacteria – evidence from geochemical and isotope studies. The American Association of Petroleum Geologists Bulletin 57, 1276-1290.

Bayrisches Landesamt für Wasserwirtschaft, 1999. Das Thermalwasservorkommen im niederbayerisch-oberösterreichischen Molassebecken, Hydrogeologisches Modell und Thermalwasser Strömungsmodell im Auftrag des Freistaates Bayern und der Republik Österreich, Kurzbericht. München.

Bechtel, A., Gratzer, R., Linzer, H.-G., Sachsenhofer, R.F., 2013. Influence of migration distance, maturity and facies on the stable isotopic composition of alkanes and on carbazole distributions in oils and source rocks of the Alpine Foreland Basin of Austria. Organic Geochemistry 62, 74-85.

Belaed, S., 2007. Charakterisierung potenzieller Muttergesteine für biogenes Erdgas in der österreichischen Molassezone. Diploma thesis: Technical University of Clausthal, Germany.

Bernard, B.B., Brooks, J.M., Sackett, W.M., 1978. Light hydrocarbons in recent Texas continental shelf and slope sediments. Journal of Geophysical Research 83, 4053-406.

Berner, U., Faber, E., 1987. Maturity related mixing model for methane, ethane and propane, based on carbon isotopes. Organic Geochemistry 13, 67-72.

Berner, U., Faber, E., 1996. Empirical carbon isotope/maturity relationships for gases from algal kerogens and terrigenous organic matter, based on dry, open-system pyrolysis. Organic Geochemistry 24, 947-955.

Berwick, L., Alexander, R., Pierce, K., 2011. Formation and reaction of alkyl adamantanes in sediments: Carbon surface reactions. Organic Geochemistry 42, 752-761.

Boreham, C.J., Murray, A.M., Dowling, L.M., 1995. Biodegradation and maturity influences on *n*-alkanes isotopic profiles in terrigenous sequences. In: Grimalt, J.O., Dorronsoro, C. (Eds.), Organic Geochemistry: Developments and Applications to Energy, Climate, Environment and Human History. A.I.G.O.A., The Basque Country, Spain, pp. 539-544.

Botz, R., Pokojski, H.-D., Schmitt, M., Thomm, M., 1996. Carbon isotope fractionation during bacterial methanogenesis by CO_2 reduction. Organic Geochemistry 25, 255-262.

Brix, F., Schultz, O., 1993. Erdöl und Erdgas in Österreich, 2 Auflage. Veröffentlichungen aus dem Naturhistorischen, Wien.

Brown, A., 2011. Identification of source carbon for microbial methane in unconventional gas reservoirs. American Association of Petroleum Geologists Bulletin 95, 1321-1338.

Cañipa-Morales, N., Galan-Vidal, C.A., Guzman-Vega, M.A., Jarvie, D.M., 2003. Effect of evaporation on C_7 light hydrocarbon parameters. Organic Geochemistry 34, 813-826.

Chen, J., Fu, J., Sheng, G., Liu, D. Zhang, J., 1996. Diamondoid hydrocarbon ratios: novel maturity indices for highly mature crude oils. Organic Geochemistry 25, 179-190.

Chung, H.M, Gormly, J.R., Squires, R.M., 1988. Origin of gaseous hydrocarbons in subsurface environments: Theoretical considerations of carbon isotope distribution. Chemical Geology 71, 97-104.

Clark, T., Knox, T.M., Mckervey, M.A., Mackle, H., Rooney, J.J., 1979. Thermochemistry of bridgehead-ring substances. Enthalpies of formation of some diamondoid hydrocarbons and perhydroquanacene-comparison with data from empirical force field calculations. Journal of American Chemical Society 101, 2404-2410.

Clayton, C., 1991. Carbon isotope fractionation during natural gas generation from kerogen. Marine and Petroleum Geology 8, 232-240.

Colemann, D.D., 2001. -70‰ methane, is it biogenic or thermogenic? American Association of Petroleum Geologists Bulletin, 85 (supplement), A39.

Covault, J.A., Hubbard, S.M., Graham, S.A., Hinsch, R., Linzer, H. 2009. Turbidite-reservoir architecture in complex foredeep-margin and wedge-top depocenters, Tertiary Molasse foreland basin system, Austria. Marine and Petroleum Geology 26, 379-396.

Dahl, J.E., Moldowan, J.M., Peters, K.E., Claypool, G.E., Rooney, M.A., Michael, G.E., Mello, M.R., Kohnen, M.L., 1999. Diamondoid hydrocarbons as indicators of natural oil cracking. Nature 399, 54-57.

Dahl, J.E., Moldowan, J.M., Wei, Z., Lipton, P.A., Denisevich, P., Gat, R., Liu, S., Schreiner, P.R., Carlson, R.M.K., 2010. Synthesis of higher diamondoids and implications for their formation in petroleum. Angewandte Chemie International Edition 49, 9881-9885.

Dai, J., 1990. Characteristics of hydrogen isotopes of paraffinic gas in China. Petroleum Exploration and Development 17, 27-32.

Davis, J.B., Squires, R.M., 1954. Detection of microbially produced gaseous hydrocarbons other than methane. Science 119, 381-382.

De Ruig, M.J. and Hubbard, S.M., 2006. Seismic facies and reservoir characteristics of a deep marine channel belt in the Molasse foreland basin. American Association of Petroleum Geologists Bulletin Bulletin 90, 735- 752.

Dimitrakopoulos, R., Muehlenbachs, K., 1987. Biodegradation of petroleum as a source of ^{13}C-enriched carbon dioxide in the formation of carbonate cement. Chemical Geology 65, 283-291.

Elster, D., Goldbrunner, J., Wessely, G., Niederbacher, P. Schubert, G., Berka, R., Philippitsch, R., Hörhan, T., 2016. Erläuterungen zur geologischen Themenkarte Thermalwässer in Österreich 1:500.000, Wien

Epstein, S., Mayeda, T., 1953. Variation of O^{18} content of waters from natural sources. Geochimica et Cosmochimica Acta 4, 213-224

Erdman, J.G., Morris, D.A., 1974. Geochemical correlation of petroleum. The American Association of Petroleum Geologists Bulletin 58, 2326-2337.

Fang, C., Xiong, Y., Liang, Q., Li, Y., 2012. Variation in abundance and distribution of diamondoids during oil cracking. Organic Geochemistry 47, 1-8.

Fang, C., Xiong, Y., Li, Y., Chen, Y., Liu, J., Zhang, H., Adedosu, T.A. Peng, P., 2013. The origin and evolution of adamantanes and diamantanes in petroleum. Geochimica et Cosmochimica Acta 120, 109-120.

Fang, C., Xiong, Y., Li, Y., Chen, Y. Tang, Y., 2015. Generation and evolution of diamondoids in source rock. Marine and Petroleum Geology 67, 197-203.

Feisthauer, S., Siegert, M., Seidel, M., Richnow, H.H., Zenger, K., Gründger, F., Krüger, M., 2010. Isotopic fingerprinting of methane and CO_2 formation from aliphatic and aromatic hydrocarbons. Organic Geochemistry 41, 482-490.

Fuex, A.N., 1977. The use of stable carbon isotopes in hydrocarbon exploration. Journal of Geochemical Exploration 7, 155-188.

Galimov, E.M., 2006. Isotope organic geochemistry. Organic Geochemistry 37, 1200-1262.

George, S.C., Boreham, C.J., Minifie, S.A., Teerman, S.C., 2002. The effect of minor to moderate biodegradation on C_5 to C_9 hydrocarbons in crude oils. Organic Geochemistry 33, 1293-1317.

Gier, S., 2000. Clay mineral and organic diagenesis of the Lower Oligocene Schöneck Fishshale, western Austrian Molasse basin. Clay Minerals 35, 709-717.

Giruts, M.V., Rusinova, G.V. and Gordadze, G.N., 2006. Generation of adamantanes and diamantanes by thermal cracking of high-molecular-mass saturated fraction of crude oils of different genotypes. Petroleum Chemistry 46, 225-236.

Giruts, M.V. and Gordadze, G.N., 2007. Generation of adamantanes and diamantanes by thermal cracking of polar components of crude oils of different genotypes. Petroleum Chemistry 47, 15-25.

Goldbrunner, J.E., 1984. Zur hydrogeologie des oberösterreichischen Molassebeckens. Steir. Beitr. Z. Hydrogeologie 36, 83-102.

Goldbrunner, J.E., 2000. Hydrogeology od deep groundwaters in Austria. Mitt. Össterr. Geol. Ges. 92(1999), 281-294

Goldbrunner, J.E., 2012. Geothermal Exploitation in the Upper Austrian Molasse Basin. Beiträge zur Hydrogeologie 59, 187-202.

Goldbrunner, J.E, 2015. Austria – Country Update. Proceedings World Geothermal Congress, Melbourne, Australia, 19-25 April 2015

Gordadze, G.N., 2008. Review: Geochemistry of cage hydrocarbons. Petroleum Chemistry 48, 243-255.

Gordadze, G.N. and Giruts, M.V., 2008. Synthesis of adamantane and diamantane hydrocarbons by high-temperature cracking of higher n-alkanes. Petroleum Chemistry 48, 412-417.

Gratzer, R., Bechtel, A., Sachsenhofer, R.F., Linzer, H.-G., Reischenbacher, D., Schulz, H.-M., 2011. Oil-oil and oil-source rock correlations in the Alpine Foreland Basin of Austria: Insights from biomarker and stable carbon isotope studies. Marine and Petroleum Geology 28, 1171-1186.

Grice, K., Alexander, R. and Kagi, R.I., 2000. Diamondoid hydrocarbon ratios as indicators of biodegradation in Australian crude oils. Organic Geochemistry 31, 67-73.

Grice, K., de Mesmay, R., Glucina, A., Wang, S., 2008, An improved and rapid 5A molecular sieve method for gas chromatography isotope ratio mass spectrometry of n-alkanes (C8–C30+): Organic Geochemistry, 39, 284–288 .

Gross, D., Sachsenhofer, R., Rech, A., Sageder, S., Geissler, M., Schnitzer, S., Troiss, W., 2015. The Trattnach Oil Field in the North Alpine Foreland Basin (Austria). Austrian Journal of Earth Sciences 108, 151-171.

Grundtner, M.-L., Pytlak, L., Gross, D., Linzer, H.-G., Sachsenhofer, R.F., 2014. Rock-fluid interactions in reservoir rocks of the Molasse Basin. EMAS 2014 – 11th Regional Workshop on Electron Probe Microanalysis Today – Practical Aspects, Leoben, Austria.

Grundtner, M.-L., Gross, D., Linzer, H.-G., Misch, D., Sachsenhofer , R.F., Scheucher, L., Gratzer, R., 2015. Diagenesis of Upper Eocene clastic reservoir rocks in the Alpine Foreland Basin (Austria). GeoBerlin, 4-7 October 2015, Berlin.

Grundtner, M.-L., Gross, D., Linzer, H.G., Neuhuber, S., Sachsenhofer, R.F., Scheucher, L., 2016. The diagenetic history of Oligocene-Miocene sandstones of the Austrian north Alpine foreland basin. Marine and Petroleum Geology 77, 418-434.

Gruner, A. Vieth-Hillebrand, A., Mangelsdorf, K., van der Kraan, G., Janka, C. Köhler, T., Morris, B.E.L., Wilkes, H., 2015. Signatures of bioactivity in petroleum reservoirs. 27th International Meeting on Organic Geochemistry, Prague, September 13-18, 2015.

Gruner, A., Jarling, R., Vieth-Hillebrand, A., Mangelsdorf, K., Janka, C., van der Kraan, G.M., Köhler, T., Morris, B.E.L., Wilkes, H., 2017. Tracing microbial hydrocarbon transformation processes in high temperature petroleum reservoir using signature metabolites. Organic Geochemistry 108, 82-93.

Grunert, P., Hinsch, R., Sachsenhofer, R.F., Bechtel, A., Ćorić, S., Harzhauser, M., Piller, W., Sperl, H., 2013. Early Burdigalian infill of the Puchkirchen Trough (North Alpine Foreland Basin, Central Paratethys): Facies development and sequence stratigraphy. Marine and Petroleum Geology 39, 164-186.

Grunert, P., Auer, G., Harzhauser, M, Piller, W.E., 2015. Stratigraphic constraints for the upper Oligocene to lower Miocene Puchkirchen group (North Alpine Foreland Basin, Central Paratethys). Newsletters on Stratigraphy 48, 111-13.

Gusterhuber, J., Dunkl, I., Hinsch, R., Linzer, H.-G., Sachsenhofer, R.F., 2012. Neogene uplift and erosion in the Alpine Foreland basin (Upper Austria and Salzburg). Geologica Carpathica 63, 295-305.

Gusterhuber, J., Hinsch, R., Linzer, H.-G., Sachsenhofer R., 2013. Hydrocarbon generation and migration from sub-thrust source rocks to foreland reservoirs: The Austrian Molasse Basin. Austrian Journal of Earth Sciences 106, 115-136.

Gusterhuber, J., Hinsch, R., Sachsenhofer, R.F., 2014. Evaluation of hydrocarbon generation and migration in the Molasse fold and thrust belt (Central Eastern Alps, Austria) using structural and thermal basin models. American Association of Petroleum Geologists Bulletin 98, 253-277.

Head, I.M., Jones, D.M., Larter, S.R., 2003. Biological activity in the deep subsurface and the origin of heavy oil. Nature 426, 344-352.

Hinrichs, K-U., Hayes, J.M., Bach, W., Spivack, A.J., Hmelo, L.R., Holm, N.G., Johnson, C.G., Sylva, S., 2006. Biological formation of ethane and propane in the deep marine subsurface. Proceeding of the National Academy of Sciences of the United States of America 103, 14684-14689.

Hinsch, R., 2013. Laterally varying structure and kinematics of the Molasse fold and thrust belt of the Central Eastern Alps: Implications for exploration. American Association of Petroleum Geologists Bulletin 97, 1805-1831.

Hoering, T.C., 1984. Thermal reactions of kerogen with added water, heavy water and pure organic substances. Organic Geochemistry 5, 267-278.

Horita, J., Ueda, A., Mizukami, K., Takatori, I., 1989. Automatic δD and $\delta^{18}O$ analyses of multi-water samples using H_2- and CO_2- water equilibration methods with a common equilibration set-up. Applied Radiation and Isotopes 40, 801-805.

Huang, H., Larter, S., 2014. Secondary microbial gas formation associated with biodegraded oils from the Liaohe Basin, NE China. Organic Geochemistry 68, 39-50.

Hubbard, S.M., de Ruig, M.J., Graham, S.A., 2005. Utilizing outcrop analogs to improve subsurface mapping of natural gas-bearing strata in the Puchkirchen Formation, Molasse Basin, Upper Austria. Austrian Journal of Earth Sciences 98, 52-66.

Hubbard S., de Ruig M.J., Graham S., 2009. Confined channel-levee complex development in an elongate depo-center: deep-water Tertiary strata of the Austria Molasse basin. Marine and Petroleum Geology 26, 85-112.

Hughes, W.B., Holba, A.G. and, Dzou, L.I.P., 1995. The ratios of dibenzothiophene to phenanthrene and pristan to phytan as indicators of depositional environment and lithology of petroleum source rocks. Geochimica et Cosmochimica Acta 59, 3581-3598.

Hunt, J.M., Huc, A.Y., Whelan, J.K., 1980. Generation of light hydrocarbons in sedimentary rocks. Nature 288, 688-690.

James, A.T., 1983. Correlation of natural gas by use of carbon isotopic distribution between hydrocarbon components. American Association of Petroleum Geologists Bulletin 67, 1176-91.

James, A.T., 1990. Correlation of Reservoired Gases Using the Carbon Isotopic Compositions of Wet Gas Components. American Association of Petroleum Geologists Bulletin 74, 1441-1458.

James, A.T., Burns, B.J., 1984. Microbial alteration of subsurface natural gas accumulations. American Association of Petroleum Geologists Bulletin 68, 957-960.

Jones., D.M, Head, I.M., Gray, N.D., Adams, J.J., Rowan, A.K., Aitken, C.M., Bennett, B., Huang, H., Brown, A., Bowler, B.F.J., Oldenburg, T., Erdmann, M., Larter, S.R., 2008. Crude-oil biodegradation via methanogenesis in subsurface petroleum reservoirs. Nature 451, 176-181.

Kamyar H.R., 2000. Verteilung der Untergrundtemperaturen an den Beispielen der Bohrlochtemperatur (BHT) – Messungen in den RAG – Konzessionen, Oberösterreichs und Salzburgs, (Molasse – und Flyschzone) (in German). Disseration zur Erlangung des akademischen Grades Doktor der Naturwissenschaften (Geophysik) an der Formal und Naturwissenschaftichen Fakultät der Universität Wien.

Kim, A.G., Douglas, L.J., 1972. Hydrocarbon gases produced in a simulated swamp environment. U.S. Bur. Mines Rept. Inv. 7690, 15.

Kniemeyer, O., Musat, F., Sievert, S., Knittel, K., Wilkes, H., Blumenberg, M., Michaelis, W., Classen, A., Bolm, C., Joye, S., Widdel, F., 2007. Anaerobic oxidation of short-chain hydrocarbons by marine sulfate-reducing bacteria. Nature 449, 898-901.

Kreutzer, N., 1993. Die ÖMV-Gas und Öllagerstätten der nieder- und ober-österreichischen Molassezone. In: Brix, F., Schultz, O., (eds.), 1993, Erdöl und Erdgas in Österreich, 2 Auflage, Wien.

Krooss, B.M., Leythaeuser, D., Schaefer, R.G., 1988. Light hydrocarbon diffusion in a caprock: Chemical Geology 71, 65-76.

Krooss, B.M., Littke, R., Müller, B., Frielingsdorf, J., Schwochau, K., Idiz, E.F., 1995. Generation of nitrogen and methane from sedimentary organic matter: implications on the dynamics of natural gas accumulations. Chemical Geology 126, 291-318

Kröll, A., Wagner, L., Wessely, G., 2006. Molassezone Salzburg – Oberösterreich 1:200.000: Geologische Karte der Molassebasis, Geol. Survesy Austria, Vienna.

Kuo, L.-C., 1994. An experimental study of crude oil alteration in reservoir rocks by water washing. Organic Geochamistry 21, 465-479.

Lafargue, E., Barker, C., 1988. Effect of water washing on crude oil compositions. American Association of Petroleum Geologists 72, 263-276.

Lafargue, E., Le Thiez, P., 1996. Effect of water washing on light ends compositional heterogeneity. Organic Geochemistry, 24, 1141-1150.

Landa S. and Machacek, V., 1933. Adamantane, a new hydrocarbon extracted from petroleum. Collections of Czechoslovak Chemical Communications 5, 1-5.

Larter, S., R., Alpin, A.C., 1994. Reservoir geochemistry: methods, applications and oppurtunities. In: England, W., Cubitt, L., (eds.) Reservoir Geochemistry. Geological Society Special Publication 86, pp. 5-32.

Larter, S., di Primo, R., 2005. Effects of biodegradation on oil and gas field PVT properties and the origin of oil rimmed gas accumulations. Organic Geochemistry 36, 299-310.

Lewan, M.D., 1993. Laboratory Simulation of Petroleum Formation. In: Engel, M.H., Macko, S.A., (eds.), 1993, Organic Geochemistry- Principles and Applications. New York, Plenum Press, pp. 419-422.

Lewan, M.D., 1997. Experiments on the role of water in petroleum formation. Geochimica et Cosmochimica Acta 61, 3691-3723.

Leythaeuser, D., Schaefer, R.G., Weiner, B., 1979. Generation of low molecular weight hydrocarbons from organic matter in source beds as a function of temperature and facies. Chemical Geology 25, 95-108.

Leythaeuser, D., Schaefer, R.G., Pooch, H., 1983. Diffusion of Light Hydrocarbons in Subsurface Sedimentary Rocks. American Association of Petroleum Geologists Bulletin 67, 889-895

Li, J., Philip, P. and, Mingzhong, C., 2000. Methyl diamantane index (MDI) as a maturity parameter for Lower Palaeozoic carbonate rocks at high maturity and overmaturity. Organic Geochemistry 31, 267-272.

Lillis, 2007. Upper Creataceous Microbial Petroleum Systems in North-Central Montana. The Mountain Geologist 44, 11-35.

Linzer, H.-G., Sachsenhofer, R. F., 2010. Submarine Large Scale Mass Movements in the Deepwater Foreland Basin of the Alps - Implications to Hydrocarbon Generation and Distribution of Source and Reservoir Rocks. AAPG Annual Convention and Exhibition-11-14 April, New Orleans.

Littke, R., Krooss, B.M., ldiz, E., Frielingsdorf, J., 1995. Molecular nitrogen in natural gas accumulations: generation from sedimentary organic matter at high temperatures. American Association of Petroleum Geologists Bulletin 79, 410-430.

Malzer, O., 1993. Muttergesteine, Speichergesteine, Migration und Lagerstättenbildung in der Molassezone und deren sedimentärem Untergrund. In: Brix, F., Schultz, O., (eds.), 1993, Erdöl und Erdgas in Österreich, 2 Auflage, Wien.

Mansoori, G.A., de Araujo, P.L.B., de Araujo, E.S., 2012. Diamondoid Molecules: With Applications in Biomedicine, Materials Science, Nanotechnology and Petroleum Science. World Scientific, pp. 1-10.

Masalimova , L.U., Lowe, D.R., McHargue, T., Derksen, R., 2015. Interplay between an axial channel belt, slope gullies and overbank deposition in the Puchkirchen Formation in the Molasse Basin, Austria. Sedimentology 62, 1717-1748.

Masterson, W.D., Dzou, L.I.P, Holba, A.G., Fincannon, A.L., Ellis, L., 2001. Evidence for biodegradation and evaporative fractionation in West Sak, Kaparuk and Prudhoe Bay field areas, North Slope, Alaska. Organic Geochemistry 32, 411-441.

Milkov, A.V., 2010. Methanogenic biodegradation of petroleum in the West Siberian Basin (Russia): Significance for formation of giant Cenomanian gas pools. American Association of Petroleum Geologists Bulletin 94, 1485-1541.

Milkov, A.V., 2011. Worldwide distribution and significance of secondary microbial methane formed during petroleum biodegradation in conventional reservoirs. Organic Geochemistry 42, 184-207.

Milkov, A.V., Dzou, L., 2007. Geochemical evidence of secondary microbial methane from very slight biodegradation of undersaturated oils in a deep hot reservoir. Geology 35, 455-458.

Morrison, J., Brockwell, T., Merren, T., Fourel, F., Phillips, A.M., 2001. On-line high-precision stable hydrogen isotopic analyses on nanoliter water samples. Analytical Chemistry 73, 3570-3575.

Murillo, W.A., Vieth-Hillebrand, A., Horsfield, B., Wilkes, H., 2016. Petroleum source, maturity, alteration and mixing in the southwestern Barents Sea: New insights from geochemical and isotope data. Marine and Petroleum Geology 70, 119-143.

Nachtmann, W., Wagner, L., 1987. Mesozoic and Early Tertiary evolution of the Alpine foreland in Upper Austria and Salzburg, Austria. Tectonophysics 137, 61-76

Napitupulu, H., Ellis, L., Mitterer, R.M., 2000. Post-generative alteration effects on petroleum in the onshore Northwest Java Basin, Indonesia. Organic Geochemistry 31, 295-315.

Ni, Y., Ma, Q., Ellis, G.S., Dai, J., Katz, B., Zhang, S., Tang, Y., 2011. Fundamental studies on kinetic isotope effect (KIE) of hydrogen isotope fractionation in natural gas systems. Geochimica et Cosmochimica Acta 75, 2696-2707.

Odden, W., Patience, R.L., Van Graas, G.W., 1998. Application of light hydrocarbons (C_4-C_{13}) to oil/source rock correlations: a study of the light hydrocarbon compositions of source rocks and test fluids from offshore Mid-Norway. Organic Geochemistry 28, 823-847.

Oremland, R.S., Whiticar, M.J., Strohmaier, F.E., Kiene, R.P., 1988. Bacterial ethane formation from reduced, ethylated sulfur compounds in anoxic sediments. Geochimica et Cosmochimica Acta 52, 1895-1904.

Orphan, V.J., Taylor, L.T., Haffenbradl, D., DeLong, E.F., 2000. Culture dependent and culture-independent characterization of microbial assemblages associated with high-temperature petroleum reservoirs. Applied and Environmental Microbiology 66, 700–711, doi: 10.1128/AEM.66.2.700–711.2000

Pallasser, R.J., 2000. Recognising biodegradation in gas/oil accumulations through the $\delta^{13}C$ compositions of gas components. Organic Geochemistry 31, 1363-1373.

Palmer, S.E., 1984. Effect of Water washing on C15+ hydrocarbon Fraction of Crude Oils from Northwest Palawan, Philippines. American Association of Petroleum Geologists Bulletin, 68, 137-149.

Palmer, S.E., 1993. Effect of biodegradation and water washing on crude oil composition. In: Engel, M.H., Macko, S.A., (eds.), Organic Geochemistry. Plenum Press, New York, pp. 511-533.

Penteado, H.B., Arauja, L.M., Fracalossi, C.P., Silva, H.Q., Reis, M.A., Cerqueira, J.R., Garcia, S.F., dos Santos, R.O., 2014. Characterization of Petroleum Compositions and the Causes for Large Heterogeneities in Deep Offshore Settings in Eastern Brazilian Marginal Basins. AAPG International Conference & Exibition, Istanbul, Turkey, September 16th.

Peters, K.E., Walters, C.C., Moldowan, J.M., 2005. The Biomarker Guide Volume II Biomarkers and Isotopes in Petroleum Exploration and Earth History, pp. 645-708.

Petrov, A.A., 1987. Petroleum Hydrocarbons. Springer-Verlag, Berlin Heidelberg, pp. 93-99.

Petrov, A.A., Arefjev, O.A., Yakubson, Z.V., 1974. Hydrocarbons of adamantane series as indices of petroleum catagenesis process. In: Tissot, B., Bienner, F., (Eds.), Advances in Organic Geochemistry. Editions Technip, Paris, France, pp. 517-522.

Prinzhofer, A., Pernaton, É., 1997. Isotopically light methane in natural gas: bacterial imprint or diffusive fractionation? Chemical Geology 142, 193-200.

Prinzhofer, A., Vega, M.A.G., Battani, A., Escudero, M., 2000. Gas geochemistry of the Macuspana Basin (Mexico): thermogenic accumulations in sediments impregnated by bacterial gas. Marine and Petroleum Geology 17, 1029-1040

Pytlak, L., Gross, D., Bechtel, A., Gratzer, R., Sachsenhofer, R.F., Linzer, H.-G., Grundtner, M.-L., Scheucher, L., 2014. Origin and Alteration of Natural Gas and Liquid Hydrocarbons Accumulated in the Austrian Molasse Basin. AAPG International Conference & Exibition, Istanbul, Turkey, September 16th.

Pytlak, L., Gross. D., Sachsenhofer, R.F., Bechtel, A., Gratzer, R., Linzer, H.-G., 2016a. Generation, mixing and alteration of thermogenic and microbial gas in oil deposits: The case of the Alpine Foreland Basin (Austria). Marine and Petroleum Geology 78, 575-592.

Pytlak, L., Gross, D., Sachsenhofer, R.F., Bechtel, A., Linzer, H.-G., 2016b. Gas accumulations in Oligocene-Miocene reservoirs in the Alpine Foreland Basin (Austria): evidence for gas mixing and gas degradation. International Journal of Earth Sciences, doi:10.1007/s00531-016-1421-1

Pytlak, L., Kowalski, A., Gross, D., Sachsenhofer, R.F., 2017. Composition of diamondoids in oil samples from the Alpine Foreland Basin, Austria: potential as indices of source rock facies, maturity and biodegradation. Journal of Petroleum Geology 40, 153-171

Radke, M., Welte, D.H., 1983. The methylphenanthrene index (MPI): a maturity parameter based on aromatic hydrocarbons. In: Bjorøy, M. (Ed.), Advances in Organic Geochemistry, 1981. Wiley, Chichester, pp. 504-512.

Radke, M., Willsch, H., Welte, D.H., 1980, Preparative hydrocarbon group type determination by automated medium pressure liquid chromatography: Analytical Chemistry 52, 406–411.

Radke, J., Bechtel, A., Gaupp, R., Püttmann, W., Schwark, L., Sachse, D., Gleixner, G., 2005. Correlation between hydrogen isotope ratios of lipid biomarkers and sediment maturity. Geochimica et Cosmochimica Acta 69, 5517–5530.

Reischenbacher, D., Sachsenhofer, R.F., 2011. Entstehung von Erdgas in der oberosterreichischen Molassezone: Daten und offene Fragen (in German). Berg- und Huttenmannische Monatshefte 156, 463-468.

Rice, D.D., Claypool, G.E., 1981. Generation, Accumulation, and Resource Potential of Biogenic Gas. American Association of Petroleum Geologists Bulletin 65, 5-25.

Roegl, F., 1999. Mediterranean and Paratethys. Facts and Hypothesis of an Oligocene to Miocene Paleogeography (short overview). Geologica Carpathica 50, 339-349.

Rooney, M.A., Claypool, G.E., Chung, H.M., 1995. Modeling thermogenic gas generation using carbon isotope ratios of natural gas hydrocarbons. Chemical Geology 126, 219-232.

Rueter, P., Rabus, R., Wilkes, H., Aeckersberg, F., Rainey, F.A., Jannasch, H.W., Widdel, F., 1994. Anaerobic oxidation of hydrocarbons in crude oil by new types of sulphate-reducing bacteria. Nature 372, 455-458.

Sachsenhofer, R.F., Schulz, H-M., 2006. Architecture of Lower Oligocene source rocks in the Alpine Foreland Basin: a model for syn- and post-depositional source-rock features in the Paratethyan realm. Petroleum Geoscience 12, 363-377.

Sachsenhofer, R.F., Gratzer, R., Tschelaut, W., Bechtel, A., 2006. Characterisation of non-producible oil in Eocene reservoir sandstones (Bad Hall Nord field, Alpine Foreland Basin, Austria). Marine and Petroleum Geology 23, 1-15.

Sachsenhofer, R.F., Leitner, B., Linzer, H.-G., Bechtel, A., Coric, S., Gratzer, R., Reischenbacher, D., Soliman, A., 2010. Deposition, Erosion and Hydrocarbon Source Potential of the Oligocene Eggerding Formation (Molasse Basin, Austria). Austrian Journal of Earth Sciences 103, 76-99.

Sackett, W.D., Nakaparskin, S., Dalrymple, D., 1970. Carbon isotope effects in methane production by thermal cracking. In: Hobson, G.D., Speers, G.C., (eds.), Advances in Organic Geochemistry, pp. 37-53.

Schaefer, R.G., Littke, R., 1988. Maturity-related compositional changes in the low-molecular-weight hydrocarbon fraction of Toarcian shales. Organic Geochemistry 13, 887-892.

Schaefer, R.G., von der Dick, H., Leythaeuser, D., 1983. C_2-C_8 hydrocarbons in sediments from deep sea drilling project leg 71, site 511, Falkland Plateau, South Atlantic. In: Blakeslee, J.H., Lee, M. (eds) Initial reports of the deep sea drilling project 71.

Schimmelmann, A., Boudou, J-P., Lewan, M.D., Wintsch, R.P., 2001. Experimental controls on D/H and $^{13}C/^{12}C$ ratios of kerogen, bitumen and oil during hydrous pyrolysis. Organic Geochemistry 32, 1009-1018.

Schimmelmann, A., Sessions, A.L, Boreham, C.J., Edwards, D.S., Logan, G.A., Summons, R.E., 2004. D/H ratios in terrestrially sourced petroleum systems. Organic Geochemistry 35, 1169-1195.

Schmidt, F., Erdoğan, L.T., 1993. Basin modelling in an overthrust area of Austria. In: Dore et al. (eds.) Basin Modelling: Advances and Applications, NPF Special Publication 3, pp. 573-581.

Schmidt, F., Erdoğan, L.T., 1996. Paleohydrodynamics in exploration. In: Wessely, G., Liebl, W., (eds) Oil and Gas in Alpidic Thrustbelts and Basin of Central and Eastern Europe, EAGE Special Publication 5, pp. 255-265.

Schoell, M., 1977. Die Erdgase der süddeutschen Molasse – Anwendung von D/H- und ^{13}C-/^{12}C- Isotopenanalysen zur Klärung ihrer Entstehung (in German). Erdöl, Erdgas Z. 93, 311-322.

Schoell, M., 1980. The hydrogen and carbon isotopic composition of methane from natural gases of various origins. Geochimica et Cosmochimica Acta 44, 649-661.

Schoell, M., 1983. Genetic characterization of natural gases. American Association of Petroleum Geologists Bulletin 67, 2225-2238.

Schoell, M., 1984. Wasserstoff und Kohlenstoffisotope in organischen Substanzen, Erdölen und Erdgasen (in German). Geologisches Jahrbuch. Reihe D, 67, Bundesanstalt für Geowissenschaften und Rohstoffe, Hannover.

Schubert, A., 1996. Tiefengrundwasseruntersuchungen im Molassebecken westlich von Linz. PhD thesis, Graz.

Schulz, H.-M., van Berk, W., 2009. Bacterial methane in the Atzbach-Schwanenstadt gas field (upper Austrian Molasse Basin), Part II: Retracing gas generation and filling history by mass balancing of organic carbon conversion applying hydrogeochemical modelling. Marine and Petroleum Geology 26, 1180-1189.

Schulz, H.-M., Sachsenhofer, R.F., Bechtel, A., Polesny, H., Wagner, L., 2002. The origin of hydrocarbon source rocks in the Austrian Molasse Basin. Marine and Petroleum Geology 19, 683-709.

Schulz, H.-M., Bechtel, A., Rainer, T., Sachsenhofer, R.F. Struck, U., 2004. Paleoceanography of the Western Central Paratethys during Early Oligocene nannoplankton zone NP23 in the Austrian Molasse Basin. Geologica Carpathica 55, 311-323.

Schulz, H.-M., Bechtel, A., Sachsenhofer, R.F., 2005. The birth of the Paratethys during the Early Oligocene: From Tethys to an ancient Black Sea analogue? Global and Planetary Change 49, 163-176.

Schulz, L.K., Wilhelms, A., Rein, E. Steen, A.S., 2001. Application of diamondoids to distinguish source rock facies. Organic Geochemistry 32, 365-375.

Seewald, J.S., Benitez-Nelson, B., Whelan, J.K., 1998. Laboratory and theoretical constrains on the generation and composition of natural gas. Geochimica et Cosmochimica Acta 62, 1599 – 1617.

Seifert, W.K., Moldowan, J.M., 1979. The effect of biodegradation on steranes and terpanes in crude oils. Geochimica et Cosmochimica Acta 43, 111-126.

Sessions, A.L., Sylva, S.P., Summons, R.E., Hayes, J.M., 2004. Isotopic exchange of carbon-bound hydrogen over geologic timescales. Geochimica et Cosmochimica Acta 68, 1545-1559

Sharaf, L.M., El Nady, M.M., 2006. Application of Light Hydrocarbon (C7+) and Biomarker Analyses in Characterizing Oil from Wells in the North and North Central Sinai, Egypt. Petroleum Science and Technology 24, 607-627.

Sorenson, T.S. Whitworth, S.M., 1990. The superacid route to 1-adamantyl cation, In: Olah, G.A., (Ed.), Cage Hydrocarbons. Wiley, New York, pp. 65-102.

Springer, M.V., Garcia, D.F., Goncalves, F.T.T., Landau, L., Azevedo, D.A., 2010. Diamondoid and biomarker characterization of oils from the Llanos Orientales Basin, Colombia. Organic Geochemistry 41, 1013-1018.

Stahl, W. J., 1977. Carbon and nitrogen isotopes in hydrocarbon research and exploration. Chemical Geology 20, 121-149.

Tang, Y., Huang, Y., Ellis, G.S., Wang, Y., Kralert, P.G., Gillaizeau, B., Ma, Q., Hwang, R., 2005. A kinetic model for thermally induced hydrogen and carbon isotope fractionation of individual *n*-alkanes in crude oil. Geochimica et Cosmochimica Acta 69, 4505-4520.

Tang, Y., Perry, J.K., Jenden, P.D., Schoell, M., 2000. Mathematical modeling of stable carbon isotope ratios in natural gases. Geochimica et Cosmochimica Acta 64, 2673-2687.

Thompson, K.F.M., 1979. Light hydrocarbons in subsurface sediments. Geochimica et Cosmochimica Acta 43, 657-672.

Thompson, K.F.M., 1983. Classification and thermal history of petroleum based on light hydrocarbons. Geochimica et Cosmochimica Acta 47, 303-316.

Thompson, K.F.M., 1987. Fractionated aromatic petroleums and the generation of gas-condensates. Organic Geochemistry 11, 573-590.

Thompson, K.F.M., 1988. Gas-condensate migration and oil fractionation in deltaic systems. Marine and Petroleum Geology 5, 237–246.

Tissot, B.P.,Welte D.H., 1984. From Kerogen to Petroleum. In: Tissot, B.P., Welte D.H., Petroleum Formation and Occurrence, Springer-Verlag, Berlin.

Veron, J., 2005. The Alpine Molasse Basin – review of petroleum geology and remaining potential. Bulletin fur Angewandte Geologie 10, 75–86.

Vieth, A., Wilkes, H., 2006. Deciphering biodegradation effects on light hydrocarbons in crude oils using their stable carbon isotopic composition: A case study from the Gullfaks oil field, offshore Norway. Geochimica et Cosmochimica Acta 70, 651-665.

Wagner, L.R, 1980. Geological Characteristic of the Main Oil and Gas Producing Formations of the Upper Austrian Molasse Basin – Part 1. The Eocene Sandstones. Erdoel-Erdgas-Zeitschrift 96, 338-345.

Wagner, L.R., 1996. Stratigraphy and hydrocarbons in upper Austrian Molasse Foredeep (active margin). In: Wessely, G., Liebl, W., (eds.), Oil and Gas in Alpidic Thrust belts and Basins of Central and Eastern Europe. European Association of Geoscientists and Engineers Special Publication 5, 217–235.

Wagner, L.R., 1998. Tectono-stratigraphy and hydrocarbons in the Molasse Foredeep of Salzburg, Upper and Lower Austria. In: Mascle, A., Puigdefabregas, C., Luterbacher, H.P., Fernandez, M., eds., Cenozoic Foreland Basins of Western Europe: Geological Society Special Publication 134, 339-369.

Weber, V.V., Maximov, S.P., 1976. Early diagenetic generation of hydrocarbon gases and their variations dependent on initial organic composition. American Association of Petroleum Geologists Bulletin 60, 287-293

Wei, Z., Moldowan, J.M, Dahl, J., Goldstein, T.P. Jarvie, D.M., 2006a. The catalytic effects of minerals on the formation of diamondoids from kerogen macromolecules. Organic Geochemistry 37, 1421-1436.

Wei, Z., Moldowan, J.M., Jarvie, D.M., Hill, R., 2006b. The fate of diamondoids in coals and sedimentary rocks. Geology 34, 1013-1016.

Wei, Z., Moldowan, J.M., Paytan, A., 2006c. Diamondoids and molecular biomarkers generated from modern sediments in the absence and presence of minerals during hydrous pyrolysis. Organic Geochemistry 37, 891-911.

Wei, Z., Moldowan, J.M., Peters, K.E., Wang, Y., Xiang, W., 2007a. The abundance and distribution of diamondoids in biodegraded oils from the San Joaquin Valley: Implications for biodegradation of diamondoids in petroleum reservoirs. Organic Geochemistry 38, 1910-1926.

Wei, Z., Moldowan, J.M., Zhang, S., Hill, R., Jarvie, D.M., Wang, H., Song, F., Fago, F., 2007b. Diamondoid hydrocarbons as a molecular proxy for thermal maturity and oil cracking: Geochemical models from hydrous pyrolysis. Organic Geochemistry 38, 227-249.

Wenger, L. M., Davis, C. L., Isaksen, G. H. 2002. Multiple controls on petroleum biodegradation and impact on oil quality. SPE Reservoir Evaluation and Engineering 5, 375–83.

Wessely, G., Schreiber, O.S., Fuchs, R., 1981. Lithofazies und mikrostratigraphie der Mittel- und Oberkreide des Molasseuntergrundes im östlichen Oberösterreich. Jahrbuch der Geologischen Bundesanstalt Band 124, 175-281

Whiticar, M.J., 1994. Correlation of natural gases with their sources. In: Magoon, L.B., Dow, W.G., (eds.), 1994, The Petroleum system – from source to trap: AAPG Memoir 60, pp. 261-283.

Whiticar, M.J., 1999. Carbon and hydrogen isotope systematics of bacterial formation and oxidation of methane. Chemical Geology 161, 291-314.

Whiticar, M.J., Suess, E., 1990. Hydrothermal hydrocarbon gases in the sediments of the King George Basin, Bransfield Strait, Antarctica. Applied Geochemistry 5, 135-147.

Whiticar, M.J., Faber, E., Schoell, M., 1986, Microbial methane formation in marine and freshwater environments: carbon dioxide reduction vs. acetate fermentation – isotope evidence. Geochimica et Cosmochimica Acta 50, 693-709.

Wiggins, W.D., Harris, P.M., Burruss, R.C., 1993, Geochemistry of post-uplift calcite in the Permian Basin of Texas and New Mexico: Geological Society of America Bulletin 105, 779-790.

Wingert, W.S., 1992. G.c.-m.s. analysis of diamondoid hydrocarbons in Smackover petroleums. Fuel 71, 37-43.

Wilkes, H., Boreham, C., Harms, G., Zengler, K., Rabus, R., 2000. Anaerobic degradation and carbon isotope fractionation of alkylbenzenes in crude oil by sulfate-reducing bacteria. Organic Geochemistry 31, 101-115.

Xia, X., Tang., Y., 2012. Isotope fractionation of methane during natural gas flow with coupled diffusion and adsorption/desorption. Geochimica et Cosmochimica Acta 77, 489-503.

Yoneyama, Y., Okamura, M., Morinaga, K., Tsubaki, N., 2002. Role of Water in Hydrogenation of Coal without Catalyst Assition. Energy Fuels 16, 48-53.

Zengler, K., Richnow H.H., Rossello-Mora, R., Michaelis, W., Widdel, F., 1999. Methane formation from long-chain alkanes by anaerobic microorganisms. Nature 401, 266-269.

Zhang, T., Krooss, B.M., 2001. Experimental investigation on the carbon isotope fractionation of methane during gas migration by diffusion through sedimentary rocks at elevated temperature and pressure. Geochimica et Cosmochimica Acta 65, 2723-2742.

Zhang, S., Huang, H., Xiao, Z., Liang, D., 2005. Geochemistry of Palaeozoic marine petroleum from the Tarim Basin, NW China. Part 2: Maturity assessment. Organic Geochemistry 36, 1215-1125.

Zhang, S., Su, J., Huang, H., He, K., Wang, Y., Wang, H., Zhang, B., Wang, X., Hu, J., 2015. Genetic origin of sour gas condensates in the Paleozoic dolomite reservoirs of the Tazhong Uplift, Tarim Basin. Marine and Petroleum Geology 68, 107-119.

13. List of figures

14. List of tables